Photoswitchable Monolayers on Si(111) and Si(100) Surfaces

vorgelegt von
M.Sc. in Organic Chemistry
Marina Vlajić
geb. in Niš, Serbien

von der Fakultät II – Mathematik und Naturwissenschaften
der Technischen Universität Berlin
zur Erlangung des akademischen Grades

Doktor der Naturwissenschaften
- Dr. rer. nat. -

genehmigte Dissertation

Promotionsausschuss:
Vorsitzende: Prof. Dr. rer. nat. Marga Lensen
Gutachterin: Prof. Dr. rer. nat. Karola Rück-Braun
Gutachterin: Prof. Dr. rer. nat. Petra Tegeder

Tag der wissenschaftlichen Aussprache: 27. April 2018

Berlin 2018

Die vorliegende Arbeit wurde
unter Leitung von Prof. Dr. Karola Rück-Braun
in der Zeit von Oktober 2013 bis Februar 2018
im Institut für Chemie der Fakultät II
der Technischen Universität Berlin angefertigt.

Abstract

Photochromic compounds, that exhibit stable and reversible change of their physical and chemical properties upon light absorption, present great potential for development of new “smart” materials. Thus, their attachment to the solid surfaces and nanostructures showed prospective in development of novel photosensitive smart materials. In that context, present work dealt with preparation of photoswitchable compounds, and their immobilization onto solid silicon surfaces.

In the first part of the work, preparation and characterization of fulgimide- and naphthopyran-linker conjugates is presented. The former being thermally stable, and latter thermally reversible; they exhibit different photochemical and photophysical properties, both in solution and on gas / solid phase interfaces. Both prepared conjugates showed reliable switching between the defined states in solution, upon several irradiation cycles. Thus, they proved to be excellent candidates for studying the photochemical behaviour on various functionalized silicon interfaces.

Second part of the work is focused on preparation of the photoswitchable structures on silicon surfaces, by employing the concept of covalently attached self-assembled monolayers (SAMs). The monolayer formation was carried out on oxide-free silicon(111) (H-terminated silicon crystal) and oxidized silicon(100) interfaces. Furthermore, various methods for the attachment of the photoswitch-linker conjugates were applied, and resulting on-chip structures were characterized. The photochemical studies of the obtained photoswitchable surfaces were carried out, and the switching on the solid phase / gas interface was studied. All developed photoswithable surface structures exhibited repeatable changes upon several irradiation cycles. It showed that the choice of photochromic compound influences the number of possible stable states on the surface. Furthermore, the properties of the underlying monolayer showed to impact the photochemical processes.

Kurzzusammenfassung

Photochrome Verbindungen, die eine stabile und reversible Änderung ihrer physikalischen und chemischen Eigenschaften bei Lichtabsorption zeigen, bieten ein großes Potenzial für die Entwicklung neuer "intelligenter" Materialien. Ihre Bindung an Festkörper und Nanostrukturen ergibt daher vielversprechende neuartige lichtempfindliche Materialien. In diesem Zusammenhang befasst sich die vorliegende Studie mit der Darstellung von photoschaltbaren Verbindungen und deren Immobilisierung auf festen Siliziumoberflächen.

Im ersten Teil der Arbeit wird die Herstellung und Charakterisierung von Fulgimid- und Naphthopyran-Linker-Konjugaten vorgestellt. Das erster System ist thermisch stabil und letzteres thermisch reversibel; sie zeigen unterschiedliche photochemische und photophysikalische Eigenschaften, sowohl in Lösung, als auch an Grenzflächen zwischen Gas und Festphase. Beide hergestellten Konjugate ergaben nach mehreren Bestrahlungszyklen ein zuverlässiges Umschalten zwischen den definierten Zuständen in Lösung. Damit erwiesen sie sich als hervorragende Kandidaten für die Untersuchung des photochemischen Verhaltens an verschiedenen funktionalisierten Silizium-Grenzflächen.

Der zweite Teil der Arbeit konzentriert sich auf die Herstellung von photoschaltbaren Strukturen auf Siliziumoberflächen, wobei das Konzept kovalent gebundener selbstorganisierter Monolagen (self-assemmbled monolayers, SAMs) verwendet wird. Die Monolagen wurden auf oxidfreien Silizium(111) (H-terminierten Siliziumkristall) und oxidierten Silizium(100) Grenzflächen aufgebracht. Darüber hinaus wurden verschiedene Methoden zur Anbindung der Photoschalter-Linker-Konjugate angewendet und die resultierenden On-Chip-Strukturen charakterisiert. Die photochemischen Untersuchungen der erhaltenen photoschaltbaren Oberflächen wurden durchgeführt, und das Schalten der Festphasen / Gas-Grenzfläche wurde untersucht. Alle entwickelten photoschaltbaren Oberflächenstrukturen zeigten wiederholbare Veränderungen bei mehreren Bestrahlungszyklen. Es zeigte sich, dass die Wahl der photochromen Verbindung die Anzahl möglicher stabiler Zustände auf der Oberfläche beeinflusst. Darüber hinaus zeigten die Oberflächeneigenschaften einen Einfluss auf die photochemischen Prozesse.

Table of Contents

1 Introduction 1

  1.1 Photochromism 1

  1.2 Self-Assembled Monolayers 3

2 Aim 9

3 Synthesis of Photoswitch-Linker Conjugates 11

  3.1 Fulgimide-Linker Conjugate 11

    3.1.1 Plan of the Synthesis 14

    3.1.2 Synthesis of the Fulgimide-Linker Conjugate 15

      3.1.2.1 Synthesis of the Fulgide Core 15

      3.1.2.2 Synthesis of the Fulgimide-Linker Conjugate for Immobilization on Silicon Surfaces 18

    3.1.3 Characterization of Photochemical Properties of Fulgimides 7, 34 and Related Compounds 19

      3.1.3.1 UV/Vis Studies of Fulgimide 34 and Related Compounds 21

  3.2 Naphthopyran-Linker Conjugate 23

    3.2.1 Plan of the Synthesis 29

    3.2.2 Synthesis of the Naphthopyran-Linker Conjugate 30

      3.2.2.1 Synthesis of the Naphthopyran Core 30

      3.2.2.2 Synthesis of the Piperazine-Based Linker 32

      3.2.2.3 Synthesis of the Naphthopyran-Linker Conjugate for Immobilization on the Silicon Surface 35

    3.2.3 Characterization of Photochemical Properties of the Naphthopyran Compounds ... 37

      3.2.3.1 UV/Vis Studies of the Naphthopyran Compounds 38

      3.2.3.2 NMR Photochemical Studies of the Naphthopyran Compounds 43

3.2.3.3 FTIR Solution Photochemical Studies of the Naphthopyran Compounds 48

4 Photoswitchable Self-Assembled-Monolayers on Silicon Surfaces..................................... 55

4.1 Preparation and Functionalization of SAMs on Si(111) Surfaces 55

4.1.1 Formation of Hydrogen-Terminated Si(111) Surface.. 57

4.1.2 Formation of Carboxy-Terminated SAMs on Si(111).. 58

4.1.3 Functionalization of Carboxy-Terminated SAMs via Amide Bond Formation Reaction on Si(111) 62

4.1.4 Fulgimide-Terminated SAMs on Si(111) 64

4.1.4.1 Photochemical Studies of Fulgimide-Terminated SAMs on Si(111) 66

4.1.5 Naphthopyran-Terminated SAMs on Si(111)... 69

4.1.5.1 Photochemical Studies of Naphthopyran-Terminated SAMs on Si(111)......... 73

4.2 Preparation and Functionalization of SAMs on Oxidized Si(100) Surfaces 78

4.2.1 Formation and Characterization of Si(100) Oxide Layer 81

4.2.2 Formation of Epoxy-Terminated SAMs on Oxidized Si(100) 82

4.2.2.1 Variation on Work-up Procedures upon Formation of Epoxy-Terminated SAMs 86

4.2.3 Formation of Alkyl-Terminated SAMs on Oxidized Si(100).................................. 88

4.2.4 Functionalization of Epoxy-Terminated SAMs via Epoxide Ring-Opening Reaction on Oxidized Si(100)... 89

4.2.5 Acetylene-Terminated SAMs on oxidized Si(100).. 90

4.2.6 Fulgimide-Terminated SAMs on Oxidized Si(100) 92

4.2.6.1 Photochemical Studies of Fulgimide-Terminated Monolayers on Oxidized Si(100) 96

5 Conclusion 101

5.1 Synthesis of Photoswitch-Linker Conjugates 101

5.2 Photochromism of Photoswitch-Linker Conjugates 103

5.3 Monolayer Structures on Si(111) and Si(100) 105

6 Experimental Section 111

6.1 General Information 111

6.2 Synthesis of Fulgimide-Linker Conjugate 113

6.3 Synthesis of Naphthopyran-Linker Conjugate 121

6.4 Preparation of the Self-Assembled Monolayers on Si(111) and Si(100) Surfaces 129

6.4.1 General Information 129

6.4.2 Procedures on Si(111) 133

6.4.3 Procedures on Oxidized Si(100) 136

6.5 Photochromic Investigations 138

6.5.1 UV/Vis Measurements 138

6.5.2 NMR Measurements 139

6.5.3 Infrared Measurements 141

7 Appendix 143

7.1 Photochemical Data 143

7.1.1 UV/Vis Data 144

7.1.2 NMR Data 155

7.1.3 Infrared Data 163

7.2 Surface Analysis 171

7.3 NMR Spectra 178

8 References 195

Table of Figures

Figure 1.1. Reversible transformation between two photoisomers A and B. 1

Figure 1.2. Various well-known photoswitches, grouped by the type of photochromism: P type: fulgide compounds (**1**), dithienylethens (**2**), and T-type: naphthopyrans (**3**), azobenzenes (**4**), spiropyrans (**5**) and hemithioindigos (**6**). 2

Figure 1.3. Schematic presentation of self-assembled monolayers on variuos silicon and gold surfaces. 4

Figure 1.4. Two different strategies for formation of SAMs on silicone surfaces, by a bottom-up method: (A) alkene on oxide-free Si(111), and (B) silane on Si/SiO$_X$ surface, with an option for further functionalization.. 6

Figure 2.1. The aim photoswitchable conjugates for the immobilization on silicon surfaces....... 9

Figure 2.2. The aim structures of photoswitchable self-assembled monolayers on silicon(111) and (100) in this work.. 10

Figure 3.1. Variation of structures of fulgide and fulgimide compounds, including the open stereoisomers and the closed photoisomer.. 11

Figure 3.2. Photoisomerisation reaction of the fulgide, upon UV and Vis light irradiation........ 12

Figure 3.3. Retrosynthetic plan for the synthesis of fulgimide-linker conjugate **7**..................... 14

Figure 3.4. Scheme of the reaction route towards obtaining Stobbe product **22**. 15

Figure 3.5. Mechanism of Stobbe condensation reaction according to the ref. 84..................... 16

Figure 3.6. Reaction scheme and conditions towards preparation of the fulgide **16**. 17

Figure 3.7. Synthetic route and conditions towards preparation of the protected fulgimide-linker conjugate **34**. 18

Figure 3.8. Deprotection of the Boc-protected fulgimide **34**, and the structure of the side product **35**.. 19

Figure 3.9. Photostationary states (PSS) of fulgide **16** and fulgimides **7** and **34** structures described in this study. 20

Figure 3.10. Absorption spectra of the PSSs of the fulgide **16** (A, B) and fulgimide **34** (C, D), at 20 °C in MeCN upon UV light irradiation - PSS(365 nm) (violet); visible light irradiation - PSS(565 nm) (green); and the initial state (black).. 21

Figure 3.11. Structures of three different stereoisomers of naphthopyran compounds, including the steric interaction of the hydrogen-atoms in the open forms. The scheme is adjusted from the scheme reported in ref. 3. 23

Figure 3.12. The resonance structures of naphthopyran with ester and electron donor substituents, in positions 5 and 6 of 2*H*-naphtho[1,2-b]pyran **38**, respectively. The scheme is adjusted from the scheme reported in ref. 87. 25

Figure 3.13. Structural modification of the chromene structures, in order to enhance the ratio of only one of the photoisomers as reported by groups of (A) Rück-Braun in ref. 93, (B) Coelho in ref. 94 and (C) Abe in ref. 97. 27

Figure 3.14. Possible photochemical and thermal reaction pathways of the chromene switching process, including the formation of the allene (A) form. 28

Figure 3.15. Retrosynthetic plan of the naphthopyran-linker conjugate **8**. 29

Figure 3.16. Three steps synthesis route, including the reaction conditions and rearrangement towards the naphthopyran **45**. 30

Figure 3.17. Side product formation via Meyer-Schuster rearrangement of the propargylacohol **47**. 31

Figure 3.18. Three steps reaction route and reaction conditions, towards obtaining Buchwald-Hartwig coupling product **63**. 32

Figure 3.19. Mechanism of the Buchwald-Hartwig amination towards preparation of the linker **63**, according to ref. 119. 34

Figure 3.20. Reaction scheme and conditions towards obtaining the piperazine-based linker **70**. 35

Figure 3.21. Formation of the naphthopyran-linker conjugate **71**, via Steglich esterification reaction. 36

Figure 3.22. Reaction scheme and conditions for the Boc-deprotection towards obtaining naphthopyran **8**. 36

Figure 3.23. General photochemical equilibrium of naphthopyran structures described in this study. 37

Figure 3.24. Absorption spectra of the PSSs of the naphthopyran **45** (A) and **71** (B) in acetonitrile: upon UV light irradiation, PSS(365 nm) (red); thermal relaxation, PSS(Δ) (blue); visible light irradiation, PSS(505 nm) (green); and the initial state (black). 38

Figure 3.25. Time-resolved spectra of the naphthopyran **45** in acetonitrile (c = 9.4 · 10^{-6} M), under (A) UV light irradiation, and (B) thermal back reaction (blue), and visible light irradiation back reaction (green). 39

Figure 3.26. Time-resolved spectra of the naphthopyran **71** in acetonitrile (c = 9.8 · 10^{-6} M), under (A) UV light irradiation, and (B) thermal back reaction (blue), and visible light irradiation back reaction (green). (D) Repeatable changes of the average absorbance in the region 458-468 nm upon reaching the PSS(365 nm) and PSS(505 nm). 40

Figure 3.27. (A) Absorption spectra of the naphthopyran **71** in tetrachloroethylene, the initial state and at the PSS(505 nm) over 3 cycles. (B) The changes in the average absorbance in the region 458-468 nm upon reaching the PSS(365 nm) and PSS(505 nm). 41

Figure 3.28. ^{1}H NMR spectra of the naphthopyran **45** in MeCN-*d3*, at 0 °C before the irradiation, upon reaching the PSS(365 nm), and upon thermal relaxation. The NMR assignations are color coded as following: CF (blue), TC (red), and TT (green). 43

Figure 3.29. ^{1}H NMR spectra of the naphthopyran **71** in MeCN-*d3*, at 0 °C before the irradiation, upon UV irradiation and reaching the PSS(365 nm), upon thermal relaxation and reaching the PSS(Δ), and upon visible light irradiation and reaching the PSS(505 nm). The NMR assignations are colour coded as following: CF (blue), TC (red), and TT (green). 44

Figure 3.30. Zoom of the ^{1}H NMR spectra of naphthopyran **71**, taken periodically at 0 °C, in order to follow the peak integral changes during (A) UV light irradiation, (B) thermal relaxation, and (C) visible light irradiation. The NMR assignations are colour coded as following: CF (blue), TC (red), and TT (green). 46

Figure 3.31. Time-resolved ^{1}H NMR spectra during the switching experiment of naphthopyrans **45** (left) and **71** (right) in MeCN-*d3* at 0 °C. 47

Figure 3.32. FTIR solution spectra of photoswitching of naphthopyran **45** in TCE, over two cycles; UV light irradiation (λ_{irr} = 365 nm) time 10 minutes, thermal relaxation time 30 minutes. The initial state (green), PSS upon UV-light irradiation in the 1st (red) and 2nd (orange) cycle, and PSS upon thermal relaxation in the 1st (blue) and 2nd (purple) cycle. 49

Figure 3.33. FTIR solution spectra of photoswitching of naphthopyran **71** in TCE (A), over two cycles; UV light irradiation (λ_{irr} = 365 nm) time 10 minutes, thermal relaxation time 20 minutes. The initial state (green), PSS upon UV-light irradiation in the 1st (red) and 2nd (orange) cycle, and

PSS upon thermal relaxation in the 1st (blue) and 2nd (purple) cycle. The changes in the intensity of the band at ~1595 cm^{-1}, in different solvents: TCE (B), MeCN (C), and DCE (D). 51

Figure 3.34. Repetable changes of the ν(C=O) methyl-ester absorption band position of naphthopyrans **45** (A) and **71** (B), upon UV-light irradiation and thermal relaxation, over two cycles, in TCE (black), MeCN (red), and DCE (blue). Dotted lines represent the PS states, upon UV-light irradiation (pink) and thermal relaxation (grey). 53

Figure 4.1. Proposed mechanism of the monolayer formation on the H-terminated Si(111) surface. 55

Figure 4.2. Hydrogen-terminated surface on Si(111). (A) Reaction conditions of the oxidation and etching reactions. (B) IR spectra of the H-terminated surface, referenced to the oxide layer, recorded in p- (black) and s-polarization (red). (C) Structure of the H-terminated Si(111) surface. 57

Figure 4.3. Synthetic route towards formation of (a) neat, and (b) diluted carboxy-terminated monolayers on Si(111). 58

Figure 4.4. IR spectra of the neat (black) and diluted (red) ester-terminated monolayer on Si(111). 59

Figure 4.5. IR spectra of ester-terminated (black) and carboxy-terminated (red) SAMs on Si(111). (A) Wide range IR spectra. (B) The zoom of the alkyl stretching region. (C) The Si-H stretching region, referenced to the silicon oxide, shows the oxidation of the Si-H bond during the hydrolysis step. 60

Figure 4.6. IR spectra of ester-terminated (black) and carboxy-terminated (red) SAMs on Si(111). (A) Wide range IR spectra. (B) The zoom of the alkyl stretching region. (C) The Si-H stretching region, referenced to the silicon oxide, shows the oxidation of the Si-H bond during the hydrolysis step. 61

Figure 4.7. Reaction conditions towards formation of photoswitchable SAMs on Si(111). 62

Figure 4.8. Boc-piperazine **62** test-coupling reaction to the carboxy-terminated SAMs on Si(111), using HCTU (black), and HATU (red) as coupling reagent. 63

Figure 4.9. IR spectra of neat ester- (black), carboxy-(red), and fulgimide-terminated SAMs on Si(111), referenced to the spectrum of H-Si(111). 64

Figure 4.10. IR spectra of diluted ester- (black), carboxy-(red), and fulgimide-terminated SAMs on Si(111), referenced to the spectrum of H-Si(111). 66

Figure 4.11. Fulgimide *Z*-to-*E* and *E*-to-*Z*, as well as *E*-to-*C* and *C*-to-*E* photochromism upon UV(365 nm) and vis(545 nm) irradiation of neat and diluted SAMs on Si(111). 67

Figure 4.12. Repeatable changes upon alternating UV and visible light irradiation of the neat (A,B) and diluted (C,D) fulgimide-terminated SAMs, upon immobilization (black), PSS(365 nm) (blue), and PSS(545 nm) (red), over 5 irradiation cycles. 68

Figure 4.13. IR spectra of ester- (black), carboxy-(red), and naphthopyran-terminated SAMs on Si(111), referenced to the spectrum of H-Si(111). 69

Figure 4.14. XPS-survey and high-resolution scans of the C1s, O1s and N1s core levels of (A) carboxy- and (B) naphthopyran-terminated SAMs on Si(111). The black lines present the recorded data, while the blue lines are fitted data. 71

Figure 4.15. Photoisomerisation of the naphthopyran **8**, on the Si(111) surface. 74

Figure 4.16. Photochemical study of naphthopyran-terminated SAMs on Si(111). Overlayed spectra of the initial state (black) upon reaching the PSSs: PSS(365 nm) (red), PSS(Δ) (blue), and PSS(545 nm) (green). (D) Steady-state difference-absorption spectra between the photostationary states, due to the ring opening (blue) and ring closure (red) of the naphthopyran ring, for the cycles (I). 75

Figure 4.17. The zoom of the ATR-FTIR spectra of the naphthopyran-terminated monolayer, upon reaching the PSSs in 2nd and 3rd cycle. Both the repeatable shift between the PSS(365 nm) and PSS(Δ), as well as an overall gradual increase of intensity in the region 1450-1250 cm^{-1} is observable. 77

Figure 4.18. Sketch of the monolayer structures obtained from tri- and monofunctional organosilanes. 78

Figure 4.19. Scheme of the proposed four-step mechanism for SAM formation on silicon oxide using organosilanes. 79

Figure 4.20. Reproducible formation of silicon oxide layers. Reaction conditions: (a) *Piranha* solution (H_2SO_4 / H_2O_2, 3:1), 100 °C, 1 h; (b) HF 2.5 % (aq), RT, 1 min; (c) *Piranha* solution (H_2SO_4 / H_2O_2, 3:1), 100 °C, 1 h. (B) IR spectra of freshly prepared silicon-oxide layer, referenced to the H-terminated sample, measured in p-polarization (black) and s-polarization (red). 81

Figure 4.21. Reaction conditions for the preparation of epoxy-terminated monolayer. 82

Figure 4.22. ATR-FTIR spectra of epoxy-terminated monolayers, prepared from toluene solution with different water concentrations: 10 ppm (black), 66 ppm (red) and toluene saturated with water (blue). (B-D) Deconvoluted IR spectra of the C-H stretching region of the epoxy-terminated monolayer. The fitted curve is color-coded according to the representation in (A). 84

Figure 4.23. (A) Three work up procedures. (B) The zoom of the C-H stretching region of the epoxy-terminated monolayer, obtained upon three different work up procedures. (C) The zoom of the C-H stretching region of the sample worked up according to the procedure (3). 87

Figure 4.24. The IR spectra of the alkyl-terminated monolayers, prepared from toluene solution with different water concentrations: ~10 ppm (black), and 66 ppm (red). (A) Reaction conditions for the preparation of the alkyl-terminated SAMs. (B-D) Deconvoluted IR spectra of the C-H stretching region of the alkyl-terminated monolayer. The fitted curve is color-coded according to the representation in (B). 88

Figure 4.25. Preparation of the acetylene- and fulgimide-terminated monolayers on oxidized Si(100). Reagents and conditions: (a) 156 mM propargylamine (**76**) in toluene, 80 °C, glove box, 24 h; (b) 5.4 mM fulgimide **7** in toluene / 1,4-dioxane (10:1), 90 °C, glove box, 24 h................ 90

Figure 4.26. The IR spectra of the epoxy- (black) and acetylene-terminated (red) monolayers, referenced to silicon-oxide. The zoom of the C-H stretching region of the epoxy- (black) and acetylene-terminated (red) monolayers. 91

Figure 4.27. The IR spectra of epoxy-terminated (black) and fulgimide-terminated monolayers (red). (B) The zoom of the C-H stretching region of the epoxy- (black) and fulgimide-terminated (red) monolayers. (C) Deconvoluted IR spectra in the same region of the fulgimide-terminated monolayer. The red curve presents the fitted curve upon the deconvolution. 93

Figure 4.28. High-resolution XPS spectra of the Si2p, C1s, N1s and O1s core levels of the epoxy- and fulgimide-terminated samples on oxidized Si(100). 94

Figure 4.29. Fulgimide *E*-to-*C* and *C*-to-*E* photochromism upon UV (λ_{irr} = 365 nm) and visible (λ_{irr} = 545 nm) light irradiation. 96

Figure 4.30. ATR-FTIR spectra of the ν_{as}(C=O) absorption band of the fulgimide-terminated monolayer at the PSSs, upon 5 UV/Vis irradiation cycles: initial state (black), PSS(365 nm) (blue), and PSS(545) (red). Broadening of the signal is observed upon several cycles: (C) 1st cycle, (D) 5th cycle. 97

Figure 4.31. Changes in wettability of the fulgimide-terminated monolayer upon reaching PSSs over five UV/Vis irradiation cycles. Dotted lines present the average position for each of the two PSSs. 98

Figure 5.1. Synthetic route towards formation of fulgimide-linker conjugate **7**. 102

Figure 5.2. Synthetic route towards formation of naphthopyran-linker conjugate **8**. 103

Figure 5.3. Time-resolved spectra of naphthopyran **45** (left) and naphthopyran-linker conjugate **71** (right) of ^{1}H NMR signals during one irradiation cycle; photoisomers: closed form (blue), TC form (red), TT form (green). 104

Figure 5.4. Overview of photoswitchable self-assembled monolayers on silicon surfaces, prepared in this work. 105

Figure 5.5. Photochemical studies of fulgimide-terminated SAMs on Si(111) and Si(100) surfaces. 108

Figure 5.6. Differences between photochemical studies of naphthopyran-linker conjugate **71** in acetonitrile solution and naphthopyran-terminated SAMs on Si(111). 109

Figure 6.1. Sample compartment of the Bruker ATR-FTIR spectrometer: (1) sample holder, (2) silicon ATR wafer, (3) mirrors, (4) polarizator, (5) detector, (6) light source. The red line is drawn to guide the eye by following the IR light beam during the measurement. 130

Figure 6.2. Sample holder unit (1) of the Bruker ATR-FTIR spectrometer with a self-prepared ATR silicon wafer (2), and irradiation elements equipped with LED diodes for both UV (365 nm) and visible light (545 nm) irradiation (3). 131

Figure 6.3. UV/Vis set-up: (1) light source, (2) optical cable, (3) sample holder with a cuvette, (4) detector, (5) LED lights, (6) temperature regulator, (7) air stream cooling. 138

Figure 6.4. Sample compartment of the UV/Vis set-up: (1) cuvette, (2) 1st LED light, (3) 2nd LED light, (4) sample holder with thermoregulation, (5) optical cable, (6) stirring mechanism, (7) air stream cooling. 139

Figure 6.5. The etched insert at the end of the optical cable; with the LED turned on, the light is distributed over the whole length of the etched insert. NMR tube mounted to the optical cable, with a spinner for inserting the tube into the NMR machine. 140

Figure 6.6. Adapter for an LED attachment to the optical cable, with and without the LED attached. 140

Figure 6.7. Cuvette for the IR measurements (1); equipped with the LED diodes set-up for irradiation (2), mounted on the cuvette holder (3). 141

Figure 6.8. Sample compartment of the Bruker FTIR spectrometer: (1) cuvette, (2) set-up with LED diodes for irradiation of the sample, (3) cuvette holder, (4) detector, (5) light source. The red line is drawn to guide the eye by following the IR light beam during the measurement. 142

Table of Tables

Table 3.1. Influence of steric effects of present substituents on the quantum yields and spectroscopic properties of the photoisomers of various fulgide molecules, recorded in toluene. The values are taken as presented in the ref. 75. 13

Table 3.2. Photochemical properties of fulgimide **16** and fulgimide **34**, investigated in acetonitrile and chloroform at 20 °C.. 22

Table 3.3. Comparison of the photochromic properties of 2,2-diphenyl-2*H*-naphtho[1,2-b]pyran and 3,3-diphenyl-3*H*-naphtho[2,1-b]pyran, recorded in diethylene-glycol bis(allyl carbonate). The values as taken as presented in ref. 23. 24

Table 3.4. Influence of substituents in the 5- and 6- position on photochromic properties of 2*H*-naphtho[1,2-b]pyrans. 25

Table 3.5. Influence of the substituents at the aromatic rings on photochromic properties of 3,3-diphenyl-3*H*-naphtho[2,1-b]pyrans. 26

Table 3.6. Spectroscopic data of naphthopyran **45** (in acetonitrile), and **71** (in acetonitrile and tetrachloroethylene). 41

Table 3.7. Spectrokinetic data of thermal bleaching of the naphthopyrans **45** (A) and **71** (B), in acetonitrile solution (c = $9.4 \cdot 10^{-6}$ M and $9.8 \cdot 10^{-6}$ M, respectively).. 42

Table 3.8. Peak assignment, position and coupling constant in ^{1}H NMR, of the three photoisomers, of naphthopyran **45** and **71** in acetonitrile-*d3* at 0 °C. 45

Table 3.9. Calculated ratios of different photoisomers of naphthopyrans **45** and **71** (10^{-2} M), upon reaching the photostationary states, in MeCN-*d3* at 0 °C, obtained from the NMR data. 47

Table 3.10. Some physical properties of the solvents used for the IR photochemical studies in solution.. 48

Table 3.11. Significant changes of the IR absorption bands and their assignments upon light illumination of naphthopyran **45** in TCE. Both changes in intensity or the position of the bands are presented. 50

Table 3.12. Significant changes of the IR absorption bands and their assignment upon photochemical study of naphthopyran **71** in TCE. Both changes in intensity or the position of the bands are presented. 52

Table 4.1. Characteristics of the components of the C1s, O1s and N1s signals obtained upon the peak fitting of the high resolution XPS spectra – assignments, binding energies (eV) and full-width at half maximum (FWHM) (eV) - for (A) carboxy- and (B) naphthopyran-terminated monolayers; The black lines present the recorded data, while the blue lines are fitted data. 72

Table 4.2. Peak positions of the $\nu_{as}(CH_3)$, $\nu_{sym}(CH_3)$, $\nu_{as}(CH_2)$ and $\nu_{sym}(CH_2)$ absorption bands and the FWHM of the $\nu_{as}(CH_2)$ and $\nu_{sym}(CH_2)$ absorption bands, for the epoxy-terminated monolayer obtained upon the peak analysis of the obtained raw FTIR data. The visualization shows changes in peak position and FWHM of $\nu_{as}(CH_2)$ and $\nu_{sym}(CH_2)$ absorption bands depending on the water concentration in toluene. 85

Table 4.3. Atomic surface composition for the epoxy- and fulgimide-terminated monolayer on oxidized Si(100) surfaces, as obtained from the XPS measurement. 94

Table 4.4. Spectral data of the components of the C1s and N1s signals obtained upon the peak fitting analysis of high-resolution XPS spectra - binding energies (eV), component peak area (%) and full-width at half maximum (FWHM) (eV) - for epoxy- and fulgimide- terminated monolayers. 95

Table 6.1. Irradiation conditions of the NMR photochemical studies of the naphthopyrans **45** and **71** 140

Table 6.2. Conditions of the in-solution FTIR photochemical studies of the naphthopyrans **45** and **71** 142

Abbreviations

abs.	absolute
aq.	aqueous
Ar	aryl
arb. unit	arbitrary unit
as	asymmetric
au	atomic units
ATR	attenuated total reflectance
Boc	*tert*-butoxycarbonyl
Boc_2O	di-*tert*-butyldicarbonate
°C	degrees Celsius
c	concentration
C, CF	closed isomer
CDI	*N*,*N'*-carbonyldiimidazole
cm^{-1}	reciprocal centimeter
COSY	correlation spectroscopy
d	doublet
DCC	*N*,*N*-dicyclohexylcarbodiimide
DCE	1,2-dichloroethane
DCM	dichloromethane
DIPEA	diisopropylethylamine
DMSO	dimethylsulfoxide
EA	elemental analysis
eq.	equivalent
ESI	electron spray ionization
Et	ethyl
et al.	and others
eV	electronvolt
FTIR	Fourier-Transformation Infrared Spectroscopy

FWHM	full width at half-maximum
FZ	Float-zone wafer
GPTMS	(3-glycidyloxypropyl)trimethoxysilane
h	hour
HATU	1-[bis(dimethylamino)methylene]-1H-1,2,3-triazolo[4,5-b]pyridinium 3-oxid hexafluorophosphate
HCTU	O-(1H-6-chlorobenzotriazole-1-yl)-1,1,3,3-tetramethyluronium hexafluorophosphate
HMBC	heteronuclear multiple bond correlation
HMQC	heteronuclear multiple quantum coherence
HR-MS	high-resolution mass spectroscopy
Hz	hertz
IR	infrared
J	coupling constant
L	ligand; liter
Lit.	literature value
m	multiplet; medium
M	mol/L
Me	methyl
MeCN	acetonitrile
min	minute
Mp	melting point
m/z	mass-to-charge ratio
NEt_3	triethylamine
nm	nanometer
NMR	nuclear magnetic resonance
o	*orto*
p	*para*
ppm	parts per million
PSS	photostationary state
PTFE	polytetrafluoroethylene

q	quartet
R	rest group
R_f	retention factor
RT	room temperature
s	singlet; strong
SAM	self-assembled monolayer
SiO_X	silicon oxide
sym	symmetric
t	triplet; time
TC	*transoid-cis* isomer
TCE	tetrachloroethylene
tech.	technical purity
THF	tetrahydrofuran
TLC	thin layer chromatography
TT	*transoid-trans* isomer
Ts	tosyl
UV	ultraviolet light
V	volume
Vis	visible light
w	weak
X	leaving group
XPS	X-ray photoelectron spectroscopy
δ	deformation vibration; chemical shift
Δ	thermal energy
Φ	quantum yield
λ	wavelength
λ_{irr}	irradiation wavelength
λ_{max}	absorption maximum
ν	wavenumber; stretching vibration
ν_{as}	asymmetric stretching vibration
ν_{sym}	symmetric stretching vibration

π^*	polarity/polarizability index
$\tau_{1/2}$	half life
Å	Ångström

1 Introduction

1.1 Photochromism

Photochromism is a light-induced reversible transformation of chemical species, between two forms - A and B - which exhibit different absorption spectra.[1] This transformation, in one or both directions, is induced by absorption of electromagnetic radiation. Upon irradiation of a thermodynamically stable form A, it undergoes transformation into form B (Figure 1.1). The back reaction may occur either by a light irradiation (photochemically, P-type photochromism) or spontaneously (thermally, T-type photochromism).[1] For most of the known photoswitchable compounds, the change in color goes from colorless or pale yellow form A, to colored form B, and is known as a positive photochromism. A negative (inverse) photochromism is described when $\lambda_{max}(A) > \lambda_{max}(B)$.

$$\mathrm{A} \quad \underset{\Delta\ /\ h\nu_2}{\overset{h\nu_1}{\leftrightarrows}} \quad \mathrm{B}$$

Figure 1.1. Reversible transformation between two photoisomers A and B.

Photochemical transformations were reported to proceed via 6π-electrocyclization reaction, *E*/*Z* isomerization, intramolecular hydrogen or group shift, dissociation reaction, or oxido-reduction.[1] Some photoswitchable compounds, e.g. fulgides and related compounds (Figure 1.2, **1**), upon UV light irradiation of the *E* isomer undergo both *E*/*Z* isomerization, as well as ring-closure reaction; however only the latter is considered an important transformation of the photochromic system.[2] Furthermore, a combination of those in a cascade reaction is also possible. Chromenes undergo ring-opening reaction, followed by *E*/*Z* isomerization towards more stable TT isomer (Figure 1.2, **3**).[3] Similarly, recently developed new class of photoswitchable compounds, donor-acceptor Stenhouse adducts (DACAs), first undergo *E*/*Z* alkene isomerization, followed by a 4π-electrocyclization reaction.[4,5]

Various well-known photoswitches are presented in Figure 1.2, grouped by the type of photochromism they exhibit. Compounds from the fulgide family **1** (X = O fulgide, X = NR fulgimide), as well as dithienylethenes (DTEs) **2** are P-type chromophores, all their photoisomers being thermodynamically stable. They undergo 6π-electrocyclic ring-closure reaction of the hexa-

1,3,5-triene unit upon UV light irradiation; the reverse ring-opening reaction is induced by visible light irradiation. T-type photoswitches, such as chromenes **3** and spiropyrans **5** undergo ring-opening reaction upon UV light irradiation. Being thermodynamically unstable, their open forms spontaneously, in the dark, undergo ring-closure reaction. Other T-type compounds, i.e. azobenzenes **4** and hemithioindigos **6**, undergo *E*/*Z* isomerization reaction upon light irradiation.

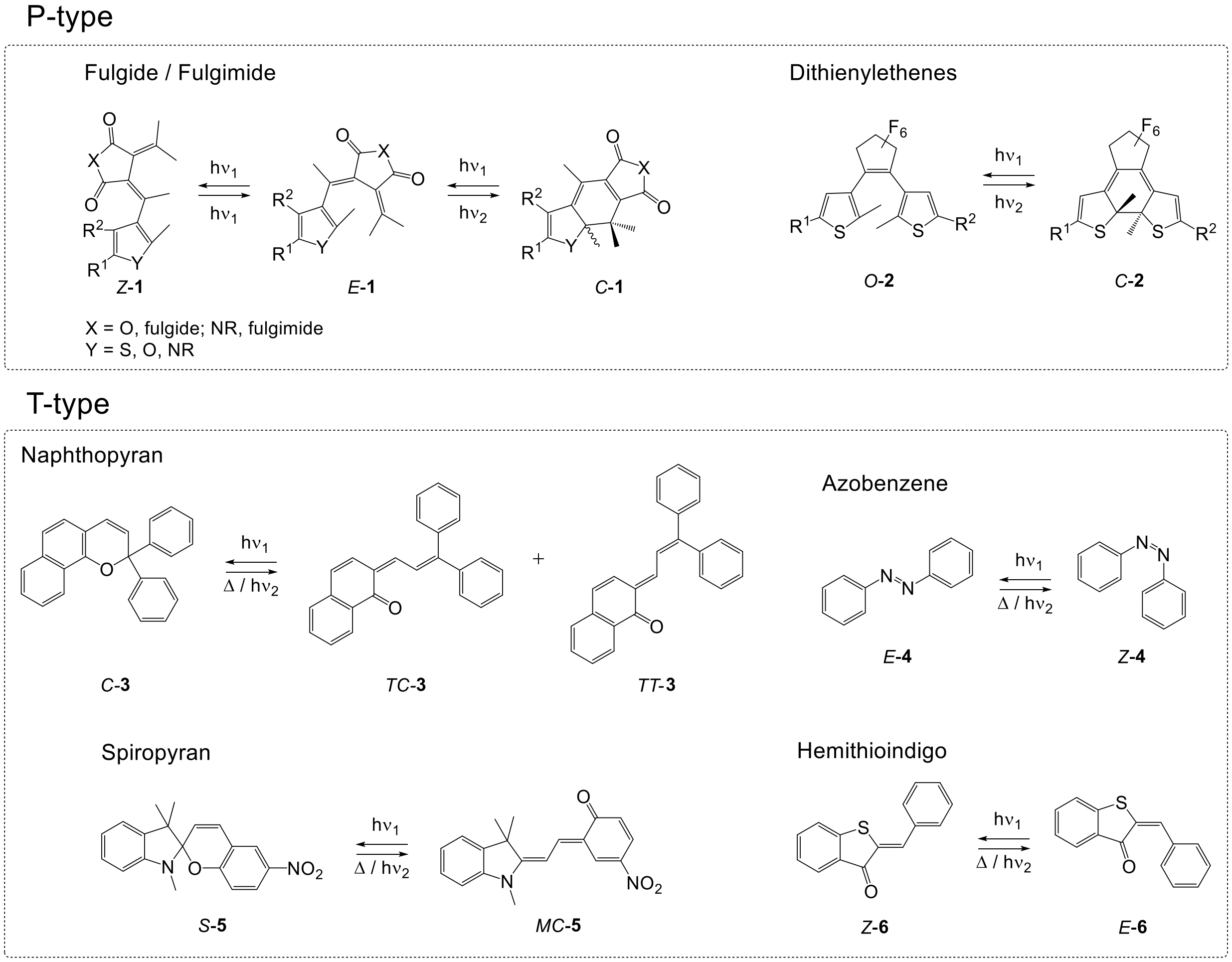
P-type
Fulgide / Fulgimide
hν1
hν1
hν1
hν2
Z-1
E-1
C-1
X = O, fulgide; NR, fulgimide
Y = S, O, NR
Dithienylethenes
hν1
hν2
O-2
C-2
T-type
Naphthopyran
hν1
Δ / hν2
C-3
TC-3
TT-3
Azobenzene
hν1
Δ / hν2
E-4
Z-4
Spiropyran
hν1
Δ / hν2
S-5
MC-5
Hemithioindigo
hν1
Δ / hν2
Z-6
E-6

Figure 1.2. Various well-known photoswitches, grouped by the type of photochromism: P type: fulgide compounds (**1**), dithienylethens (**2**), and T-type: naphthopyrans (**3**), azobenzenes (**4**), spiropyrans (**5**) and hemithioindigos (**6**).

Photochromic compounds have found various applications. Many have been incorporated into various biological systems, i.e. nucleic acids, peptides, enzymes, proteins, ligands, etc.[6–11] P-type photoswitches, due to their bistable nature, are good choice for molecular memories and switches.[2,12] Furthermore, fulgides and related compounds show excellent switching reversibility, resistance to fatigue in solution, and nondestructive readout ability. Immobilized on the solid substrate, they allow photochemical studies with the obtained photoswitchable surfaces, due to the changes of their vibrational modes upon light-induced ring-opening and -closing reactions.[13,14] Additionally, large changes in the first-order molecular hyperpolarizability between different forms are observed upon photoisomerization, allowing their application in the formation of effective two-dimensional confined nonlinear optics (NLO) switching materials.[15] Moreover, due to their properties, they found application in various fields, e.g. optical data storage, energy switchable devices, nonlinear optics, etc.[16–21] Naphthopyrans are known for their high photocoloration, fast color bleaching, and low degree of fatigue. Mainly, they are widely used in production of ophthalmic lenses.[22–24] Furthermore, they have been embedded in different polymer structures, thin films, and immobilized on nanostructures (e.g. nanoparticles and nanofibers).[25–30] Towards development of new photoresponsive materials, they found increasing application in textile industry.[31,32] Recent developments suggested possible use of modified naphthopyran compounds stabilized by a steric force for application in molecular logic gates and optical data storage devices.[33]

1.2 Self-Assembled Monolayers

Customized and well-defined hybrid surface structures on the nanometer scale are the foundation of future technological applications. The main approach towards designing surfaces with molecular control is by using the concept of self-assembled monolayers (SAMs) of organic molecules. Obtaining hybrid systems by employing SAMs already showed to possess potential application in variety molecular systems, including molecular electronics, optoelectronic devices, photovoltaics, biochips, (bio)chemical sensors, and biomaterials.[34–36]

In general sense, the self-assembled monolayers are spontaneously formed monolayers on the surface, when appropriate conditions are met.[35] Considering diversity in properties and reactivity of different materials and monolayer molecules, the appropriate conditions may involve simple deposition in the solution of monolayer molecules, or require activation by employing heating, illumination or applied bias. At present, two types of SAMs are generally most researched: 1) alkanethiol monolayers on gold, and 2) organic monolayers on silicon substrate.[35] Monolayer formation on silicon and other non-metal surfaces is highly advantageous alternative over formation on metal surfaces, since the monolayer is covalently bound to the surface. Organic monolayers on Si surfaces can be generally divided into two main strategical approaches: a) monolayers on a thin silicon oxide layer (SiO_X) prepared mostly through silane chemistry, and b) monolayers on oxide-free Si surface by formation of Si-C bond.

Monolayer molecules generally consist of three parts (Figure 1.3):[35] 1) an anchoring group that has a high affinity towards the surface, and is responsible for anchoring the molecules, 2) a linker which is generally an alkyl or aryl chain, and has a crucial role in the ordering and packing of the monolayer, due to van der Waals and electrostatic forces, and 3) a terminal group that introduces the functionality into the monolayer system, allows secondary functionalization, and defines physical and chemical properties of the surface.

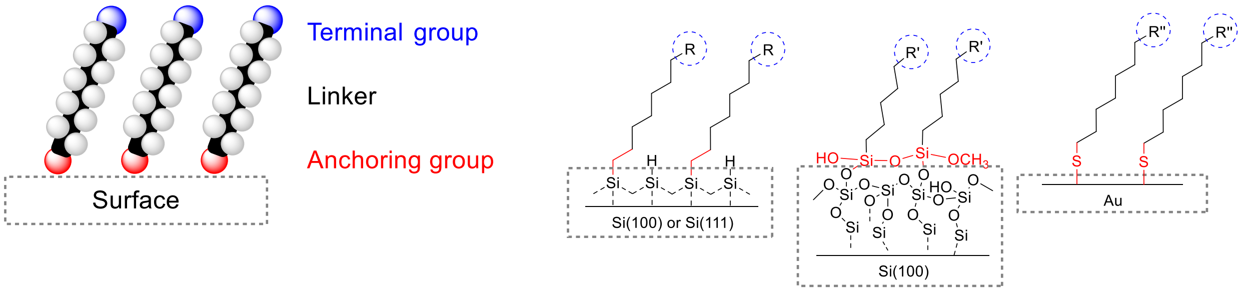

Figure 1.3. Schematic presentation of self-assembled monolayers on variuos silicon and gold surfaces.

Two main synthetic strategies are known for the formation of the functionalized SAMs on the surface.[35] The bottom-up method is a stepwise strategy, in which first the SAM is formed, and later further functionalized in an on-chip reaction. This approach ensures formation of densely packed monolayers, and allows formation of mixed or multicomponent structures.[37,38] Here, the stability of the formed monolayers towards the following on-chip reactions is required; however, it is advantageous in the case when secondary functionality is labile under SAMs formation reaction conditions. The top-down method is the SAMs formation of the pre-synthesized monolayer molecules, with the secondary functionality already embedded in the monolayer molecule. Here, the composition of the surface is known, due to absence of the unreacted functionalities at the terminal end; however, the bulkiness of the structure at the terminal end influences the formation of non-densely packed monolayers. This strategy does not require further on-chip reactions, which is advantageous in the case when the substrate is labile under necessary reaction condition. Both of these approaches are widely used, in research and industrial oriented applications.

In this work, the aim is formation of high-quality, densely packed photoswitchable monolayers, thus the bottom-up method is used for all developed structures. The formation of the self-assembled monolayers on silicon surfaces is approached from different immobilization strategies (Figure 1.4):

1) Monolayer formation on oxide-free H-terminated silicon(111) surface by thermally induced hydrosilylation. Hydrosilylation is the most reported strategy for formation of SAMs on H-terminated silicon surface - the reaction of a silicon hydride species with unsaturated carbon-carbon bonds (i.e. 1-alkenes or 1-alkynes), and formation of Si-C bond.[39,40] This approach is similarly also available for Si-heteroatom bond formation, i.e. Si-O-C, Si-N, Si-S bond. The resulting monolayer is covalently attached to the surface, highly stable and does not hydrolyze due to the non-polar covalent Si-C bond. The monolayers on Si(111) are characterized with highly-ordered, densely-packed structures with the headgroups located on top of the monolayer. The advantage of this approach is the ease of preparation, and formation of high-quality monolayers. However, the main disadvantage is the reproducibility of the monolayer formation - it proves to be difficult to achieve good quality samples without formation of some oxide. For futher functionalization, the attachment efficiency is limited by the steric demand of the photoswitch itself.

2) Monolayer formation on Si(100)/SiO_X interface by silanization of the organosilanes, such as trichloro- or trialkoxysilanes.[41,42] The resulting monolayer is covalently attached to the surface, with cross-linked network of Si-O-Si bonds between the monolayer molecules, suggesting increase of the stability of the monolayer. The advantage of this approach comes with the fact that Si/SiO_X interfaces are technologically relevant for various applications, including molecular electronic systems. However, amorphous silicon-oxide layers with non-defined amount of hydroxyl groups on top, difficulties to distinguish chemisorbed and physisorbed molecules on the surface, and high dependency between the quality of the resulting layer structure and the external influences such as water traces are the downsides of the method. Furthermore, the monolayers on oxidized Si(100) are less ordered, not as densely-packed monolayer structures on the surface compared to structures on oxide-free Si(111). The headgroups are not densely ordered on top of the monolayer, too, some are embedded into the monolayer. The further functionalization efficiency is thus influenced by the amount of available headgroups on top of the monolayer.

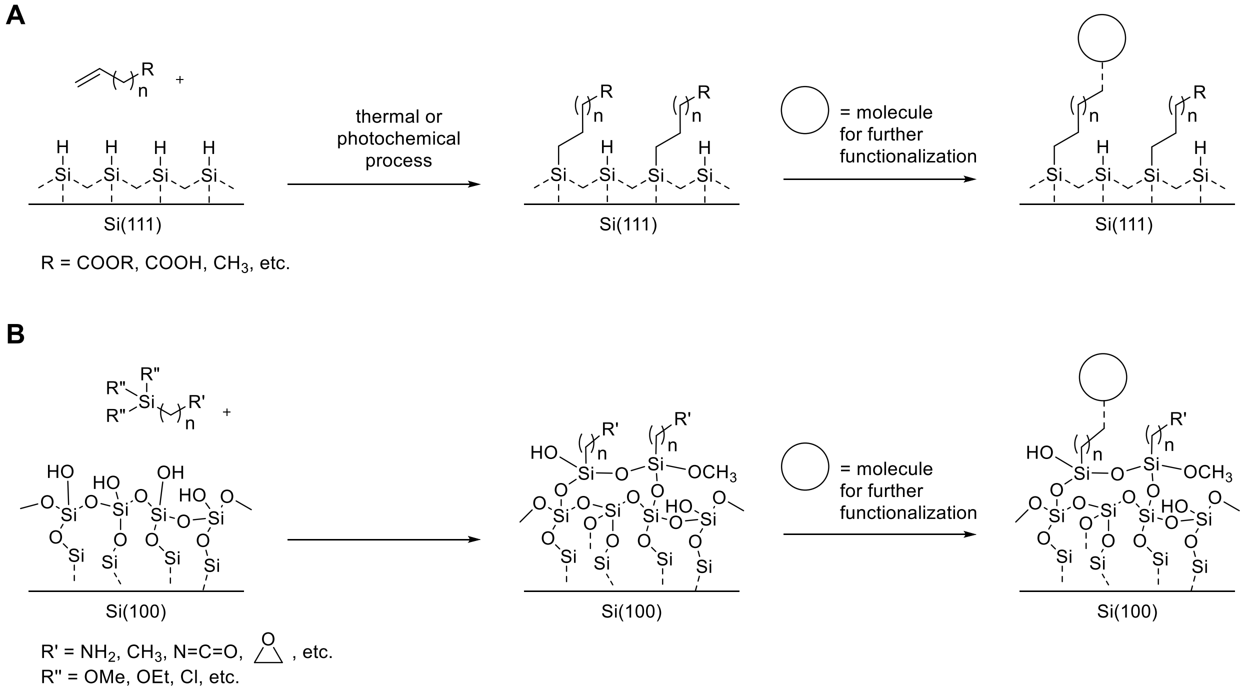
A
R
n
+
H H H H
Si Si Si Si
Si(111)
R = COOR, COOH, CH3, etc.
thermal or
photochemical
process
= molecule
for further
functionalization
B
R"
R"
Si
R'
R"
n
+
HO HO OH HO
Si(100)
R' = NH2, CH3, N=C=O, , etc.
R" = OMe, OEt, Cl, etc.
OCH3

Figure 1.4. Two different strategies for formation of SAMs on silicone surfaces, by a bottom-up method: (A) alkene on oxide-free Si(111), and (B) silane on Si/SiO$_X$ surface, with an option for further functionalization.

Both synthetic strategies for the formation of SAMs on silicon surfaces have their advantages when it comes to applications of these structures. Various biologically active molecules were immobilized on silicon materials towards production of biological microarrays, i.e. protein and DNA microarrays.[43–46] For the purpose of biosensors, different capture agents can be attached to the silicon surface (i.e. aptamers, proteins, biotin, single strand nucleic acid, etc.).[47–53] Additionally, various chemical approaches have been employed for the immobilization of peptides and nucleotides on oxidized Si(100), involving reaction with surface amine, epoxide, aldehyde or acetylene groups.[54–57] Similarly, the biomolecules have been immobilized on oxide-free Si(111) surface, by reaction with surface epoxide, semicarbazide, or carboxylic acid functionalities.[51,58–61] Moreover, sensors are developed employing the supramolecular concept of host-guest interactions. Structures with cavitands grafted on silicon surfaces were developed, being able to detect aromatic compounds, as a benzene-detection molecular device,[62] or with a selectivity for Na$^+$ ions over other alkali metal ions.[63] Ayadim *et al.* reported of antracene modified monolayers, that behaved as pH probe depending on the protonation state of the amine.[64]

Immobilization of photochromic compounds allows development of the photoresponsive “smart” new materials, towards their applications, among others, in optical memories and logic gates. Different photoswitchable compounds immobilized on silicon surfaces have been previously reported. In the group of Rück-Braun, azobenzene and fulgimide modified Si(111) were developed, by the reaction with the surface carboxylic acid functionalities.[13,14,65] Furthermore, azobenzene SAMs on oxide-free Si(111) were also reported by others.[66] Diarylethenes immobilized on H-terminated Si(111) via grafting of the acetylene linker showed light-controlled reversible current changes upon switching.[67] On oxidized silicon surface, immobilization and reversible switching of coumarin[68], azobenzene[69,70], and spiropyran[70,71] compounds were reported. Recently, reversible dimerization of anthracene derivatives immobilized on oxidized silicon surface upon alternation of UV and visible light was published, too.[72]

In order to obtain a satisfactory level of surface analysis, it is necessary to use more than one characterization method to study the monolayer quality, each providing specific information about the surface structure. Additionally, they are useful for the on-chip photochemical investigations. The following methods were utilized in this work:

- Fourier transform infrared spectroscopy (FTIR) is used for determination of the functional groups being present on the surface, thus allowing the evaluation of the on-chip reaction steps. Furthermore, it provides information on packing density and ordering of the monolayers, and allows distinguishing between different photoisomers, thus enabling evaluation of the switching process of the photoswitchable monolayers.
- X-ray photoelectron spectroscopy (XPS) provides information on elemental composition of the monolayer. The obtained data can be further used for the evaluation of the efficiency of the on-chip reaction steps, and for calculations providing the information on surface coverage.
- Contact angle goniometry, is used to investigate polarity and roughness of a SAM. These informations further can be used for evaluation of the on-chip reaction steps, ordering of a SAM, and evaluation of the on-surface switching process.
- Ellipsometry provides information on the thickness of the monolayer structure on the surface surface.

2 Aim

The aim of the work is to prepare photoswitchable self-assembled monolayers on various silicon surfaces.

The first part of this work is focused on synthesis of two different photoswitchable conjugates – indolylfulgimide **7** (P-type) and 2*H*-naphthopyran **8** (T-type) (Figure 2.1). For their further immobilization onto surfaces and later on-surface studies, an adequate linker should be incorporated into their structure, consisting of available free amine functionality, which allows a variety of attachment chemistries for the immobilization onto the surface. For this reason, different linkers – being flexible (i.e. ethylenediamine based), or more rigid (i.e. piperazine based) – are possible options to be incorporated into their structures.

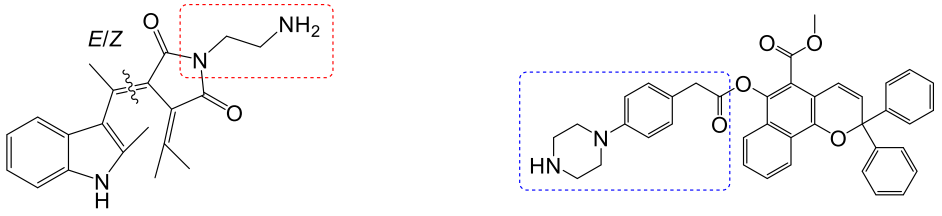

Fulgimide-linker conjugate **7**

Naphthopyran-linker conjugate **8**

Figure 2.1. The aim photoswitchable conjugates for the immobilization on silicon surfaces.

The second part of this work is focused on the immobilization of the prepared photoswitchable-linker conjugates on various silicon surfaces, using different attachment chemistries. The procedures for the formation of the high-quality self-assembled monolayers on both H-terminated silicon (111) and oxidized silicon(100) surfaces should be applied. Different functionalities on the terminal end of the monolayer molecules should allow for different attachment chemistries. Additionally, they would offer different immediate environment for the photoswitchable compounds once attached (Figure 2.2). In order to evaluate the quality of the obtained surface structures, characterization using various methods is required (ATR-FTIR measurements, XPS measurements, ellipsometry and contact angle measurements).

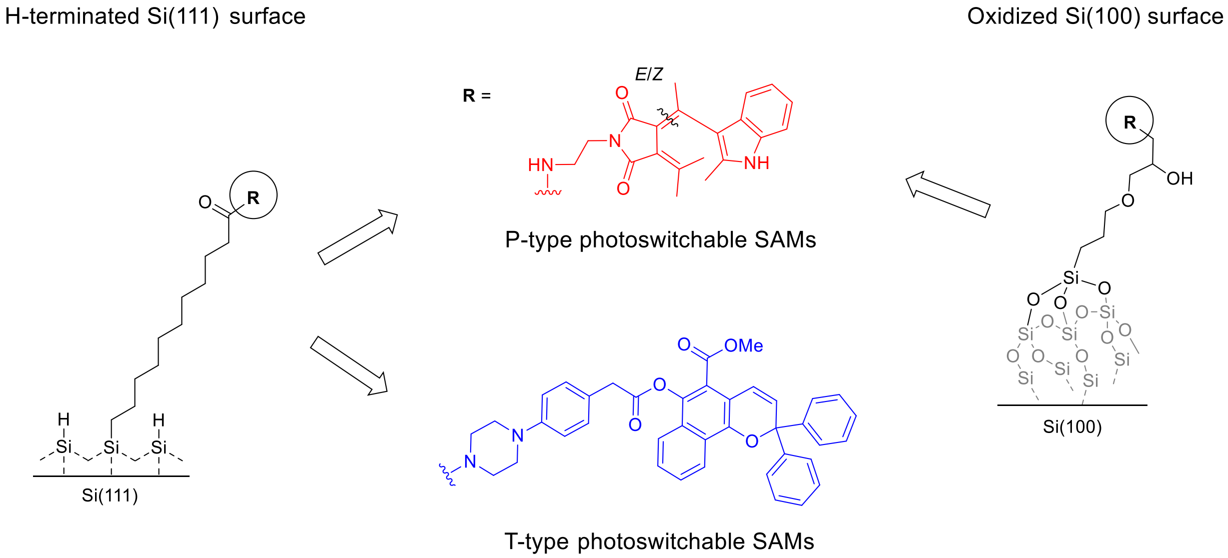
H-terminated Si(111) surface
Oxidized Si(100) surface
R =
E/Z
HN
N
O
NH
P-type photoswitchable SAMs
T-type photoswitchable SAMs
OMe
N
Si(111)
Si(100)
OH
R

Figure 2.2. The aim structures of photoswitchable self-assembled monolayers on silicon(111) and (100) in this work.

Finally, in order to understand the photochemical processes on the surface, the photochemical properties of the prepared compounds need to be first investigated in solution (i.e. UV/Vis studies, NMR and FTIR measurements). Upon successful immobilization on the silicon SAMs, the characterization of the photoswitching processes of all prepared, P-type and T-type, photoswitchable surfaces is to be done using FTIR and contact angle measurements.

3 Synthesis of Photoswitch-Linker Conjugates

3.1 Fulgimide-Linker Conjugate

In order to have photochromic properties, a fulgide (and related fulgimide) structure requires at least one of the four substituents on the *exo*-methylene carbon atom to be an aromatic ring (e.g. furyl, thienyl, indolyl, pyrryl) (Figure 3.1).[73] This substitution allows the formation of a hexa-1,3,5-triene structure that may undergo 6π-electron pericyclic ring closure and ring opening reactions.[2,73]

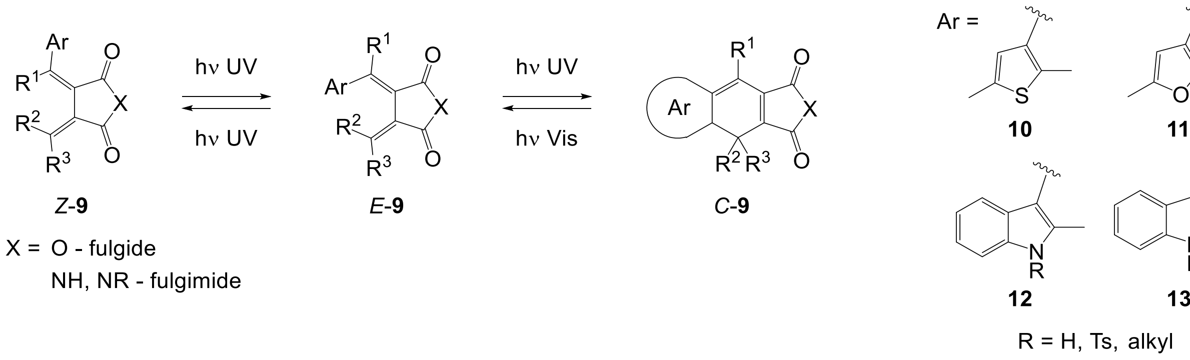

Figure 3.1. Variation of structures of fulgide and fulgimide compounds, including the open stereoisomers and the closed photoisomer.

Upon the UV light irradiation, a fulgide undergoes 6π-electrocyclization of its open *E*-form towards the almost planar cyclic closed *C*-form.[2] In order for the photocyclization reaction to occur, the three conjugated double bonds of the hexa-1,3,5-triene unit require the *cis-cis-cis* orientation, so that carbon atoms that form the new bond would come sufficiently close for the ring-closure reaction (Figure 3.2). Only the *E*-form, opposed to the other open isomer *Z*, can assume the appropriate orientation of the double bonds towards electrocyclization reaction.[2] Additionally, under the UV light irradiation, there is also the *E*-to-Z and *Z*-to-*E* isomerization pathway, that occurs between the two open form isomers. Due to all photoisomers being thermally stable, reverse ring-opening reaction, from the closed form towards the *E* isomer, occurs under the visible light irradiation. Additionally, the choice of the aromatic ring, as well as the other substituents, can significantly influence the photochromic properties, through variation of the steric and electronic effects.[2]

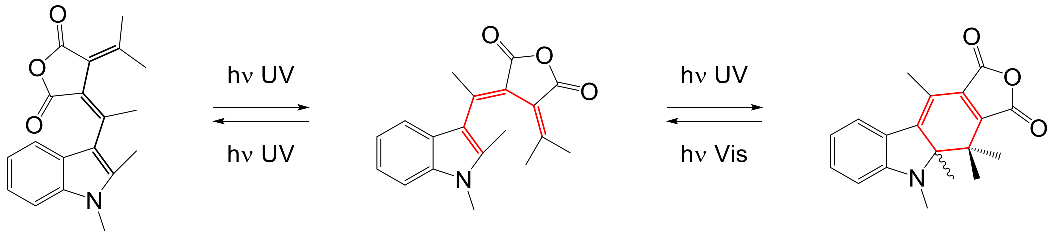

14 *Z*-form **14** *E*-form **14** *C*-form

Figure 3.2. Photoisomerisation reaction of the fulgide, upon UV and Vis light irradiation.

In the work of Kaneko *et al.*, various fulgides were prepared, varying the choice of the heteroaromatic ring at the substituent.[74] They reported that the closed forms of various pyrrylfulgides absorb at longer wavelengths (λ_{max} > 600 nm), compared to the other fulgides in the study. However, it is reported that indolylfulgides and thiazolylfulgides show high fatigue resistance and low medium dependence, compared to furyl, thienyl and pyrryl analogs, which they attributed to the high chemical stabilities of the heterocyclic groups. Additionally, the indolylfulgide also showed excellent thermal stability.[74]

Uchida *et al.*[75] studied how steric effects of the substituents can influence the photochromic properties of indolylfulgides. As shown in Table 3.1, when substituent R^1 is hydrogen atom, the fulgide is neither photochromic nor thermochromic.[73] Instead, when R^1 is an alkyl group, the photochromic properties depend on its steric effects. Generally, the bulkiness of the R^1 substituent increases the quantum yield of the UV irradiation. Furthermore, the increase of bulkiness of both the R^1 group and the substitution on the isopropylidene group, increases the bleaching quantum yield of the visible irradiation. It is reported that the bleaching quantum yield increases significantly when adamantylidene, instead of the isopropylidene, group is present.[75] Additionally, increasing the size of the substituent R^2, results in significant decrease in both $\Phi_{E\rightarrow C}$(UV) and $\Phi_{C\rightarrow E}$(Vis), as well as a bathochromic shift of the λ_{max} of the closed form. In general, the λ_{max} of the open forms are not particularly influenced by the steric effects of the substituents, while the deviation of the λ_{max} of the closed form is significant.

Table 3.1. Influence of steric effects of present substituents on the quantum yields and spectroscopic properties of the photoisomers of various fulgide molecules, recorded in toluene. The values are taken as presented in the ref. 75.

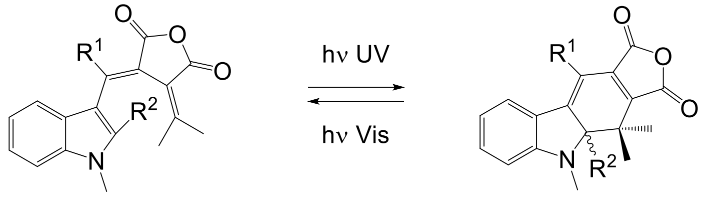

E-**15** *C*-**15**

R^1	R^2	$\Phi_{E \rightarrow C}$(UV)	$\Phi_{C \rightarrow E}$(Vis)[a]	$\Phi_{C \rightarrow E}$(Vis)[b]	λ_{max} **E [Z]** (nm)	λ_{max} **C** (nm)
H	Me	-	-	-	-	-
Me	Me	0.045	0.16	0.051	385 [397]	584
n-Pr	Me	0.14	0.12	0.049	385	587
i-Pr	Me	0.23	0.31	0.054	385	574
Me	Et	0.023	0.087	0.066	384 [395]	616

[a] Irradiation with 403 nm light. [b] Irradiation with 608 nm light.

Yokoyama *et al.* studied the electronic effects of substituents on indolylfulgides.[76] The electron-donating substituent introduced in the 5-position of the indole ring exhibit a bathochromic shift in the absorption maximum of the closed form. Additionally, both the $\Phi_{E \rightarrow C}$(UV) and the $\Phi_{C \rightarrow E}$(Vis) decreased as the electron-donating ability of the substituent increased.

Fulgimides are the most important class of fulgide analogs. Their spectroscopic properties, photochemical reversibility and thermal stability showed to be closely related to the respective fulgide analogs.[77] For this reason, their structure is found convenient for the attachment of another substituent onto fulgimide core (e.g. a fluorophore)[78], or introduction of fulgimide molecule into various environments, without significant change of their photochromic properties[13,14]. Additionally, opposite to fulgides, the respective fulgimides showed high resistance to solvolytic degradation in hydroxylic media.[77]

3.1.1 Plan of the Synthesis

For the efficient attachment of the photoswitch to the surface, its structure requires an appropriate linker. Fulgimide molecules were previously attached to the linker system via Sonogashira-coupling reaction of the 6-bromo substituted indolylfulgimide.[79] Additionally, attachment to the surfaces via linker developed from N-substitution of the fulgimide imide structure has been reported.[13,14] For the attachment to the variously functionalized silicon surfaces (i.e. carboxy- and epoxy-terminated surfaces), the fulgimide-linker conjugate **7** with a primary amine functionality was developed, according to the retrosynthetic route shown in Figure 3.3. The introduction of the linker is carried out during the fulgimide synthesis step, from the respective fulgide **16**.

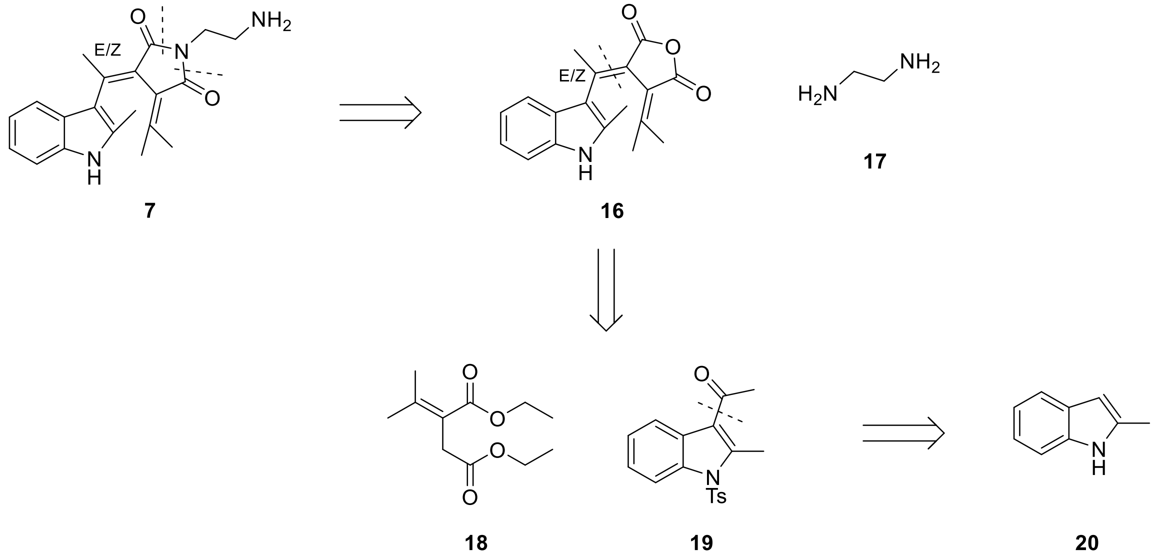

Figure 3.3. Retrosynthetic plan for the synthesis of fulgimide-linker conjugate **7**.

The synthesis of fulgide and fulgimide compounds were previously well established in the group of Rück-Braun.[80–82] The N-methyl substitution on the indole ring showed to give lower ratio of the closed form in the photostationary state upon UV light irradiation, compared to unsusbstituted analogs, for both fulgide **16** and fulgimide **7**.[80] The preparation of the fulgide moiety proceeds via Stobbe reaction, from two main synthetic units – diethyl 2-(propan-2-ylidene)succinate (**18)** and indol fragment **19**.

3.1.2 Synthesis of the Fulgimide-Linker Conjugate

3.1.2.1 Synthesis of the Fulgide Core

Indolylfulgide **16** was obtained in 5 reaction steps, starting from the commercially available 2-methyl-1*H*-indole (**20**).

The synthesis of the fulgide **16** starts with an acylation of the 2-methylindole **20** via a Vilsmeier-Haack reaction with a *N*,*N*-dimethylacetamide (DMA), in presence of phosphoryl chloride (Figure 3.4).[80] The introduction of the acyl group in the 3-position of the indole ring is crucial for the following Stobbe reaction. Upon recrystallization from ethanol, the product 1-(2-methyl-indol-3-yl)ethan-1-one (**21**) was obtained in 81 % yield.

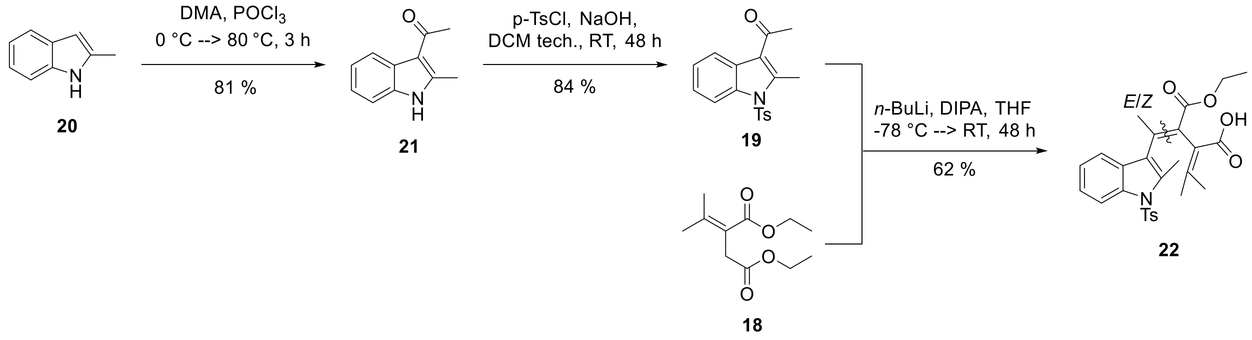

Figure 3.4. Scheme of the reaction route towards obtaining Stobbe product **22**.

Before the Stobbe condensation reaction, which proceeds under strong basic conditions, the protection of the indole amine was necessary. When not protected, the alkaline conditions in this step causes deprotonation of the indole amine, which thus increases electron density at the carbonyl carbon of the acyl group. This further leads to poor reactivity and lower yield of the desired Stobbe product.[81] However, it is already known that the use of *p*-toluenesulfonyl as a protection group, apart from being stable towards alkaline conditions, is beneficial in the Stobbe reaction as well, since its electron withdrawing ability increases the reactivity at the carbonyl carbon in the acyl group.[81] In the research group of Rück-Braun, the procedure using *p*-toluenesulfonyl chloride in technical DCM, in presence of sodium hydroxide as a base, was previously developed. The greater amount of water traces in the tech. DCM, allows for higher concentration of the base dissolved in the reaction mixture, and thus increases the yield of the reaction, compared to procedure carried out in dry solvent.[81] Upon prolonged reaction time at room temperature, and subsequent recrystallization in cyclohexane, the protected product **19** was obtained in 84 % yield.

The Stobbe condensation was first described by Stobbe in 1893,[83] as an aldol-type condensation reaction between the α-methylene group of the succinate ester and a carbonyl group of ketone or aldehyde, yielding a half-ester product.[84] The mechanism of the reaction is shown in Figure 3.5. The reaction starts with a deprotonation at the α-methylene position of the succinate ester, forming an enolate **23**. A nucleophilic attack of the enolate at the carboyl carbon of the ketone **24** leads to the formation of an alkoxide **25**. The formed alkoxide undergoes intramolecular nucleophilic attack at the carbonyl carbon of the ester, and by elimination of ethyl alkoxide, forms a 5-membered ring lactone **27**. Alternative pathway, a nucleophilic attack at the carbonyl carbon of the other ester group, would lead to formation of an unfavorable 4-membered ring. Deprotonation at the α-hydrogen of the ester, leads to elimination, opening of the lactone and formation of the double bond. The newly formed double bond gives two regioisomers, *E* and *Z*. Opening of the lactone leads to formation of a salt of the half-ester, which upon acidic work-up yields a half-ester Stobbe product **30**.

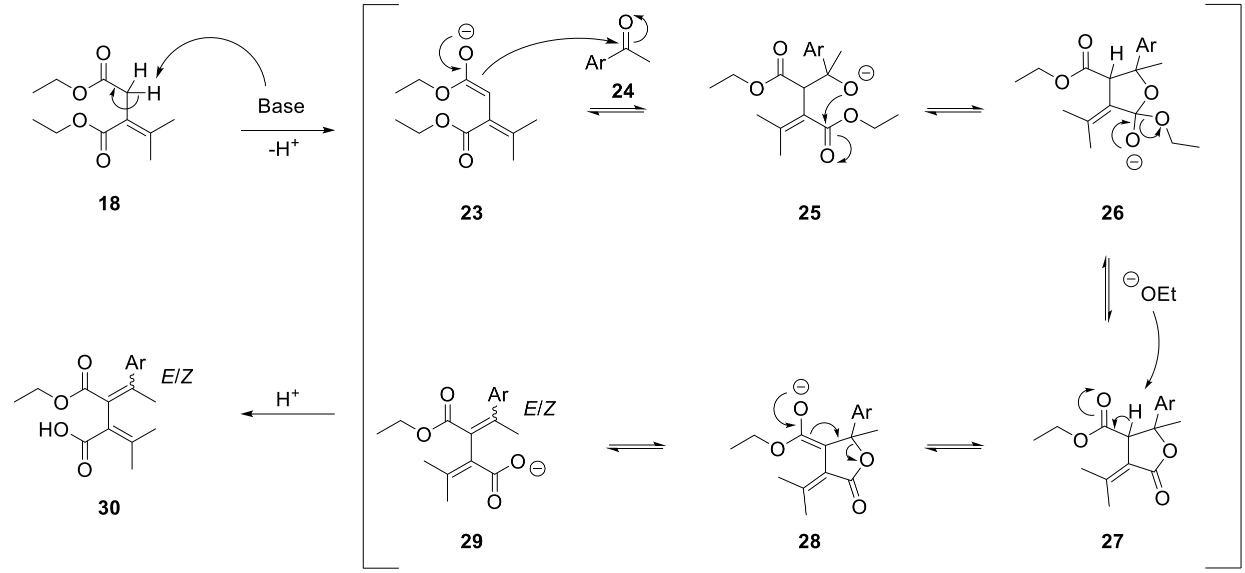

Figure 3.5. Mechanism of Stobbe condensation reaction according to the ref. 84.

The reaction conditions for the Stobbe condensations of the indole derivate **19** and diethyl 2-(propan-2-ylidene)succinate (**18**) were previously optimized in the group of Rück-Braun,[80] and are presented in Figure 3.4. The reaction was carried out under dry inert conditions, using LDA as a base, prepared *in situ* from diisopropylamine and *n*-butyllithium. After prolonged reaction time at room temperature, the reaction mixture was acidified to yield a half-ester **22**. Purification of the product on column chromatography was previously established,[81] using a mixture of cyclohexane / ethyl acetate 2:1 with 0.1 % NEt_3 as an eluent, to deprotonate the carboxylic acid of the product on the column, and thus allow it to bind to the silica, while eluting other components. Finally, the product was eluted from the column using cyclohexane / ethyl acetate with 0.2 % acetic acid as the eluent system, reprotonating the product. The ratio of the two open isomers obtained upon Stobbe reaction, *E* and *Z*, can be determined from the integrals of appropriate ^{1}H NMR signals. The signals assigned to protons of the tosyl-group, doublets at 7.60 and 7.68 ppm for the *E* and *Z* isomer, respectively, are separated enough to allow the use of their integrals to determine the ratio of 74:26 (*E*:*Z*).

Towards obtaining fulgide **16**, the half-ester required saponification to yield a diacid compound **25** (Figure 3.6). Under the reaction conditions, 20% aq. potassium hydroxide / ethanol (V/V 1:1), hydrolysis of the ester group occurs rapidly. However, for complete deprotection of the N-tosyl protection group, a longer reaction time is necessary.[81] As previously reported, for obtaining a high yield of the following coupling reaction, complete conversion to the N-deprotected diacid product **31** was crucial.[81] Additionally, it was not necessary to purify the obtained diacid **31** before the fulgide coupling reaction; however, it was shown that for the efficiency of the coupling reaction, the raw product needed to be meticulously dried.[81] For this reason, the yield of the saponification reaction was not determined.

The coupling of the two carboxylic acid groups towards an anhydride was carried out in the presence of *N*,*N*-dicyclohexylcarbodiimide (DCC) in freshly distilled DCM, under dark conditions at room temperature (Figure 3.6).

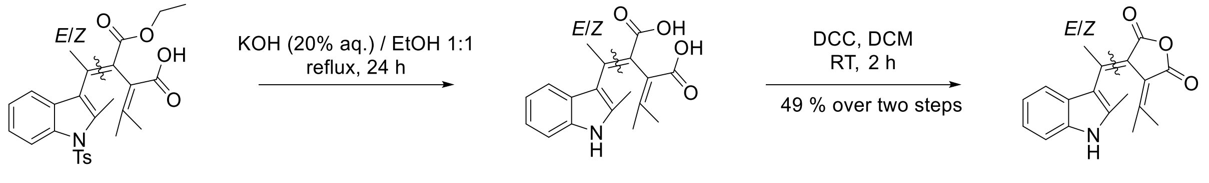

22 **31** **16**

Figure 3.6. Reaction scheme and conditions towards preparation of the fulgide **16**.

DCC is known to mediate an anhydride formation under mild conditions, and short reaction times.[85] For the formation of the fulgide **16**, in the group of Rück-Braun, several coupling reagents were previously tested; DCC showed to be the most successful both for the isolated yields and the reaction times.[80,86] The fulgide **16** was obtained as a mixture of regioisomers, *E* and *Z* in a ratio of 85:15, according to ^{1}H NMR.

3.1.2.2 Synthesis of the Fulgimide-Linker Conjugate for Immobilization on Silicon Surfaces

Transformation of the fulgide **16** towards a fulgimide **7** for the purpose of attaching the latter to the silicon surfaces, was done with an amine linker, commercially available ethylenediamine (**17**). Before fulgimide preparation, the linker was necessary to be protected on one side, to avoid formation of di-fulgimide product. For this purpose, a simple Boc-protection was introduced, in a reaction with the amine compound in excess, and slow addition of di-*tert*-butyl dicarbonate, in order to avoid formation of the di-protection product (Figure 3.7). The reaction proceeded at room temperature in DCM, over prolonged reaction time, and yielded the desired linker in 80 % yield.

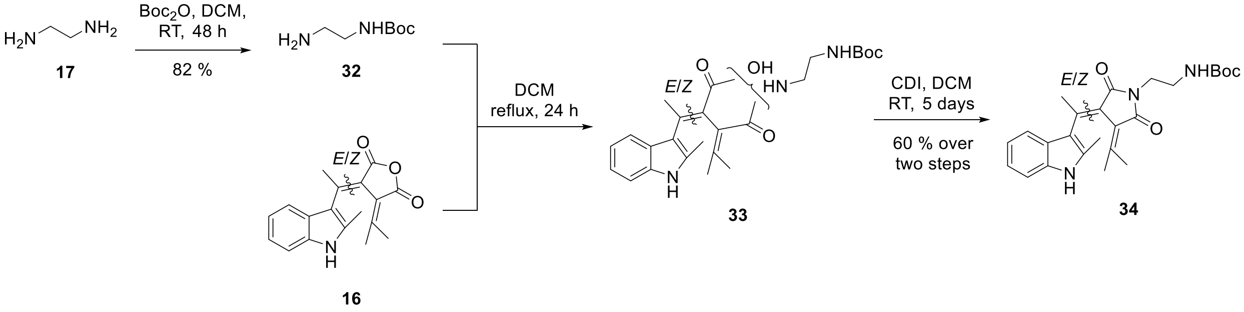

Figure 3.7. Synthetic route and conditions towards preparation of the protected fulgimide-linker conjugate **34**.

Fulgimide preparation was then proceeded in the one-pot synthesis procedure, previously developed and optimized in the group of Rück-Braun.[81] The fulgide **16** was first refluxed in DCM in the presence of the prepared linker, to establish the mixture of regioisomers of the acid/amide compound **33**, both as the *E*- and *Z*-isomers of the double bond (Figure 3.7). Without isolation of the products, the next step proceeded in the presence of the coupling reagent, *N*,*N'*-carbonyldiimidazole (CDI), in DCM at room temperature, over prolonged reaction time (5 days). Several different coupling reagents and procedures were previously tested, towards obtaining fulgimide product **34**; the reported route with CDI as a coupling reagent showed to be superior compared to the other tested coupling reagents (HCTU, EDC, DCC, DIC, and a method employing phenacyl bromide)[a], the one-pot method being more efficient than 2 steps synthetic routes.[81] Crude isolated product was purified on column chromatography, and compound **34** obtained as a mixture of isomers (*E*:*Z*, 85:15, according to the ^{1}H NMR), in 60 % yield over two steps.

Finally, the last synthetic step prior to immobilization of fulgimide conjugate onto the silicon surface is deprotection of the Boc-protected amine, under acidic conditions (Figure 3.8). Previously, it was shown that efficiency of the deprotection, as well as side product formation, is dependent on both the solvent and the acid used in the deprotection reaction.[81]

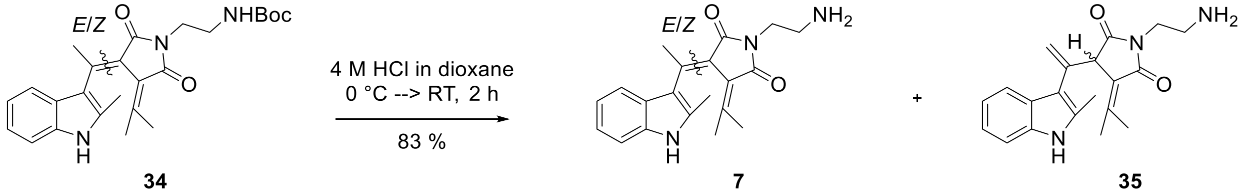

Figure 3.8. Deprotection of the Boc-protected fulgimide **34**, and the structure of the side product **35**.

The commercially available 4 M HCl in dioxane, when added slowly in cooled reaction mixture (0 °C), resulted in high yield of the deprotected product. Upon washing in alkaline solution (0.1 M NaOH aq.), and purification by column chromatography, the free amine fulgimide-linker conjugate was obtained in 83 % yield (*E*:*Z* 85:15, according to ^{1}H NMR). By this procedure, the side product **35** was formed in traces (isolated in < 6%), and was detected by ^{1}H NMR by the geminal alkene protons at 5.26 and 5.48 ppm.[81]

3.1.3 Characterization of Photochemical Properties of Fulgimides 7, 34 and Related Compounds

Photochemical isomerization of fulgides and fulgimides proceeds under UV light irradiation, via 6π-electrocyclization reation of their *E*-open isomer, as previously described. Furthermore, under UV light irradiation, the additional *E*-to-*Z* and *Z*-to-*E*-isomerization occur (Figure 3.9). Once the photostationary state (PSS) is reached, all three forms are in equilibrium. Upon removing the UV light source, the ratio of isomers remains and does not change, since all isomers are being thermodynamically stable. Finally, upon visible light irradiation, the closed form undergoes the ring-opening reaction, yielding the open isomer *E*.

---

[a] EDC - 1-ethyl-3-(3-dimethylaminopropyl)carbodiimide, DIC - *N*,*N'*-Diisopropylcarbodiimide.

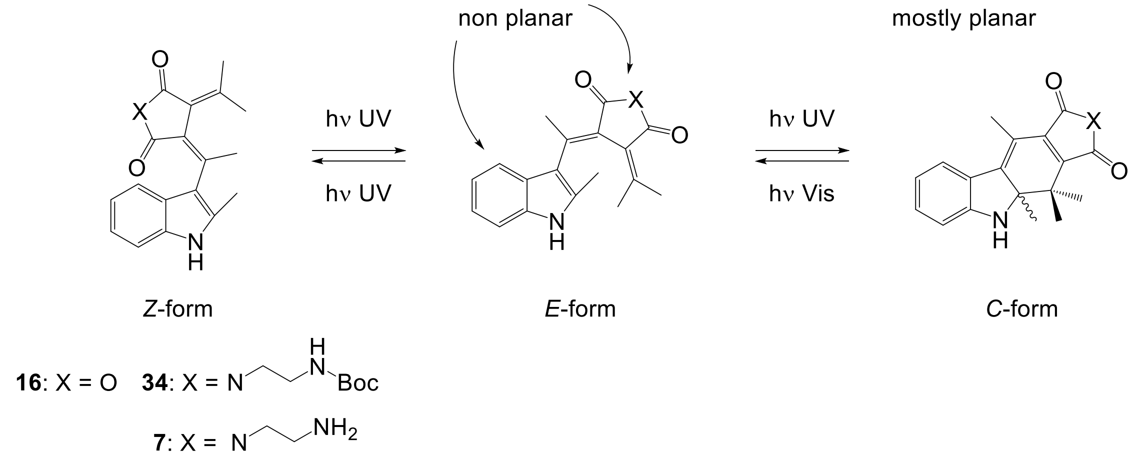

Figure 3.9. Photostationary states (PSS) of fulgide **16** and fulgimides **7** and **34** structures described in this study.

The light absorption of the fulgide family compounds is attributed to a π-π* transition. For the non-planar open forms, the conjugation of the π-electrons is limited, and thus the open isomers absorb at shorter wavelengths, typically in the UV region. On the other side, the closed form is mostly planar, and absorbs in the visible spectral range; thus, different photoisomers can be identified via UV/Vis measurements. The UV/Vis studies were carried out for both, fulgide **16** and fulgimide **34**, under the same conditions. Furthermore, switching reliability was investigated by performing several cycles and comparing the absorbance at λ_{max} at photostationary states in acetonitrile solutions.

The photochemical studies of fulgimide **34**, evaluated via FTIR spectroscopy in solution, were previously carried out in the group of Rück-Braun.[81] The data recorded in benzene solution show that both ν_{as}(C=O) and ν_{sym}(C=O) absorption bands exhibit changes in the peak position in different photostationary states. At PSS(365 nm), the bands are found at 1693 and 1754 cm^{-1}, for ν_{as}(C=O) and ν_{sym}(C=O); at PSS(545 nm) signals shift to 1686 and 1737 cm^{-1}, respectively.[81] The change of the peak position at different photostationay states is a crucial information for an investigation of the switching process of fulgimide-terminated surfaces.[14]

Additionally, the ratio of the different photoisomers upon reaching the PSSs were studied. It was shown that in benzene solution, at PSS(365 nm), the ratio of the photoisomers *E*:*Z*:*C* is 15:6:79 (HPLC), while at PSS(545 nm) the ratio is 94:6:0, respectively.[14]

3.1.3.1 UV/Vis Studies of Fulgimide 34 and Related Compounds

The samples for the UV/Vis photochemical studies were prepared in both chloroform and acetonitrile. All measurements were carried out under constant stirring of the solution, at a temperature of 20 °C.

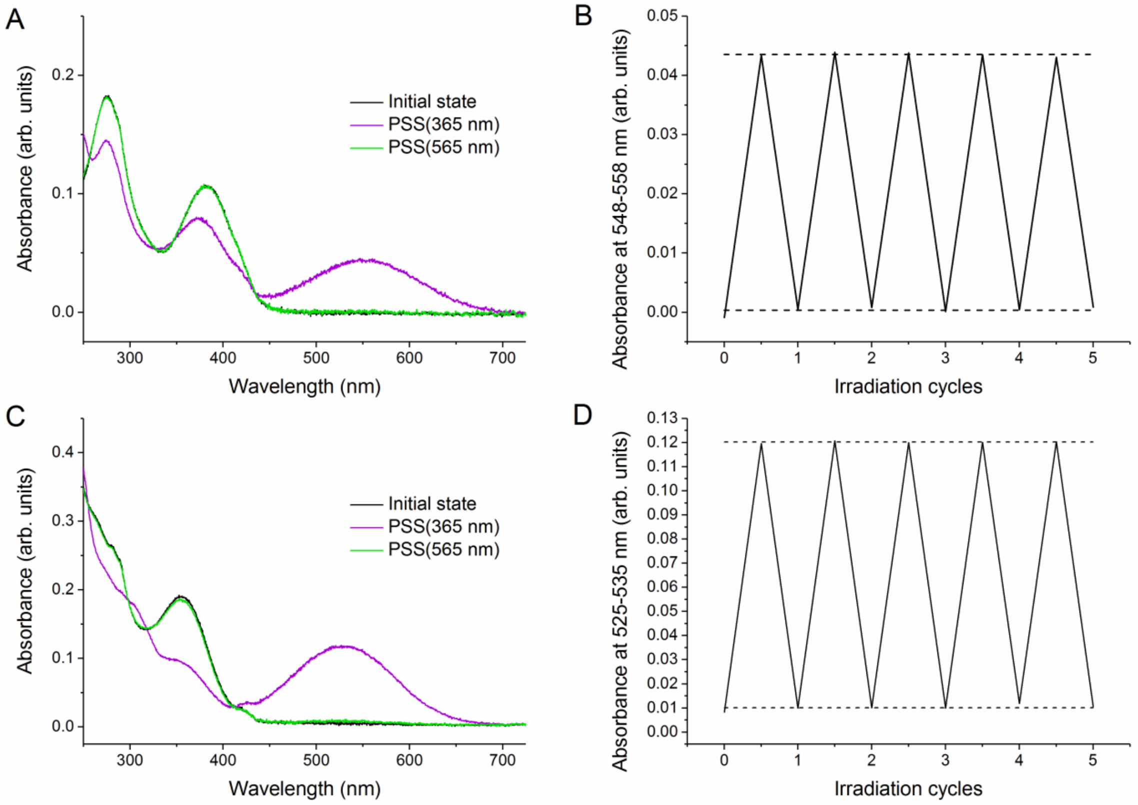

Figure 3.10. Absorption spectra of the PSSs of the fulgide **16** (A, B) and fulgimide **34** (C, D), at 20 °C in MeCN upon UV light irradiation - PSS(365 nm) (violet); visible light irradiation - PSS(565 nm) (green); and the initial state (black).

At the initial state, fulgide **16** is a mixture of the open *E* and *Z*-forms, 85:15 respectively. Upon the UV light irradiation (λ_{irr} = 365 nm), an increase in the absorbance at 553 nm and simultaneous decrease in the absorbance at 275 and 382 nm suggests the ring-closure reaction upon which the amount of closed isomer in the solution increases, while the open isomers decrease (values are given for acetonitrile solution, for the data in chloroform, see Table 3.2). The photoisomerisation between the *E*- and *Z*-isomers cannot be evaluated via UV/Vis studies, due to the similar properties of the open forms. Irradiation with visible light (λ_{irr} = 565 nm) furnishes a decrease in the absorbance at 553 nm, and an increase in the absorbance in the UV region.

Table 3.2. Photochemical properties of fulgimide **16** and fulgimide **34**, investigated in acetonitrile and chloroform at 20 °C.

Compound	**Solvent**	**λ_{max} open forms** (nm)	**λ_{max} closed form** (nm)	**λ_{isosb}** (nm)
16	MeCN	275, 382	274, 373, 553	257, 326, 345, 433
	$CHCl_3$	274, 381	274, 374, 547	256, 329, 337, 435
34	MeCN	280, 354	303, 344, 529	255, 297, 317, 408
	$CHCl_3$	282, 359	307, 353, 536	297, 321, 410

Fulgimide **34**, at the initial state consists of 85:15 ratio of *E*/*Z* photosiomers. Similarly, upon UV light irradiation, an increase at 529 nm, and a decrease of the absorbance in the UV region (280 and 354 nm), is observed, due to the ring-closure reaction (Figure 3.10B). At the same time, due to the *E*-to-*Z* and *Z*-to-*E*-isomerisation, the *E* and *Z* content is changed. Visible light irradiation, reverts the reaction towards the *E*-form. The λ_{max} of the closed form of fulgimide **34** is blue-shifted compared to fulgide **16**, in both investigated solvents, as already reported for the related fulgide and fulgimide structures.[73] The data obtained from the measurements in both acetonitrile and chloroform are presented in Table 3.2.

Alteration between UV and visible light irradiation allows for evaluation of the reliability of the switching process. The changes of the closed-form λ_{max} was evaluated over five irradiation cycles, for both fulgide **16** and fulgimide **34** (Figure 3.10, B and D, respectively). These measurements show a repeatable change in absorbance of the closed form between the PSS(365 nm) and PSS(565 nm); the dotted lines are the average absorption over five irradiation cycles.

3.2 Naphthopyran-Linker Conjugate

Chromenes, i.e. benzo- and naphthopyrans, are photochromic systems that undergo reversible ring opening of the heterocycle due to C-O bond cleavage upon UV light irradiation (Figure 3.11).[3] The open forms that are generated absorb at longer wavelength, exhibit different absorption spectra, have different geometries and other physical and chemical properties compared to the closed isomer. The equilibrium composition and ratios of different photoisomers is influenced by the electronic and steric factors of the chromene core and its substituents, as well as experimental conditions, i.e. the choice of solvent and temperature.[3]

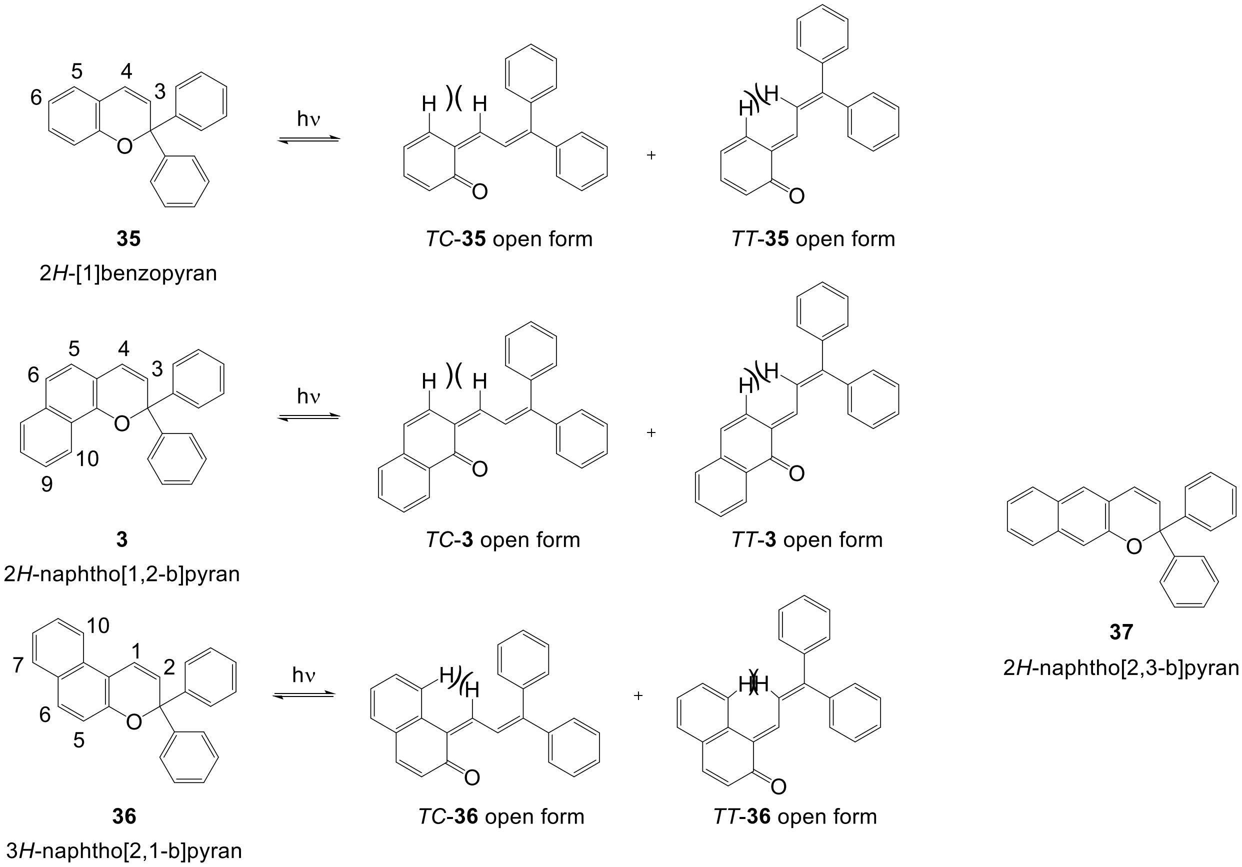

35
2*H*-[1]benzopyran

TC-**35** open form

TT-**35** open form

3
2*H*-naphtho[1,2-b]pyran

TC-**3** open form

TT-**3** open form

37
2*H*-naphtho[2,3-b]pyran

36
3*H*-naphtho[2,1-b]pyran

TC-**36** open form

TT-**36** open form

Figure 3.11. Structures of three different stereoisomers of naphthopyran compounds, including the steric interaction of the hydrogen-atoms in the open forms. The scheme is adjusted from the scheme reported in ref. 3.

The two main types of naphthopyran compounds are 3*H*-naphtho[2,1-b]pyran (**36**) and 2*H*-naphtho[1,2-b]pyran (**3**). Other possible structural isomers (e.g. the linear 2*H*-naphtho[2,3-b]pyran (**37**)) show no significant photochromic response at ambient temperature (Figure 3.11).

The structural differences between the core structures of these naphthopyran compounds play a role in the photochromic properties, i.e. absorption maximum of the open forms and the bleaching rate (Table 3.3). In the PSS, 2*H*-naphtho[1,2-b]pyrans show higher equilibrium concentration of the open forms, compared to 3*H*-naphtho[2,1-b]pyrans.[3] Additionally, their λ_{max} is bathochromically shifted, and open isomers have slower fading rates. The difference in fading rate can be attributed to the different steric interactions of the protons in the open forms – more significant steric interaction between the H-1 and H-10 in the 3*H*-naphtho[2,1-b]pyran than the interaction between H-4 and H-5 in the 2*H*-naphtho[1,2-b]pyrans (Figure 3.11).

Table 3.3. Comparison of the photochromic properties of 2,2-diphenyl-2*H*-naphtho[1,2-b]pyran and 3,3-diphenyl-3*H*-naphtho[2,1-b]pyran, recorded in diethylene-glycol bis(allyl carbonate). The values as taken as presented in ref. 23.

Compound	**λ_{max} visible** (nm)	**λ_{max} UV** (nm)	**$\tau_{1/2}$** (s)
2*H*-naphtho[1,2-b]pyran	476	355	> 1800
3*H*-naphtho[2,1-b]pyran	432	359	45

In order to tune the photochromic properties of 2*H*-naphtho[1,2-b]pyrans, substituents are introduced in the 5- and 6- position, in an attempt to mimic the steric interaction observed for the 3*H*-naphtho[2,1-b]pyran structures. As it can be seen in Table 3.4, the introduction of a small substituent such as a methyl group at position 5, already significantly reduces the fading rate of the open forms sterically; the fading rate is additionally reduced upon introduction of an ester group. Furthermore, when the substituent at position 6- is an electron donor group (e.g. MeO), it leads to a slower fading rate, due to its electronic influence on the stability of the open form. The resonance structures obtained in this case are presented in Figure 3.12. The MeO is in conjugation with the ester functionality in the position 5. The *orto*-quinoidal structure of the ring-open form additionally stabilizes the open forms. The ring adjacent to the pyran unit has lost some of its π-electron character in the open form, and thus the open form is in favor due to the fact that ring-opened isomers are preferred when the aromaticity of the ring is diminished.[87]

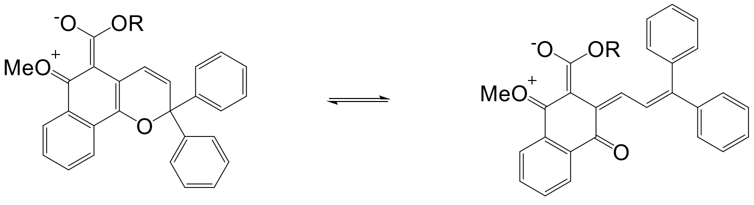

Figure 3.12. The resonance structures of naphthopyran with ester and electron donor substituents, in positions 5 and 6 of 2*H*-naphtho[1,2-b]pyran **38**, respectively. The scheme is adjusted from the scheme reported in ref. 87.

Table 3.4. Influence of substituents in the 5- and 6- position on photochromic properties of 2*H*-naphtho[1,2-b]pyrans.

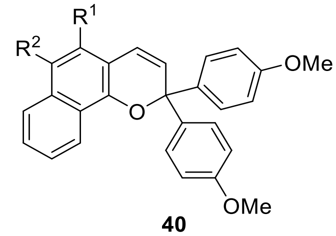

40

R^1	**R**^{2}	λ_{max} **open forms** (nm)[a]	$\tau_{1/2}$ (s)
H	H	412, 508	> 1800
Me	H	416, 496	178
Me	Me	421, 494	66
Ph	Ph	418, 508	20
COOMe	H	492	2
COOEt	H	493[b]	3[b]
COOMe	Me	416, 492, 476[d]	4, 217[d]
COOMe	Ph	416, 506	7
COOMe	OMe	501[c]	74[c]
COOMe	$OCOC_2H_5$	499[c]	19[c]
COOMe	OH	497[d]	235[d]
COOMe	$OCH_2COOC_2H_5$	508[d]	211[d]
COOMe	$OCOCH_3$	490[e]	-

[a] Data values are taken from ref. 88, recorded in toluene, at 21 °C. [b] Data taken from the ref. 87, recorded in toluene. [c] Data taken from ref. 89, recorded in toluene, at 20 °C. [d] Data taken from ref. 90, recorded in diethylene-glycol bis(allyl carbonate). [e] Data taken from ref. 91, recorded in ethanol.

The choice of the substituent at the aromatic rings in the position 3 of the 3,3-diphenyl-3*H*-naphtho[2,1-b]pyrans can further fine-tune the required photochromic properties of the photoswitch (Table 3.5). The electron donating group in the *para*-positions leads to a bathochromic shift of the λ_{max}, and an increase in the fading rate. The authors report that the mono 3-(4-methoxyphenyl) derivative fades faster than the unsubstituted analogue; an additional methoxy-substituent (dimethoxyphenyl) further enhances the fading rate.[92] However, no values for the half-lives were reported. On contrary, the electron-withdrawing groups cause a blue shift, and the fading rate of the open forms is slower; this influence depends on the withdrawing strength of the substituents. The trifluoromethylphenyl derivative fades at a slower rate than the corresponding fluorophenyl compound.[92]

Table 3.5. Influence of the substituents at the aromatic rings on photochromic properties of 3,3-diphenyl-3*H*-naphtho[2,1-b]pyrans.

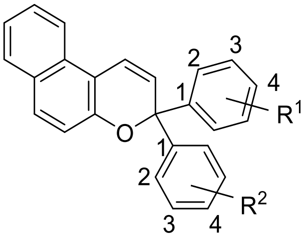

41

R^1	**R^2**	λ_{max} (nm)^a
H	H	430
H	4-MeO	458
4-MeO	4-MeO	475
4-MeO	4-NMe$_2$	512
H	4-NMe$_2$	528
4-NMe$_2$	4-NMe$_2$	544, 442
4-F	4-F	428
2-F	4-F	419
H	CF$_3$	422

^{a} Data recorded in toluene. The values as taken as presented in the ref 3.

The fading rate of the naphthopyran compounds can be further modified, by an inhibition of formation of the more stable TT isomer. Thus, substitution may influence the ratio between the isomers in the open form, by e.g. introducing a sterically demanding group, stabilizing one of the isomers via intramolecular hydrogen bonding, or structural restrictions towards double bond isomerization. In all of the following examples in Figure 3.13, the bleaching of the naphthopyran was accelerated due to introduced structural changes. In the group of Rück-Braun, sterically demanding substituent (i.e. CN) was introduced at 2-position of 2*H*-benzo[2,1-b]pyran, resulting in very fast relaxation time (t = 12 μs), suggesting formation of only short-lived TC isomer at room temperature, while due to the sterical reasons, there was no isomerization towards the TT isomer.[93] More recently, in the group of Coelho, a series of bridged naphthopyrans were developed, which prohibit isomerization towards the long-lived TT form.[94–96] Finally, the group of Abe recently developed an approach, in which by introduction of an alkoxy- group at 10-position of a 3*H*-naphtho[2,1-b]pyran, formation of the TT form is reduced due to the intramolecular hydrogen bonding between the oxygen atom of the alkoxy- group and the olefinic proton in the TC form.[97]

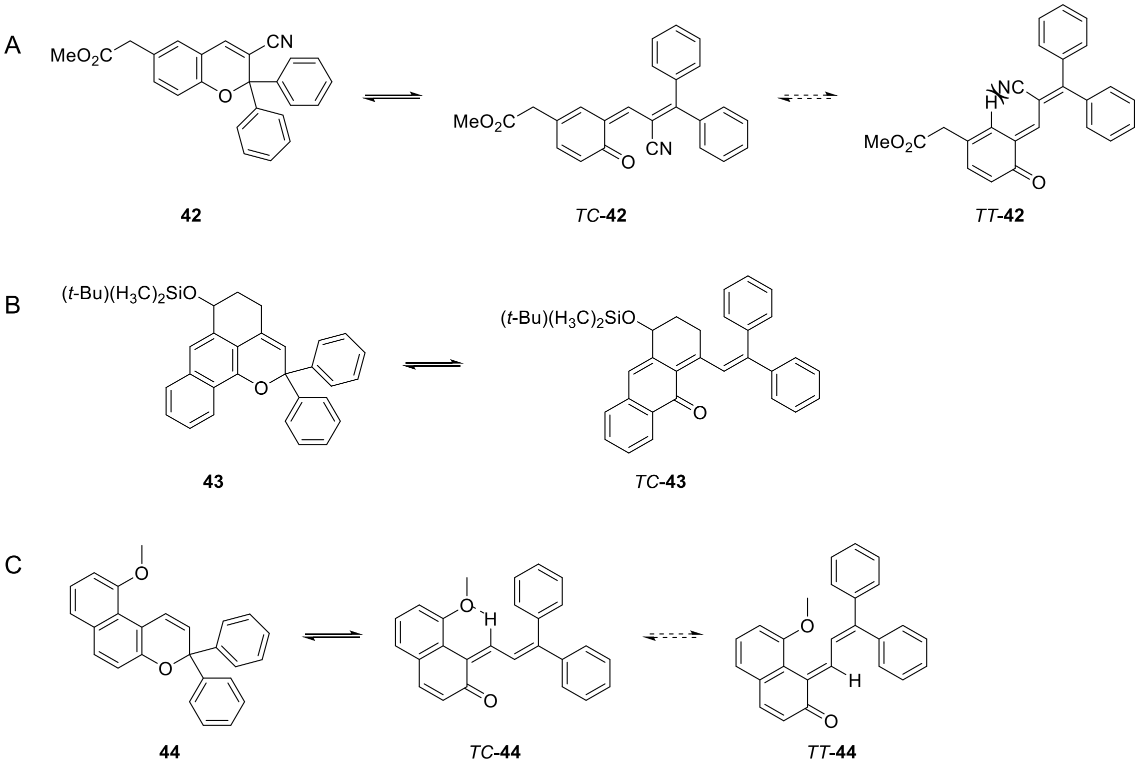

Figure 3.13. Structural modification of the chromene structures, in order to enhance the ratio of only one of the photoisomers as reported by groups of (A) Rück-Braun in ref. 93, (B) Coelho in ref. 94 and (C) Abe in ref. 97.

Upon UV-light irradiation, a naphthopyran molecule undergoes C-O bond cleavage, thus ring-opening of the pyran moiety occurs, yielding the open forms (Figure 3.14). Initially formed *transoid-cis* (TC)-form is thermally unstable, and thus it either quickly reverts to the closed form (CF), or under further UV irradiation undergoes C=C isomerization yielding the more stable *transoid-trans* (TT)-form. The *cis-trans* isomerisation between the two open forms is a slow process, and happens upon UV irradiation. Other possible isomers, *cisoid-cis* (CC) and *cisoid-trans* (CT), are under detection limit at room temperature, and do not influence the photochemical properties of the PSS. Upon removal of the UV-light source, the thermally unstable TC form rapidly returns to the closed form. The thermal bleaching of the more stable TT form occurs slowly; the process involves two steps - isomerisation from TT to TC form (slow process), and further ring closure, from TC to the closed form (fast process). Under visible light irradiation, color-fading of the TT forms occurs faster.

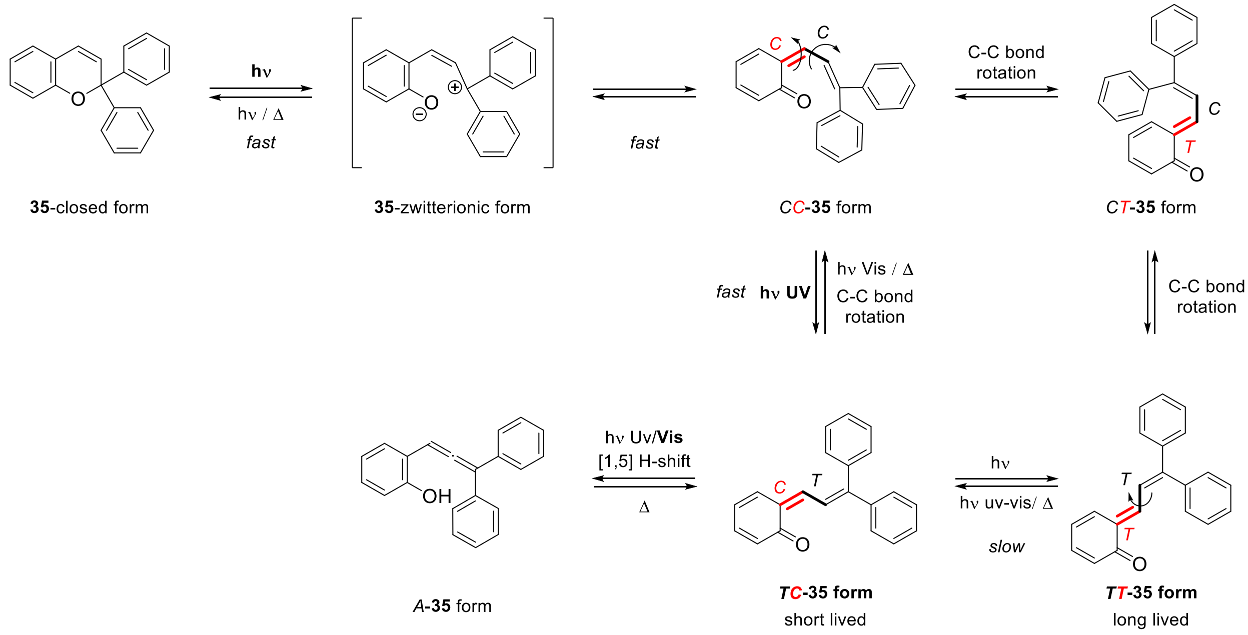
hν
hν / Δ
fast
fast
C-C bond rotation
35-closed form
35-zwitterionic form
CC-35 form
CT-35 form
fast hν UV
hν Vis / Δ
C-C bond rotation
C-C bond rotation
hν Uv/Vis
[1,5] H-shift
Δ
hν
hν uv-vis/ Δ
slow
A-35 form
TC-35 form
short lived
TT-35 form
long lived

Figure 3.14. Possible photochemical and thermal reaction pathways of the chromene switching process, including the formation of the allene (A) form.

The NMR studies is a widely employed method for understanding the kinetics of the photochemical isomerization of chromene compounds. On the example of difluorophenyl substituted benzopyran, Delabere *et al.* investigated photochemical and thermal reactions of the switching process.[98,99] Upon UV irradiation, apart from the TC and TT isomers, small amount of the additional allene (A) isomer is formed, and detected by ^{19}F NMR. Under visible light irradiation also the TC→A isomerization occurs at room temperature. The allene form was confirmed for differently substituted 3*H*-naphtho[2,1-b]pyrans in various solvents.[100–103] However, the NMR investigations of various 2*H*-naphtho[1,2-b]pyrans showed no allene isomer formation at low temperature, upon photochemical investigations in any of the tested solvents.[104–107]

3.2.1 Plan of the Synthesis

For the attachment to the surface, a synthetic route of the amino-functionalized naphthopyran-linker conjugate was developed, according to the retrosynthetic scheme in Figure 3.15. The substitution pattern was chosen to fine-tune the desired properties of the photoswitch, in order to follow the photochromic changes when attached to the Si(111) surface. The methyl ester functionality at 5-position was introduced in order to reduce the thermal back reaction fading rate. Additionally, the ester functionality makes a useful substitution choice for further characterizations, due to its strong absorption in the IR. The hydroxyl-functionality of the naphthopyran core **45**, was introduced as a coupling functionality for the attachment of the linker. The synthesis of the naphthopyran core **45** was previously well established in the group of Rück-Braun, and based on the procedure earlier reported by Gabbutt *et al.*[87]

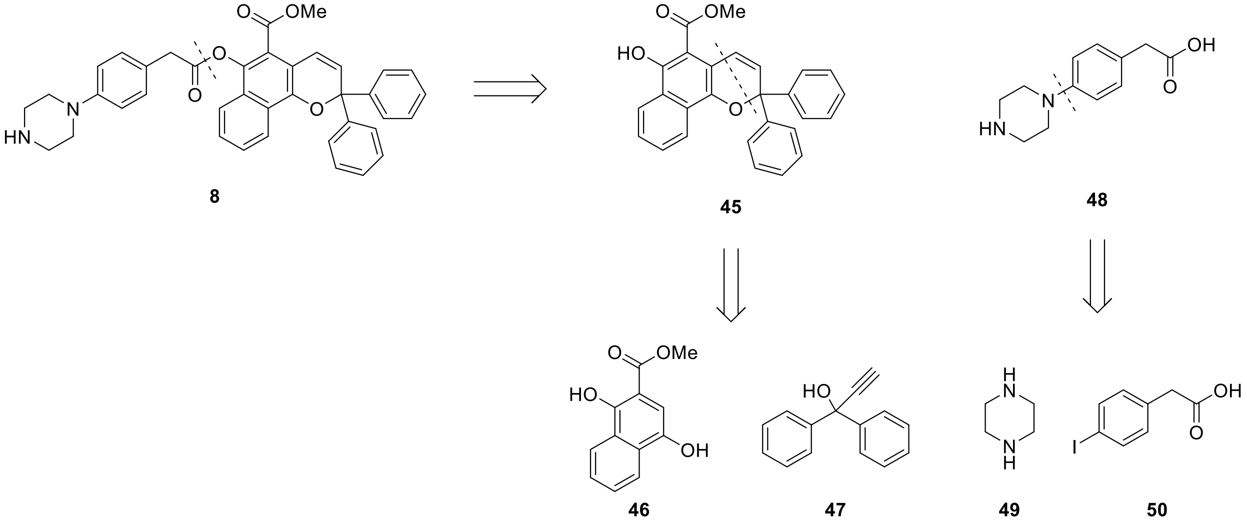

Figure 3.15. Retrosynthetic plan of the naphthopyran-linker conjugate **8**.

An amine linker, based on the rigid piperazine structure, was designed with the aim to attach the final naphthopyran-linker conjugate **8** to the carboxy-terminated Si(111) surface. The mono-Boc protected piperazine was coupled to the methyl 2-(4-iodophenyl)acetate in a Buchwald-Hartwig amination reaction, to yield a linker arm. The prepared linker, deprotected to the carboxylic acid, was coupled with the core naphthopyran **45** in a Steglich esterification reaction, to yield the desired conjugate for surface attachment.

3.2.2 Synthesis of the Naphthopyran-Linker Conjugate

3.2.2.1 Synthesis of the Naphthopyran Core

Naphthopyran core **45** was obtained in a three-step reaction sequence, starting from commercially available 1,4-dihydroxy-2-naphthoic acid (**51**) and benzophenone (**52**).

First, 1,4-dihydroxy-2-naphthoic acid (**51**) was protected in a selective methylation reaction, to afford the desired 1,4-dihydroxy-2-naphthoat (Figure 3.16).[108]

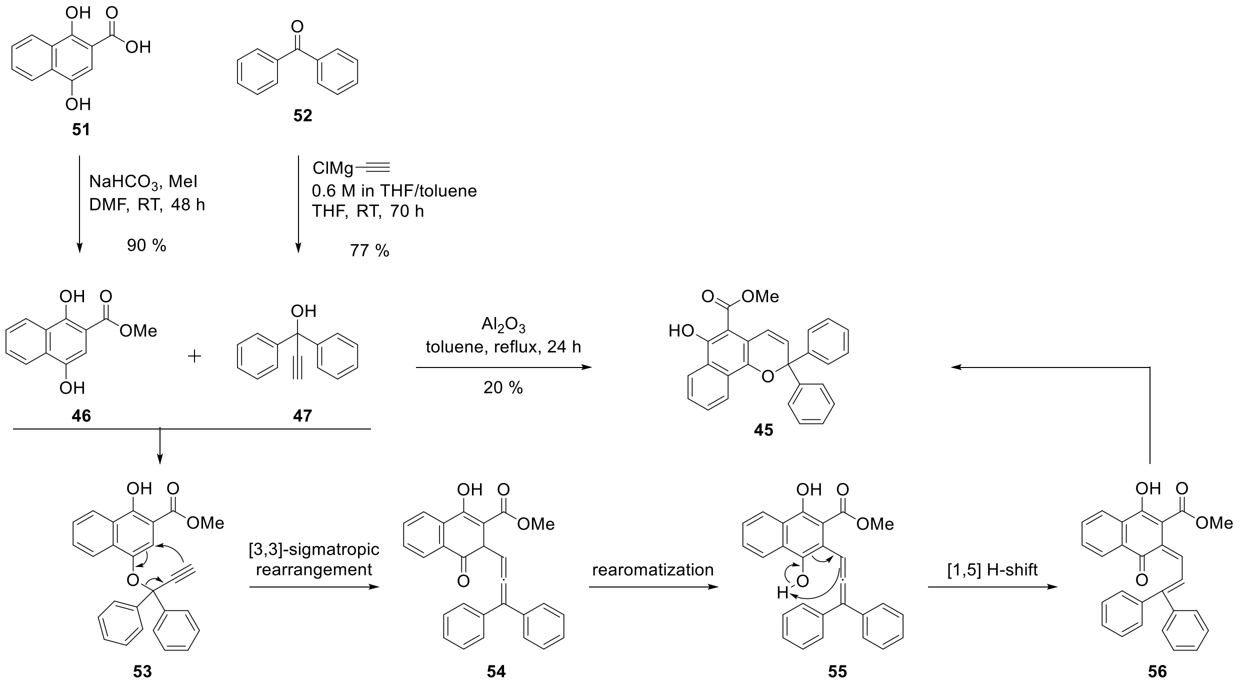
51
52
NaHCO3, MeI
DMF, RT, 48 h
90 %
ClMg
0.6 M in THF/toluene
THF, RT, 70 h
77 %
46
47
Al2O3
toluene, reflux, 24 h
20 %
45
[3,3]-sigmatropic rearrangement
rearomatization
[1,5] H-shift
53
54
55
56

Figure 3.16. Three steps synthesis route, including the reaction conditions and rearrangement towards the naphthopyran **45**.

As a methylation reagent, methyl iodide was used, and mixed with the naphthopyran building block **51** in DMF under basic conditions, at room temperature, over prolonged reaction time. Upon the purification by column chromatography, the desired methyl ester **46** was obtained in 90% yield. Here, classical Fisher esterification reaction conditions (methanol, under acidic conditions) would not have resulted in the desired product, as previously reported.[109]

1,1-diphenylprop-2-yn-1-ol (**47**) was obtained from commercially available benzophenone (**52**) in a Grignard reaction with ethylene magnesium chloride in abs. THF, at room temperature, over prolonged reaction time (Figure 3.16).[93] The purification of the product was a challenge, due to its instability under acidic conditions; the propargylalcohol undergoes side product formation to 3,3-diphenylacrylaldehyde (**60**), when the alkyne-substituted carbocation is intercepted with water followed by tautomerisation via Meyer-Schuster rearrangement (Figure 3.17).[110] Thus, purification of the product on column chromatography using silica was not an option, due to its slightly acidic properties. The fractional-bulb distillation showed to be an unsuccessful method, since upon two separate attempts, it led to obtaining only the mixed fractions. Finally, the product was purified by column chromatography, using neutral aluminium oxide (Alox) as a stationary phase, and pentane / ethyl acetate 5:1 as eluents, and obtained in 77% yield.

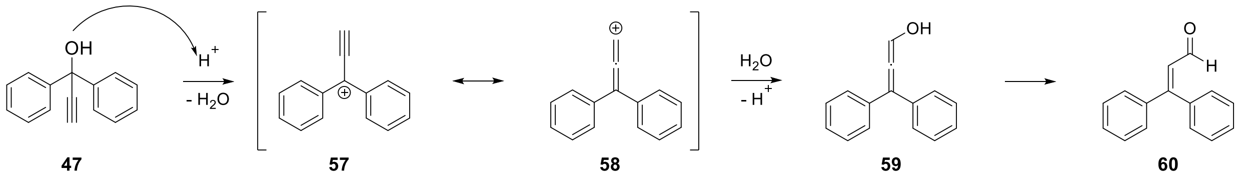

Figure 3.17. Side product formation via Meyer-Schuster rearrangement of the propargylacohol **47**.

The preparation of naphthopyran **45** was carried out in apolar toluene, under acidic catalysis (aluminum oxide, refluxing overnight), according to Gabbutt *et al.*[87] Reaction proceeds via acidic catalyzed condensation of the naphthol **46** and propargylalcohol **47** towards alkynyl aryl ether **53** (Figure 3.16). The reaction further proceeds via [3,3]-sigmatropic Claisen rearrangement to obtain allene **54**, which undergoes rearomatization and [1,5] hydrogen-shift to yield naphthopyran **45** in the open form. Upon the electrocyclization reaction, the naphthopyran **45** was obtained and isolated in 20% yield. A screening of different acidic catalyst, for the preparation of chromene compounds from the respective propargylalcohols, was previously tested in the group of Rück-Braun.[108] It was shown for a series of different benzo- and naphthopyrans, that the procedure according to Gabbutt *et al.* is more efficient compared to the other previously reported alternatives.[108] In this work, for the here designed chromene, no investigation in this matter were carried out.

There are several reasons for the low yield of the reaction. Even after 24 h reaction time, the turnover was incomplete; TLC control showed remaining naphtol in the reaction mixture, upon all of the propargylacohol was used up. Thus, the poor yield was influenced by the formation of the side-product **60** via the Meyer-Schuster rearrangement of the propargylacohol in the reaction mixture, catalyzed by the acidic aluminum oxide (Figure 3.17).[111] The formation of the aldehyde **60** was confirmed in the ^{1}H NMR spectrum, via a doublet at 9.51 ppm (^3J = 8.0 Hz) assigned to the aldehyde proton.[112] Additionally, the reaction is known to be less efficient when 1-naphtol is employed in the reaction, compared to 2-naphtol used for the synthesis of 3*H*-naphtho[2,1-b]pyrans, resulting in generally higher yield of the aldehyde side product.[110]

3.2.2.2 Synthesis of the Piperazine-Based Linker

The linker was prepared following a four-step procedure, starting from the commercially available 2-(4-iodophenyl)acetic acid (**50**) and piperazine (**49**). The synthesis of the linker was designed to proceed by a metal mediated amination of methyl iodophenyl acetate **61** and mono Boc-protected piperazine **62** (Figure 3.18).

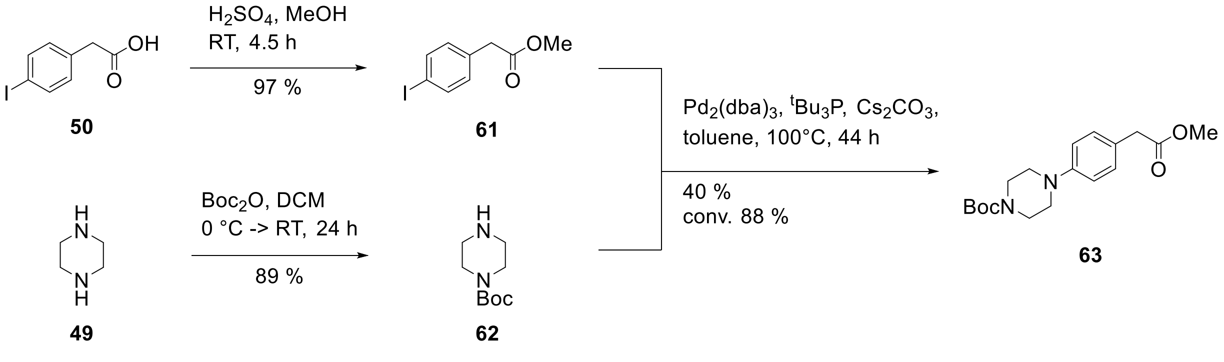

Figure 3.18. Three steps reaction route and reaction conditions, towards obtaining Buchwald-Hartwig coupling product **63**.

Methyl 2-(4-iodophenyl)acetate was obtained according to the procedure described by Yu *et al.*[113] 2-(4-Iodophenyl)acetic acid (**50**) was dissolved in methanol, esterification reaction proceeded under acidic conditions via Fisher esterification mechanism, by refluxing over a period of 4.5 h

(Figure 3.18). Since reactants and the products are in equilibrium, methanol was used in excess to shift the equilibrium towards the product, resulting in 97 % yield, without requiring a purification step.

Before the metal-mediated amination, the commercially available piperazine requires a selective mono-protection, in order to avoid formation of a di-coupled product. Since the amination reaction proceeds under basic conditions, the Boc-protecting group was chosen for amine protection, due to its stability towards bases and inertness towards many other nucleophilic reagents.[114] Piperazine was protected using Boc_2O and piperazine in excess, in DCM starting at 0 °C and slowly warming up to room temperature over prolonged reaction time (Figure 3.18).[115] Upon work-up, the desired product, *tert*-butyl piperazine-1-carboxylate (**62**) was afforded in 89% yield, without further purification.

The coupling of two linker units proceeded via Buchwald Hartwig amination reaction, which allows formation of aryl amine compounds, starting from aryl halides and primary or secondary amines, in a palladium-mediated coupling reaction.[116,117] Herein, the obtained methyl 2-(4-iodophenyl)acetate (**61**) was coupled with the Boc-protected piperazine **62**, using tris(dibenzylideneacetone)dipalladium(0) ($Pd_2(dba)_3$) as a precatalyst, and tri-*tert*-butylphosphine as a ligand, in the presence of Cs_2CO_3 as the base, and heating in toluene.[118]

The mechanism of the reaction starts with the oxidative addition of the aryl iodide **61** (**I**). In the next, the complex is coordinated by the secondary amine and subsequently deprotonated by the present base, yielding the complex **66** (**II**) (Figure 3.19).[119] Finally, the new C-N bond is formed via the reductive elimination (**III**), leading to the desired product **63** and the regenerated catalyst. The reaction did not reach completion even after prolonged reaction time (48 h), according to TLC control. The product was isolated in 40% yield; the starting aryl iodide was recovered by a column chromatography after quenching of the reaction, resulting in an overall conversion of 88%. Furthermore, the obtained yield may be influenced by side product formation via the β-H elimination reaction (**IV**) (Figure 3.19, B).[120] Imine **67** and a dehalogenated product **69** are the most likely products of the β-H elimination.[120] Additionally, disproportionation of the arylpalladium halide complex towards dihalo- and diarylpalladium complexes has been reported; the latter may lead to formation of biaryl side product via reductive elimination.[119,121]

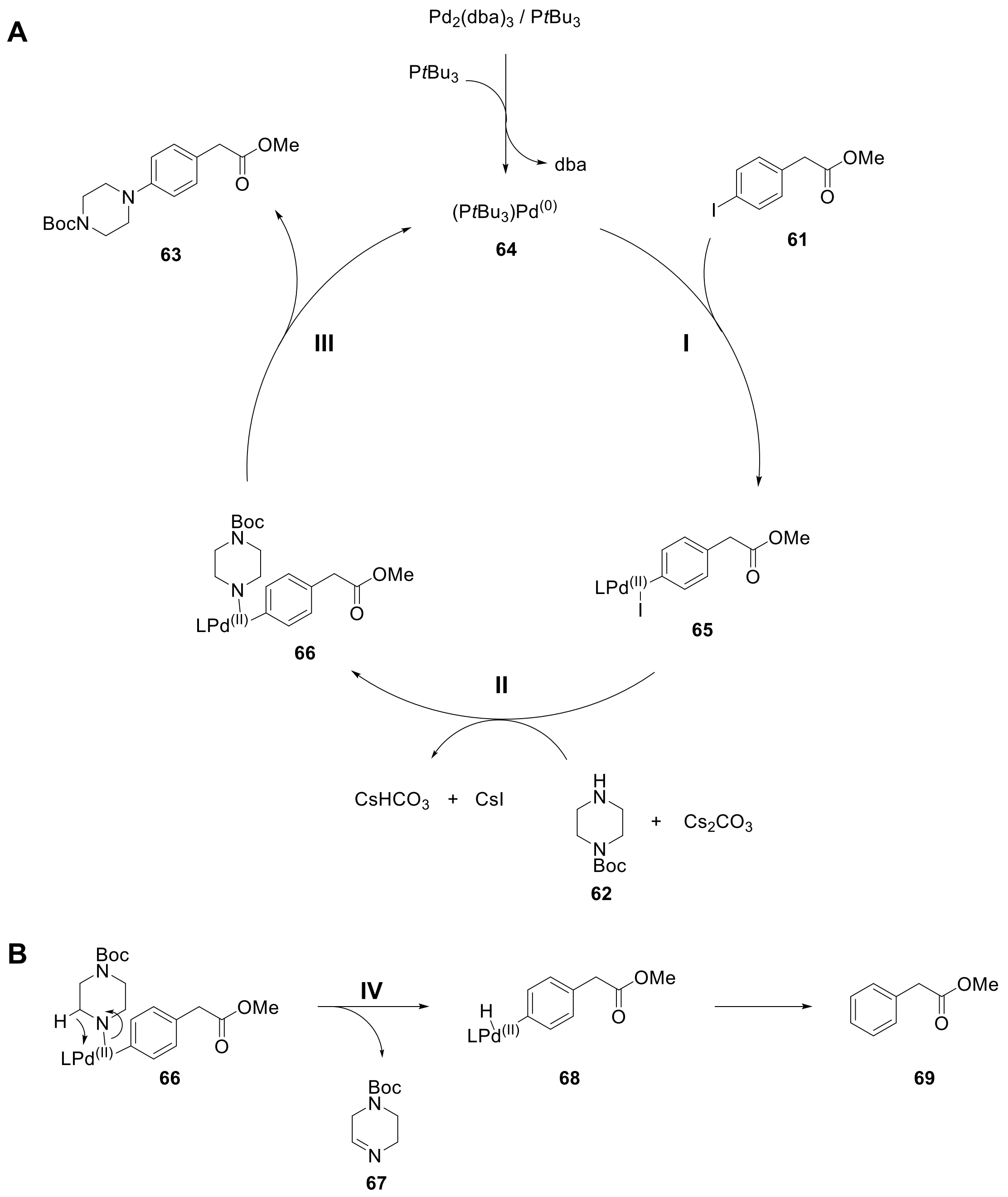
A
Pd2(dba)3 / PtBu3
PtBu3
dba
(PtBu3)Pd(0)
64
OMe
O
BocN
N
63
OMe
O
I
61
III
I
Boc
N
N
LPd(II)
OMe
O
66
LPd(II)
I
OMe
O
65
II
CsHCO3 + CsI
H
N
N
Boc
62
+ Cs2CO3
B
Boc
N
H
N
LPd(II)
OMe
O
66
IV
H
LPd(II)
OMe
O
68
Boc
N
N
67
OMe
O
69

Figure 3.19. Mechanism of the Buchwald-Hartwig amination towards preparation of the linker **63**, according to ref. 119.

Additionally, the amination reaction was tested under the Ullmann reaction conditions, using copper iodide as the catalyst in the metal-mediated coupling reaction.[122,123] However, under the tested conditions – CuI as the catalyst, tetramethylethylenediamine (TMEDA) as the ligand, potassium phosphate as the base, in abs. toluene at 80 °C,[124] after prolonged reaction time (30 h), no conversion of the educt was observed. The starting material was entirely recovered via column chromatography.

In this work, no additional experiments were carried out towards optimization of the amination reaction. Although the Buchwald-Hartwig cross-coupling reactions always follow the general catalytic cycle route, the catalytic species, and thus the rate limiting step as well, can vary for different substrates and overall reaction conditions. There are many variables that must be taken into account (i.e. choice of ligand, solvent, palladium-to-ligand ratio, temperature, etc), since they can significantly influence the efficiency of the reaction.[125,126] It is reasonable to believe that investigation towards tuning the reaction conditions may lead to improved conversion and overall yield of the reaction.[127,128]

In the final step, the linker ester group was hydrolyzed under basic conditions,[114] in order to obtain the carboxyl-functionality, available for further coupling reaction with the naphthopyran core (Figure 3.20). The hydrolysis was carried out in 2 M NaOH aq. / THF solution, at room temperature overnight. The reaction yielded 94% of the desired product without further purification.

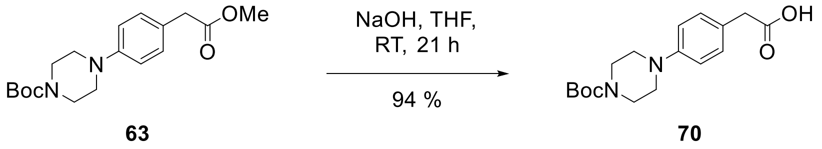

Figure 3.20. Reaction scheme and conditions towards obtaining the piperazine-based linker **70**.

3.2.2.3 Synthesis of the Naphthopyran-Linker Conjugate for Immobilization on the Silicon Surface

The coupling of the naphthopyran core **45**, and the linker **70** was carried out in a Steglich esterification reaction (Figure 3.21).[129] *N*,*N*'-Dicyclohexylcarbodiimide (DCC) was used as a coupling reagent, and 4-dimethylaminopyridine (DMAP) as a catalyst in the coupling reaction, in dry DCM, according to the procedure previously reported for phenols in ref. 130. The reaction was carried out in the dark, and afforded the desired naphthopyran **71** in 70 % yield upon purification.

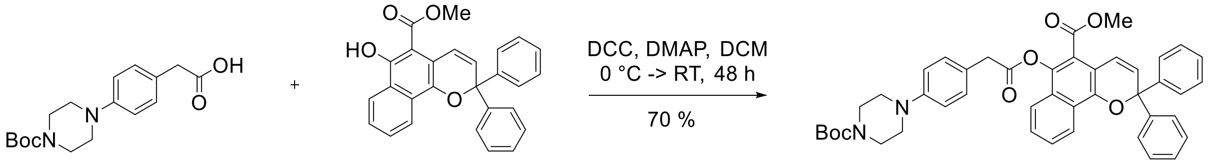

70 **45** **71**

Figure 3.21. Formation of the naphthopyran-linker conjugate **71**, via Steglich esterification reaction.

The TLC monitoring of the reaction showed incomplete conversion of the starting naphthopyran **45**, after prolonged reaction time (48 h). Furthermore, the purification of the product proved to be a challenge. The column chromatography with different eluent systems – pentane / ethyl acetate = 5:1, 2:1, 1:1, 1:10 – showed to be unsuccessful towards obtaining pure product, due it strongly binding to the silica. Additionally, the recrystallization was tested as a purification method, due to the difference in the polarities of the educts and the product, using varying ratios of ethyl acetate and cyclohexane (cyclohexane / ethyl acetate = 50:50, 10:50, 50:10, 99:1, 1:99) under reflux, but all efforts were unsuccessful. Finally, the column chromatography on silica, using pentane / ethyl acetate = 5:1, with addition of a base (0.1 % NEt_3), afforded the pure product. The addition of the base reduced the acidity of silica, and thus allowed elution of the product which otherwise remained attached to the column material.

The final step of the naphthopyran-linker conjugate synthesis is the Boc-deprotection, furnishing the free secondary amine for the attachment to the carboxy-terminated silicon surface. Boc-cleavage is carried out under acidic conditions;[114] using HCl in dioxane at 0 °C (Figure 3.22). The final product was isolated quantitatively, without further purification, in form of the chloride salt.

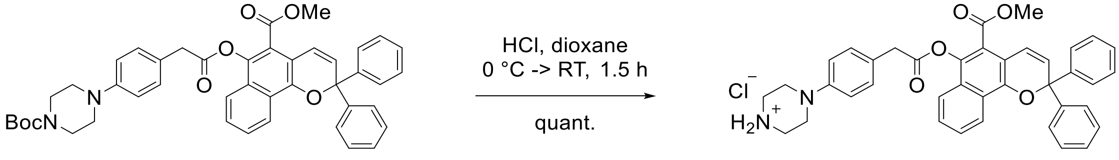

71 **8**

Figure 3.22. Reaction scheme and conditions for the Boc-deprotection towards obtaining naphthopyran **8**.

3.2.3 Characterization of Photochemical Properties of the Naphthopyran Compounds

Photochemical isomerisation of the naphthopyran compounds occur upon UV light irradiation of the closed structure. Ring-opening reaction, as previously described, leads to formation of two main photoisomers, the short lived TC and more stable, long lived TT-form (Figure 3.23). Under UV irradiation, the amount of the closed form is decreased, while the amounts of the open-form photoisomers increase. Once the photostationary state is reached, all three forms are in equilibrium, and the ratio between them should remain unchanged as long as the same light source is employed. Due to thermal instability of the open isomers, removing the light source influences ring-closure reaction, and the equilibrium shifts towards formation of the closed form.

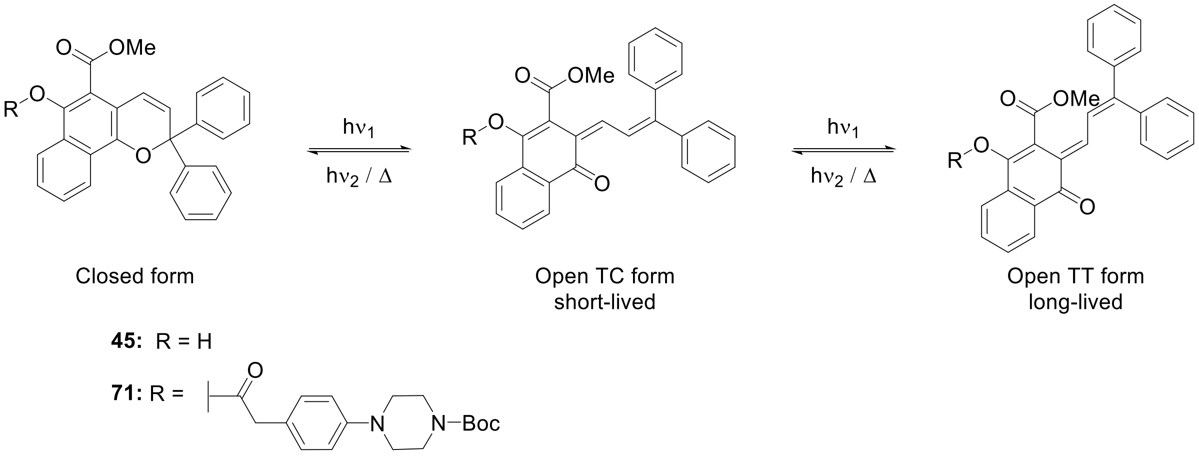

Figure 3.23. General photochemical equilibrium of naphthopyran structures described in this study.

The photostationary states are possible to identify via UV/Vis measurement, since the absorbance at the λ_{max} stays constant once the equilibrium is reached. UV/Vis measurements were carried out for both prepared naphthopyran compounds, **45** and **71**, under the same conditions. Furthermore, fatigue resistance was confirmed by performing several cycles and comparing the absorbance at λ_{max} in the photostationary states.

Additionally, NMR mesurements allow identification of the isomer ratios in the photostationary states, but also the ratios of photoisomers at different points of the photochemical reaction. This method was employed in order to evaluate the switching process of the prepared naphthopyran compounds. For identifying the open isomers by elucidation of molecular structure, and determination of the ratio of isomers in the PSSs. Furthermore, this method was previously used and reported as a usefull approach to study the switching mechanism between the different isomers, and analyze the kinetics of the photochemical and thermal reactions.[131]

Finally, the photochemical reactions were investigated via infrared spectroscopy in solution. These studies do not necesserily allow identification of each of the photoisomers upon the switching reactions, due to the signals of TC and TT being similar. Rather, it allows observation of the changes of the significant signals of the isomers in the different photostationary states, obtained by bond cleavage, isomerizations and bond formation reactions. Additionally, the data obtained for these compounds in solution, plays crucial role in evaluation of the switching process on the photoswitchable silicon surfaces.

3.2.3.1 UV/Vis Studies of the Naphthopyran Compounds

The samples for the UV/Vis photochemical studies were prepared in acetonitrile and degassed with stream of argon for 15 min. The studies of naphthopyran **71** were additionally done in tetrachloroethylene (TCE). The measurements were carried out under constant stirring of the solutions, at a temperature of 21.8 °C ± 0.2, unless otherwise stated.

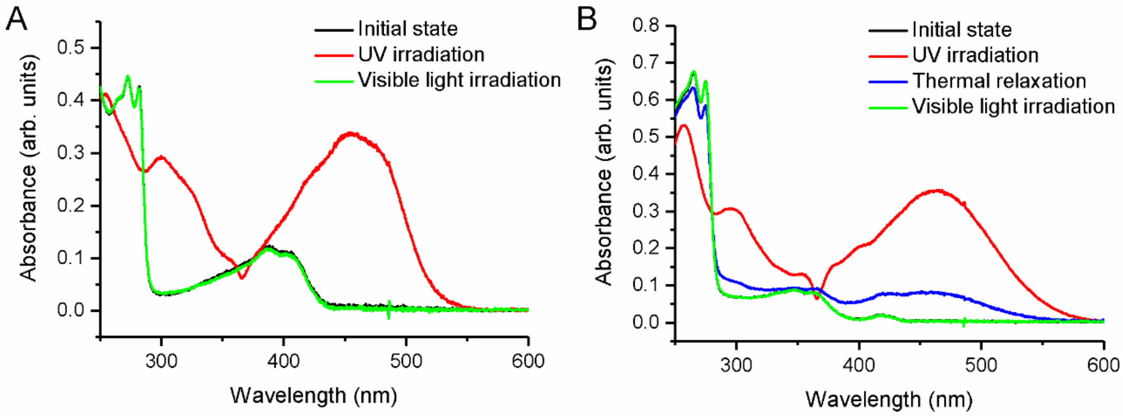

Figure 3.24. Absorption spectra of the PSSs of the naphthopyran **45** (A) and **71** (B) in acetonitrile: upon UV light irradiation, PSS(365 nm) (red); thermal relaxation, PSS(Δ) (blue); visible light irradiation, PSS(505 nm) (green); and the initial state (black).

Upon the ring-opening reaction of naphthopyran **45** in acetonitrile solution, under the UV light irradiation (λ_{irr} = 365 nm) the spectra shows increase in the absorbance at 455 nm caused by the extended delocalization of the π-electrons over both the naphthopyrane moiety and the phenyl rings (PSS(365 nm)) (Figure 3.24A). A time-resolved photochemical study shows rapid increase in absorbance at λ_{max} and very slow return to the closed form, both under thermal relaxation and visible light irradiation (λ_{irr} = 505 nm) (Figure 3.25). For comparison, both back reactions are carried out immediately upon 60 s of irradiation of the samples with the 365 nm light (Figure 3.25B). The thermal relaxation was monitored in the dark at 21.8 °C. For the visible light irradiation back reaction, simultaneously was the UV light source turned off and visible light turned on. The visible light irradiation for 50 min increased the temperature to 27.3 °C; the final spectra was taken upon cooling to the initial temperature. The spectroscopic data are presented in Table 3.6.

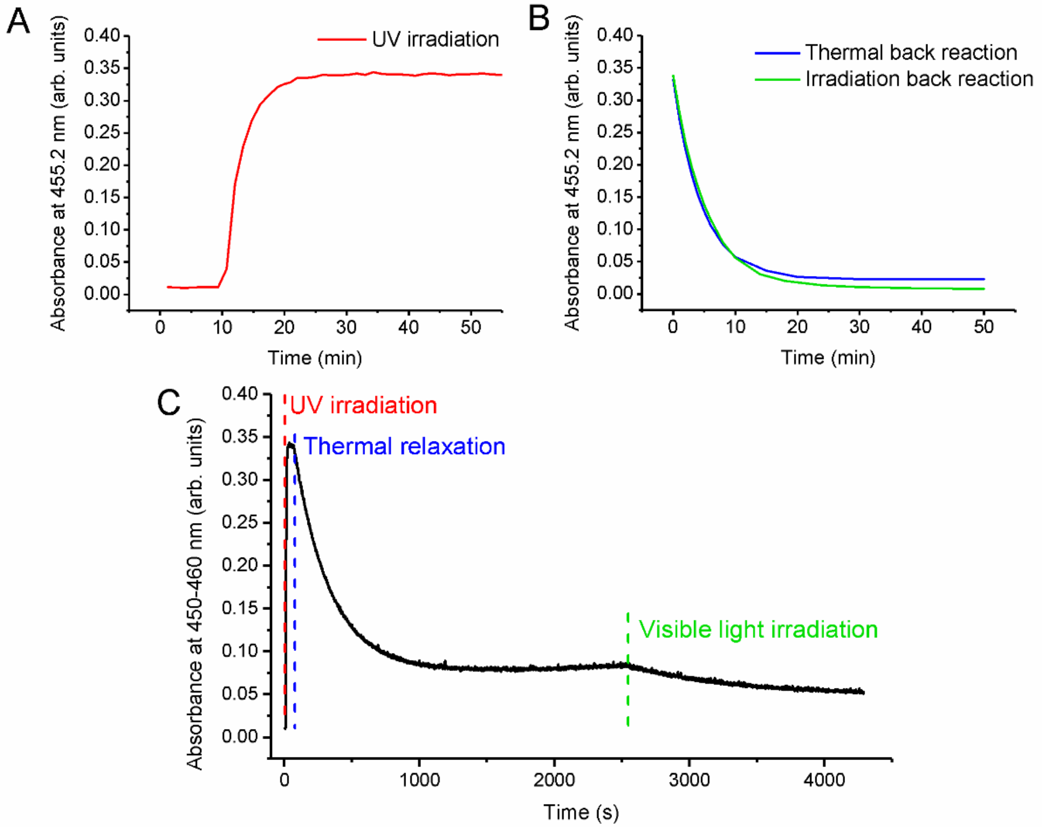

Figure 3.25. Time-resolved spectra of the naphthopyran **45** in acetonitrile (c = 9.4 · 10^{-6} M), under (A) UV light irradiation, and (B) thermal back reaction (blue), and visible light irradiation back reaction (green).

For the naphthopyran **71**, similarly, upon the 365 nm light irradiation, at the PSS(365 nm), the spectra shows the absorbance maximum at 463 nm (Figure 3.24B). A time-resolved study shows thermal relaxation in the dark to be fast, due to the fast bleaching of the TC and formation of the closed form (PSS(Δ)) (Figure 3.26). Ring closure of the more stable TT-form proceeds very slowly, and thus the timeresolved spectra reaches a plateau. The complete return to the closed forms occurs upon visible light irradiation (PSS(505 nm)). For comparison, both back reaction are carried out upon 60 s of irradiation of the samples with the 365 nm light (Figure 3.26B). The spectroscopic data are presented in Table 3.6.

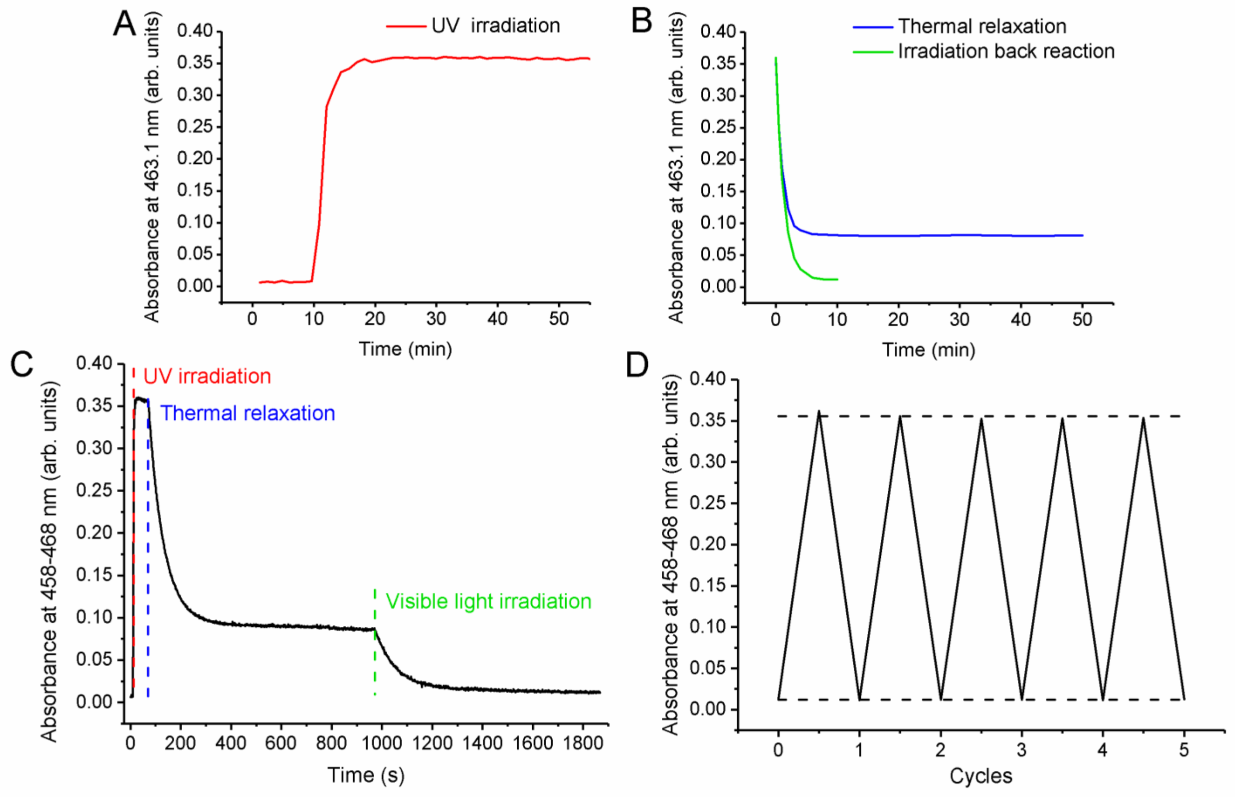

Figure 3.26. Time-resolved spectra of the naphthopyran **71** in acetonitrile (c = 9.8 · 10^{-6} M), under (A) UV light irradiation, and (B) thermal back reaction (blue), and visible light irradiation back reaction (green). (D) Repeatable changes of the average absorbance in the region 458-468 nm upon reaching the PSS(365 nm) and PSS(505 nm).

Since the visible-light irradiation back reaction allows for fast complete regeneration of closed form of the naphthopyran **71**, the alternation between UV- and visible-light irradiations allows the evaluation of the fatigue resistance. Figure 3.26D shows the repeatable absorption change upon several UV/visible-light irradiation cycles of the naphthopyran **71** in acetonitrile solution. The cycles, consisted of 60 s irradiation with UV-light, followed by the immediate 10 min visible-light irradiation. upon irradiation with 505 nm LED light, the temperature of the sample increased from 21.8 °C to ~25.5 °C; the spectra of the PSS(505 nm) were taken upon cooling down to the initial temperature. Remarkable reproducibility without decomposition or side-product formation during this process was observed upon 5 cycles (Figure 3.26D, the dotted lines present the average values of the absorbance for the PSSs over 5 cycles).

Tetrachloroethylene (TCE) is one of the solvents of choice for the investigation of the switching in solution via FTIR spectroscopy. For this reason, the fatigue resistance was also tested in tetrachloroethylene and proved reproducibility over several cycles at the λ_{max} of the open forms. However, some slight inconsistencies were observed in the area below 450 nm (Figure 3.27), most probably due to reactivity of tetrachloroethylene towards [2+2] photocycloaddition under prolonged UV light irradiation (λ = 350 nm).[132] For this reason, TCE was not further used for UV/Vis investigations of naphthopyran compounds.

Table 3.6. Spectroscopic data of naphthopyran **45** (in acetonitrile), and **71** (in acetonitrile and tetrachloroethylene).

Compound	**Solvent**	**λ_{max} closed form** (nm)	**λ_{max} open forms** (nm)	**λ_{isosb}** (nm)
Naphthopyran **45**	MeCN	273, 282, 388, 402[a]	254, 300, 455	252, 260, 285
Naphthopyran **71**	MeCN	265, 275, 348, 361[a]	257, 294, 463	280
	TCE	351, 369[a]	462	-[b]

[a] observed sholder. [b] TCE UV cut-off wavelength is at 290 nm.

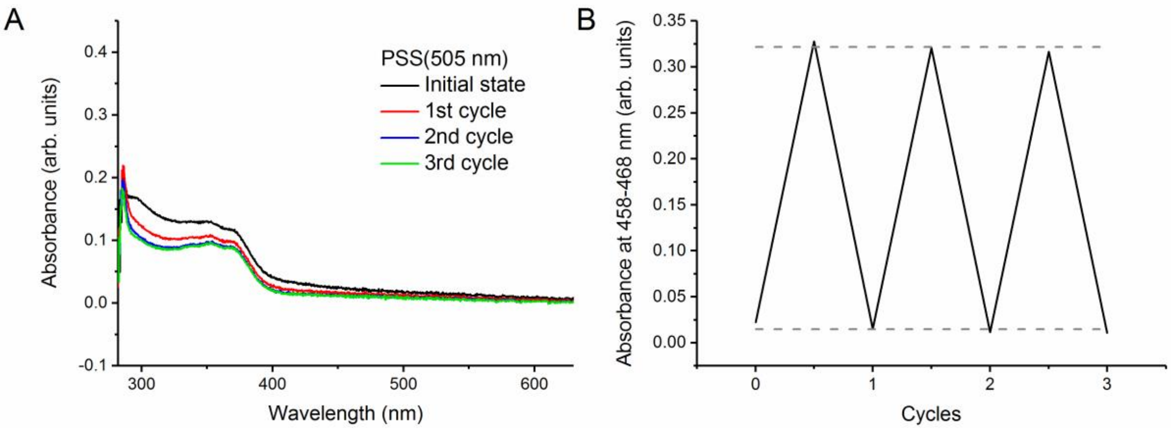

Figure 3.27. (A) Absorption spectra of the naphthopyran **71** in tetrachloroethylene, the initial state and at the PSS(505 nm) over 3 cycles. (B) The changes in the average absorbance in the region 458-468 nm upon reaching the PSS(365 nm) and PSS(505 nm).

The kinetics of thermal bleaching of the naphthopyran compounds can be analyzed from time-resolved absorption spectra, by fitting the experimentally obtained data from the measurements in acetonitrile to a biexponential (second-order) decay[133,134]:

$$A(\tau) = A_1 e^{-k_1 \tau} + A_2 e^{-k_2 \tau} + A_{th}$$

Where $A(\tau)$ is the absorbance at the λ_{max}, A_1 and A_2 are contributions to the initial absorbance A_0, k_1 and k_2 are rate constants of fast and slow components, respectively, and A_{th} is the residual absorbance when time approaches infinity. The biexponential decay fitting provided correlation coefficients of >0.99 (Table 3.7). Additionally, a common way of describing the bleaching of the colored forms is by introduction of $\tau_{1/2}$ and $\tau_{3/4}$ values, which are defined as the time taken for the initial absorbance (A_0) to reduce by ½ and ¾, respectively. All spectrokinetic data are presented in Table 3.7.

Table 3.7. Spectrokinetic data of thermal bleaching of the naphthopyrans **45** (A) and **71** (B), in acetonitrile solution (c = $9.4 \cdot 10^{-6}$ M and $9.8 \cdot 10^{-6}$ M, respectively).

Compound	λ_{max} (nm)	k_1 (10^{-3} s^{-1})	k_2 (10^{-3} s^{-1})	$\tau_{1/2}$ (s)	$\tau_{3/4}$ (s)	A_0	A_1	A_2	A_{th}
45	455	3.634	0.752	213	453	0.3316	0.3085	0.0007	0.018
71	463	16.38	2.128	67	230	0.3565	0.2651	0.0091	0.0824

The values for the λ_{max}, $\tau_{1/2}$, $\tau_{3/4}$ and A_0 are obtained from the experimental data; k_1, k_2, A_1, A_2 and A_{th} are obtained from the biexponential decay fitting of the experimental data.

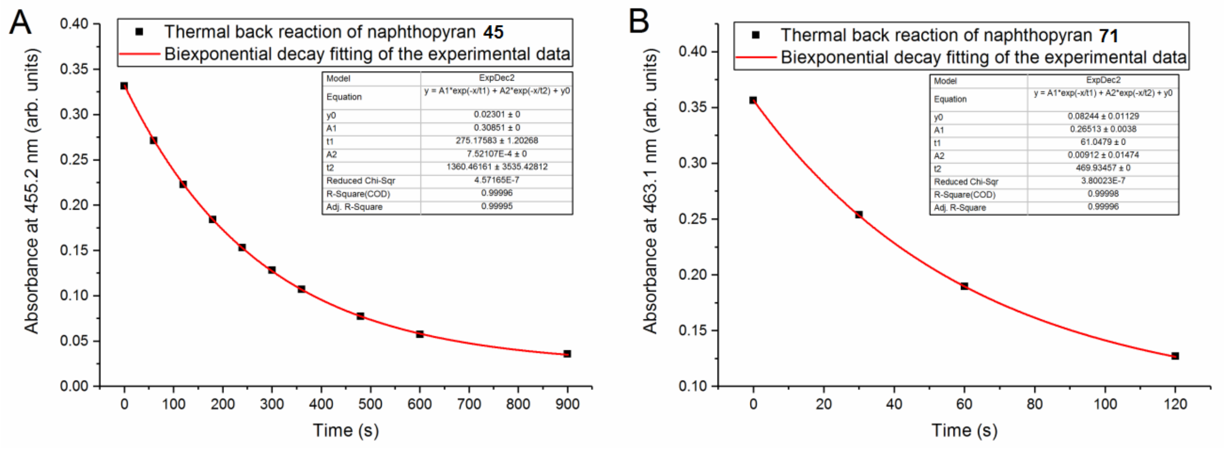

Model	ExpDec2
Equation	y = A1*exp(-x/t1) + A2*exp(-x/t2) + y0
y0	0.02301 ± 0
A1	0.30851 ± 0
t1	275.17583 ± 1.20268
A2	7.52107E-4 ± 0
t2	1360.46161 ± 3535.42812
Reduced Chi-Sqr	4.57165E-7
R-Square(COD)	0.99996
Adj. R-Square	0.99995

Model	ExpDec2
Equation	y = A1*exp(-x/t1) + A2*exp(-x/t2) + y0
y0	0.08244 ± 0.01129
A1	0.26513 ± 0.0038
t1	61.0479 ± 0
A2	0.00912 ± 0.01474
t2	469.93457 ± 0
Reduced Chi-Sqr	3.80023E-7
R-Square(COD)	0.99998
Adj. R-Square	0.99996

The obtained bleaching rate constants, k_1 and k_2, for both naphthopyrans, show faster bleaching kinetics for compound **71**, compared to the compound **45** (Table 3.7). Additionally, the fading times, $\tau_{1/2}$ and $\tau_{3/4}$, for the naphthopyran **45** are significantly higher than the fading times of the naphthopyran **71**. This behaviour of the two naphthopyrans in the solution can be assigned to two different factors: (1) stabilization from the electron donating group in the 6-position, stabilizing the open forms, as previously shown in Figure 3.12, (2) hydrogen bonding formation between the carbonyl oxygen of the open forms and the free hydroxyl group in the case of compound **45**, thereby stabilizing the open forms. The influence of the hydrogen bonding on the stabilization of the open forms has been described before.[28,135] Naphthopyran **71**, due to the additional linker, does not undergo the latter kind of stabilization of its open forms. The bleaching of the opened forms upon the visible-light irradiation is also slower for naphthopyran **45** (Figure 3.25), for the same reason.

3.2.3.2 NMR Photochemical Studies of the Naphthopyran Compounds

Naphthopyran samples (acetonitrile-*d3*, c = 10^{-2} M, 0 °C) were irradiated directly in the NMR tube, and the spectroscopic changes were followed by periodical recording of ^{1}H NMR spectra during the irradiation and relaxation reactions. The conditions for the measurements are comparable to the previous NMR work published in the field of 2*H*-naphthopyrans switching experiments.[106] The assignments were made on the basis of chemical shifts, coupling constants of the measured ^{1}H and the 2D NMR H,H-COSY experiments. Coupling constants provide crucial information in assignation of the peaks, due to observed differences in the values between different protons in CF, TC and TT form.[104,131]

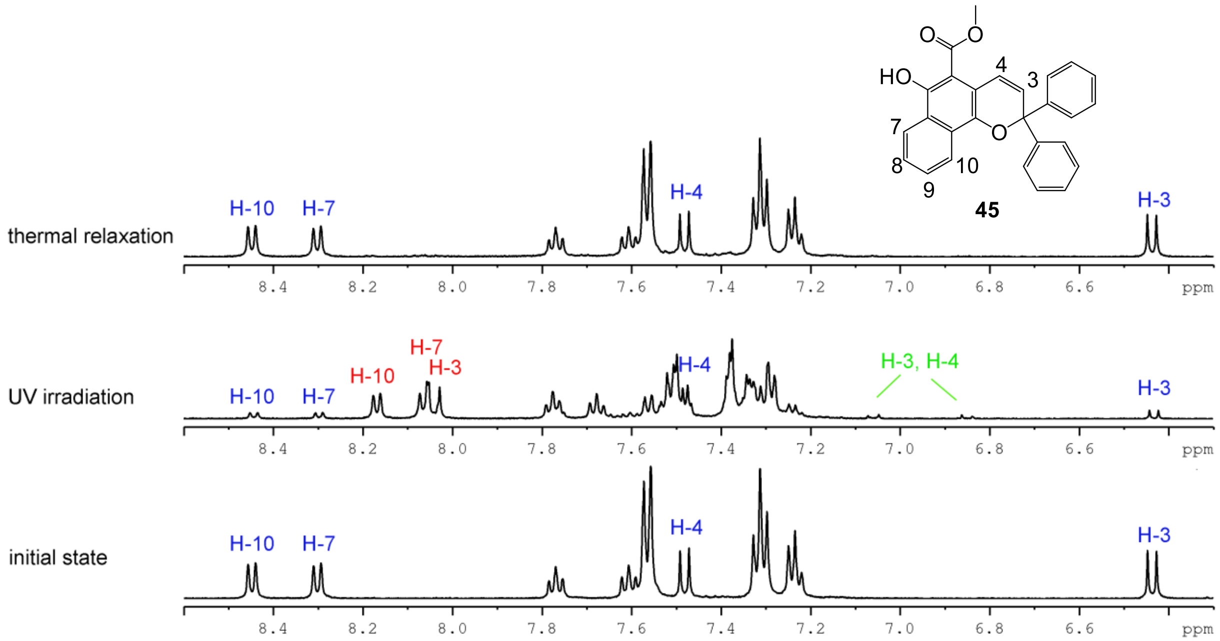

Figure 3.28. ^{1}H NMR spectra of the naphthopyran **45** in MeCN-*d3*, at 0 °C before the irradiation, upon reaching the PSS(365 nm), and upon thermal relaxation. The NMR assignations are color coded as following: CF (blue), TC (red), and TT (green).

In the ^{1}H NMR spectra of the initial state of the naphthopyran **45**, where only the close form is present, two pairs of doublets are observed (Figure 3.28). The doublets at 6.44 and 7.48 ppm, with a coupling constant J = 10 Hz, are assigned to the protons H-3 and H-4, respectively. The other pair of doublets, at 8.30 and 8.45 ppm, with a coupling constant J = 8.2 Hz are assigned to the protons H-7 and H-10, respectively. Upon UV light irradiation, integrals of these peaks decrease, while the new signals appear in the spectra. In the PSS(365 nm), the new doublets at 8.17 and 8.06 ppm, with a coupling constant of 7.8 Hz and 8 Hz, are assigned to the H-10 and H-7 of the TC form, respectively. The doublet at 8.04 ppm, with the coupling constant J = 12 Hz is assigned to H-3 of the TC form. The H-4 of the TC form could not be easily identified due to the overlapping with other aromatic signals. A pair of weak doublets observed at 6.85 and 7.06 ppm, with a vicinal coupling constant of 12.2 Hz, is assigned to the H-4 and H-3 protons of the TT form, respectively. Upon thermal back reaction, the signals for both TC and TT decrease, and finally disappear, while the signals for the closed form increase.

^{1}H NMR spectra of naphthopyran **71** upon reaching the PSSs is showed in Figure 3.29.

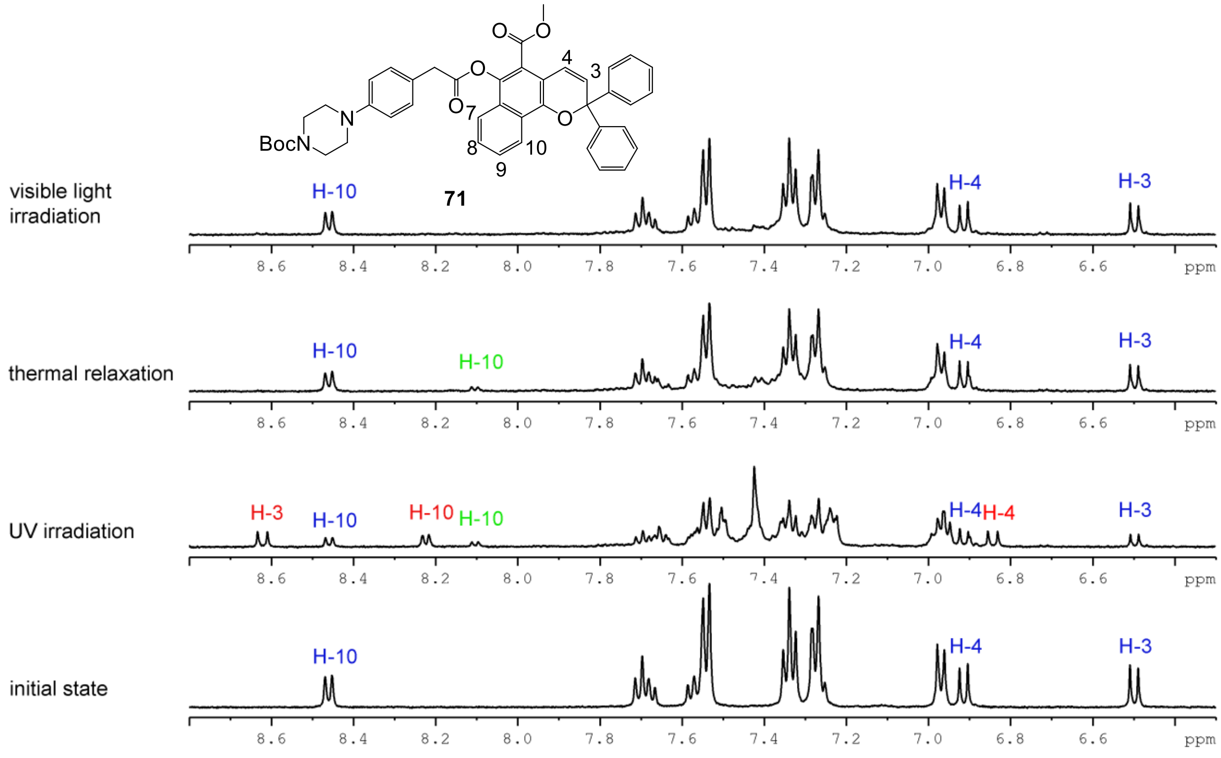

Figure 3.29. ^{1}H NMR spectra of the naphthopyran **71** in MeCN-*d3*, at 0 °C before the irradiation, upon UV irradiation and reaching the PSS(365 nm), upon thermal relaxation and reaching the PSS(Δ), and upon visible light irradiation and reaching the PSS(505 nm). The NMR assignations are colour coded as following: CF (blue), TC (red), and TT (green).

Before the UV-light irradiation, the system of two doublets at 6.50 and 6.91 ppm, with a vicinal coupling constant of 10 Hz was assigned to H-3 and H-4 of the closed form, respectively. Furthermore, the signal found at 8.46 ppm for the closed form (*J* = 8.4 Hz) is assigned to H-10. Upon the UV-light irradiation and formation of the open forms, the new system of doublets appear at 8.62 and 6.84 ppm, with a vicinal coupling constant of 11.9 Hz, assigned to the H-3 and H-4 of the TC form. However, due to the overlap of several aromatic signals, it was not possible to identify the H-3 and H-4 protons for the TT form. Furthermore, upon the UV-light irradiation, this signal at 6.46 ppm decreases in intensity, while the doublets at 8.22 (*J* = 7.8 Hz) and 8.10 ppm (*J* = 7.8 Hz) increase, assigned to the H-10 for TC and TT form, respectively.

During the thermal relaxation, the signals assigned to the TC form decrease, and finally disappear from the spectra. At the PSS(Δ) only signals assigned to the closed form and the TT form are observed. Irradiation with visible light (λ_{irr} = 505 nm), leads to TT back reaction towards the TC form, which finally forms the closed form. The finally obtained ^{1}H NMR spectra show only signals assigned to the closed form.

Table 3.8. Peak assignment, position and coupling constant in ^{1}H NMR, of the three photoisomers, of naphthopyran **45** and **71** in acetonitrile-*d3* at 0 °C.

Compound	**Assigned proton in NMR**	**Proton position** (ppm) **[Coupling constant** (Hz)**]** CF	TC	TT
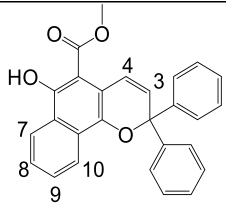 **45**	3	6.44 [10]	8.04 [12]	7.06 [12.2]
	4	7.48 [10]	-	6.85 [12.2]
	7	8.30 [8.2]	8.06 [8]	-
	10	8.45 [8.2]	8.17 [7.8]	-
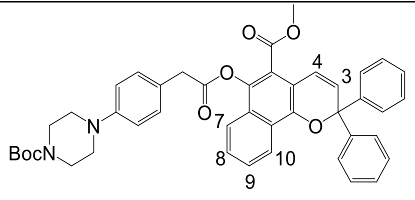 BocN N O O O O O 4 3 7 8 9 10 **71**	3	6.50 [10]	8.62 [12.2]	-
	4	6.91 [10]	6.84 [12.2]	-
	10	8.46 [8.4]	8.22 [7.8]	8.10 [7.8]

In order to follow the kinetics of the switching process, the ^{1}H NMR spectra were taken periodically in regular intervals, during the switching process at 0 °C (Figure 3.30). Gradual change of signal integrals is observed during different parts of the photochemical cycles (A-C), which allows determination of the photoisomers ratio over time.

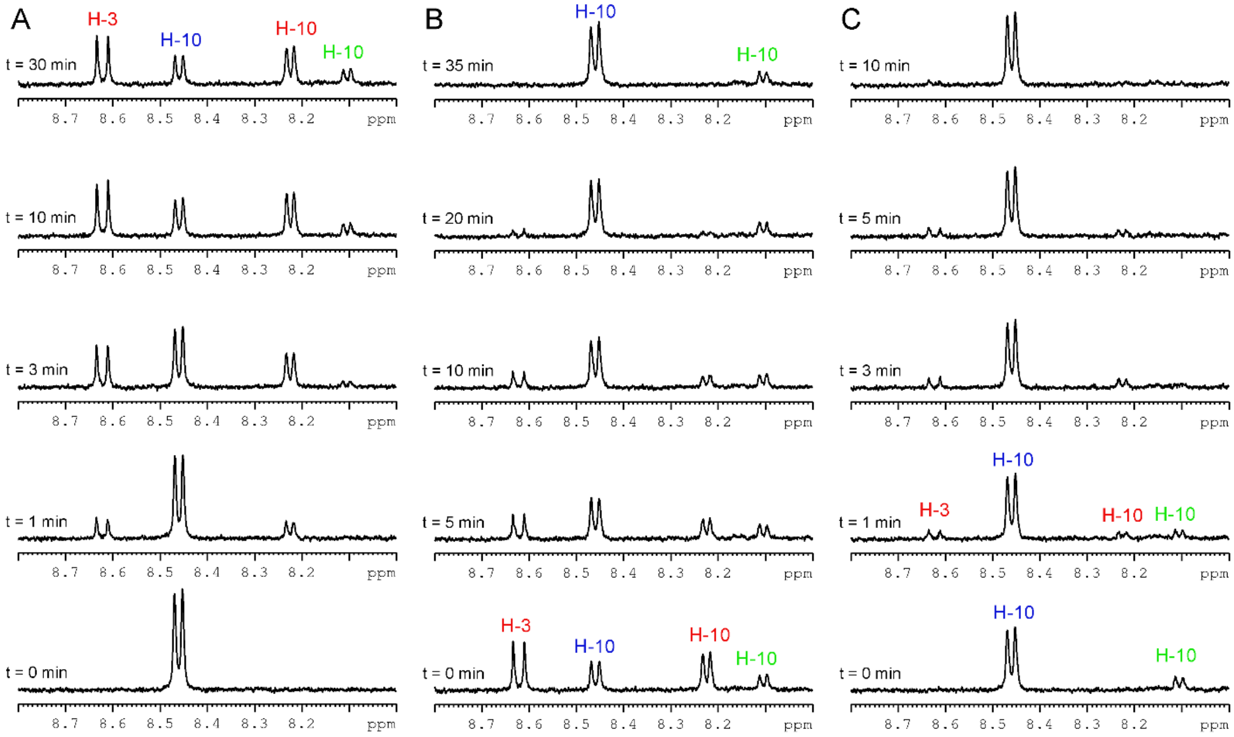

Figure 3.30. Zoom of the ^{1}H NMR spectra of naphthopyran **71**, taken periodically at 0 °C, in order to follow the peak integral changes during (A) UV light irradiation, (B) thermal relaxation, and (C) visible light irradiation. The NMR assignations are colour coded as following: CF (blue), TC (red), and TT (green).

The time-resolved spectra were obtained by plotting the signal integrals over time (Figure 3.31). For the time-resolved analysis, the peaks in the ^{1}H NMR spectra needed to show no overlapping with the neighboring signals. For both naphthopyran compounds, it can be observed that upon UV-light irradiation, the signals for CF decrease in intensity, while signals for both TC and TT increase. For naphthopyran **45**, the thermal back reaction TC→CF is drastically slowed down, as previously observed during the UV/Vis investigations. During the thermal back reaction, gradual decrease of the signals for both TC and TT form is observed, while the signals for closed form increase. A strong stabilization of the open forms is observed (hydrogen bonding), and thus both TC and TT form simultaneously revert back to the closed form.

In the case of naphthopyran **71**, during the thermal relaxation in the dark, signals for CF increase, and TC decrease, due to the spontaneous TC→CF reaction; however, the intensity of the TT signals remain unchanged. At the PSS(Δ), only the closed form and more stable open form, TT, are present. Finally, by irradiation with the 505 nm light, TT undergoes conversion to TC form at first, which is observable as simultaneous increase of the TC signal and decrease of the TT signal. Over time, both decrease, while the CF intensity increases. The ratios of the photoisomers at PSSs at 0 °C are presented in Table 3.9.

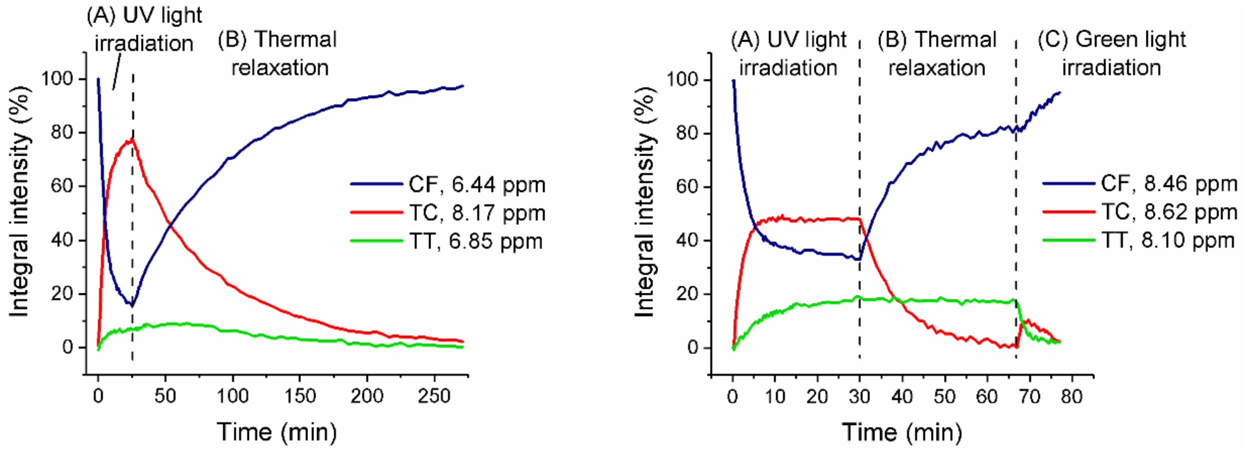

Figure 3.31. Time-resolved ^{1}H NMR spectra during the switching experiment of naphthopyrans **45** (left) and **71** (right) in MeCN-*d3* at 0 °C.

Table 3.9. Calculated ratios of different photoisomers of naphthopyrans **45** and **71** (10^{-2} M), upon reaching the photostationary states, in MeCN-*d3* at 0 °C, obtained from the NMR data.

Compound	Photostationary state	Ratio CF:TC:TT
45	PSS(365 nm)	16:77:7
71	PSS(365 nm)	34:48:18
	PSS(Δ)	83:0:17

It is significant to address the greater stabilization of the open forms present for the compound **45**, as previously observed during the UV/Vis measurements. From the determined ratios of the photoisomers, we can observe that there is almost twice the amount of closed isomer at the PSS(365 nm) of compound **71** compared to **45**. Additionally, the ratios between the TC and TT isomers at the PSS(365 nm) further emphasize the influence of the stabilization. In the case of compound **45**, the firstly formed TC isomer is strongly stabilized (via hydrogen bonding), thus further transformation to the TT form occurs at a lower rate, yielding the tenfold ratio between the open isomers. For conjugate **71**, the ratio between open isomers is ~2.5. Therefore, the stabilization attributed to both resonance and hydrogen-bonding effects, favors not just the open to the closed isomer, but also the TC to the TT isomer.

3.2.3.3 FTIR Solution Photochemical Studies of the Naphthopyran Compounds

Photochemical studies in solution were performed in a concentration of the photoswitch of $3\cdot 10^{-2}$ M in the following solvents: TCE, MeCN, and DCE. Different solvents are chosen due to their different properties (Table 3.10). All photochemical studies were performed in two cycles.

Table 3.10. Some physical properties of the solvents used for the IR photochemical studies in solution.

Solvent	**Dielectric constant** (20 °C)	**Polarity/ polarizability index** (π*)	**Viscosity** (cp, 20 °C)	**Boiling point** (in °C)
TCE	2.5	0.28	0.89	121
MeCN	37.50	0.75	0.37	82
DCE	10.36	0.81	0.79	83

The initial state of the naphthopyran **45** in all three used solvents show significant peaks in the carbonyl region, at 1655 cm^{-1}, due to the methyl-ester functionality (TCE, Figure 3.32). The position maximum of the peaks is shifted to lower wavenumbers compared to peak positions expected for the esters of aromatic acids (1740-1705 cm^{-1})[136], because of intramolecular hydrogen bonding with the *o*-hydroxyl group.[a] The peak of smaller intensity, observed at 1719 cm^{-1} in MeCN (most polar of the solvents), but not in DCE and TCE, is assigned to the non-hydrogen bonded ester carbonyl vibration. The peak at ~1448 cm^{-1} is due to the asymmetric bending vibration of the CH_3 residue of the methyl ester. Signal assignments are listed in Table 3.11.

---

[a] Ref. 136, page 115.

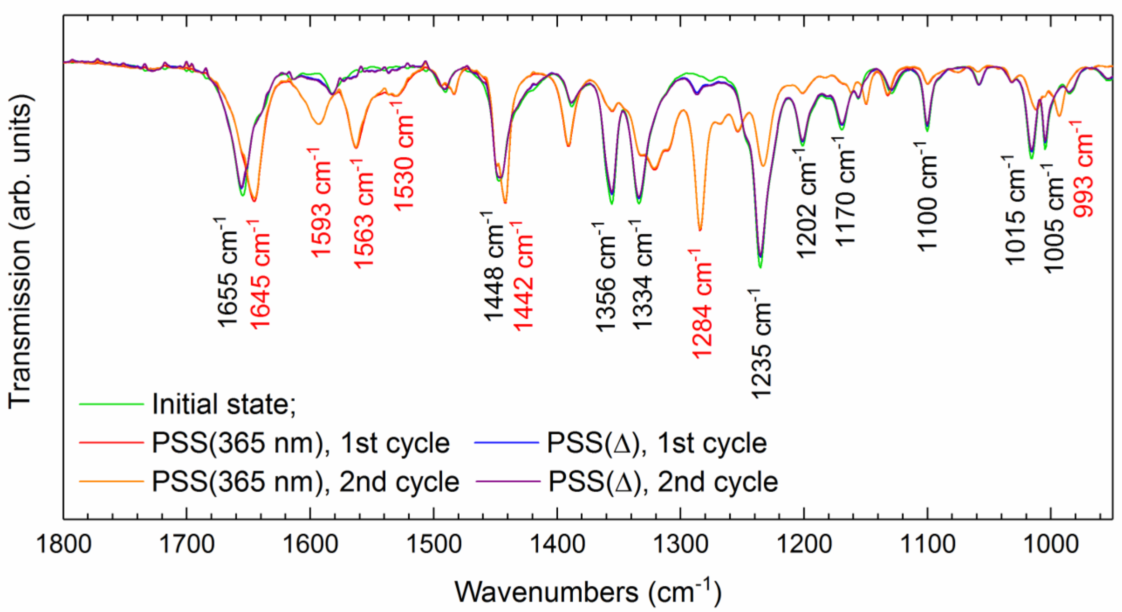

Figure 3.32. FTIR solution spectra of photoswitching of naphthopyran **45** in TCE, over two cycles; UV light irradiation (λ_{irr} = 365 nm) time 10 minutes, thermal relaxation time 30 minutes. The initial state (green), PSS upon UV-light irradiation in the 1st (red) and 2nd (orange) cycle, and PSS upon thermal relaxation in the 1st (blue) and 2nd (purple) cycle.

Upon irradiation with UV light (λ_{irr} = 365 nm), three additional peaks appear at the PSS(365 nm), at 1593, 1563 and 1530 cm^{-1}, assigned to the C=C stretching vibration of the conjugated double bonds and extended conjugation including the naphthalene ring.[a] The band that would be assigned to the ketone vibration, which is expected upon ring-opening reaction, cannot be observed, due to the overlapping of the very strong ester band at ~1650 cm^{-1}. Both the ν(C=O) and $\delta(CH_3)$ absorption bands of the ester bond experience a shift to lower wavenumbers upon switching to the open forms, to 1645 and 1442 cm^{-1}, respectively (this behaviour is observable in all three different solvents, and thus does not depend on the solvent properties). This shift of the ester band may be due to different ratio of superpositioned bands in the two PSSs (ester and ketone), and/or stronger hydrogen bonding of the *o*-hydroxyl group upon extended conjugation in the ring-opened forms. Two peaks assigned to bending and in-plane deformation of the phenol O-H bond, observable at 1356 and 1334 cm^{-1} at the initial state, are both shifted and decreased in intensity upon UV irradiation, observable at 1336 and 1321 cm^{-1}, respectively. The absorption band at 1284 cm^{-1}, observable only in the PSS(365 nm) is the ketone ν(C-CO-C) band, thus confirming the formation of ketone in the ring-opened forms. Additionally, the broader peak of the ester carbonyl in MeCN, compared to other solvents comes from the water impurities in the solvent, due to O-H bending vibrations observable as a shoulder at ~1640 cm^{-1}. The significant changes of the signals between the PSSs are presented in Table 3.11.

---

[a] Ref. 136, Table 3.1.

Table 3.11. Significant changes of the IR absorption bands and their assignments upon light illumination of naphthopyran **45** in TCE. Both changes in intensity or the position of the bands are presented.

IR Absorption bands (cm^{-1})		**Assignment**	**Literature**[136]
Initial, PSS(Δ)	**PSS(365 nm)**		
1655	1645	ν(C=O) ester, H-bonded [a]	~ 1650 (s)
-	1593	C=C conjugated with C=C or C=O	1660-1580 (s-m)
-	1563	C=C conjugated with C=C or C=O	(1600-1500) (v)
-	1530		
1448	1442	$\delta_{as}(CH_3)$ bending	1475-1445 (m-s)
1356	1356	COH bending (phenol)	1410-1310 (s)
1334	1321	in-plane O-H def vib (phenol)	1410-1310 (s)
1286	1284	ν(C-CO-C) aryl ketone	~ 1300 (m)
1235	1233	ν_{asym}(C-O-C) ester	1275-1185 (s)

The initial state of the naphthopyran **71** shows three absorption bands in the carbonyl region: at 1773, 1729 and 1703 cm^{-1}, assigned to phenylacetic acid ester, aromatic methyl ester and the carbamate protection group (TCE, Figure 3.33A). Upon irradiation with 365 nm light, only small changes in intensities and positions of certain bands are observable. The new band at 1650 cm^{-1} is assigned to the conjugated ketone carbonyl vibration (this band is not observable in MeCN, due to the O-H bending vibrations of the water impurities). Additionally, two bands are observable in the aromatic stretching region, at 1595 and 1545 cm^{-1}, assigned to extended conjugation of the C=C double bond and the naphthalene ring, respectively.[a] Slight changes in the intensity in different photostationary states were observable for the signals at 1288 cm^{-1} (increase due to ν(C-CO-C) aryl ketone), and decrease of the signal at 1227 cm^{-1} (ν_{as}(C-O-C) ester), comparable to the changes observed for the naphthopyran **45**. The significant changes of the signals between the PSSs are presented in Table 3.12.

---

[a] The -CH=CH- in conjugation with aryl moiety, shows a vibration of a medium intensity in the range 1640-1610 cm^{-1}.[136] However, this band is only observable as a shoulder of a more intense C=O stretching vibration.

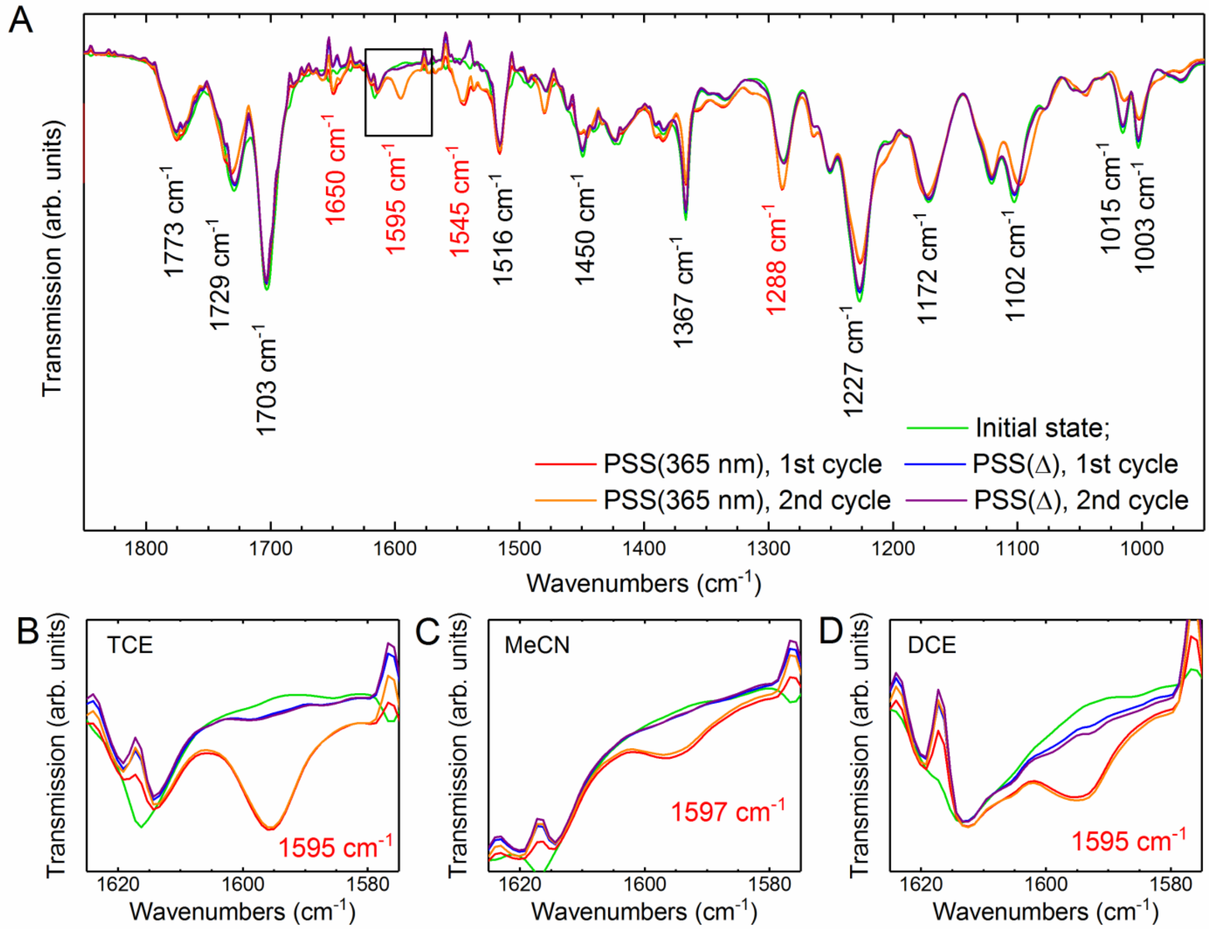

Figure 3.33. FTIR solution spectra of photoswitching of naphthopyran **71** in TCE (A), over two cycles; UV light irradiation (λ_{irr} = 365 nm) time 10 minutes, thermal relaxation time 20 minutes. The initial state (green), PSS upon UV-light irradiation in the 1st (red) and 2nd (orange) cycle, and PSS upon thermal relaxation in the 1st (blue) and 2nd (purple) cycle. The changes in the intensity of the band at ~1595 cm^{-1}, in different solvents: TCE (B), MeCN (C), and DCE (D).

The negative peaks at 1617, 1577, 1570, 1559 and 1540 cm^{-1} are observed for all three different solvents, and show increase in the intensity over time (Figure 3.33). These negative peaks are caused by the decreased s/n ratio (higher noise in this region of the spectra) caused by the water adsorbed on the detector. Because of this reason, it is not possible to accurately analyze changes in the intensity of the peak at ~1546 cm^{-1} related to the switching of naphthopyran, since the noise signals influence the shape and intensity of this band. However, this influence of the noise is not observed for the band at ~1595 cm^{-1}, and thus we used changes in the intensity of this band to analyze the switching process in solution.

---

[a] Ref. 136, Table 3.1.

Table 3.12. Significant changes of the IR absorption bands and their assignment upon photochemical study of naphthopyran **71** in TCE. Both changes in intensity or the position of the bands are presented.

IR Absorption bands (cm^{-1})		**Assignment**	**Literature**[136]
Initial, PSS(Δ)	**PSS(365 nm)**		
1773	1775	ν(C=O) phenyl ester	1800-1750 (s)
1729	1731	ν(C=O) methyl ester	1740-1705 (s)
-	1650	ν(C=O) ketone conjugated	1680-1650 (s)
-	1595	-C=C- aromatic ring str extended conjugation	(1600-1500) (v)
-	1545		
1288	1289	ν(O-C(aromatic))	1310-1230 (s)
1227	1227	ν(C-O-C) ester	1275-1185 (s)

Additionally, the lower ratio of open-to-closed forms at PSS(365 nm) for the naphthopyran **71**, compared to **45**, previously observed in the ^{1}H NMR, is observable due to smaller changes in the IR signature upon photochemical switching of the compound.

The photochemical process of naphthopyran-linker conjugate **71** can be monitored by following the changes in the intensity of the band at 1595 cm^{-1} (Figure 3.33). The intensity of the band increases with the UV-light irradiation, and decreases during the thermal relaxation. As previously observed in the NMR study, accumulation of the TT form occurs due to a slow TT→TC reaction under these conditions. Thus, upon 20 min of thermal relaxation, in none of the solvents, complete return to the initial state was observed.

The methyl-ester ν(C=O) band at 1729.2 cm^{-1} (in TCE) experiences a shift to higher wavenumbers upon UV irradiation, observable at 1731.4 cm^{-1}, and upon thermal relaxation, this band shifts back to 1728.7 cm^{-1}. This blue shift upon UV irradiation, and the red shift upon thermal relaxation is observable in all three used solvents, suggesting that the shift is not influenced or assisted by any of the solvent properties, but due to changes in the vibration energies of the naphthopyran itself (Figure 3.34 B). The repeatable shift in the position of the methyl-ester ν(C=O) band is also observable for the naphthopyran **45** upon photochemical studies in different solvents (Figure 3.34A).

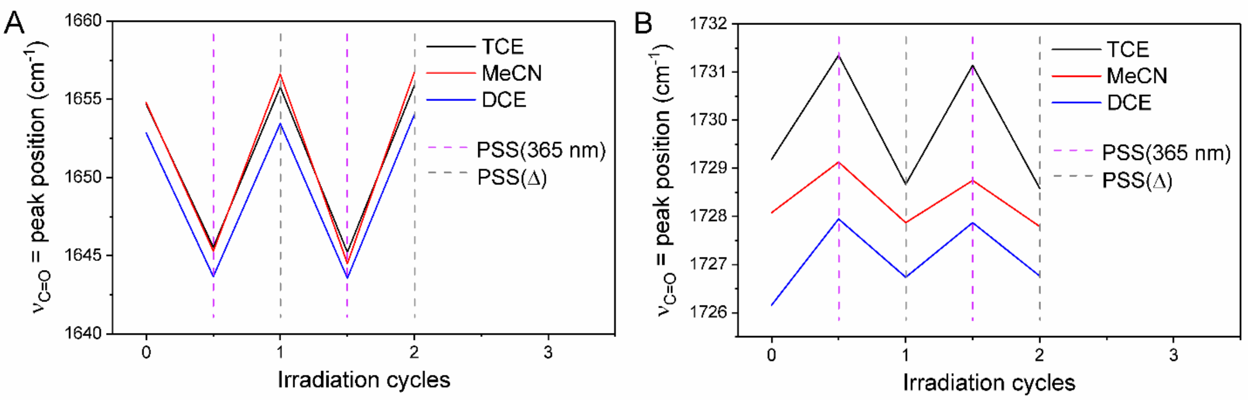

Figure 3.34. Repetable changes of the ν(C=O) methyl-ester absorption band position of naphthopyrans **45** (A) and **71** (B), upon UV-light irradiation and thermal relaxation, over two cycles, in TCE (black), MeCN (red), and DCE (blue). Dotted lines represent the PS states, upon UV-light irradiation (pink) and thermal relaxation (grey).

Additionally, for naphthopyran **71**, there is a correlation between the average ν(C=O) band positions (in both photostationary states) and the used solvents, which goes along with the solvent index of polarity/polarizability (π*), and measures the ability of the solvent to stabilize a charge or a dipole.[137] The stabilization of the dipole decreases the vibration frequency and shifts the ν(C=O) absorption band to lower wavenumbers. The higher this index is, the better the solvent stabilizes the C=O dipole, and the band at lower wavenummber is observed. However, this correlation between the π* and ν(C=O) band positions is not observable for the naphthopyran **45**, due to the methyl-ester bond being already highly stabilized by hydrogen-bonding to the free hydroxyl group in the *orto*-position.

4 Photoswitchable Self-Assembled Monolayers on Silicon Surfaces

4.1 Preparation and Functionalization of SAMs on Si(111) Surfaces

Hydrosilylation reaction allows for easy functionalization of the hydrogen-terminated silicon surfaces with an unsaturated bond, i.e. carbon-carbon, carbon-oxygen (mainly alkene, alkyne, and aldehyde).[39] The reaction has been shown to be mediated thermally or photochemically, in order to prepare a surface radical, which reacts with an unsaturated bond in order to form a Si-C bond. The proposed mechanism of the hydrosilylation reaction starts at radical cation at the Si surface (Figure 4.1).[138] The reaction with the unsaturated carbon-carbon bond leads to formation of the carbon-centered radical, the intermediate state, which may abstract hydrogen atom from the neighboring surface Si-H bond, creating a new dangling bond and a stable Si-C bond.[139–141] The formed dangling bond proceeds the reaction via the radical chain mechanism.

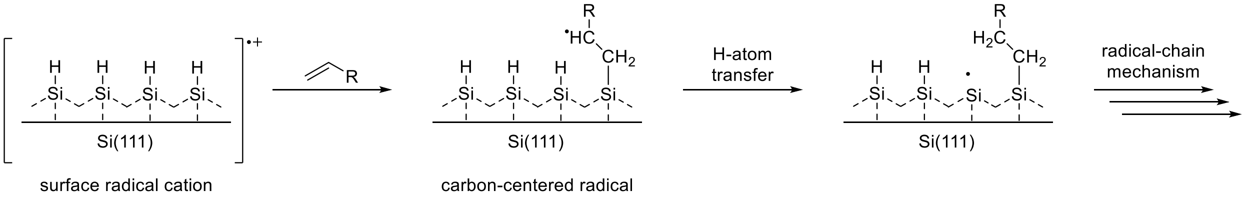

Figure 4.1. Proposed mechanism of the monolayer formation on the H-terminated Si(111) surface.

The formed monolayers are thermodynamically and kinetically stable, due to the stability and strength of the covalent Si-C bond. Thus, side reactions or degradation due to the oxidation are not likely to occur. Additional advantage is the existence of only one coupling point between surface and each monolayer molecule attached, which ensures no multilayer or irregular structure formation, coming from the hydrosilylation reaction itself. The main disadvantage of this approach is the difficulty in avoiding oxidation of the surface; thus the procedure requires working under inert atmosphere and use of dried and degassed chemicals.

The choice of the functionality at the terminal end of the monolayer molecule is crucial for the preparation of high quality densely packed SAMs, as well as for the further functionalization of the surface. One of the limiting factors is the reactivity of the H-Si bond of the hydrogen-terminated surface towards variety of functional groups, e.g. alcohols[142,143], aldehydes[142–144], carboxylic acids[145–148], amines[149], etc. SAMs preparations using the carboxylic acid functionality at the terminal end have been previously reported, however they do, in low level, show also the reverse attachment to the surface, competing with the preferred reaction between CH_2=CH- and the substrate, leading to Si-O(CO)R bond formation.[145,146] Compared to the SAMs prepared from the ester-functionalized monolayer molecules, these structures also show lower level of ordering and packing on the surface.[150,151] Additionally, the direct grafting of the monolayer molecules with a carboxy-functionalities at the terminal end may form dimers during the process, thus induce formation of a bilayer structures on the surface.[148] Thus the ester grafting, and subsequent hydrolysis, makes a better synthetic approach. Furthermore, preparation of the high-quality diluted monolayers, by mixing the carboxy-terminated monolayer with an alkene (e.g. 1-decene), proved to challenging due to the segregation of the structures on the surface.[152] The dilution of surface functional groups allows formation of the less crowded functionalities at the terminal end of the monolayer, which showed to be especially beneficial for the sterically demanding reactions at the terminal end.[153] Additionally, the dilution may change the properties of the surface at the terminal end, i.e. polarity, and thus provide different immediate environment for the attached photoswitch-linker conjugate.

In the group of Rück-Braun, the procedures for the formation of the SAMs on Si(111) have been already established and the obtained monolayers characterized, including both neat and diluted carboxy-terminated monolayers, obtained via hydrolysis of the ester-terminated SAMs.[13,14,65,82] The neat self-assembled monolayers are prepared by grafting of methyl 10-undeceonoate, while for the diluted SAMs the methyl 10-undecenoate is mixed with 1-decene, and as a mixture grafted on the surface via thermal hydrosylilation reaction; the following hydrolysis under acidic conditions yields carboxy-terminated monolayers. This way prepared carboxy-terminated monolayers were used for coupling of alcohols and amines, using HCTU as a coupling reagent, towards formation of ester[65] and amide[14] bonds on the surface, respectively. In this work, the carboxy-terminated surfaces were coupled with both primary and secondary amine photoswitch-linker-conjugates, towards preparation of the amide-bond coupled photoswitchable surfaces on Si(111).

4.1.1 Formation of Hydrogen-Terminated Si(111) Surface

Double side polished wafers (*Sil'tronix*, double side polished Si(111) ± 0.02°, FZ, n-type (P-doped) were cut in rectangle shape (1.1 cm x 2.5 cm). For preparation of ATR crystals, the shorter rim was grinded to a 45° angle, and finally polished. After cleaning in organic solvents, the wafers were ready for further use. For the preparation of hydrogen-terminated Si(111) surface, the wafer was first oxidized in *Piranha* solution (H_2SO_4 / H_2O_2, 3:1), to remove any chemisorbed or physisorbed impurities from the surface (organic and inorganic contaminants, including dust, silica, silicon and metals). In order to remove the oxide layer, the wafer was etched in 40% NH_4F aq. solution,[154,155] to which 50 mM ammonium sulfite monohydrate was added as an oxygen scavenger[156]. This allowed for anisotropic etching of the surface, resulting in no defect structures, steps and islands.[148] Thus, the obtained surface was nearly-atomically smooth, with the terrace structures, Si-H bonds being oriented perpendicular to the surface. The surface density of the Si-H bonds was determined to be $7.83 \cdot 10^{14}$ / cm^2.[148,155]

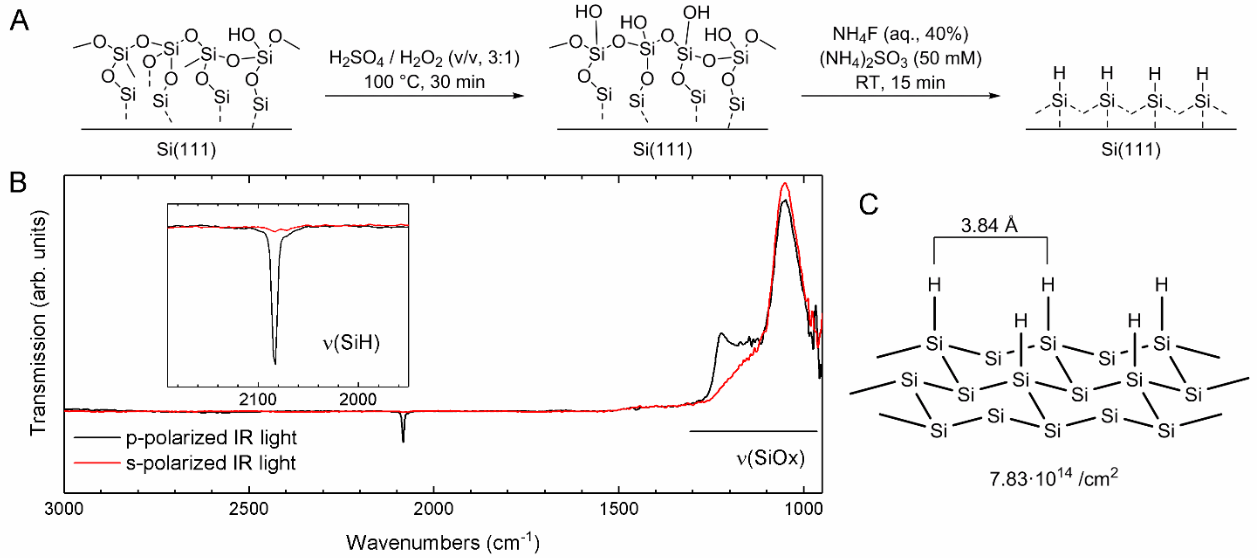
A
H_2SO_4 / H_2O_2 (v/v, 3:1)
100 °C, 30 min
NH_4F (aq., 40%)
$(NH_4)_2SO_3$ (50 mM)
RT, 15 min
Si(111)
Si(111)
Si(111)
B
Transmission (arb. units)
ν(SiH)
2100
2000
p-polarized IR light
s-polarized IR light
ν(SiOx)
3000
2500
2000
1500
1000
Wavenumbers (cm^{-1})
C
3.84 Å
$7.83 \cdot 10^{14}$ /cm^2

Figure 4.2. Hydrogen-terminated surface on Si(111). (A) Reaction conditions of the oxidation and etching reactions. (B) IR spectra of the H-terminated surface, referenced to the oxide layer, recorded in p- (black) and s-polarization (red). (C) Structure of the H-terminated Si(111) surface.

The orientation of hydrogen atoms on the surface was confirmed by the ATR-FTIR spectroscopy – the hydrogen-terminated surface, references to the Si/SiO_X, shows a single signal at 2083.7 cm^{-1} in p-polarization, responsible for the Si-H stretching vibration; no signal is observable in s-polarization mode (Figure 4.2).[148,157] The negative signals were observed for the ν(SiO_X)

absorption bands at 1055 cm^{-1} (detected by both s- and p-polarized light, transverse optical mode) and at 1226 cm^{-1} (detected only by p-polarized light, longitudinal optical mode).[158] The transverse optical mode corresponds to the vibration parallel to the plane of the oxide surface, while the longitudinal optical mode responds to vibrations that are orthogonal to this plane.

4.1.2 Formation of Carboxy-Terminated SAMs on Si(111)

Monolayers were prepared on a freshly obtained H-terminated Si surface, employing the process of thermal hydrosilylation at high temperature, in the glove box.[81] Methyl 10-undecenoate (**72**) or a mixture of methyl 10-undecenoate and 1-decene (**73**) (V/V, 1:1) were grafted, to obtain neat and diluted ester-terminated monolayers, respectively (Figure 4.3). Dilution of the monolayer reduces the concentration of functionalities at the terminal end, and allows the formation of densely packed and order monolayers compared to the neat SAMs. It is important to note, however, that the ratio of the monolayer units in the solution does not necessarily reflect the ratio on the surface, and the here given ratios are reported as the initial solution values.

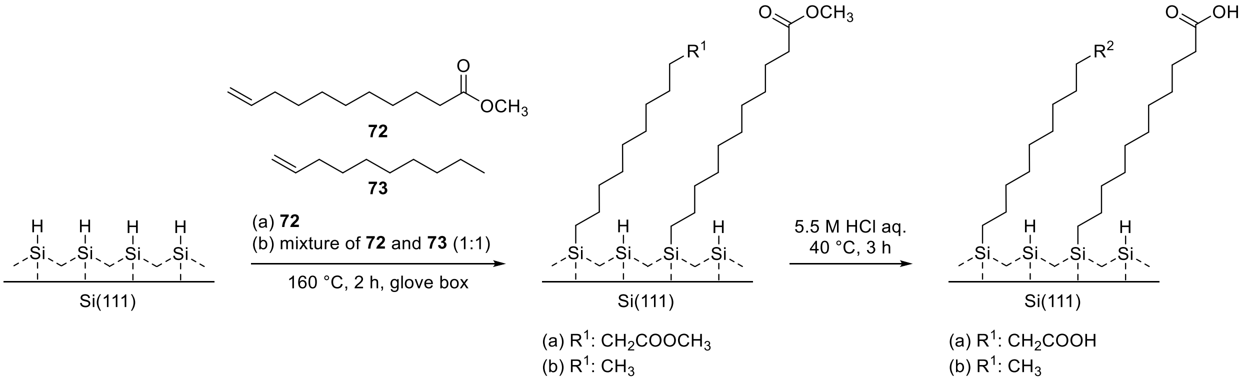

Figure 4.3. Synthetic route towards formation of (a) neat, and (b) diluted carboxy-terminated monolayers on Si(111).

Upon formation of the monolayer, the IR spectra show an intense signal at 1746 cm^{-1}, assigned to the methyl-ester carbonyl stretching vibration (Figure 4.4A). This band is expectedly of lower intensity for the diluted monolayer, due to less concentration of ester monolayer molecules on the surface, compared to the neat monolayer.

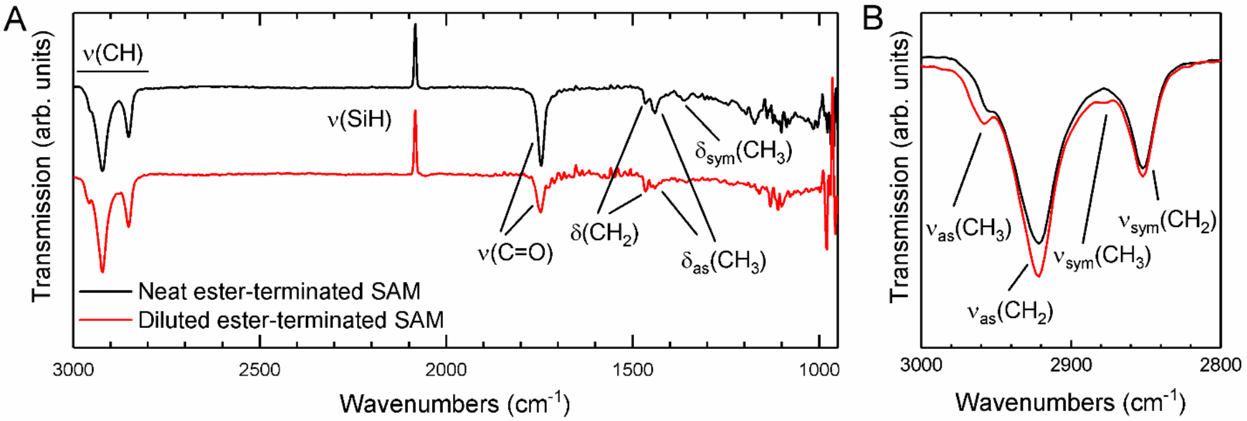

Figure 4.4. IR spectra of the neat (black) and diluted (red) ester-terminated monolayer on Si(111).

Additionally, the IR spectra shows strong signals at 2852 and 2922 cm^{-1}, which correspond to the $\nu_{sym}(CH_2)$ and $\nu_{as}(CH_2)$ absorption bands, present in both neat and diluted monolayers (Figure 4.4B). The positions of these peaks in the alkyl stretching region gives qualitative information on the ordering and packing of the monolayer – the shift of the $\nu_{as}(CH_2)$ band towards the value for the crystalline-pure alkyl-monolayer (2917 cm^{-1}) suggest better ordering of the monolayer.[159] Thus, both neat and diluted monolayers show high quality of ordered and densely packed structures. Furthermore, comparing the obtained monolayers, the signals for diluted monolayer are of slightly higher intensity (Figure 4.4B). This may be due to a higher coverage of the monolayer molecules on the surface, due to the reduced bulkiness of the functionalities on the terminal end when 1-decene is introduced. Additionally, the intensity of the $\nu_{as}(CH_3)$ and $\nu_{sym}(CH_3)$ are both higher for the diluted monolayer, which also suggests a higher concentration of the monolayer molecules on the surface. The bending CH absorption bands - $\delta(CH_2)$, $\delta_{as}(CH_3)$, and $\delta_{sym}(CH_3)$ are observed at 1466, 1440, and 1365 cm^{-1}, respectively. The absence of the signals in the Si-O stretching region (1250-1000 cm^{-1}) suggests no substrate oxidation during the thermal grafting reaction.

Finally, upon the hydrolysis of the ester functionality in a 5.5 M HCl solution (degassed with an argon stream prior to the reaction for 1 h), at 40 °C for 3 h, carboxy-terminated SAMs are obtained. The conditions for the hydrolysis reaction of the ester-terminated monolayer were previously optimized in the research group of Rück-Braun.[82] The efficiency of the reaction is evaluated by the position of ν(C=O) signal (Figure 4.5); the ν(C=O) absorption band is observed at 1714 cm^{-1}, due to formation of the carboxy-functionality upon the hydrolysis reaction, suggesting the complete hydrolysis.

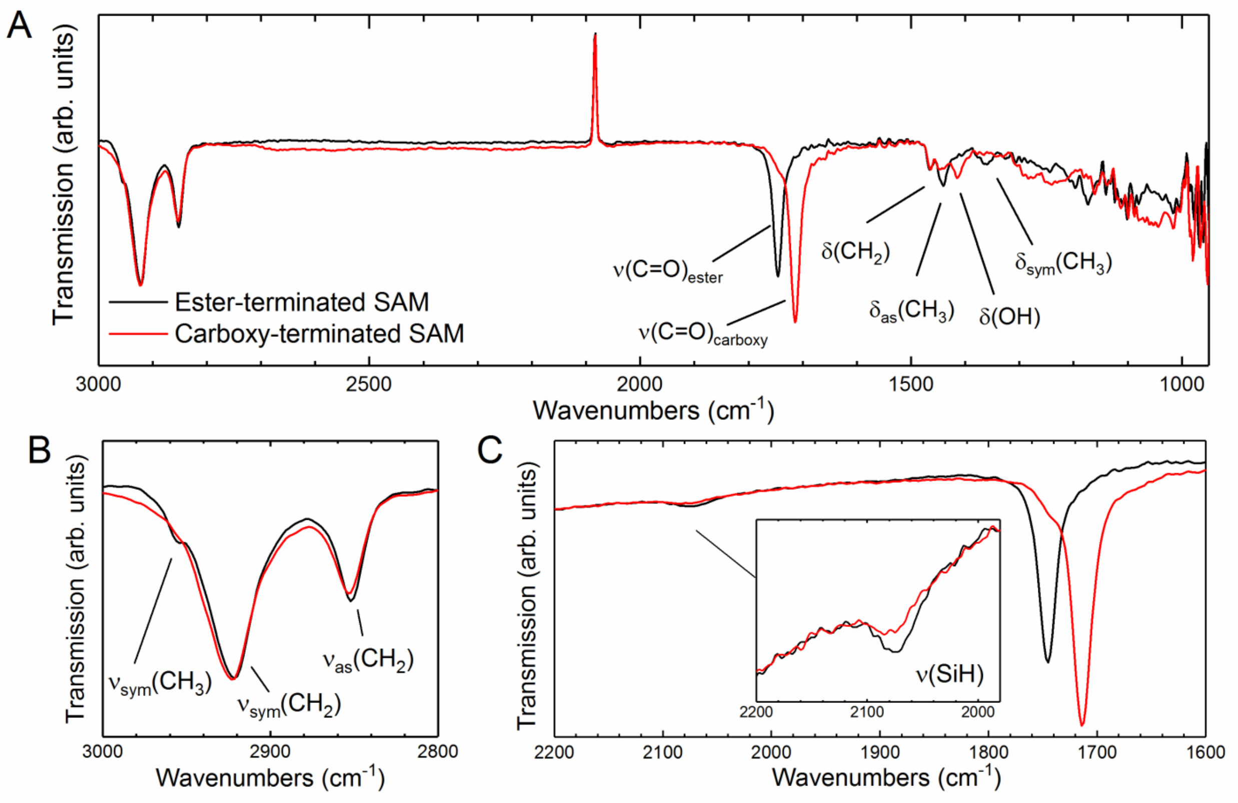

Figure 4.5. IR spectra of ester-terminated (black) and carboxy-terminated (red) SAMs on Si(111). (A) Wide range IR spectra. (B) The zoom of the alkyl stretching region. (C) The Si-H stretching region, referenced to the silicon oxide, shows the oxidation of the Si-H bond during the hydrolysis step.

In the alkyl region, the decrease in the intensity of the $\nu_{sym}(CH_3)$ of the carboxy-terminated SAMs goes along with the successful hydrolysis reaction. The comparison between the $\nu(CH_2)$ absorption bands of ester- and carboxy terminated monolayers show no changes in the monolayer structure upon the hydrolysis reaction. Additionally, the $\delta(CH_2)$ absorption band at 1466 cm^{-1}, remains unchanged after the reaction. However, both sym and as $\delta(CH_3)$ absorption bands, at 1440 and 1365 cm^{-1}, decrease in intensity, as expected. The absorption band of the $\delta(OH)$, of the carboxy-functionality, is assigned to the new signal at 1415 cm^{-1}.

The oxidation of the unreacted Si-H bonds occurs during the hydrolysis reaction. In the IR spectra, referenced to the silicon oxide, this can be observed as the decrease in the Si-H signal at 2077 cm^{-1}, upon the hydrolysis reaction (Figure 4.5C). Additionally, the slight change in the intensity of the signals in the Si-O stretching region, below 1250 cm^{-1}, suggests the oxidation of the silicon substrate.

The hydrolysis reaction of the diluted monolayers proceeds under the same conditions. The completion of the hydrolysis reaction is again confirmed by the position of the ν(C=O), for carboxy-terminated SAM assigned at 1714 cm^{-1} (Figure 4.6A). The alkyl stretching region here does not change significantly upon the hydrolysis reaction, as observed for the neat monolayer as well; the $\nu_{as}(CH_3)$ absorption band at 2958 cm^{-1} only slightly decreases in intensity, due to methyl groups still being present on the surface of the decene moieties. Similarly, the intensity of the $\delta_{as}(CH_3)$ absorption band at 1440 cm^{-1} also does not change significantly, only a slight decrease in intensity is observed, while the $\delta(CH_2)$ at 1463 cm^{-1} stays unchanged as observed for the neat SAMs. Furthermore, the signal of the δ(OH) absorption band is here observable at 1410 cm^{-1}.

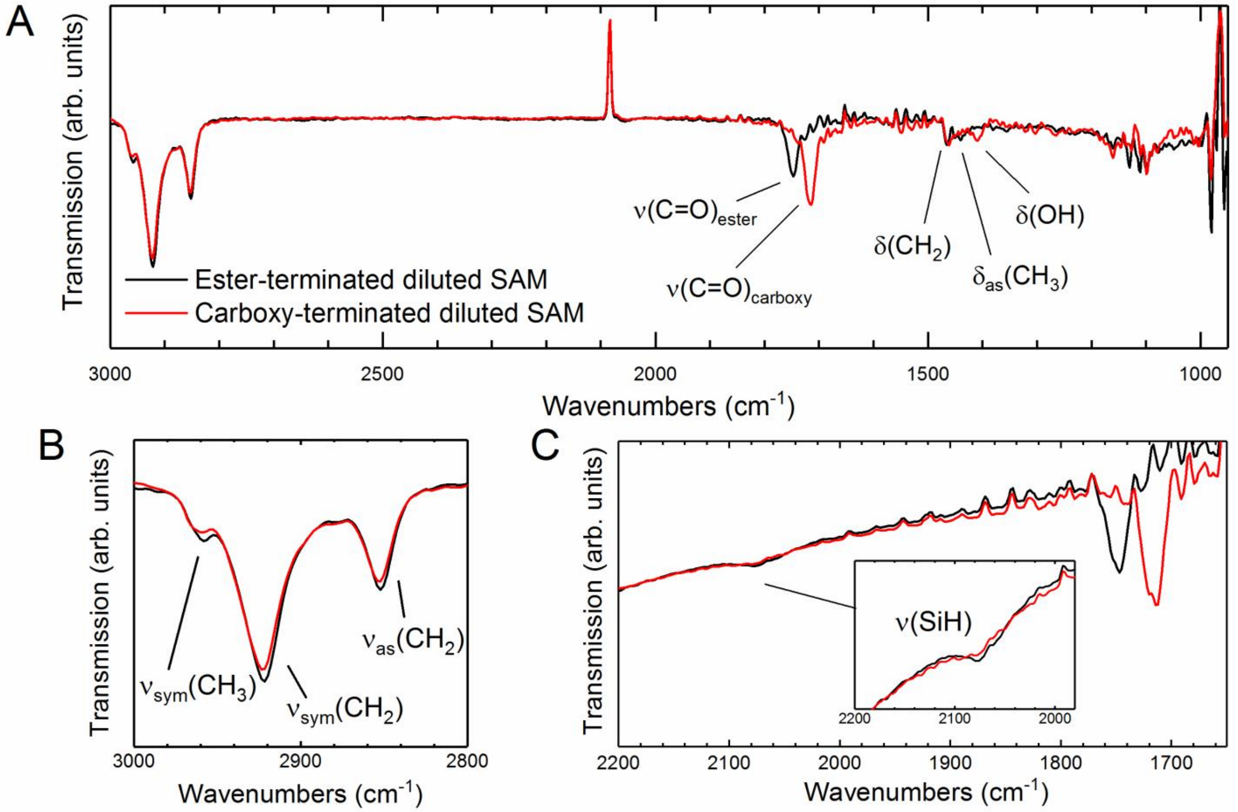

Figure 4.6. IR spectra of ester-terminated (black) and carboxy-terminated (red) SAMs on Si(111). (A) Wide range IR spectra. (B) The zoom of the alkyl stretching region. (C) The Si-H stretching region, referenced to the silicon oxide, shows the oxidation of the Si-H bond during the hydrolysis step.

Only slight oxidation of the substrate is observable, due to the changes in the Si-O stretching region (below 1250 cm^{-1}, Figure 4.6B), as well as the Si-H signal referenced to the silicon oxide, at 2077 cm^{-1} (Figure 4.6C).

4.1.3 Functionalization of Carboxy-Terminated SAMs via Amide Bond Formation Reaction on Si(111)

The Si(111) wafers were further functionalized via the amide-bond formation, coupling the amine photoswitch-linker-conjugate to the carboxy-functionality at the terminal end of the monolayer, using HCTU as a coupling reagent, under inert conditions (glove box). Fulgimide-linker conjugate **7** immobilization was carried out on both neat and diluted SAMs, following the procedure by Michalik.[81]

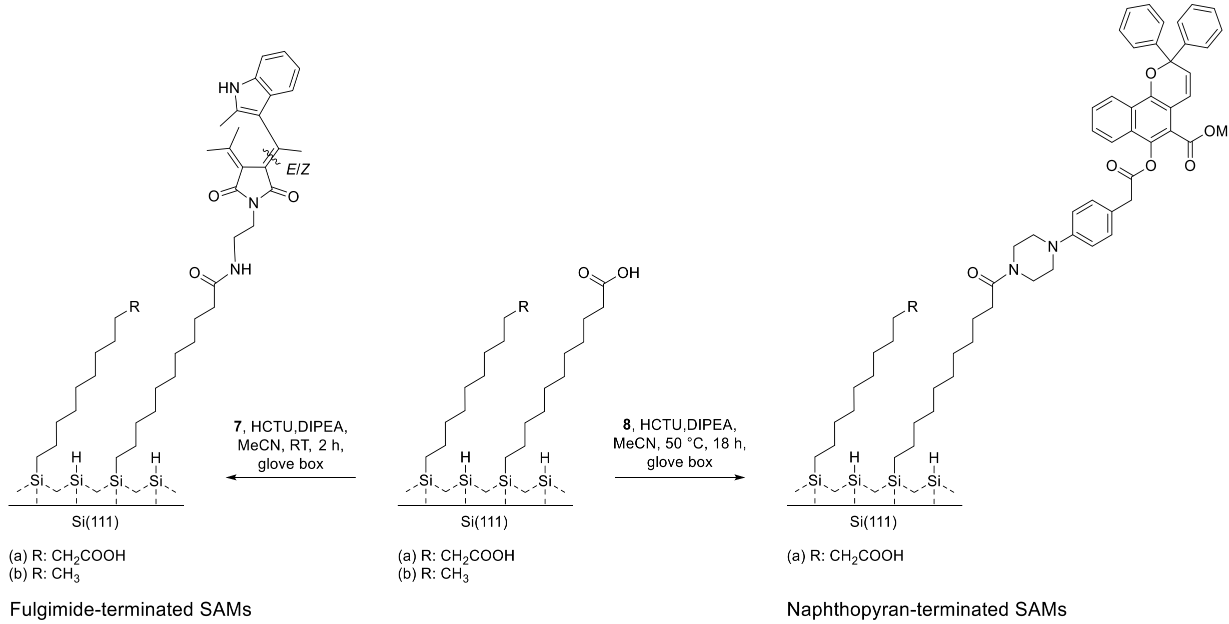
HN
E/Z
O
N
O
O
NH
R
H
H
Si
Si
Si
Si
Si(111)
(a) R: CH$_2$COOH
(b) R: CH$_3$
Fulgimide-terminated SAMs
7, HCTU,DIPEA,
MeCN, RT, 2 h,
glove box
O
OH
R
Si(111)
(a) R: CH$_2$COOH
(b) R: CH$_3$
8, HCTU,DIPEA,
MeCN, 50 °C, 18 h,
glove box
O
OMe
O
O
O
N
N
O
R
Si(111)
(a) R: CH$_2$COOH
Naphthopyran-terminated SAMs

Figure 4.7. Reaction conditions towards formation of photoswitchable SAMs on Si(111).

In order to test the coupling reaction of the secondary amine naphthopyran-linker conjugate on the surface, the coupling of the linker (Boc-protected piperazine **62**) was first tested. HCTU as a coupling reagent, at 50 °C, 5 h in glove box, proved to be effective enough for the sterically demanding piperazine secondary amine on densily packed carboxy-terinated monolayer. Additionally, HATU as a coupling reagent was also tested under the same reaction conditions, but two showed comparable results in the IR (Figure 4.8). The dominant bands assigned to the $\nu_{as}(CH_2)$ and $\nu_{sym}(CH_2)$ of the monolayer molecules, are located at 2922 and 2852 cm^{-1}, respectively. Additionally, the strong band, asymmetrical in shape, with the maximum at 1643 cm^{-1} is assigned to the amide bond, and a shoulder at 1657 cm^{-1} to the hydrogen bonded carbamate bond. The non-hydrogen bonded carbamate carbonyl bond shows a weak band at 1692 cm^{-1}. The intense band with the peak maximum at 1427 cm^{-1} is caused by bending vibrations of the CH_2 of the piperizine unit, and CH_3 of the *tert*-butyl group.

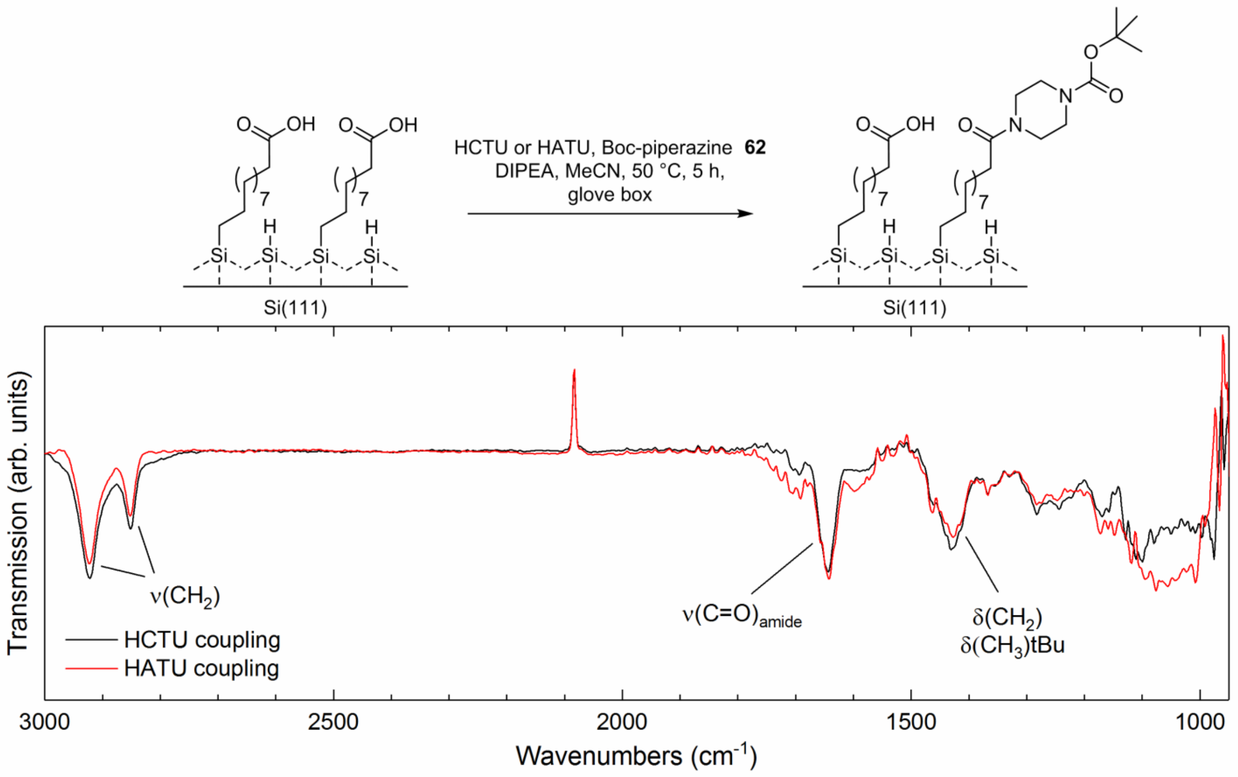

Figure 4.8. Boc-piperazine **62** test-coupling reaction to the carboxy-terminated SAMs on Si(111), using HCTU (black), and HATU (red) as coupling reagent.

Furthermore, the immobilization of the naphthopyran-linker conjugate was proceeded using HCTU, at 50 °C, over longer reaction time (18 h) in the glove box, and resulted in formation of the photoswitchable SAMs.

4.1.4 Fulgimide-Terminated SAMs on Si(111)

Fulgimide-terminated monolayers were prepared on both neat and diluted samples on Si(111). For immobilizations of fulgimide-linker conjugate **7** (*E*/*Z*, 85:15) on both neat and diluted SAMs, the same reaction conditions were employed (HCTU, DIPEA, room temperature, 2 h, in glove box). Samples were washed with acetonitrile and DCM, and stored under argon.

Upon immobilization of the fulgimide-linker conjugate on the neat SAMs, the alkyl stretching region does not change significantly (Figure 4.9). The peak positions of both $\nu_{as}(CH_2)$ and $\nu_{sym}(CH_2)$, observed at 2922 and 2852 cm^{-1}, respectively, do not change, suggesting that the densely packed monolayer is not disturbed by the photoswitch attachment reaction. Additionally, the signals slightly increase in intensity after the coupling reaction, which is expected due to the added methylene moieties of the ethylene diamine linker.

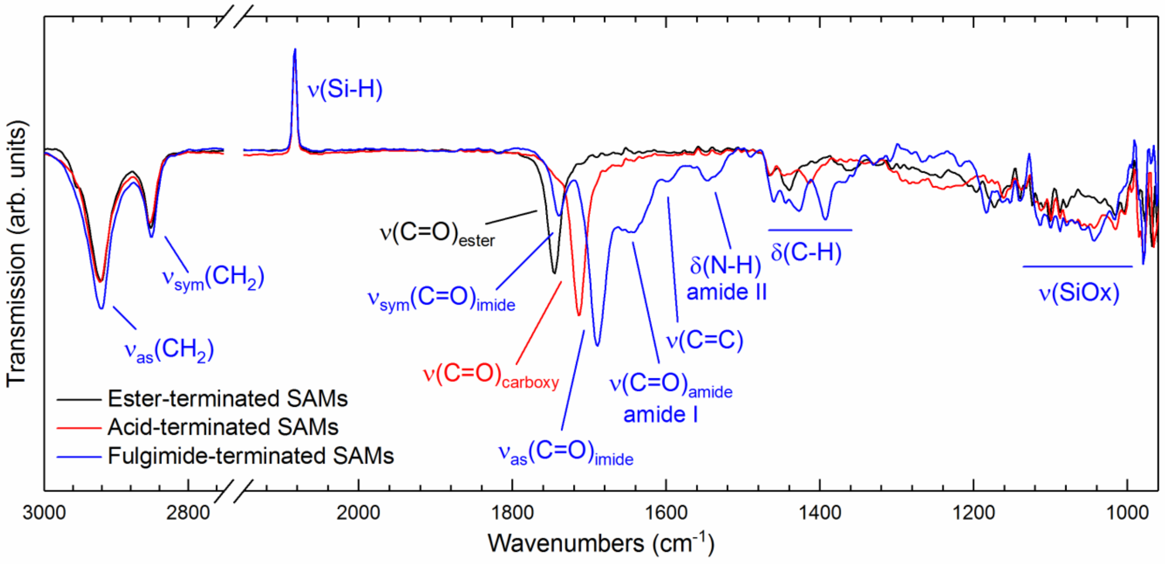

Figure 4.9. IR spectra of neat ester- (black), carboxy-(red), and fulgimide-terminated SAMs on Si(111), referenced to the spectrum of H-Si(111).

The ν(C=O) absorption band of the newly formed amide bond, also known as amide I vibration, is located at 1649 cm^{-1}. In concentrated samples, this band is observable in the region 1680-1630 cm^{-1}, due to the hydrogen bonding between the amide bonds.[a]

---

[a] For dilute solutions, when the amide bond does not participate in hydrogen bonding, the amide I band is observable in the region 1700-1665 cm^{-1}.[136]

Hydrogen bonds decrease the C=O bond frequency, and thus the band is observed at lower wavenumbers. Contrary, in the diluted monolayers, the hydrogen bonding is not present due to reduced amount of carboxy-functionalities on the surface, and the band is observed at the higher wavenumbers. Here, it is assumed that the densely packed structure with fulgimide head-groups on the surface is obtained, with hydrogen-bonds formed both between the photoswitch units and with unreacted carboxy-functionalities on the surface. Amide II band is mainly responsible for the N-H bending motion, combined with the C-N stretching vibration, here observed at 1547 cm^{-1}. The imide functionality usually exhibits two absorption bands, being assigned to symmetric and asymmetric stretching vibrations of the C=O bonds.[160] An intense signal at 1689 cm^{-1} and a weaker at 1739 cm^{-1} are assigned to the ν_{as}(C=O) and ν_{sym}(C=O) imide absorption bands, respectively. The C=C stretching vibration, conjugated with either the indole ring or the imide carbonyl bond, is responsible for a weak signal at 1601 cm^{-1}; a signal ~1600 cm^{-1} is caused by the presence of an alkene conjugation.[136] Several weak bands in the region 1460 to 1360 cm^{-1} are mainly due to the different C-H deformation motions of various functionalities, including the methylene and methyl C-H bending motions, scissoring modes, and alkene C-H in-plane vibrations. A slight increase in the intensity of the bands in the 1250-1000 cm^{-1} region is due to the oxidation of the silicon substrate, during the fulgimide coupling reaction.

The IR spectra of the diluted fulgimide-terminated SAMs is shown in Figure 4.10. The intense absorption band at 1689 cm^{-1} is assigned to the asymmetric, while the weak band at 1739 cm^{-1} is assigned to the symmetric stretching vibration of the imide carbonyl groups of the fulgimide moieties. The bands at 1658 cm^{-1} and 1548 cm^{-1} are assigned to the amide I and amide II absorption bands, respectively. When compared to the neatly prepared SAMs, a shift of the amide I band is observed for the diluted SAMs, from 1649 to 1658 cm^{-1}, respectively. This goes along with the reduced amount of hydrogen bonding between the surface amide- and carboxy-functionalities, due to the dilution of the monolayer. The signal assigned to the ν(C=C) stretching vibration responsible for the presence of further alkene conjugation is observed at 1595 cm^{-1}. Additionally, several weak signals, responsible for the various C-H bending deformations, are found in the 1460-1350 cm^{-1}. The slight substrate oxidation is also observed for the diluted fulgimide-terminated monolayers, due to an increase in the intensity of the region 1250-1000 cm^{-1}.

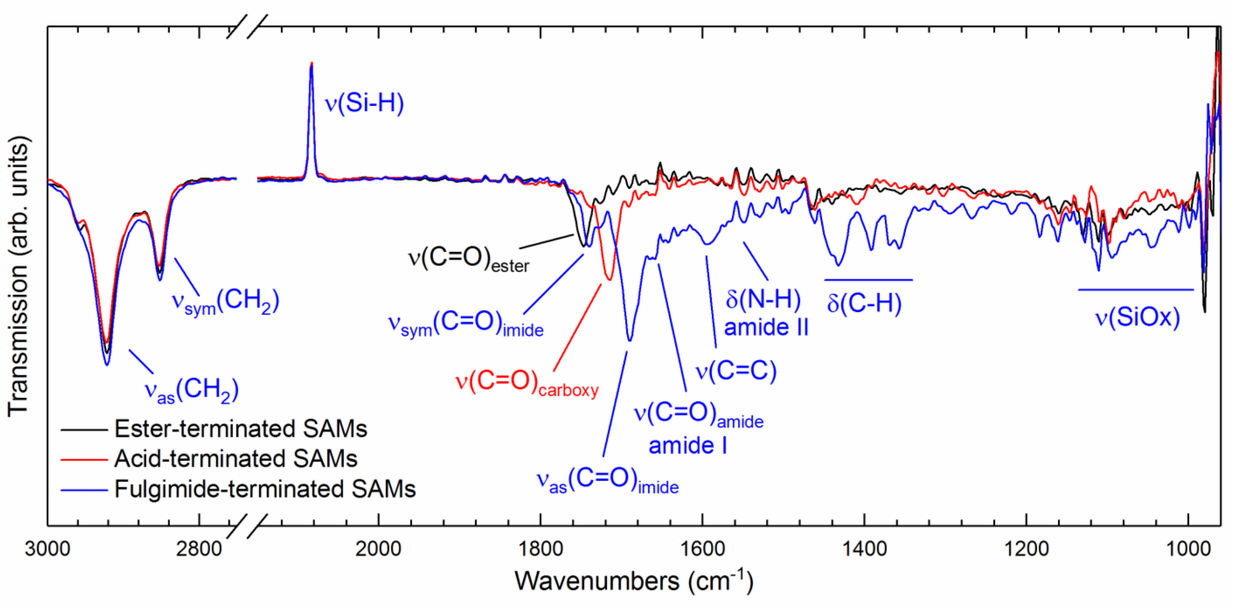

Figure 4.10. IR spectra of diluted ester- (black), carboxy-(red), and fulgimide-terminated SAMs on Si(111), referenced to the spectrum of H-Si(111).

4.1.4.1 Photochemical Studies of Fulgimide-Terminated SAMs on Si(111)

The photochemical studies of both the neat and the diluted fulgimide-terminated monolayers, were carried out via ATR-FTIR spectroscopy. Upon UV-light irradiation, the fulgimide head groups of the fulgimide-terminated monolayer were switched from the open *E*-form to the closed *C*-form. Additionally, under UV irradiation, also the *Z*-to-*E* and *E*-to-*Z* isomerization takes place (Figure 4.11). The switching of the fulgimide-terminated SAMs were conducted by alternations of UV and visible light irradiation, and the two photostationary states PSS, PSS(365 nm) and PSS(545 nm), respectively, were evaluated by ATR-FTIR spectroscopy. The switching experiments with the fulgimide head groups were carried out under inert gas atmosphere (nitrogen), and were allowed for 30 min per irradiation period. Apart from that, the samples were stored in the dark.

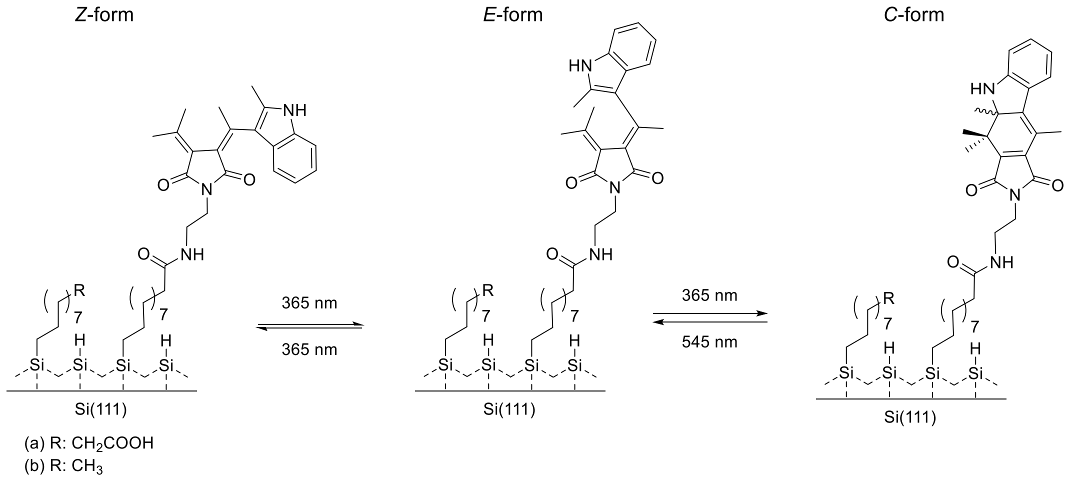

Figure 4.11. Fulgimide *Z*-to-*E* and *E*-to-*Z*, as well as *E*-to-*C* and *C*-to-*E* photochromism upon UV(365 nm) and vis(545 nm) irradiation of neat and diluted SAMs on Si(111).

Evaluation of the two photostationary states by ATR-FTIR spectroscopy is possible due to the changes in the position and intensity of the ν_{as}(C=O) imide absorption bands that fulgimide moieties exhibit upon ring-opening and –closure reactions. For the neat SAMs, upon immobilization of fulgimide-linker conjugate **7** (85:15, *E*/*Z*), the imide ν_{as}(C=O) absorption band is found at 1689.5 cm^{-1} (Figure 4.12). Upon UV light irradiation (λ_{irr} = 365 nm), ring-closure reaction occurs, yielding an increase closed-form ratio on the surface, and the band shifts to 1695 cm^{-1} PSS(365 nm). Irradiation with visible light (λ_{irr} = 545 nm), induces the ring-opening back reaction increasing the ratio of the open forms at PSS(545 nm). The ν_{as}(C=O) imide absorption band shifts to 1691 cm^{-1}. The *E*/*Z* photoisomerisation is not detectable by IR spectroscopy. The alternation of the UV and visible light irradiation, over 5 cycles, results in repeatable shifting of this band between, on average, 1695 cm^{-1} (PSS(365 nm)) and 1691 cm^{-1} (PSS(545 nm)). No sign of decomposition or fatigue of the photoswitching process on the surface was observed over 5 irradiation cycles.

Similarly, the same trend was observed for the photochemical studies of diluted SAMs Si(111) surfaces (Figure 4.12). In the initial state, upon immobilization of the fulgimide-linker conjugate **7**, the imide ν_{as}(C=O) absorption band was found at 1689.5 cm^{-1}. Upon alteration of the UV and visible light irradiation, the imide C=O band shifts, on average, between 1693 and 1691 cm^{-1}, for PSS(365 nm) and PSS(545 nm), respectively. This sample suffered from lower signal-to-noise ratio, leading to the peaks not having a regular shape, which may be the reason for shorter range of peak shifting between the two photostationary states, compared to the neatly prepared SAMs.

Additionally, both the neat and diluted sample show repeatable changes in the position and intensity of the ν_{sym}(C=O) absorption band, observed at 1739 cm^{-1} in the initial state upon immobilization; this band shifts to 1758 cm^{-1} upon reaching the PSS(365 nm), and shifts back to 1739 cm^{-1} at the PSS(545 nm) (Figure 4.12).

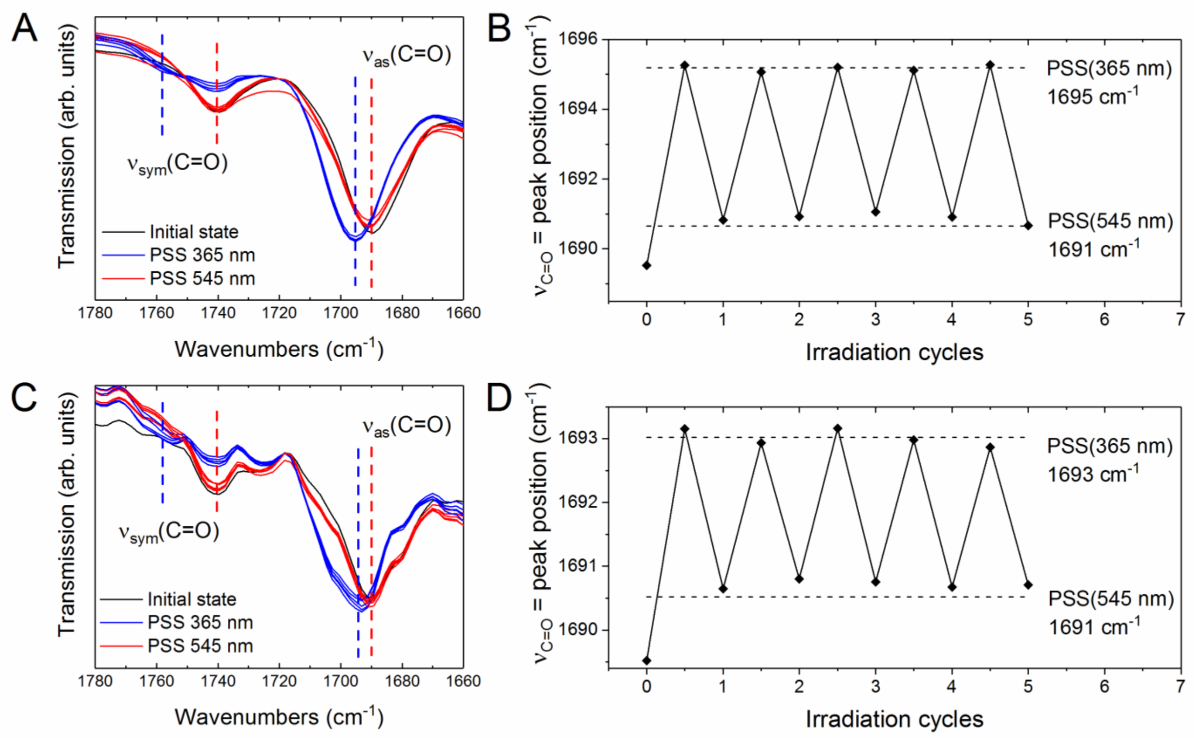

Figure 4.12. Repeatable changes upon alternating UV and visible light irradiation of the neat (A,B) and diluted (C,D) fulgimide-terminated SAMs, upon immobilization (black), PSS(365 nm) (blue), and PSS(545 nm) (red), over 5 irradiation cycles.

4.1.5 Naphthopyran-Terminated SAMs on Si(111)

Upon the coupling reaction with naphthopyran **8** (at 50 °C in MeCN, in the glove box, over 18 h), the band responsible for the C=O stretching vibration is found at 1641 cm^{-1}, assigned to the amide stretching vibration of the newly formed bond (Figure 4.13). The observed O-H bending vibration from the carboxy-functionality at 1415 cm^{-1} is reduced in the intensity, as expected. Additionally, the two ester ν(C=O) absorption bands are now observable, due to the ester functionalities present in the naphthopyran moiety: at 1765 and 1725 cm^{-1}, corresponding to the naphthyl- and methyl ester, respectively. Both ester groups are located at lower frequencies compared to the values detected in solution studies. This can be explained by the changes in vibration of the C=O bond via hydrogen bonding with the unreacted carboxy-functionalities from the surface, which influence the decrease in frequency of the bond. The absorption bands at 1612 and 1517 cm^{-1} are assigned to the stretching vibration of the aromatic units.

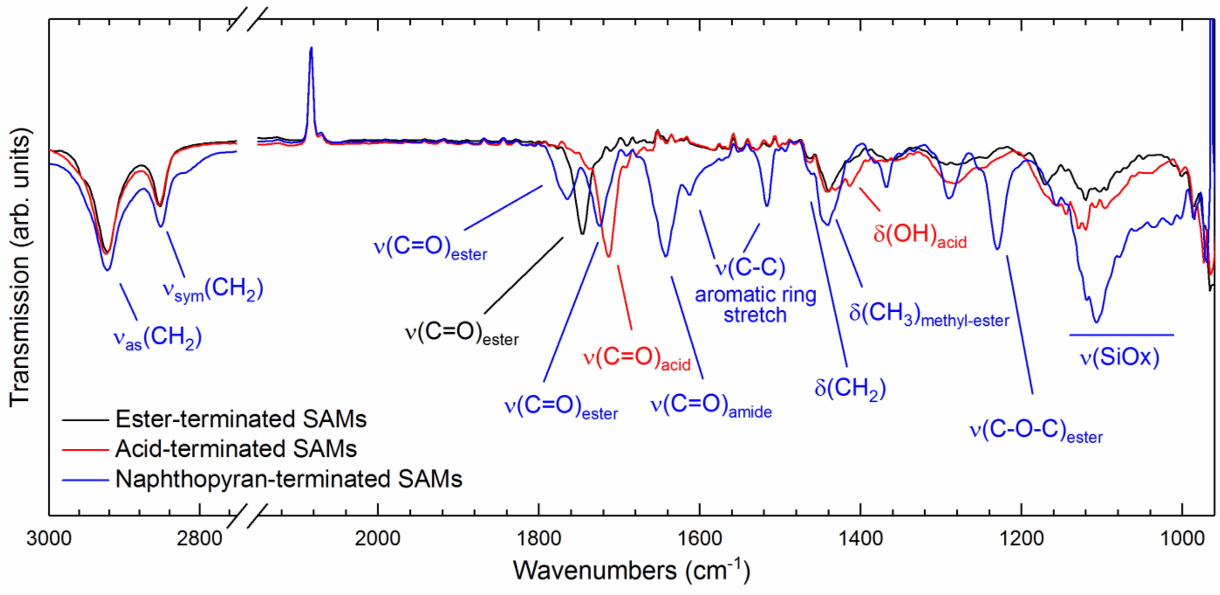

Figure 4.13. IR spectra of ester- (black), carboxy-(red), and naphthopyran-terminated SAMs on Si(111), referenced to the spectrum of H-Si(111).

Additionally, vibrations corresponding to the bending motion of C-H bonds, of the CH_2 and CH_3 units are observed at 1446 and 1465 cm^{-1}. Furthermore, the intensive band with the maximum at 1230 cm^{-1} is assigned to the C-O-C stretching vibration of the ester units of the naphthopyran moiety. The wide band in the region 1200-1000 cm^{-1} is assigned to the C-O stretching vibrations from the naphthopyran moiety, and Si-O stretching vibration due to the oxidation of the substrate upon the naphthopyran coupling reaction.

In Figure 4.14, the survey XPS and high-resolution spectra for carboxy- and naphthopyran-terminated monolayers are presented.[a] For both samples, Si (2s and 2p), C1s and O1s, were observable as major peaks. Additionally, the sample with the naphthopyan-terminated monolayers contains the N1s signal, due to the nitrogen atoms present in the naphthopyran moiety. The high-resolution XPS spectra of both the carboxy- and naphthopyran-terminated sample were analyzed, and fitted data are presented in Table 4.1.

The C1s peak of the carboxy-terminated sample shows the expected signature, already known in the literature,[14] dominated by a high intensity peak for the C-C bond from the alkyl backbone of the monolayer at 284.8 eV. Additionally, the peak at lower energy, at 283.6 eV is assigned to the Si-C bond of the carbon atom directly attached to the silicon surface. At higher energy, peak at 289.5 eV is assigned to the C=O bond of the carboxy-functionality. Upon the naphthopyran immobilization, the peak analysis of the C1s scan shows additional signals due to existence of carbons with different chemical environments. The signal responsible for carbon attached to the oxygen or nitrogen atoms (C-O, C-N) is now observable at 285.7 eV. At the higher energies, the two peaks are responsible for C=O bonds, from the amide and ester functionalities, at 287.4 and 289.1 eV. A wide signal of small intensity at 292.0 eV is assigned to the π-π* satellite peak. The single- and double-bonded oxygen of the carboxy-functionality is observed in O1s spectra, at 532.8 and 532.0 eV, respectively. Additionally, a small contribution is observable by a peak at 531.5 eV, assigned to Si-O, observable due to a surface oxidation.

After the naphthopyran coupling reaction, the ratio of the components in the O1s spectra changes. Higher intensity of the peak at 531.3 eV suggests substrate oxidation, as previously observed in the FTIR data. The C-O and C=O peaks change the ratio, C=O now being the most dominant peak, due to two ester and the amide functionalities from the naphthopyran-terminated monolayer. The C-O peak is attributed to the C-O bonds of the two esters functionalities and the remaining unreacted carboxy-groups of the monolayer moieties on the surface. Additionally, due to these different contributions, the full-width at half maximum (FWHM) increases for both C-O and C=O upon the coupling reaction. Peak fitting analysis of the N1s peak of the naphthopyran-terminated monolayer gave two component peaks, located at 399.5 and 400.0 eV, which were assigned to amine and amide C-N bonds, respectively.

---

[a] The XPS spectra were taken in the research group of Prof. Dr. Arne Thomas (Institute of Chemistry, Technische Universität Berlin)

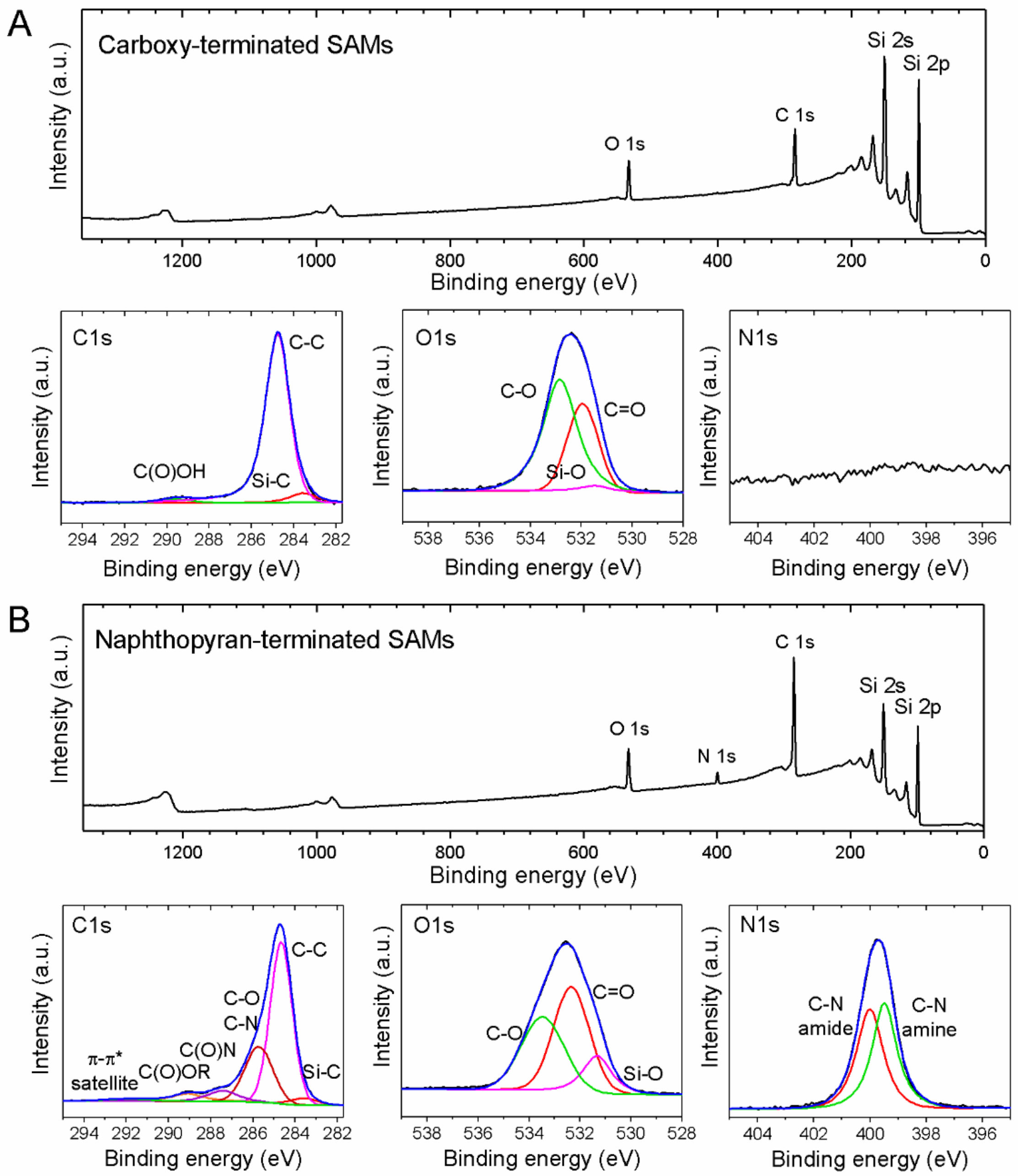

Figure 4.14. XPS-survey and high-resolution scans of the C1s, O1s and N1s core levels of (A) carboxy- and (B) naphthopyran-terminated SAMs on Si(111). The black lines present the recorded data, while the blue lines are fitted data.

Table 4.1. Characteristics of the components of the C1s, O1s and N1s signals obtained upon the peak fitting of the high resolution XPS spectra – assignments, binding energies (eV) and full-width at half maximum (FWHM) (eV) - for (A) carboxy- and (B) naphthopyran-terminated monolayers; The black lines present the recorded data, while the blue lines are fitted data.

Sample	**Assignment**		**Binding energy** (eV)	**FWHM** (eV)
(**A**) Carboxy-terminated monolayer	C1s	Si-C	283.6	1.5
		C-C	284.8	1.3
		COOH	289.5	1.6
	O1s	Si-O	531.5	1.5
		C=O	532.0	1.4
		C-O	532.8	1.6
(**B**) Naphthopyran-terminated monolayer	C1s	Si-C	283.6	1.6
		C-C	284.7	1.3
		C-O, C-N	285.7	1.6
		C(O)N	287.4	1.8
		COOR	289.1	1.8
		π-π* satellite	292.0	2.6
	O1s	Si-O	531.3	1.4
		C=O	532.3	1.7
		C-O	533.5	2.0
	N1s	C-N amine	399.5	1.0
		C-N amide	400.0	1.1

The calculation reported in ref. 14, allows evaluation of the efficiency of the amide coupling, on the basis of an increase of the C1s signal. The C1s signal for the naphthopyran-terminated monolayer is larger by a factor of ~2.3 than the signal for carboxy-terminated monolayer. The naphthopyran moiety contains 39, while the linker contains 11 carbon atoms. Since the work is comparable to the one in ref. 14 due to the same alkyl linker in the monolayer, and the attachment of the heavy photoswitch on top, it is assumed that the same damping effect of the XPS signal in the molecular level takes place. Thus, the same factor of 0.6 is used, the authors introduced to explain the XPS intensities.[14] Therefore, using the final calculation developed by the authors, we obtain the surface to consist of ~0.48 of naphthopyran molecules per 1 monolayer molecule: (0.48 · 39 + 0.6 · 11)/11 = 2.3. Therefore, it can be concluded a high density of the functionalized monolayer molecules, where on average every second alkyl linker is functionalized with a naphthopyran moiety.

4.1.5.1 Photochemical Studies of Naphthopyran-Terminated SAMs on Si(111)

As learned from the naphthopyran **71** photochemical studies in solution, upon UV irradiation, the ring-opening reaction occurs, leading to an increase of both open TC and TT form, and a decrease in the amount of the closed form (Figure 4.15); PSS(365 nm) consists all three photoisomers. Thermal relaxation leads to quick fading of the short lived TC form, leading to a mixture consisting only CF and slowly fading TT form (plateau formation, Figure 3.26) at PSS(Δ). Finally, irradiation with visible light (505 nm) induces the ring-closure reaction of the TT form; the resulting PSS(505 nm) contains only the closed form. On the surface, a photochemical study was carried out with the naphthopyran-terminated sample under inert conditions. Two strategically different switching experiments were done: (I) Photochemical cycles consisting of UV irradiation (λ_{irr} = 365 nm) and thermal relaxation, alternating between PSS(365 nm) and PSS(Δ), and (II) Photochemical cycles consisting of UV irradiation, thermal relaxation and visible light irradiation (λ_{irr} = 545 nm), overall resulting in switching between three states - PSS(365 nm), PSS(Δ), and PSS(545 nm). It is important to note here that visible light irradiation was done with the 545 nm LED, compared to the 505 nm used for the solution studies, due to the set-up limitations. For both UV irradiation and thermal relaxation, it was allowed 30 min per photochemical and thermal reactions; however, for visible light irradiation with 545 nm light, it was allowed for 50 min irradiation periods.

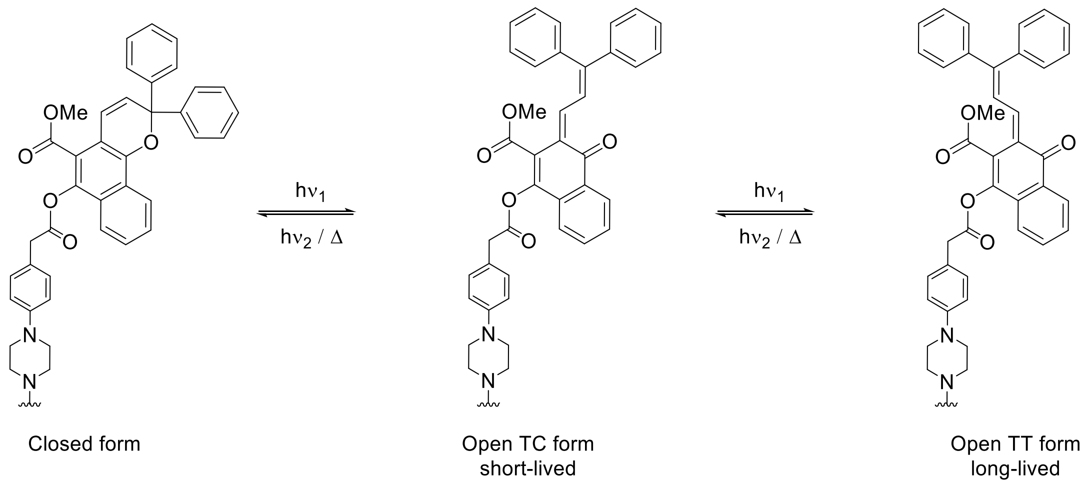

Figure 4.15. Photoisomerisation of the naphthopyran **8**, on the Si(111) surface.

Studies in solution suggested that changes in the peak maximum position of the methyl-ester ν(C=O) absorption band are an indicator of the switching process; thus, the changes in the position of the ν(C=O) methyl-ester absorption bands may give a valuable insight into the switching behaviour on the surface. Upon immobilization of the naphthopyran on the surface, the position of the C=O band is found at 1724.9 cm^{-1}. Upon UV light irradiation, the band shifts to 1725.5 cm^{-1}. Yet, upon thermal relaxation, the absorption band does not shift back to the initial value, but reaches the 1725.3 cm^{-1} (PSS(Δ)). Repeatable changes are observed for the 3 irradiation cycles (Figure 4.16B, cycles (I)), where the ν(C=O) absorption band shifts, on average, from 1725.5 to 1725.3 cm^{-1}, between the PSS(365 nm) and PSS(Δ), respectively. Visible irradiation of the sample at PSS(Δ) caused further shift of the ν(C=O) absorption band towards lower wavenumbers, reaching the position at 1725.1 cm^{-1}, on average. Since the irradiation with visible light was not carried out with an optimal light wavelength, the complete return to the initial state was not obtained, but instead a new photostationary state (PSS(545 nm)). Repeatable changes are recorded over three cycles going from 1725.5 cm^{-1} at PSS(365 nm), over 1725.3 cm^{-1} at PSS(Δ) towards the 1725.1 cm^{-1} at PSS(545 nm), as shown in Figure 4.16B (cycles (II)).

Furthermore, the switching may be evaluated by following the changes in the intensity of the band at 1595 cm^{-1} (Figure 4.16C). There is a significant increase in the intensity of the peak upon the first UV light irradiation, from the initial state (black) to PSS(365 nm) (red). At the PSS(Δ) upon thermal relaxation, the intensity of the band decreased (blue). During the cycles (II), visible light irradiation further decreased the intensity of the band (green); however the initial state was not reached.

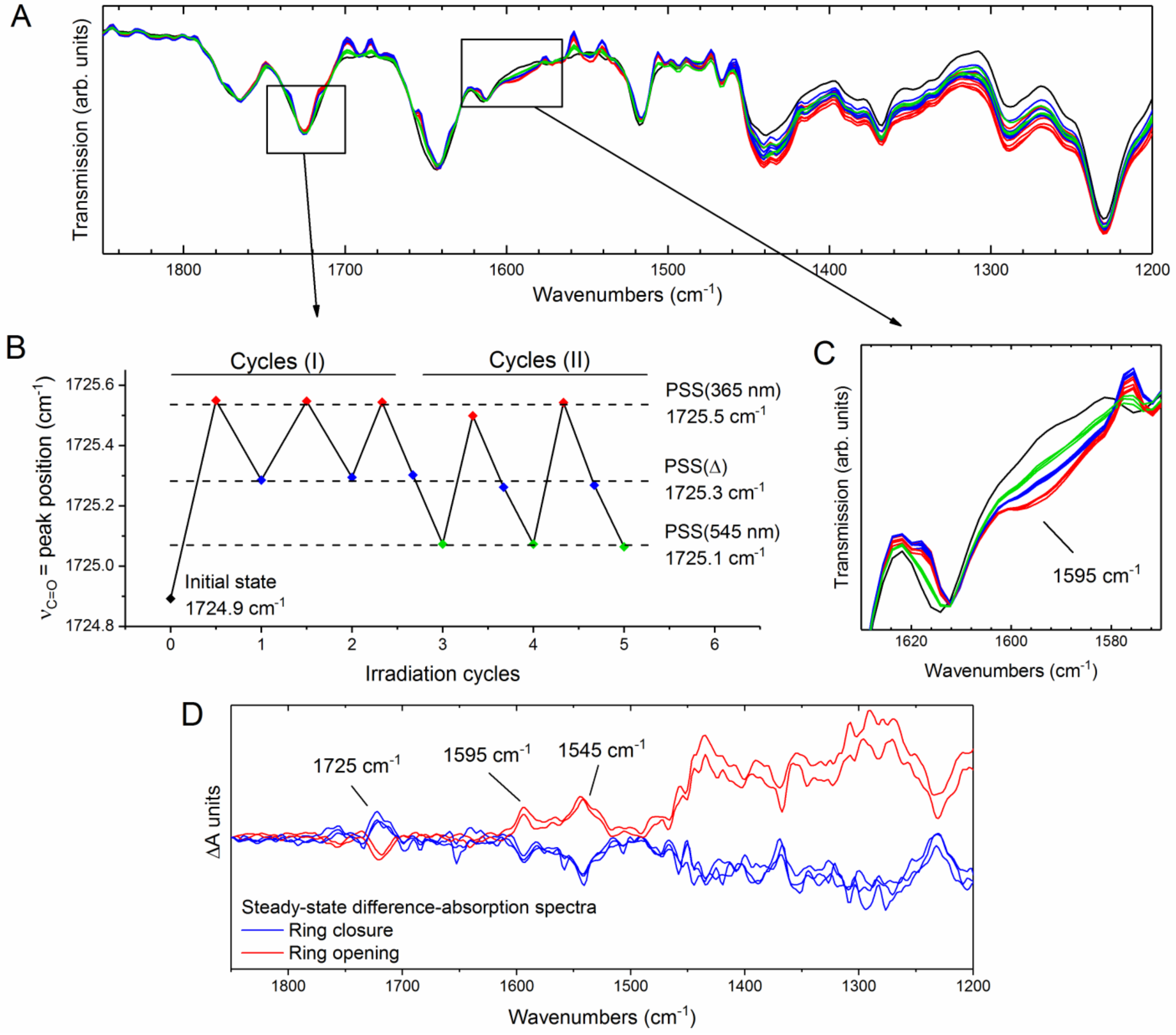

Figure 4.16. Photochemical study of naphthopyran-terminated SAMs on Si(111). Overlayed spectra of the initial state (black) upon reaching the PSSs: PSS(365 nm) (red), PSS(Δ) (blue), and PSS(545 nm) (green). (D) Steady-state difference-absorption spectra between the photostationary states, due to the ring opening (blue) and ring closure (red) of the naphthopyran ring, for the cycles (I).

The steady-state difference-absorption spectra between the photostationary states of naphthopyran-terminated SAM show repetable changes of the IR signature (Figure 4.16D). The main changes in the intensities between the PSS(365 nm) (blue lines) and PSS(Δ) (red lines) are in the methyl ester ν(C=O) absorption bands at ~1725 cm^{-1}, the C=C stretching vibration of the conjugated double bond and extended conjugation of the naphthalene ring at 1595 and 1545 cm^{-1}.

These changes go along with the changes observed during the IR studies of naphthopyran **71** in solution.

The three-state system observed during photochemical studies on the surface goes along with the slow bleaching of the TT form, previously observed in studies in solution. During the first cycle, the most significant change in the position of the band is observed, due to CF → TC, and TC → TT. A slow fading of the TT form is detected, reaching a plateau on the surface, and does not returned to closed form PSS(Δ). However, the slow bleaching of the open forms may be additionally influenced by the properties of the surface itself. Due to the carboxy-terminated surface in the vicinity of the naphthopyran head groups, the acid-functionality can influence the switching process by stabilizing the open forms due to the hydrogen bond formation / proton-transfer between the ketone-oxygen and carboxy-functionality of the surface.[28,135] This would explain the more prominent shift upon the first UV-light irradiation, during which the open forms are formed. The open forms are then stabilized, and the system does not completely revert back to the closed form. Only a small portion of naphthopyran head-groups are then able to switch during the irradiation / thermal relaxation cycles. The slow back reactions, both under thermal relaxation and upon visible irradiation conditions, proved to be slower when hydrogen bonding is present, due to the stabilization of the TC open form, as seen in the solution studies of compound **45**.

Additionally, naphthopyrans require an approximetely 90° rotation of the half of the molecule, when switching between the closed and open forms; thus the trend observed for the changes in the position of ν(C=O) methyl ester absorption band can be also influenced by to the limiting factors of the densily packed monolayers. The reduced switching properties, due to the lateral steric hindrance, of the chromophoric compounds attached to the densily packed self-assembled monolayers has been reported before for Si and Au surfaces.[13,161] Additionally, the slow color fading reaction of naphthopyrans embedded into polymer matrices has been reported before; the densily packed structures can limit movement of the naphthopyran molecules, reduce the possible rotations, and thus slow down both ring-opening and ring-closure reaction.[27,162]

The observed changes in the intensity of the bands at 1595 cm^{-1}, as well as the shift of the ν(C=O) ester band, upon UV irradiation in solution, were not as strongly observable on the surface, as in solution studies. This may be due to several different reasons: 1) The concentration of naphthopyran molecules on top of the monolayer is much lower than the concentration in the solution studies, so the changes in the IR are of lower intensity, 2) due to the densily packed monolayer, the naphtopyran moieties are switching in confined space, which may influence the partial reduction and blocking of the vibrations, and 3) switching in the liquid medium differently influences the kinetics compared to switching in densely packed naphthopyran moieties in the solid phase / gas interface on the surface.

Additionally, the intensity of the IR signature in the region from 1450-1250 cm^{-1} slightly increases with each cycle during the irradiation process, and decreases upon thermal relaxation. In Figure 4.17 changes in the 2nd and 3rd cycle are shown; the signature for PSS(365 nm) reached in 2nd cycle (red) decreases in the intensity when the PSS(Δ) is reached (blue), additional UV light irradiation increases the intensity of the signals (PSS(365 nm), 3rd cycle, orange) even further, which again decreases during the thermal relaxation (PSS(Δ), 3rd cycle, violet). Finally, the prolonged visible light irradiation (50 min) does not influence the intensity of the signals (PSS(545 nm), 3rd cycle, green). Overall, a gradual shift of the intensity is observed over 5 performed cycles (Figure 4.16A).

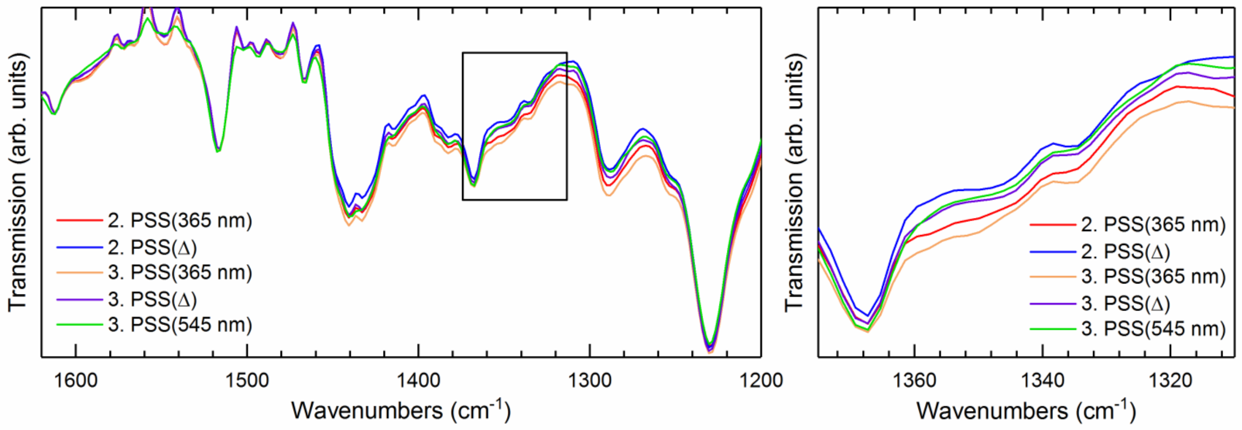

Figure 4.17. The zoom of the ATR-FTIR spectra of the naphthopyran-terminated monolayer, upon reaching the PSSs in 2nd and 3rd cycle. Both the repeatable shift between the PSS(365 nm) and PSS(Δ), as well as an overall gradual increase of intensity in the region 1450-1250 cm^{-1} is observable.

These repetable changes and the shift in the intensity in this region were not observed in the solution studies of the naphthopyran **71**, and thus are attributed to the changes on the silicon surface. One of the possible explanations for this phenomenon is that this behaviour might be influenced by warming up the sample upon prolonged irradiation with UV light causing the increase in the intensity, and subsequently cooling down during the thermal relaxation. However, since this observation was not previously observed for the fulgimide-terminated SAMs on silicon(111), there might be additional naphthopyran-based properties influencing this behaviour.

4.2 Preparation and Functionalization of SAMs on Oxidized Si(100) Surfaces

Trifunctional organosilanes are attractive in terms of the obtained monolayer structure – a threefold functionality at the anchoring end allows them to form bonds directly with the hydroxyls on the surface, as well as a cross-linked network with the neighboring monolayer molecules (Figure 4.18). This network increases surface coverage and stability of the monolayer, compared to structures developed from monofunctional organosilanes. The main disadvantage of the trifunctional organosilanes comes from the poor reproducibility, due to the possibility for the formation of oligomers and thus attachment of aggregates to the surface, resulting in disordered and multilayer structures. The silane deposition process strongly depends on several parameters such as water content[42,163,164], solvent[163], silane concentration[165,166], temperature[167,168], humidity,[47] and deposition time[169]. In comparison, the monofunctional organosilanes (R_3SiX, most common $R(CH_3)_2SiX$) are favored in terms of reproducibility of the resulting monolayer on the surface, since they can form only one type of bond ($Si_{surface}$-O-Si_{silane}), thus attachment of the aggregates to the surfaces and formation of multilayers is not possible. The limitations of using monofunctional organosilanes is lower surface coverage compared to trifunctional organosilanes[165], which is limited by the size of the hydrocarbon side groups[170].

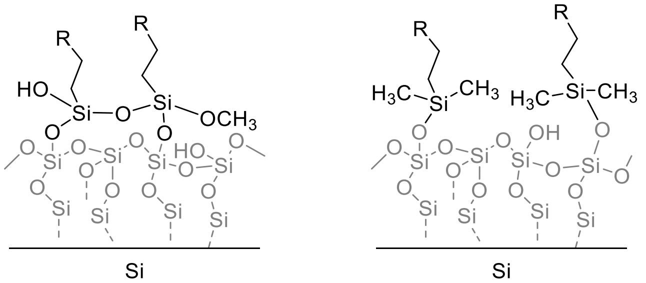

Figure 4.18. Sketch of the monolayer structures obtained from tri- and monofunctional organosilanes.

Self-assembled monolayer formation during the silanization process goes through a four-step mechanism[42,164] (Figure 4.19). In the first step, silane molecules are physisorbed at the surfaces mediated by the thin water layer that is already absorbed by the polar oxide surface. In the next step, the silanes get hydrolyzed by the water molecules, creating corresponding hydroxysilanes ($RSi(OH)_3$). These hydroxysilanes are hydrogen bonded to the polar oxide surface, but still capable of lateral movements across the surface. In the third step, the hydrogen bonded species undergo aggregation through lateral movement via attractive forces, such as van der Waals forces between the hydrocarbon chains, dipol-dipol interactions and hydrogen bond interactions. Once aggregated, the species become significantly less mobile. Finally, in the last step, condensation between anchored hydroxysilanes and the surface Si-OH bonds occurs, resulting in the formation of covalent Si-O-Si bonds. In the same step, the polymerization with the neighboring silane species (cross-linking) takes place, yielding the covalent network between the monolayer molecules, which increases stability.

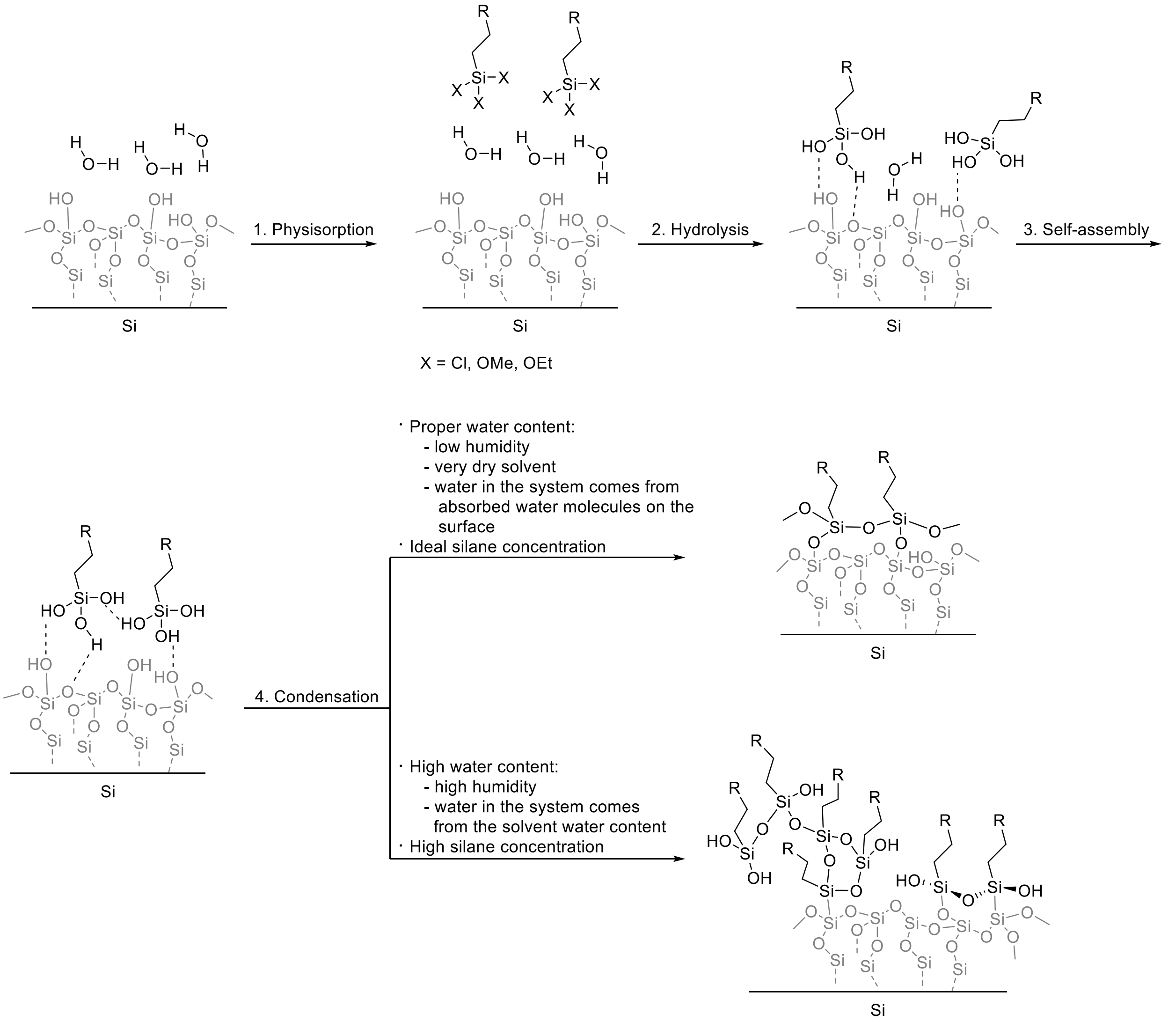
1. Physisorption
2. Hydrolysis
3. Self-assembly
4. Condensation
X = Cl, OMe, OEt
Si
· Proper water content:
- low humidity
- very dry solvent
- water in the system comes from absorbed water molecules on the surface
· Ideal silane concentration
· High water content:
- high humidity
- water in the system comes from the solvent water content
· High silane concentration

Figure 4.19. Scheme of the proposed four-step mechanism for SAM formation on silicon oxide using organosilanes.

The water content can highly influence the quality of the formed monolayer. It was suggested in Sagiv's early work[171] that water absorbed on the surface was crucial to hydrolyze chlorosilane molecules. Thus, when an optimal amount of water is present in the system, hydrolysis of organosilanes occurs only in the proximity of the surface. In this case, molecules attach to the surface one by one; cross-link polymerization results in formation of the monolayer. Prolonged reaction times do not induce formation of the multilayers.[172] Additional physisorbed monolayer molecules can later be removed by proper washing procedures. In the case when there is an insufficient amount of water molecules in the system, hydrolysis of the silane molecules does not fully occur, and silanization reactions result in incomplete surface coverage.[42] On the contrary, if the water concentration in the system is high, hydrolysis of silane molecules occur in the bulk solution, resulting in formation of large, extensively cross-linked aggregates, which attach to the surface with just a few covalent bonds.[172] Thus, the resulting structure has multi-layer assembly.

In order to obtain SAMs with an epoxide functionality at the terminal end, (3-glycidyloxypropyl)trimethoxysilane (GPTMS) was used. Epoxysilanes are compounds often used for monolayer preparation on hydroxylated surfaces, including silicon oxide[56,169], glass slides[173], oxidized platinum surfaces[174] and silicon nitride surfaces[54]. GPTMS is often used in commercial applications for coatings on fibers, and has been used to make organic/inorganic hybrid materials in epoxy/amine systems.[175] Epoxy-terminated monolayers are attractive because they can react with various amino-functionalized molecules[56,173,175,176], thus being used for immobilization of peptides[177]. They were also studied in the reaction with glycols[178] and carboxy-terminated polymers[179].

Czochralski method grown crystals (CZ) showed to be of poorer quality compared to Float zone (FZ) silicon wafers. This mainly comes from the higher impurity concentration (oxygen level in CZ and FZ silicon is $\sim 5\cdot 10^{17}$ atoms/cm^3 and $\sim 5\cdot 10^{15}$ atoms/cm^3, respectively). This higher interstitial oxygen concentration in CZ silicon can be observed in the IR data, in the region below 1120 cm^{-1} [180]. For this reason, the silanization experiments were performed on float zone silicon wafers.

4.2.1 Formation and Characterization of Si(100) Oxide Layer

Double side polished wafers (*Sil'tronix*, Si(100) ± 0.5°, FZ, p-doped (Boron); Si(100) ± 0.5°, FZ, non-doped) were cut in rectangle shape (1.1 cm x 2.5 cm). For preparation of ATR crystals, the shorter rim was grinded to a 45° angle, and polished. After cleaning in organic solvents, the wafers were ready for further use. In order to obtain a reproducible formation of Si/SiO_X interfaces for further modification, a three-step process was employed (Figure 4.20): (a) Silicon wafers were first oxidized in *Piranha* solution (H_2SO_4 / H_2O_2, 3:1), to remove any chemisorbed or physisorbed impurities from the surface. (b) The freshly oxidized surface was then etched in 2.5 % aqueous HF solution, in order to completely remove the oxide layer and form Si-H termination. During this step metal ions that may have diffused into silicon oxide during the oxidation step, e.g. from the external contaminants, are eliminated.[181] (c) Finally, the wafer was oxidized in *Piranha* solution, in order to form a silicon oxide layer[182] and to maximize the number of hydroxyl groups[35].

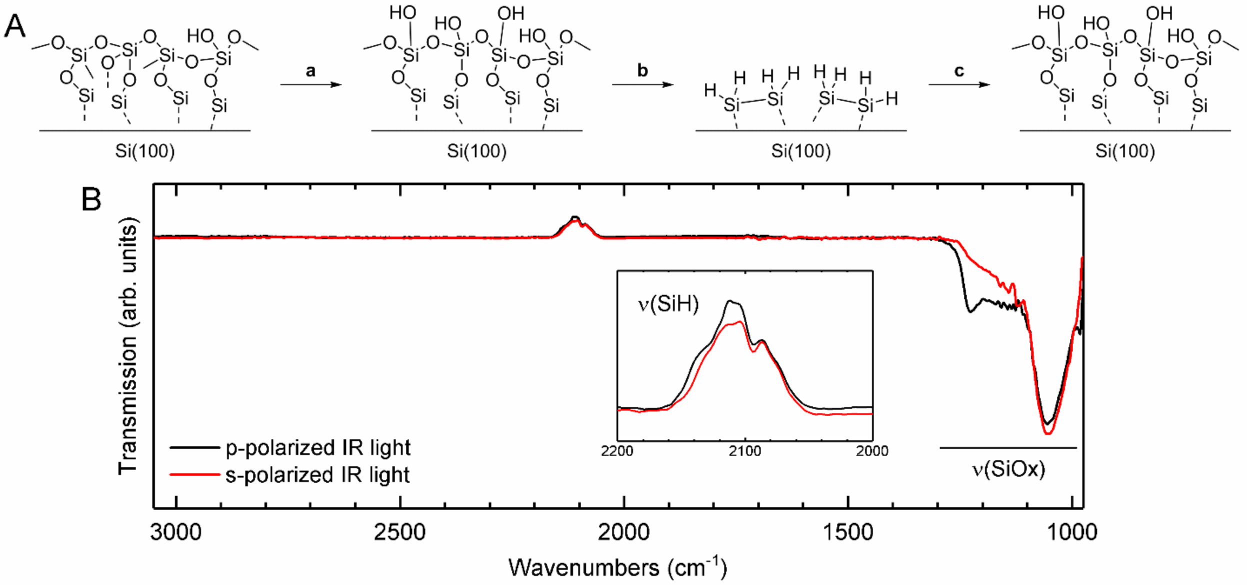

Figure 4.20. Reproducible formation of silicon oxide layers. Reaction conditions: (a) *Piranha* solution (H_2SO_4 / H_2O_2, 3:1), 100 °C, 1 h; (b) HF 2.5 % (aq), RT, 1 min; (c) *Piranha* solution (H_2SO_4 / H_2O_2, 3:1), 100 °C, 1 h. (B) IR spectra of freshly prepared silicon-oxide layer, referenced to the H-terminated sample, measured in p-polarization (black) and s-polarization (red).

In the IR spectra of the silicon oxide layer referenced against the H-terminated silicon surface, the dominant peaks were observed at 1055 cm^{-1} (detected by both s- and p-polarized light, transverse optical mode) and at 1226 cm^{-1} (detected only by p-polarized light, longitudinal optical mode)

(Figure 4. 20).[158] Other absorption bands in the area, including the shoulder at around 1150 cm^{-1} (detected by s-polarized light) indicate the formation of defects in the oxide layer.[183]The negative peaks in the area 2150 to 2050 cm^{-1} correspond to the loss of Si-H bonds, due to oxidation. The dominant peak in this range at 2112 cm^{-1} is assigned to the absorption band of the unstrained dihydrides, the predominant structure of H-terminated Si(100).[184] The peak at 2087 cm^{-1} is assigned to the vibration of monohydride Si-H species. The shoulder at ~2129 cm^{-1} suggests strained monohydride species, which is an indication of the non-atomically flat surface structure.[184]

The thickness of the freshly prepared oxide layer was verified via ellipsometry measurement, carried out with a Sentech SE 850 ellipsometer, in the research group of Prof. Dr. K. Petermann (Institute of Hochfrequenztechnik-Photonik, Technische Universität Berlin). The thickness of the SiO_2 layer alone was determined from reference samples, and was calculated to have a value of 1.49 nm.

4.2.2 Formation of Epoxy-Terminated SAMs on Oxidized Si(100)

Monolayers were prepared on freshly oxidized wafers, in the glove box, using 1% volume concentration of (3-glycidyloxypropyl)trimethoxysilane (**74**, GPTMS) in toluene, and reaction times of 24 h (Figure 4.21).

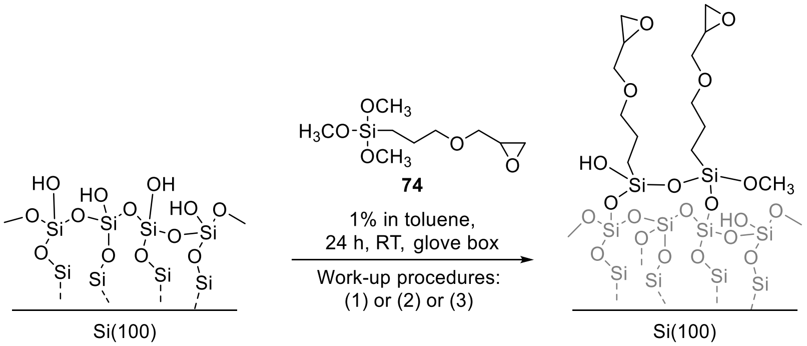

Figure 4.21. Reaction conditions for the preparation of epoxy-terminated monolayer.

The water presence is known to be crucial for monolayer formation with trimethoxysilanes.[171] Only for water concentrations ≤10 ppm in toluene ATR-FTIR analysis of the epoxy-terminated monolayer obtained from GPTMS showed characteristics of a monolayer, whereas samples prepared in toluene with higher water content (> 66 ppm) provided signatures known for multilayer formation and generation of aggregates.[a]

The intensity of the signals in the ν(C-H) absorption region is higher with the increase of the water content in the solvent, suggesting higher amount of molecules attached to the surface (Figure 4.22). The $\nu_{as}(CH_3)$ absorption band at ~2963 cm^{-1} indicates incomplete hydrolysis of the silane methoxy-groups, and this signal was observed for the sample prepared with ~10 and 66 ppm water. However, this band was not observed for the sample prepared in toluene saturated with water. These two observations can be explained due to two competing processes happening at the same time – (1) the condensation reaction at the surface, and (2) the hydrolysis of the remaining methoxy-groups.[166] With a low amount of water in the solvent, the hydrolysis reaction is happening with the water molecules already being adsorbed on the polar surface; the hydrolysis and the condensation in the bulk solution, as well as the condensation reaction on the surface are slow.[166] In the sample saturated with water, both reactions are fast and are happening in the bulk solution; thus all methoxy-groups are hydrolyzed, allowing the formation of silane oligomers and aggregates in the bulk solution, and the aggregates were attached to the surface.

Peak analysis (deconvolution) of the signal in the alkyl region allowed for analysis of peak maxima position and full width at half-maximum (FWHM). The area below the absorption bands was deconvoluted, using Gaussian curve to fit the raw spectra (Figure 4.22, B-D). The fitting procedure was applied to the exact same region in all the data sets (software used is Origin v9.2). The obtained values are presented in Table 4.2.

---

[a] Water content in toluene samples were determined by a Karl-Fisher titration, carried out in the research group of Prof. Dr. Matthias Drieß (Institute of Chemistry, Technische Universität Berlin).

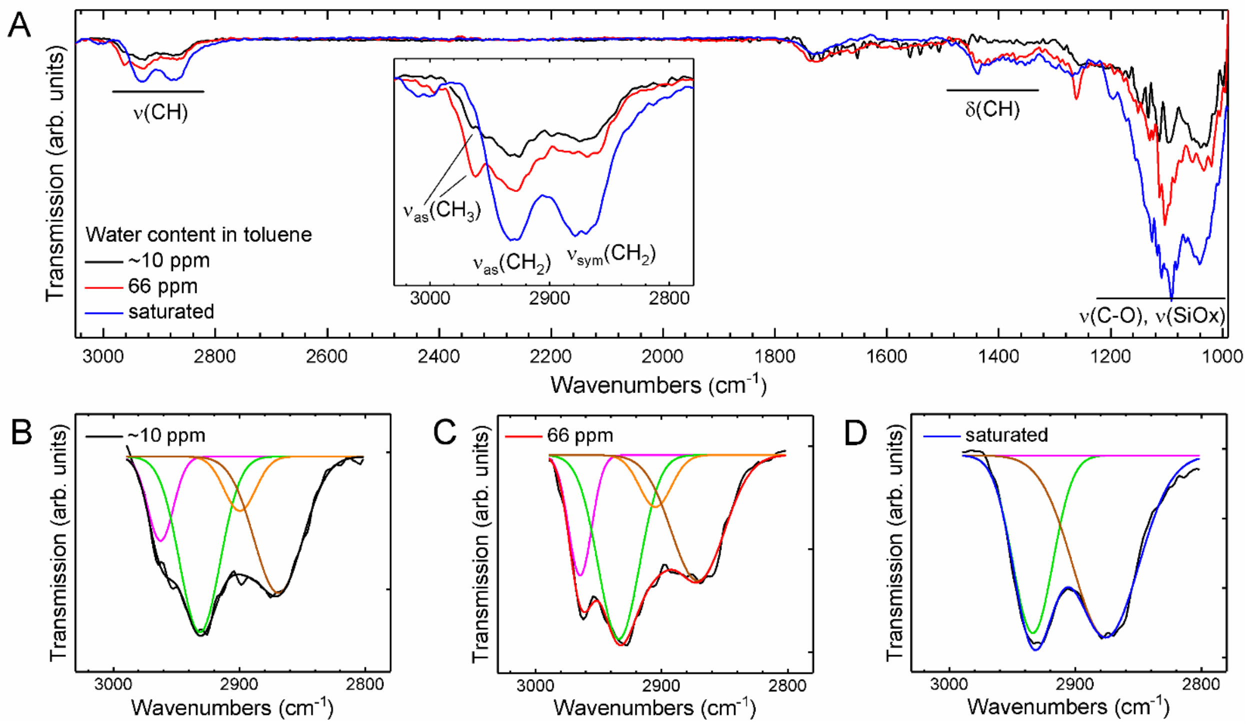

Figure 4.22. ATR-FTIR spectra of epoxy-terminated monolayers, prepared from toluene solution with different water concentrations: 10 ppm (black), 66 ppm (red) and toluene saturated with water (blue). (B-D) Deconvoluted IR spectra of the C-H stretching region of the epoxy-terminated monolayer. The fitted curve is color-coded according to the representation in (A).

For the sample saturated with water, the intensity of the $\nu_{as}(CH_2)$ and $\nu_{sym}(CH_2)$ absorption bands were the highest, and observed at 2933.7 and 2875.9 cm^{-1}, respectively. By lowering toluene water content to 10 ppm, the peak positions for both $\nu_{as}(CH_2)$ and $\nu_{sym}(CH_2)$ absorption bands showed the significant shift to lower wavenumbers, to 2931.3 and 2869.0 cm^{-1}, respectively. This shift indicates a better ordering and packing of the monolayer molecules on the surfaces.[185]

The analysis of the full width at half-maximum of the $\nu_{as}(CH_2)$ and $\nu_{sym}(CH_2)$ stretching vibrations provided additional information on orientation and packing of the monolayers,[186] because with lower water content their FWHM value decreased (Table 4.2). This difference in FWHM value is caused by the local variation in molecular packing around the oscillating dipoles and/or by increasing the number of molecules in all-trans conformation, thus resulting in improved packing due to the lower water content in toluene.[186]

Table 4.2. Peak positions of the $\nu_{as}(CH_3)$, $\nu_{sym}(CH_3)$, $\nu_{as}(CH_2)$ and $\nu_{sym}(CH_2)$ absorption bands and the FWHM of the $\nu_{as}(CH_2)$ and $\nu_{sym}(CH_2)$ absorption bands, for the epoxy-terminated monolayer obtained upon the peak analysis of the obtained raw FTIR data. The visualization shows changes in peak position and FWHM of $\nu_{as}(CH_2)$ and $\nu_{sym}(CH_2)$ absorption bands depending on the water concentration in toluene.

Toluene water	**Position of the absorption bands** (cm^{-1})				**FWHM** (cm^{-1})	
content (ppm)	$\nu_{as}(CH_3)$	$\nu_{sym}(CH_3)$	$\nu_{as}(CH_2)$	$\nu_{sym}(CH_2)$	$\nu_{as}(CH_2)$	$\nu_{sym}(CH_2)$
10	2962.5	2899.6	2931.3	2869.0	37.6	45.5
66	2964.6	2904.8	2933.9	2871.3	38.3	49.5
saturated	-	-	2933.7	2875.9	37.2	61.5

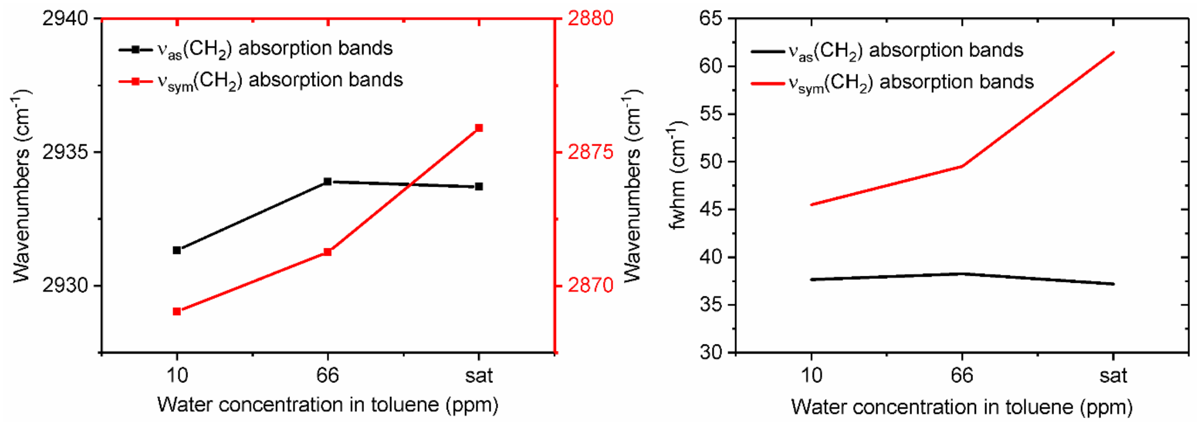

The higher intensities of the signals in the region below 1280 cm^{-1} with the increase of the water concentration in toluene, go along with the previously reported IR analyses of monolayer formation at various humidity levels,[47] suggesting the presence of irregular multilayer structures[168]. However, this region presents a challenge for the appropriate assignation of the spectra due to overlapping of different bands: Si-O-Si vibrational modes (bonds between silane molecules and the oxide surface, and cross-linked networks between monolayer molecules on the surface), non-hydrolyzed Si-O-C bonds, C-O bonds from the glycidoxy group and C-H bending vibrations. The band at 1194 cm^{-1} can be assigned to both the CH_2 wagging absorption band of the -$(CH_2)_3$- chain (reported at 1196 cm^{-1} in ref. 187, and at 1200 cm^{-1} in ref. 188) and the rocking absorption band of the C-H bonds in O-CH_3 (reported at 1190 and 1191 cm^{-1} in ref. 189). The band at 1100 cm^{-1} is assigned to the ν(C-O) absorption band of the glycidoxy group.[187] A complex mode involving C-O stretching motion coupled with Si-O stretching and CH_3 rocking motions is located at ~1091 cm^{-1}.[168,187,190–193] The epoxide ring stretching vibration (at ~1260 cm^{-1})[187], is not often observable in the IR spectra, due to its very low absorption intensity. However, a signal is observed at 1263 cm^{-1} (66 ppm sample, a shoulder 10 ppm and saturated sample), an indication of an additional vibrational contributions, e.g. C-H deformation band in $SiOCH_3$[189], or Si-C deformation band in Si-CH_2-R[136,189]. In the range 1480-1360 cm^{-1} bending vibration absorption bands of the alkyl chains are expected.

The water contact angle for the GPTMS monolayers (10 ppm sample) was 54.1° ± 2.7, and in accordance to the literature.[69,166] It is was previously reported that multilayer formation goes along with an increase in contact angle.[69] Here, for the 66 ppm samples an angle of 62.0° ± 2.5 was determined.

The thickness of the monolayer was determined for the sample prepared in 10 ppm toluene. Two-layer model SiO_2/GPTMS was used, refractive indices of the epoxysilane monolayer and the silicon oxide are assumed to be constant and equal to the bulk values of 1.429 and 1.461, respectively. Thickness of the oxide below the organic layer was calculated to be in range 1.30-1.42 nm. The monolayer thickness was determined to be 0.9 nm, which goes along with the previously reported values for the GPTMS monolayer (0.85 ± 0.15 nm),[169] and is in agreement with the extended conformation of the GPTMS molecule (0.9-1.0 nm). This suggests, on average, an orthogonal orientation of the molecules and their head groups towards the surface.

4.2.2.1 Variation on Work-up Procedures upon Formation of Epoxy-Terminated SAMs

The work-up procedure after the silanization reaction and monolayer formation is crucial. In the literature removal of all physisorbed molecules was described with either ethanol or toluene,[56,194,195] and also by additional sonication using these solvents.[168,169,173,175,196] Herein three different work-up procedures were tested for epoxide-terminated monolayer formation with 10 ppm samples (Figure 4.23): procedure (1) washing of the wafer with toluene (3 × 5 ml) and ethanol (3 × 5 ml), and subsequent sonication in ethanol for 20 minutes; procedure (2) washing of the wafer with toluene (3 × 5 ml) and ethanol (3 × 5 ml), and subsequent sonication in toluene for 20 minutes; procedure (3) washing of the wafer with toluene (5 × 5 ml) and subsequent sonication in toluene for 10 minutes). Furthermore, all samples were baked in the oven at 150 °C for 10 minutes.

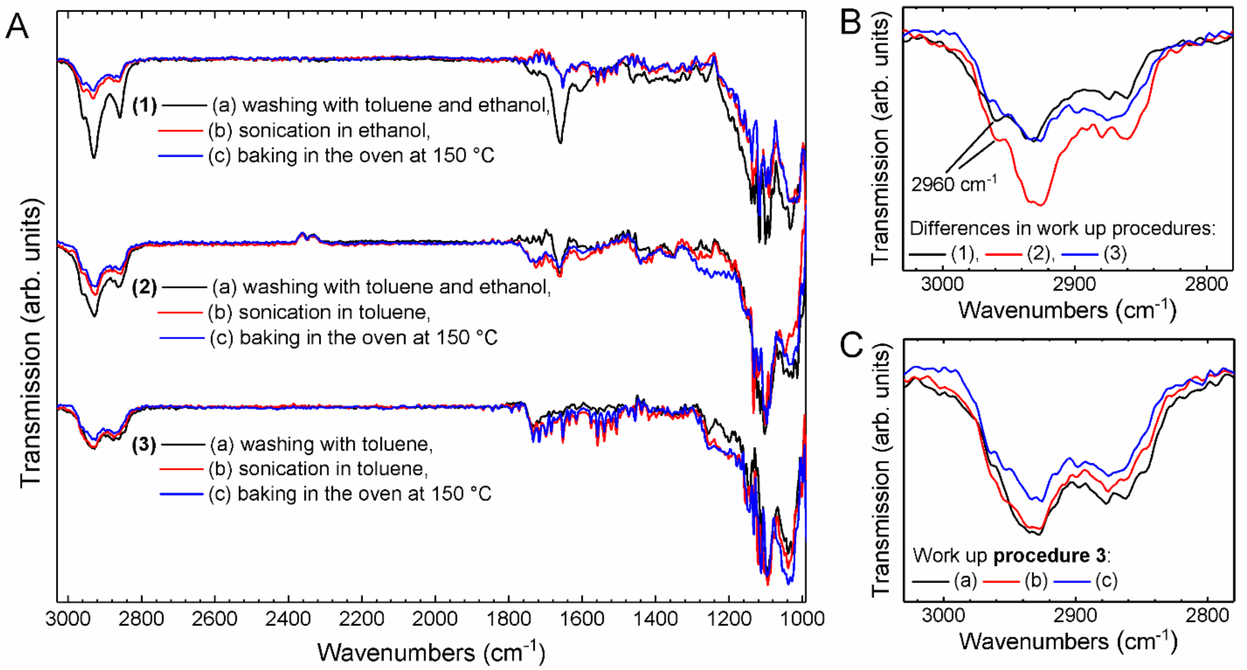

Figure 4.23. (A) Three work up procedures. (B) The zoom of the C-H stretching region of the epoxy-terminated monolayer, obtained upon three different work up procedures. (C) The zoom of the C-H stretching region of the sample worked up according to the procedure (3).

Various washing procedures showed a significant difference in shape and intensity of the IR bands only in the alkyl-stretching region. Only samples including ethanol in the washing procedure showed a significant contribution to the $\nu_{as}(CH_3)$ absorption band at ~2960 cm^{-1} (Figure 4.23A), probably due to adsorption of ethanol molecules to the monolayer. However, toluene guaranteed removal of adsorbed and/or weakly bound monolayer molecules during the washing and sonication procedures, and no detectable adsorption (Figure 4.23B). Strong signal at ~1650 cm^{-1} observable for the work-up procedures (1) and (2) is assigned to the O-H bending vibration of remaining ethanol absorbed on the surface upon washing.

Baking of the wafer after formation of the monolayer, promotes condensation of hydrogen bonded silanols to form siloxane bonds, both towards the surface and for cross-network formation.[195]

4.2.3 Formation of Alkyl-Terminated SAMs on Oxidized Si(100)

In order to confirm the results obtained for the epoxy-terminated monolayer derived from GPTMS, alkyl SAMs were prepared following the same procedure, using trimethoxy(propyl)silane (**75**) (Figure 4.24).

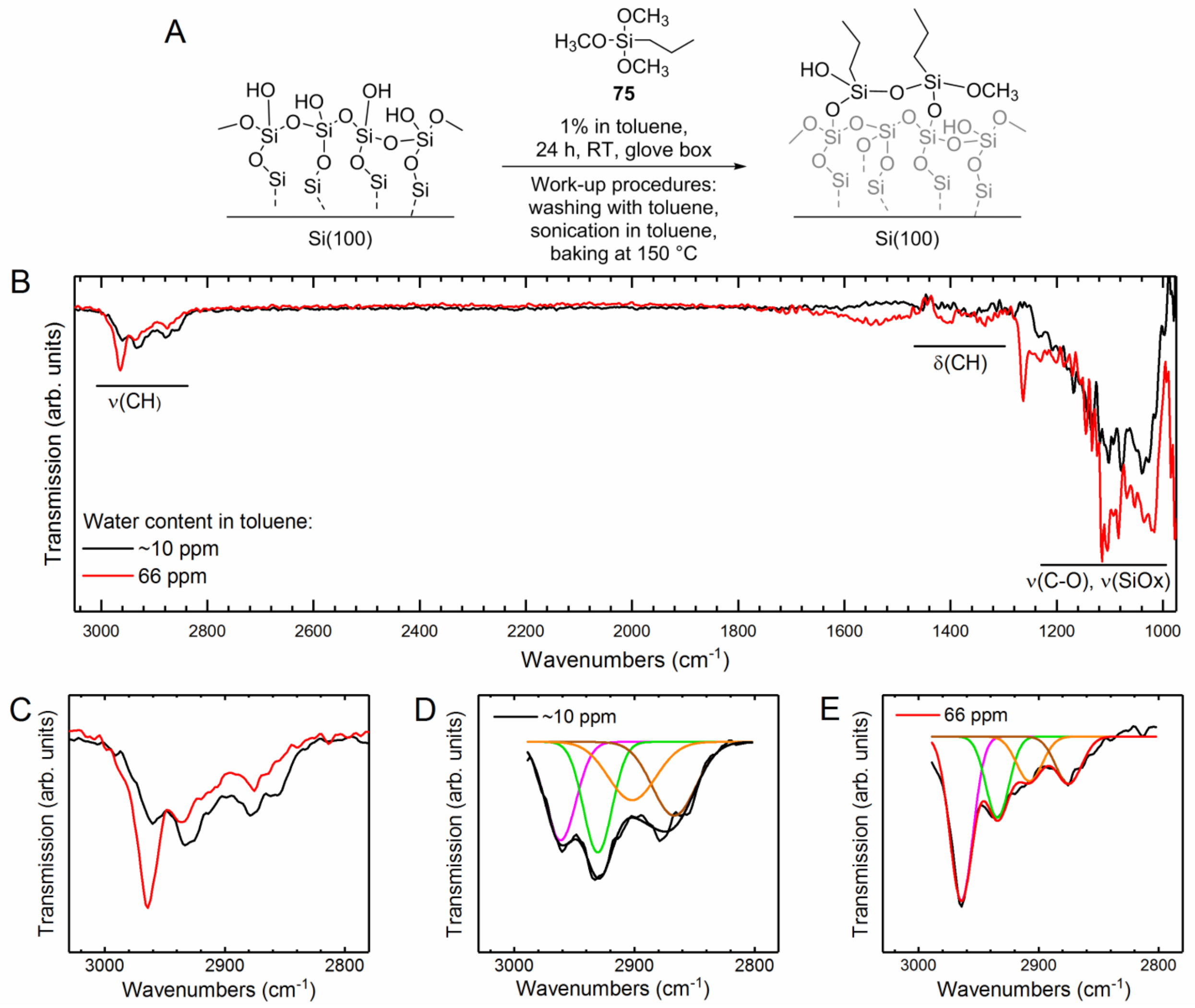

Figure 4.24. The IR spectra of the alkyl-terminated monolayers, prepared from toluene solution with different water concentrations: ~10 ppm (black), and 66 ppm (red). (A) Reaction conditions for the preparation of the alkyl-terminated SAMs. (B-D) Deconvoluted IR spectra of the C-H stretching region of the alkyl-terminated monolayer. The fitted curve is color-coded according to the representation in (B).

In the IR, again the higher intensities of the bands in both C-H and Si-O stretching vibration region are observed for the sample prepared in toluene with higher water content (66 ppm). Furthermore, the higher intensity of the $\nu_{as}(CH_3)$ absorption band (2964 cm^{-1}) and C-H deformation band in $SiOCH_3$ (1263 cm^{-1}) is observable for the sample prepared in toluene (66 ppm), suggesting incomplete hydrolysis of methoxy-groups, possibly due to formation of aggregates and irregular structures. Additionally, upon deconvolution of the ν(CH) region, a shift towards lower wavenumbers of the bands is observed in the sample prepared with lower water content ($\nu_{as}(CH_3)$: from 2964 to 2960 cm^{-1}, $\nu_{as}(CH_2)$: from 2931 to 2927 cm^{-1}, and $\nu_{sym}(CH_2)$: from 2871 to 2860 cm^{-1}), thus suggesting better ordering and packing of the monolayer.

Static contact angle for the samples prepared in toluene with the lowest water content (10 ppm) were determined to be 51.2° ± 2.3. As described for the epoxy-terminated monolayer, the sample prepared in toluene with higher water content tend to form multilayer structures, and thus the contact angle increases;[69] the contact angle for the samples prepared in toluene (66 ppm) was determined to be 64.2° ± 2.9.

4.2.4 Functionalization of Epoxy-Terminated SAMs via Epoxide Ring-Opening Reaction on Oxidized Si(100)

The ring-opening reaction on the epoxy-terminated monolayer with fulgimide-linker-conjugate **7** proved to be challenging, and after some initial experiments model studies towards an acetylene-terminated monolayer were investigated using propargylamine (**76**). However, reactions in toluene (156 mM) at room temperature or 60 °C (glove box) for 4 h according to Escorhuela *et al.*[56] gave no turnover according to IR-analysis. Moreover, activation of the epoxide using Lewis acids ($TiCl_4$ in DCM, $Ti(iOPr)_4$ in DCM, and $BF_3 \cdot OEt_2$ in THF; 156 mM) failed. Finally, after the improvement of the whole process starting with the silanization reaction for high quality epoxide-terminated monolayers, ring-opening with propargylamine (156 mM) in toluene proceeded at elevated temperature (80 °C) during 24 h reaction time (Figure 4.25). The reaction was also tested in N-methyl-2-pyrrolidone (NMP) for 20 h at 90 °C,[197] but was unsuccessful.

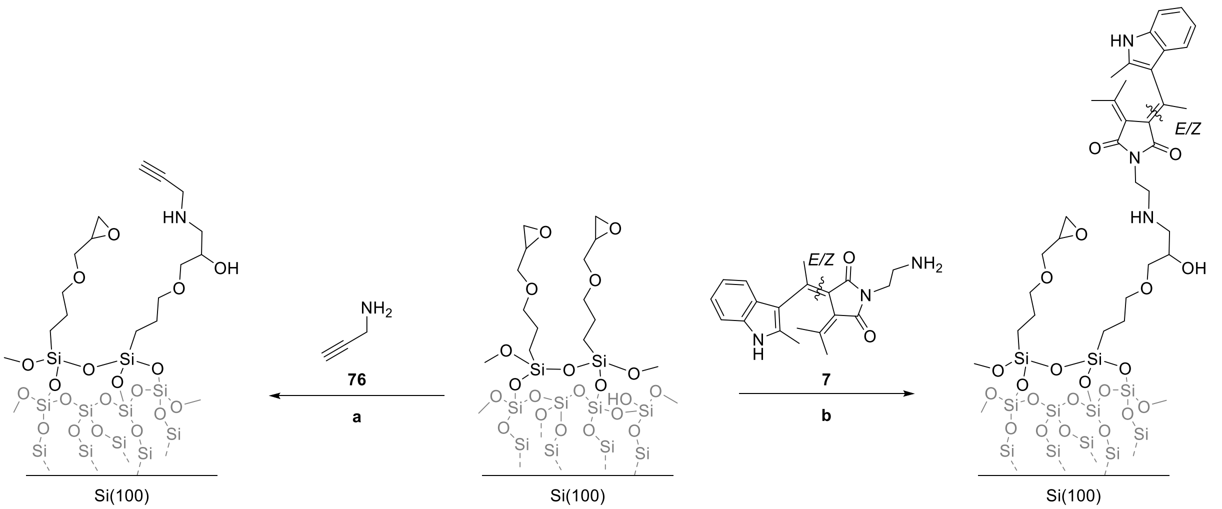

Figure 4.25. Preparation of the acetylene- and fulgimide-terminated monolayers on oxidized Si(100). Reagents and conditions: (a) 156 mM propargylamine (**76**) in toluene, 80 °C, glove box, 24 h; (b) 5.4 mM fulgimide **7** in toluene / 1,4-dioxane (10:1), 90 °C, glove box, 24 h.

4.2.5 Acetylene-Terminated SAMs on oxidized Si(100)

Upon the ring-opening reaction with propargylamine (**76**), the shape and the positions of the peak maxima in the C-H stretching region did not change significantly (Figure 4.26). The intensity increased for both $\nu_{as}(CH_2)$ and $\nu_{sym}(CH_2)$ absorption bands, because of the additional CH_2 group from the propargylamine moiety. Additionally, a slight shift to lower wavenumbers was observed for both CH_2 absorption bands (from 2931.3 to 2928.9 cm^{-1} for $\nu_{as}(CH_2)$, and from 2869.0 to 2862.7 cm^{-1} for $\nu_{sym}(CH_2)$), thereby suggesting adjustment in packing due to loss of sterically demanding epoxide ring head groups. A weak absorption band at 2121 cm^{-1} originates from the C≡C bond vibration. A wide asymmetric band with the peak maximum at 1612 cm^{-1} was assigned to δ(N-H) absorption bands of the secondary amine, both in its protonated and non-protonated form. Protonated secondary amines (NH_2^+) show vibrations in a region from 1620-1560 cm^{-1}, while the vibrations of the non-protonated amines (NH) are located at 1580-1490 cm^{-1}.[136] In addition, asymmetry and high intensity of the bands suggest overlapping with the water O-H bending vibration from the water adsorbed on the surface.

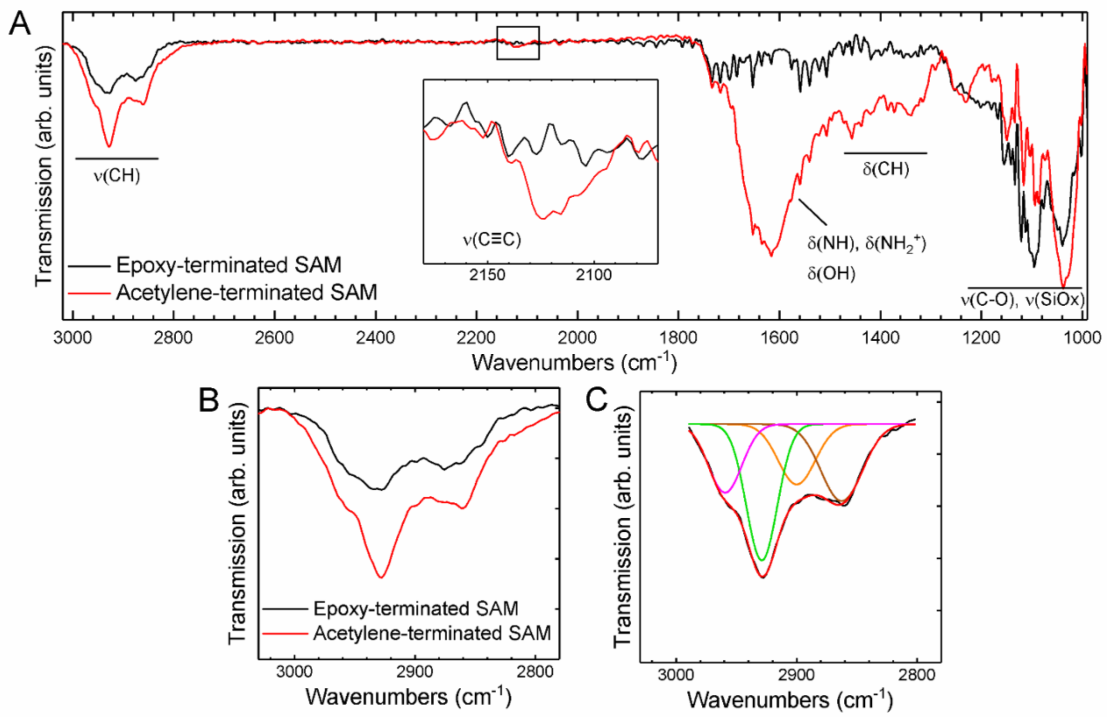

Figure 4.26. The IR spectra of the epoxy- (black) and acetylene-terminated (red) monolayers, referenced to silicon-oxide. The zoom of the C-H stretching region of the epoxy- (black) and acetylene-terminated (red) monolayers.

The area with two broad absorption bands with maxima at 1438 and 1373 cm^{-1} contains a variety of weak-medium vibrations. The alcohol O-H in plane vibration band is a broad signal with a peak at 1370 cm^{-1}, also occurring as two absorption bands. C-H wagging vibrations of secondary alcohols are located in the range 1400-1330 cm^{-1}, while the position of the C-H deformation vibration depends on the hydrogen bonding, being located at 1440-1400 cm^{-1} when bonded, and 1410-1350 cm^{-1} when not involved in hydrogen bonding. Additionally, absorption bands observed in this region are the C-H wagging vibration overtone of C≡C-H (1375-1225 cm^{-1}), and CH_2 deformation vibrations (1485-1430 cm^{-1}). Small changes in the intensity of the signals in the region below 1200 cm^{-1} suggest only minor changes in the Si-O-Si network, due to oxidation of the substrate upon the epoxide ring-opening reaction.

4.2.6 Fulgimide-Terminated SAMs on Oxidized Si(100)

Ring-opening of the epoxide-terminated monolayer with the fulgimide-linker-conjugate **7** (*E/Z* = 85:15) was hampered by the low solubility in toluene, and 3 mM or 4.8 mM concentrations of compound **7** (15, or 24 µmol) in toluene at 80 °C for 20 h did not furnish monolayer functionalization. Changing the solvent to a mixture of toluene/1,4-dioxane (10:1, 27 µmol, 5.4 mM), increased the amount of fulgimide **7** in solution, thus proved to be successful at 90 °C, but only by mildly stirring the solution, and ensuring that the silicon wafer would not get mechanically damaged. The reaction at 80 °C, without stirring the solution did not yield in monolayer functionalization. When conducting epoxide opening in the glove box, ATR-FTIR-analysis showed no further oxidation of the monolayer or the substrate itself.

Upon the fulgimide immobilization on the surface, characteristic ν_{sym}(C=O) and ν_{as}(C=O) absorption bands of the imide group of the fulgimide head group were observed at ~1734 and ~1700 cm^{-1}, respectively (Figure 4.27), previously also observed for fulgimide-terminated SAMs on Si(111). Furthermore, a wide asymmetric band with a peak maximum at 1608 cm^{-1} was observable and assigned to the δ(N-H) absorption bands of the secondary amine, both in its protonated and non-protonated form, and δ(O-H) from the water adsorbed on the surface. Two broad absorption bands with maxima at ~1455 and ~1350 cm^{-1}, are also observable upon epoxide ring-opening, corresponding to an overlap of a variety of weak-medium vibrations. A weaker intensity of this band compared to the one observed for the acetylene-terminated monolayer indicates a possible lower conversion for the epoxide ring-opening with fulgimide-linker-conjugate **7** than with propargylamine. This might be due to the size of both molecules, with the fulgimide-linker-conjugate being sterically more demanding resulting in lower coverage of the surface.

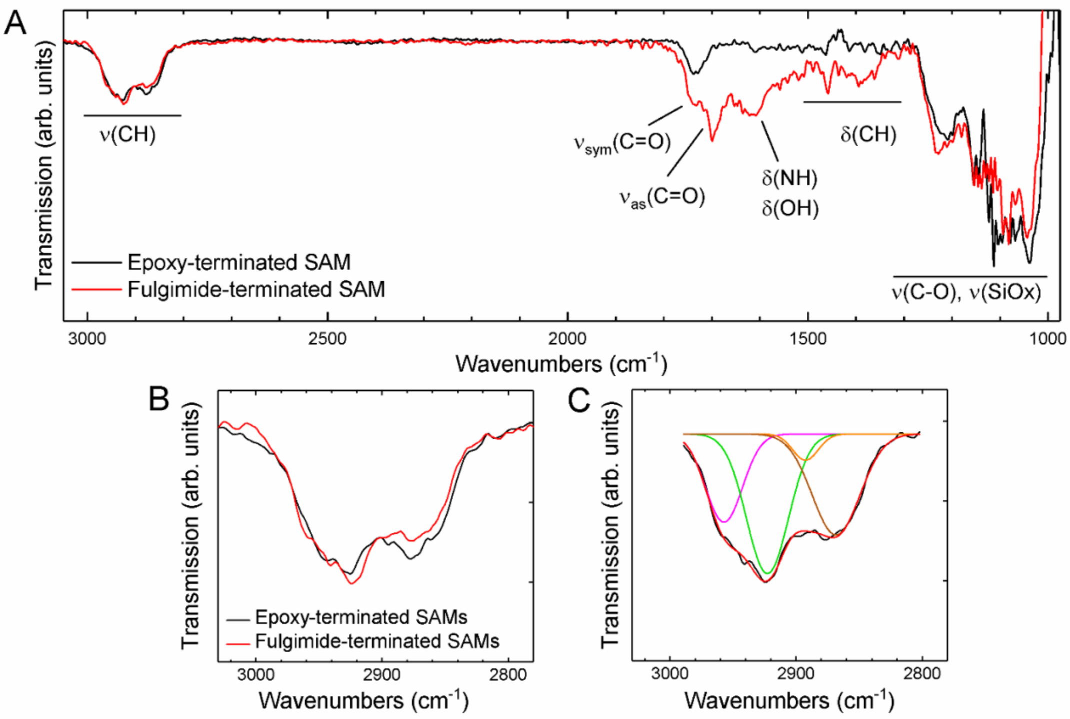

Figure 4.27. The IR spectra of epoxy-terminated (black) and fulgimide-terminated monolayers (red). (B) The zoom of the C-H stretching region of the epoxy- (black) and fulgimide-terminated (red) monolayers. (C) Deconvoluted IR spectra in the same region of the fulgimide-terminated monolayer. The red curve presents the fitted curve upon the deconvolution.

Furthermore, the shape of the C-H stretching region did not change significantly upon the ring opening with the fulgimide. Although the ring opening reaction adds a few methylene groups for each fulgimide linker, the intensities of the $\nu_{as}(CH_2)$ and $\nu_{sym}(CH_2)$ absorption bands stayed almost the same. One of the reasons for this may be partial reduction and blocking of the vibrations of the methylene groups, because of influences of the neighborhood of the molecules and hydrogen bonding. The fulgimide molecules are also not necessarily located on top of the monolayer due to the rough surface, in comparison to the work on Si(111).[14]

In Figure 4.28 the highly resolved XPS spectra of the epoxy- and fulgimide-terminated monolayers are presented.[a] The Si2p, C1s, O1s and N1s are observable as major peaks in the survey, and their contribution to the surface composition is shown in Table 4.3. The N1s signal in the XPS spectrum of the fulgimide-terminated sample comprises contributions from N-atoms of the fulgimide moiety, secondary amine N species of the linker unit, and from impurities observed for the epoxy-terminated monolayer. Nitrogen impurities are known to be present in the samples,[198] and may go along with samples being stored under nitrogen gas over longer time periods.

---

[a] XPS measurements were carried out in the research group of Prof. Dr. Wolfgang Unger at the BAM Federal Institute for Materials Research and Testing, Berlin.

Table 4.3. Atomic surface composition for the epoxy- and fulgimide-terminated monolayer on oxidized Si(100) surfaces, as obtained from the XPS measurement.

Sample	**Elemental composition (surface concentrations** [at%]**)**			
	Si	O	C	N
Epoxy-terminated SAMs	47.55	35.45	16.45	0.40
Fulgimide-terminated SAMs	41.25	31.60	23.85	1.85

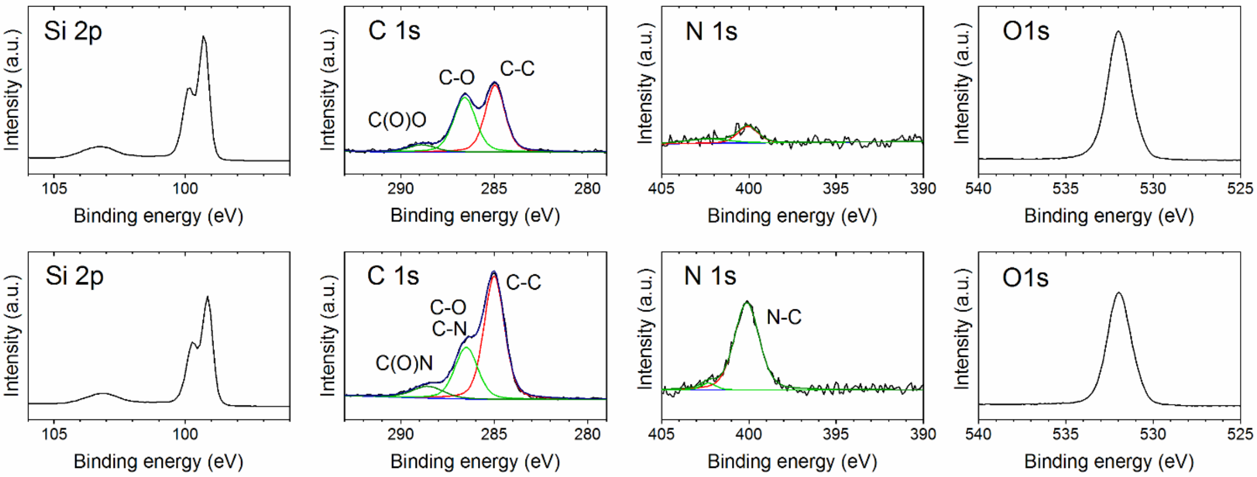

Figure 4.28. High-resolution XPS spectra of the Si2p, C1s, N1s and O1s core levels of the epoxy- and fulgimide-terminated samples on oxidized Si(100).

Peak-fitting analysis of the XPS data for C1s gave insight into chemical environments of the observable C-atoms (Table 4.4). The spectra of the epoxy-terminated sample exhibited a peak at 285.0 eV, originating from C-C and C-H bonds. Ether and epoxide C-O bonds are not distinguishable, appearing at 286.1-288.0 and 286.1-287.1 eV, respectively;[199] here observed at 286.6 eV. Additionally a peak above 288.6 eV is assigned to (O=C-O) groups; the existence of this peak for epoxy-terminated monolayers was reported before,[56,166,194] and it might be an indication for a surface modification with atmospheric carbon dioxide at high temperature in the oven.[200] The deconvoluted C1s spectra of the fulgimide-terminated monolayer showed increase in the C-C component, due to the additional contribution of the fulgimide head-groups. Comparable to the epoxy-terminated sample, peaks are observed at 286.7 eV (C-O, C-N) and 288.9 eV (O=C-O(N)).

Peak fitting analysis of the N1s peak of the fulgimide-terminated monolayer gave two component peaks: a strong signal at 400.1 eV assigned to aromatic/imide C-N bonds and aliphatic C-N bonds. An additional signal is observable at 402.3 eV and assigned to charged amine species (both protonated and hydrogen-bonded).[200,201] In the ATR-FTIR spectra of the fulgimide-terminated monolayers absorption bands for protonated and hydrogen bonded amine species were observed, too (Figure 4.27). The highly resolved O1s region showed only one signal, at 532.0 eV, assigned to Si-O bonds, as well as various C-O bonds from the monolayer and fulgimide moieties.

Table 4.4. Spectral data of the components of the C1s and N1s signals obtained upon the peak fitting analysis of high-resolution XPS spectra - binding energies (eV), component peak area (%) and full-width at half maximum (FWHM) (eV) - for epoxy- and fulgimide- terminated monolayers.

Sample on Si(100)	Assignment (group)	Binding energy position (eV)	Area (%)	FWHM (eV)
Epoxide	C-C, C-H	285.0	48.5	1.2
	C-O	286.6	44.4	1.4
	O=C-O	288.9	7.1	1.7
Fulgimide	C-C, C-H	285.0	61.9	1.3
	C-O, C-N	286.5	29.1	1.4
	O=C-O(N)	288.6	9.0	2.0
	N-C	400.1	95.5	1.7
	N-C (charged)	402.3	4.5	1.0

For the fulgimide-terminated monolayer an immobilization yield was calculated from the C/N ratio of the surface. The chemical formula of the molecules forming this monolayer comprises 26 C-atoms and 3 N-atoms. In the case of a full coverage, the C/N ratio would be 26/3 = 8.67. However, the experimentally obtained C/N ratio for the fulgimide-terminated sample is higher: 23.85 / 1.85 = 12.89 (Table 4.3). Therefore, it can be concluded that the immobilization yield is not 100%. From the nitrogen surface concentration of the fulgimide-terminated surface, the calculated carbon surface concentration for fulgimide-termination is 1.85 · 8.67 = 16.04, and the residual amount of carbon detected on the surface is derived from unreacted epoxide units: 23.85 – 16.04 = 7.81. Since the epoxy-terminated monolayer has 6 carbon atoms per immobilized molecule, the fulgimide:epoxide ratio can be calculated:

fulgimide : epoxide = $\frac{16.04}{26} : \frac{7.81}{6}$ = 0.61 : 1.30 ≈ 1.0 : 2.13.

Accordingly, we may speculate that one out of every three epoxy-head groups of the monolayer is modified with fulgimide-linker-conjugate **7**, giving an estimate for the overall derivatisation efficiency for the on-chip epoxide ring-opening reaction in the order of 32 %.

4.2.6.1 Photochemical Studies of Fulgimide-Terminated Monolayers on Oxidized Si(100)

Upon UV-light irradiation, the fulgimide head groups of the fulgimide-terminated monolayer were switched from the open *E*-form to the closed *C*-form (Figure 4.29). The switching of the fulgimide-terminated SAMs were conducted by alternations of UV and visible light irradiation, and the two photostationary states, PSS(365 nm) and PSS(545 nm), were evaluated by ATR-FTIR spectroscopy and water contact angle measurements. The switching experiments were carried out comparable to the fulgimide-terminated samples on Si(111), under inert gas and were allowed for 30 min per irradiation period. Apart from that, the samples were stored in the dark.

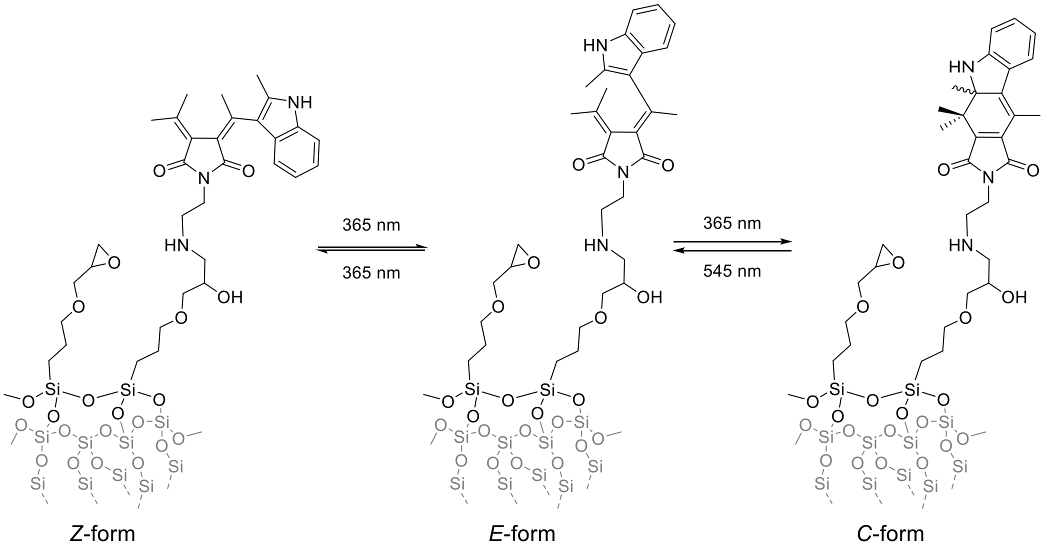

Figure 4.29. Fulgimide *E*-to-*C* and *C*-to-*E* photochromism upon UV (λ_{irr} = 365 nm) and visible (λ_{irr} = 545 nm) light irradiation.

After the immobilization procedure with fulgimide **7** (*E*/*Z* = 85:15), the ν_{as}(C=O) absorption band was located at 1698.9 cm^{-1} (Figure 4.30). Upon irradiation, the imide absorption band is shifted from 1699.5 to 1698.7 cm^{-1} (in PSS(365 nm) and PSS(545 nm), respectively) in the first cycle. However, a gradual shift of the position of the ν_{as}(C=O) absorption band of the open forms

(PSS(545 nm)) over five cycles is observed, from 1698.9 (after immobilization) to 1698.4 cm^{-1} (Figure 4.30B). For this, changes in the orientation, location and the ratios of the photoisomers of the fulgimide molecules might be responsible, and additionally variations in water content and surface temperature. In addition, there is a decrease in the intensity and broadening of ν_{as}(C=O) absorption bands in both PSS, over five cycles (Figure 4.30, C,D). This broadening of the signals, and the appearance of a shoulder at lower frequency (1694 cm^{-1}) might be an indication for weakening of the C=O bond. The hydrogen bonding is capable of lowering frequency of the C=O bond, and thus the peak is observed at lower wavenumbers.[136] Additionally, the alterations in water content and hydrogen bonding may partially impede the vibration of the C=O bonds, leading to a decrease of the intensity of these absorption bands over time.

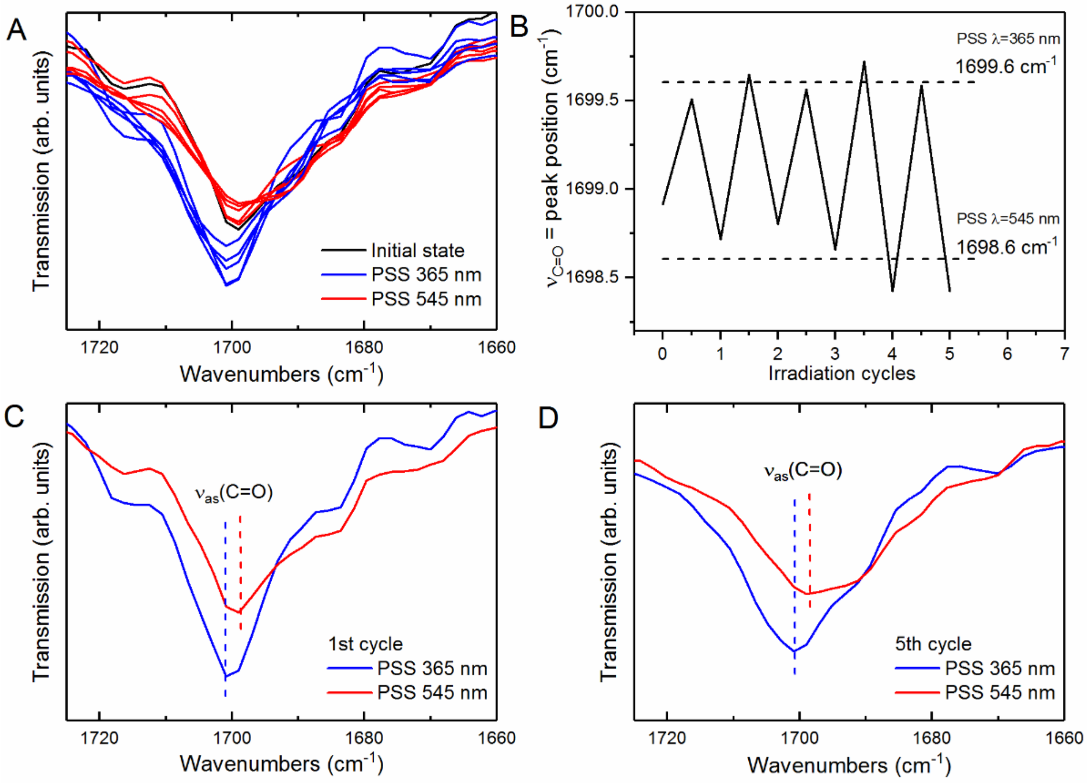

Figure 4.30. ATR-FTIR spectra of the ν_{as}(C=O) absorption band of the fulgimide-terminated monolayer at the PSSs, upon 5 UV/Vis irradiation cycles: initial state (black), PSS(365 nm) (blue), and PSS(545) (red). Broadening of the signal is observed upon several cycles: (C) 1st cycle, (D) 5th cycle.

Monolayer formation on silicon oxide suffers from a lower level of ordering of the monolayer itself, due to the roughness of the oxide surface. Therefore, monolayer molecules can adopt various orientations, resulting in some terminal functionalities being hidden or hindered,[173] causing different environments for the photoswitchable molecules and capacities for water. These possible variations may dictate differences in the vibrational energy of the imide C=O bonds of the various fulgimide molecules on the surface, leading to the observed broadening of the absorption bands over several irradiation cycles. Photoswitchable SAMs on highly ordered S(111) did not show this kind of shift, since all of the fulgimide moieties are being located on top of the monolayer.

Additionally, the switching process was studied by water contact angle measurements. The wettability of the surface directly depends on the surface composition, and due to ring-opening and ring-closing of the fulgimide molecules upon UV/Vis irradiation, repeatable changes in wettability over several cycles are expected. Therefore, the switching process was monitored over five cycles, and the contact angles were measured after each irradiation process (Figure 4.31). After the immobilization of the (*E*/*Z*)-fulgimide-linker-conjugate **7** (*E*/*Z* = 85:15) a contact angle of 64.0° was recorded. Irradiation with 365 nm light, furnished the PSS(365 nm) containing the *C*-form and a more polar surface (contact angle 57.7°). The ring-opening reaction with 545 nm light reproducibly gave a less polar surface and a contact angle of 62.5° for PSS(545 nm), and thus a lower value in comparison to the value for the starting 85:15 (*E*/*Z*)-mixture.

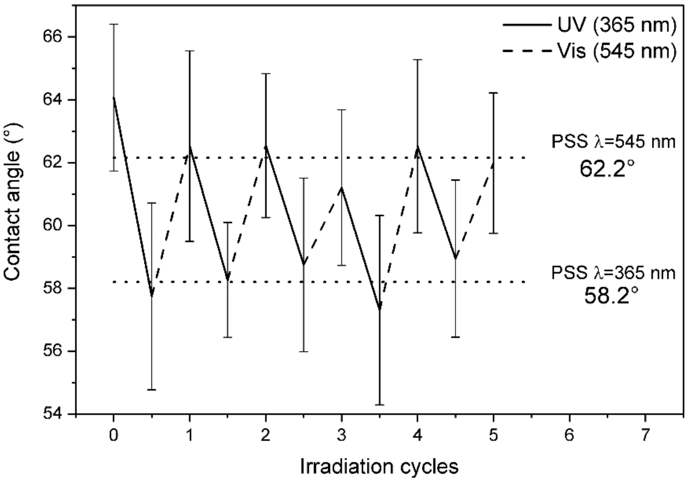

Figure 4.31. Changes in wettability of the fulgimide-terminated monolayer upon reaching PSSs over five UV/Vis irradiation cycles. Dotted lines present the average position for each of the two PSSs.

The dipole moments were previously calculated for all fulgimide forms (*E*-form: 2.409 au, *Z*-form: 1.337 au, and *C*-form: 1.980 au).[15] However, the changes in wettability observed from the contact angle measurements upon photoisomerisation do not go along with the changes of the calculated dipole moments, which would assume a more polar surface for the PSS(545 nm) with the (*E*/*Z*)-forms, but only when reaching a defined orientation of the dipole moments. However, the *C*-form was reported to have very high averaged hyperpolarizability compared to the open forms, 37224 au compared to 1811 and 683 au, respectively. In addition, surrounding water molecules due to their own electric dipole moment can increase this effect, thereby making the fulgimide-terminated monolayer with the PSS(365 nm) enriched in *C*-form more polar furnishing a better wettability of the surface.

5 Conclusion

In this work, the unique property of photochromic compounds to reproducibly switch between different states were used to functionalize silicon wafers, with the aim of preparation of light-sensitive smart materials. Two types of photochromic compounds, fulgimides and naphthopyrans, were synthesized and fully characterized. Their photochromic properties were investigated using various different methods – UV/Vis measurements, NMR and FTIR spectroscopy. Their different thermodynamic stability governs their photochemical properties; fulgimide photoisomers being stable, thus the switching alternates between two states only upon light irradiation. On contrary, naphthopyran open isomers are thermodynamically labile, thus their switching is directed both by light irradiation and thermal relaxation in the dark. Both systems showed remarkable fatigue resistance during the investigations in solution.

For their immobilization onto silicon wafers, the concept of self-assembled monolayers was employed. Immobilization of the photochromic compounds was carried out on monolayers on oxide-free Si(111) and oxidized Si(100) surfaces. For the evaluation of the obtained monolayer structures, several analytical methods were used, such as ATR-FTIR spectroscopy, X-ray photoelectron spectroscopy, ellipsometry and contact angle goniometry; they confirmed high quality of the prepared monolayer structures. Furthermore, they allowed examination of photochromism of the photoswitch-functionalized surfaces. For all prepared photoswitchable surfaces, repeatable changes between the states were observed upon light-illumination and/or thermal relaxation in the dark. Furthermore, comparison between the various photoswitchable monolayers suggested influence of the underlying monolayer properties onto the photochemical behavior of the photochromic moieties on top.

5.1 Synthesis of Photoswitch-Linker Conjugates

In this work, fulgimide-linker conjugate **7** with free primary amine functionality was synthesized, with the aim of attachment to the variously terminated surfaces. The synthesis proceeded in nine reaction steps, from commercially available 2-methylindole **20**, to yield fulgimide conjugate **7** (*E*/*Z* ratio 85:15, ^{1}H NMR) in 8.4 % overall yield (Figure 5.1).

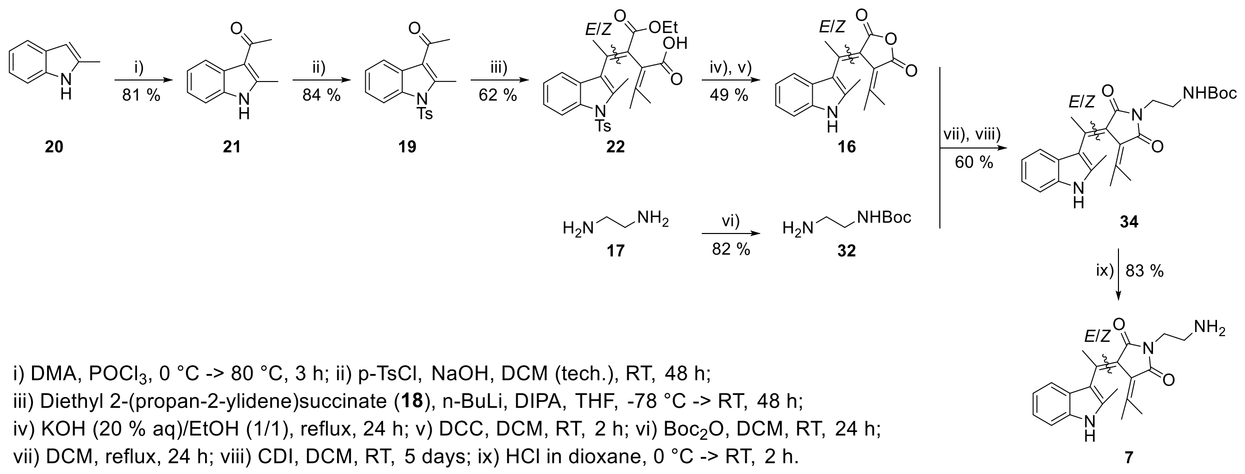

i) DMA, $POCl_3$, 0 °C -> 80 °C, 3 h; ii) p-TsCl, NaOH, DCM (tech.), RT, 48 h;
iii) Diethyl 2-(propan-2-ylidene)succinate (**18**), n-BuLi, DIPA, THF, -78 °C -> RT, 48 h;
iv) KOH (20 % aq)/EtOH (1/1), reflux, 24 h; v) DCC, DCM, RT, 2 h; vi) Boc_2O, DCM, RT, 24 h;
vii) DCM, reflux, 24 h; viii) CDI, DCM, RT, 5 days; ix) HCl in dioxane, 0 °C -> RT, 2 h.

Figure 5.1. Synthetic route towards formation of fulgimide-linker conjugate **7**.

Furthermore. naphthopyran-linker-conjugate **8** was synthesized and characterized. Contrary to the linker attached to the fulgimide structure, here a more rigid, piperazine-based linker was used. The synthesis proceeded via the nine-step synthetic route presented in Figure 5.2, affording the desired naphthopyran compound **8** as a salt, in 3.1 % overall yield.

In the linker synthetic route, the Buchwald-Hartwig amination reaction (Figure 5.2, iii) did not show complete conversion in toluene at 100 °C over 44 h, and side product formation of imine and dehalogenated educt was speculated as possible reason for lowering the yield of this reaction (Chapter 3.2.2.2, Figure 3.19). An optimization of this reaction step, including the choice of the catalyst source, ligand, base, solvent and temperature were not investigated in this work. However, it is believed that future optimization of this step may increase the obtained yield of the reaction.

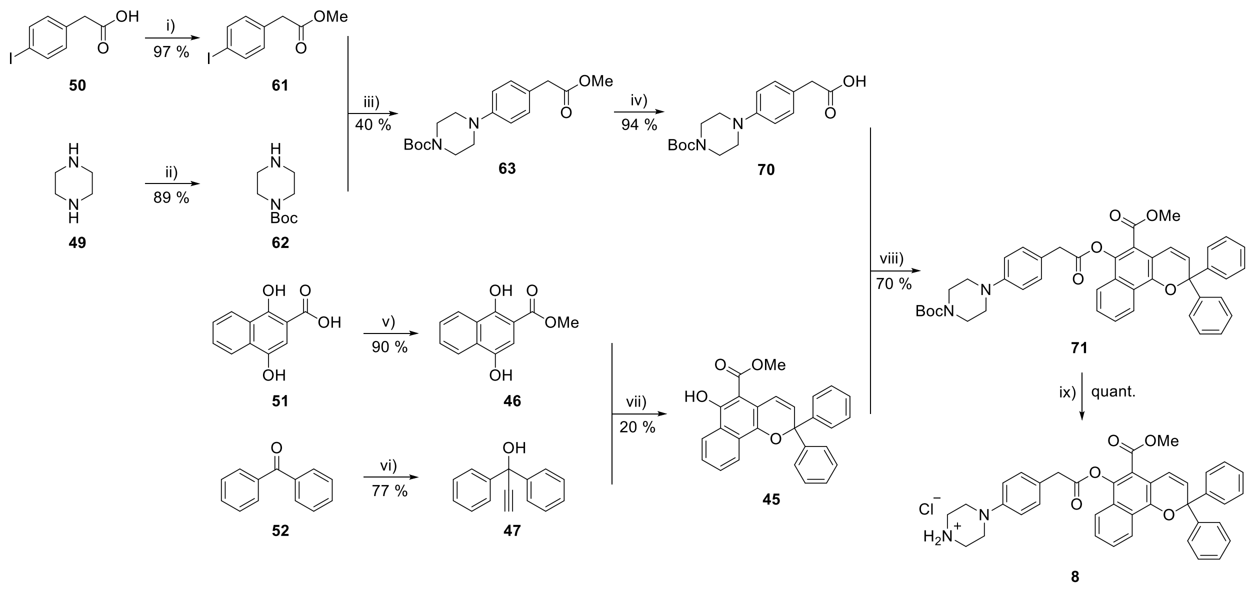

i) H_2SO_4, MeOH, RT, 4.5 h; ii) Boc_2O, DCM, 0 °C -> RT, 24 h; iii) $Pd_2(dba)_3$, $^t\mathrm{Bu}_3P$, Cs_2CO_3, toluene, 100 °C, 44 h; iv) NaOH, THF, RT, 21 h; v) $NaHCO_3$, MeI, DMF, RT, 23 h; vi) CHCMgCl (0.6 M in THF/toluene), THF, RT, 70 h; vii) Al_2O_3, toluene, reflux, 24 h; viii) DCC, DMAP, DCM, 0 °C -> RT, 48 h; ix) HCl in dioxane, 0 °C -> RT, 1.5 h.

Figure 5.2. Synthetic route towards formation of naphthopyran-linker conjugate **8**.

5.2 Photochromism of Photoswitch-Linker Conjugates

Photochemical studies were performed for both fulgimide-linker conjugate **7**, and related fulgide analogue **16**, with the use of UV/Vis measurements. Both photochromic compounds were investigated in acetonitrile and chloroform. Additionally, for both compounds, as expected, a complete reproducible switching without signs of fatigue in solution were observed in measurements in acetonitrile, upon alternation of UV (λ_{irr} = 365 nm) and visible light (λ_{irr} = 565 nm) irradiations, over 5 cycles.[14]

The switching of both the naphthopyran core **45** and naphthopyran-linker conjugate **71** were characterized in detail. Both UV/Vis time-resolved and ^{1}H NMR time-resolved spectra of the photochemical studies showed the open forms reaching a plateau upon thermal relaxation for both naphthopyran compounds; compound **45** was bleaching significantly slower compared to the conjugate **71** (Figure 5.3). From the ^{1}H NMR investigations, it was shown that naphthopyran building block **45**, contained a ratio of the photoisomeric species at PSS(365 nm) of 16:77:7 (CF:TC:TT). The thermal back reaction was very slow, so that signals of both open isomers were fading simultaneously. For the naphthopyran-linker-conjugate **71** the ratio of photoisomers at PSS(365 nm) was determined to be 34:48:18 (CF:TC:TT). Additionally, the TC→CF transformation occurs fast; at PSS(Δ) only the CF and TT forms were observed (83:17, respectively). The closed form was completely restored upon visible light irradiation. The slow **45**-TC bleaching is assigned to stabilization from the electron-donating group (OH) in 6-position, as well as hydrogen bonding of the phenyl OH, stabilizing the carbonyl oxygen of the open forms; this effect is not observed for the naphthopyran-linker conjugate **71**.

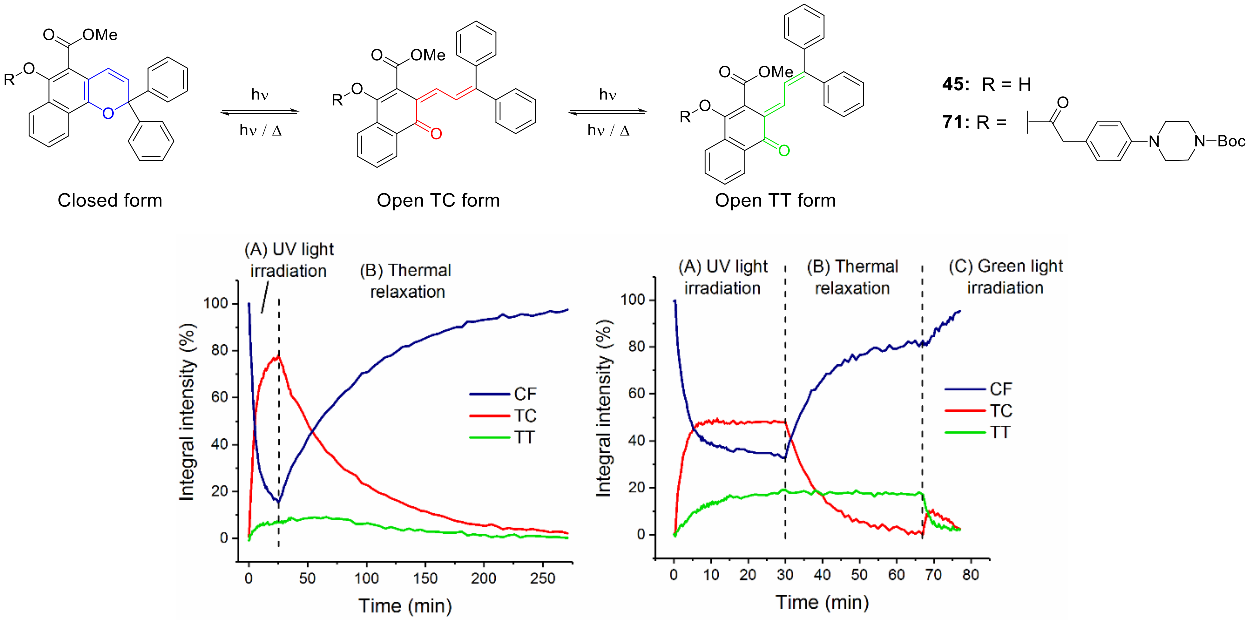

Figure 5.3. Time-resolved spectra of naphthopyran **45** (left) and naphthopyran-linker conjugate **71** (right) of ^{1}H NMR signals during one irradiation cycle; photoisomers: closed form (blue), TC form (red), TT form (green).

The photochemical switching was analyzed in solution via FTIR spectroscopy for both naphthopyran compounds **45** and **71**, in solvents of different polarity, i.e. TCE, MeCN and DCE. Photochemical studies by alternation of irradiation with UV light (λ_{irr} = 365 nm) and thermal relaxation were conducted, and revealed, amongst others, repeatable changes in the position of methyl ester ν(C=O) absorption band, independent from the solvent used, and changes in the intensity of the signal responsible for the conjugated C=C bond vibration at ~1595 cm^{-1}.[136,202]

Additionally, UV/Vis absorption studies of naphthopyran **71** in acetonitrile showed completely reproducible photochemical cycles without a sign of fatigue upon alternation of UV (λ_{irr} = 365 nm) and visible light (λ_{irr} = 505 nm) irradiation.

5.3 Monolayer Structures on Si(111) and Si(100)

Self-assembled monolayers were prepared on oxide-free silicon(111) and oxidized silicon(100) wafers (Figure 5.4).

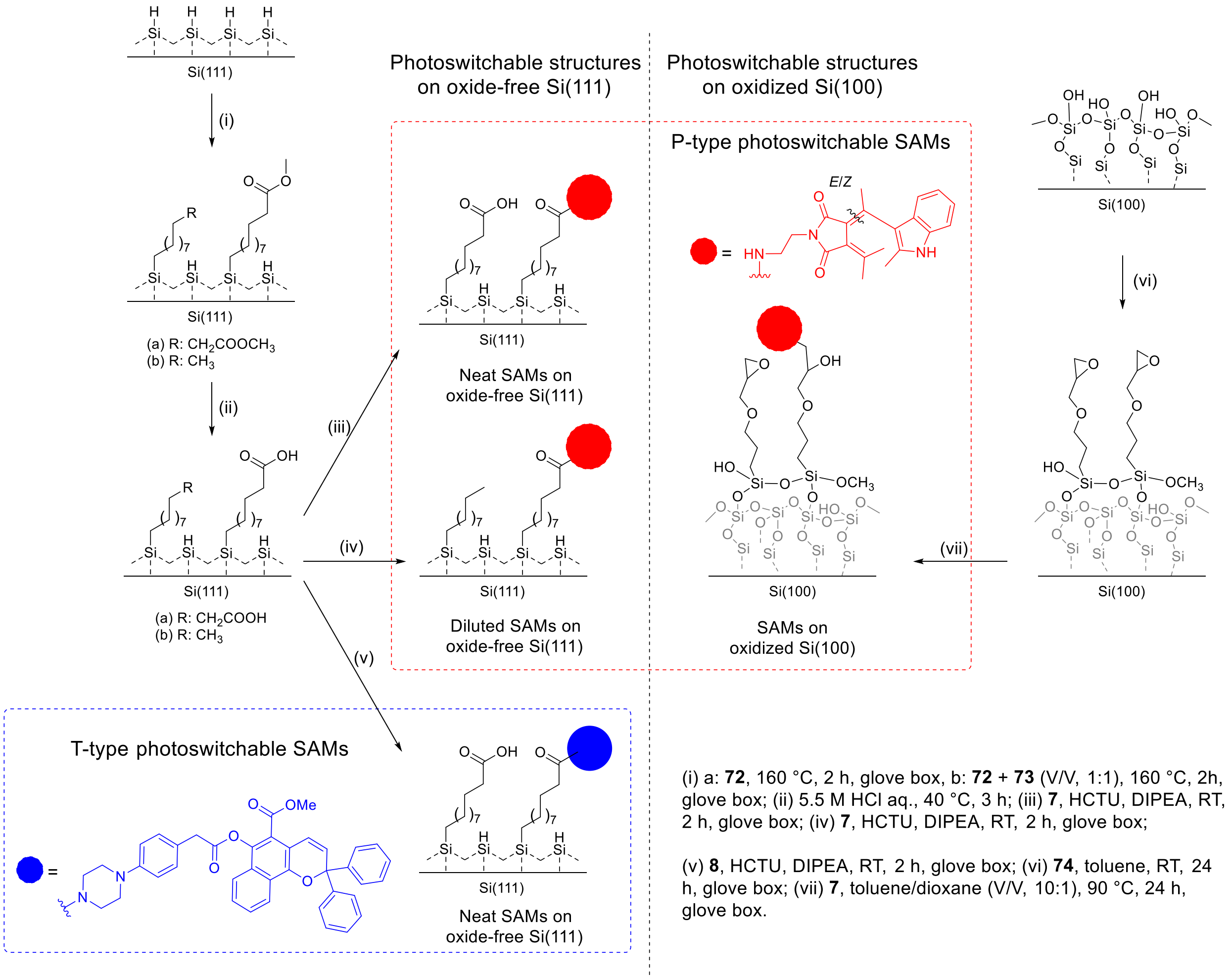
Si(111)
(i)
(a) R: CH2COOCH3
(b) R: CH3
(ii)
(a) R: CH2COOH
(b) R: CH3
(iii)
(iv)
(v)
Photoswitchable structures on oxide-free Si(111)
Photoswitchable structures on oxidized Si(100)
P-type photoswitchable SAMs
E/Z
Neat SAMs on oxide-free Si(111)
Diluted SAMs on oxide-free Si(111)
SAMs on oxidized Si(100)
Si(100)
(vi)
(vii)
T-type photoswitchable SAMs
OMe
Neat SAMs on oxide-free Si(111)

(i) a: **72**, 160 °C, 2 h, glove box, b: **72** + **73** (V/V, 1:1), 160 °C, 2h, glove box; (ii) 5.5 M HCl aq., 40 °C, 3 h; (iii) **7**, HCTU, DIPEA, RT, 2 h, glove box; (iv) **7**, HCTU, DIPEA, RT, 2 h, glove box;

(v) **8**, HCTU, DIPEA, RT, 2 h, glove box; (vi) **74**, toluene, RT, 24 h, glove box; (vii) **7**, toluene/dioxane (V/V, 10:1), 90 °C, 24 h, glove box.

Figure 5.4. Overview of photoswitchable self-assembled monolayers on silicon surfaces, prepared in this work.

On Si(111) SAMs were prepared via hydrosilylation of methyl-10-undecenoate (**72**) on H-terminated Si(111) surface. Diluted monolayers, with a reduced number of functionalities at the terminal end, were obtained by grafting a mixture of methyl undecenoate and 1-decene (**73**) (V/V, 1:1). Subsequent hydrolysis of ester-terminated SAMs, yielded a carboxy-terminated monolayer. Further functionalization of the carboxy-terminated oxide-free Si(111) surfaces were carried out with both fulgimide- **7** and naphthopyran-linker conjugate **8**, via amide bond formation, using HCTU as a coupling reagent. Results previously reported for neat fulgimide-terminated SAMs on Si(111) showed efficiency of the coverage of ~50 %, suggesting that every other monolayer carboxylic acid head-group is functionalized with a fulgimide moiety[14]. A dilution of carboxylic acid functionalities at the terminal end of the SAMs, prepared in this work using a 1:1 ratio of the monolayer molecules (methyl-10-undecenoate and 1-decene), suggests ~50 % of groups at the terminal end of the SAM carrying a carboxylic acid functionality. Thus, maximum coverage of fulgimide **7** onto the diluted monolayer would yield a structure where every second monolayer linker is functionalized: the complete functionalization of carboxylic acid head groups. Consequently, this results in the same possible coverage of both neat and diluted monolayers. However, the main difference comes from the polarity of the underlying monolayer in the immediate vicinity of the fulgimide moieties; the neat SAMs contain very polar unreacted carboxylic acid functionalities, while the diluted SAMs mainly contain nonpolar methyl groups from the decene monolayer units.

The coupling efficiency of the naphthopyran **8** attachment was also determined, using X-ray photoelectron spectroscopy (XPS) and a comparable approach previously applied to the fulgimide neat SAMs in ref. 14. The grafting efficiency was determined to be ~50 %, resulting in high density of the naphthopyran units on top of the SAMs, where every second monolayer molecule is decorated with a photoswitch unit. This suggest similar packing density and concentration of the photoswitch on top of the surface, for both P-type and T-type photoswitchable SAM structures on Si(111).

On oxidized Si(100), epoxy-terminated self-assembled monolayer was prepared, by silanization reaction with (3-glycidyloxypropyl)trimethoxysilane (**74**). The amount of water present in the solvent during the silanization reaction proved to be essential for the formation of reproducible and high quality monolayers. Analysis of the $\nu(CH_2)$ peak positions provided information on ordering and packing of the monolayer molecules, suggesting that more densely packed structures were prepared with toluene of low water content (10 ppm). This was further confirmed by applying the same procedures on preparation of an alkyl-terminated monolayer without a functionality at the terminal end, by silanization of trimethoxy(propyl)silane (**75**). Additionally, the choice of solvent for the work-up procedure after monolayer formation also was crucial. According to obtained IR data, only toluene gave reproducible results; procedures involving ethanol often resulted in adsorption of solvent on top of the monolayer. High-quality monolayers were further confirmed via contanct-angle and ellipsometry measurements. Contact angle for epoxy-terminated monolayer was determined to be 54.1°, which is in accordance with the literature values for regular monolayer structures. Thickness of the monolayer was determined to be 0.9 nm, which is in agreement with the extended conformation of the GPTMS molecule (0.9-1.0 nm), and previously reported values for the GPTMS monolayer structures.

Functionalization of the monolayer was carried out via an epoxide ring-opening reaction with propargylamine (**76**) and fulgimide-linker-conjugate **7**. XPS investigation of the fulgimide-terminated SAMs on oxidized Si(100) suggested ≈32 % derivatisation yield of fulgimide-linker-conjugate **7**; a lower yield than previously observed for the amide bond formation on densely packed carboxy-terminated Si(111) surfaces.[14]

On-chip photochemical studies on fulgimide-terminated monolayers, both on Si(111) and Si(100), exhibited repeatable changes of ν_{as}(C=O) absorption bands, upon alternation of UV (λ_{irr} = 365 nm) and visible light irradiation (λ_{irr} = 545 nm). Highly ordered monolayers on Si(111), where fulgimide moieties are located on top of the monolayers show regular changes between two photostationary states (PSS(365 nm) and PSS(545 nm)), over 5 irradiation cycles. Contrary, due to the roughness of the oxide surface, the structure of monolayers on oxidized Si(100) suffers from a lower level of ordering of the monolayer itself. Thus, monolayer molecules can adopt various orientations causing different environments for the fulgimide head-groups (some embedded in the monolayers, while others being on top). These possible variations, as well as monolayer ability to adsorb water on its surface, may have an influence on vibrational energy of the imide C=O bonds of the various fulgimide molecules immobilized on the surface, leading to the observed broadening of the absorption bands over several irradiation cycles. The shoulder at lower wavenumbers (~1680 cm^{-1}) was observed for fulgimide samples on oxidized Si(100) and diluted SAMs on Si(111). Different level of ordering of the monolayers influence switching read-out of the fulgimide decorated monolayers. However, obviously for all scenarios a two state system was evaluated with IR spectroscopy.

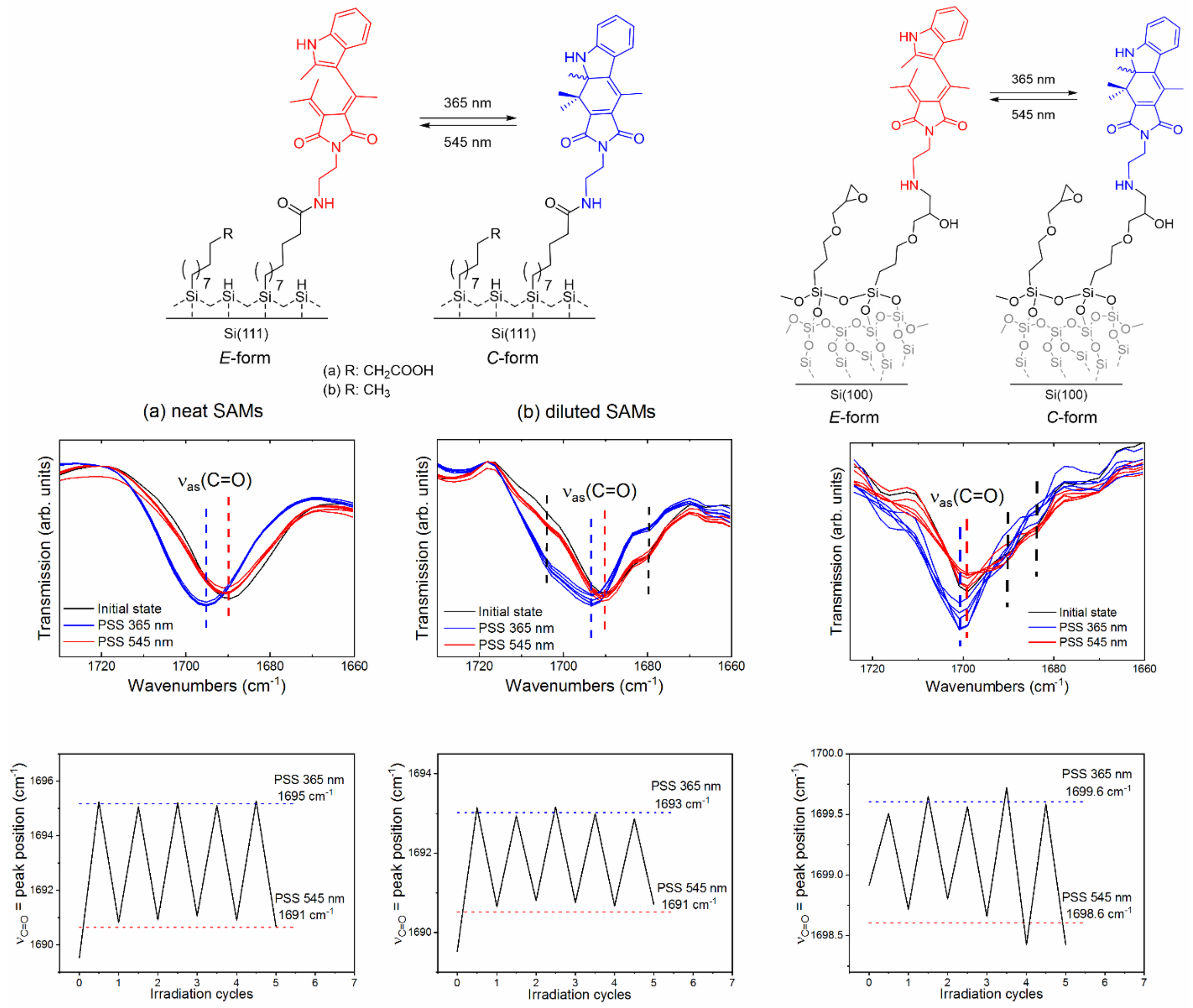

Figure 5.5. Photochemical studies of fulgimide-terminated SAMs on Si(111) and Si(100) surfaces.

Additionally, the contact angle measurements of fulgimide-terminated SAM on oxidized Si(100) surface revealed repeatable changes in wettability upon alternating UV and visible light irradiation. These changes are shown to depend, amongst others, upon the hyperpolarizability of the different fulgimide photoisomers.[15]

The photo-induced switching of the naphthopyran-terminated Si(111) surface was evaluated by ATR-FTIR spectroscopy, by following the changes in the methyl ester ν(C=O) absorption band position (1725 cm^{-1}), as well as the intensity of the conjugated C=C bond stretching vibration (1595 cm^{-1}), upon several cycles.

Compared to the solution studies, the accumulation of the open forms is higher on the surface; it is caused by the fading rate on surface being slower compared to solution studies. This can be explained by the different immediate environments of the naphthopyran compounds - the fading rate being different in liquid medium compared to solid phase / gas interface observed for the surface studies. Moreover, the confined space of the densely packed naphthopyran moieties on the surface can also impact the reduction of the fading rate. Furthermore, stabilization of the naphthopyran open forms via hydrogen bonding with the unreacted carboxy-terminated surface may additionally cause accumulation of the open forms. As silimar intramolecular stabilization via hydrogen bonding was previously observed in the solution studies of naphthopyran **45**. The existence of the stabilization results in a three state cycle of naphthopyran-terminated SAMs going through three different states: PSS(365 nm) → PSS(Δ) → PSS(545 nm). From the PSS(545 nm) upon UV light irradiation, PSS(365 nm) is again reachable. Thus, the switching between the states is a one-directional process.

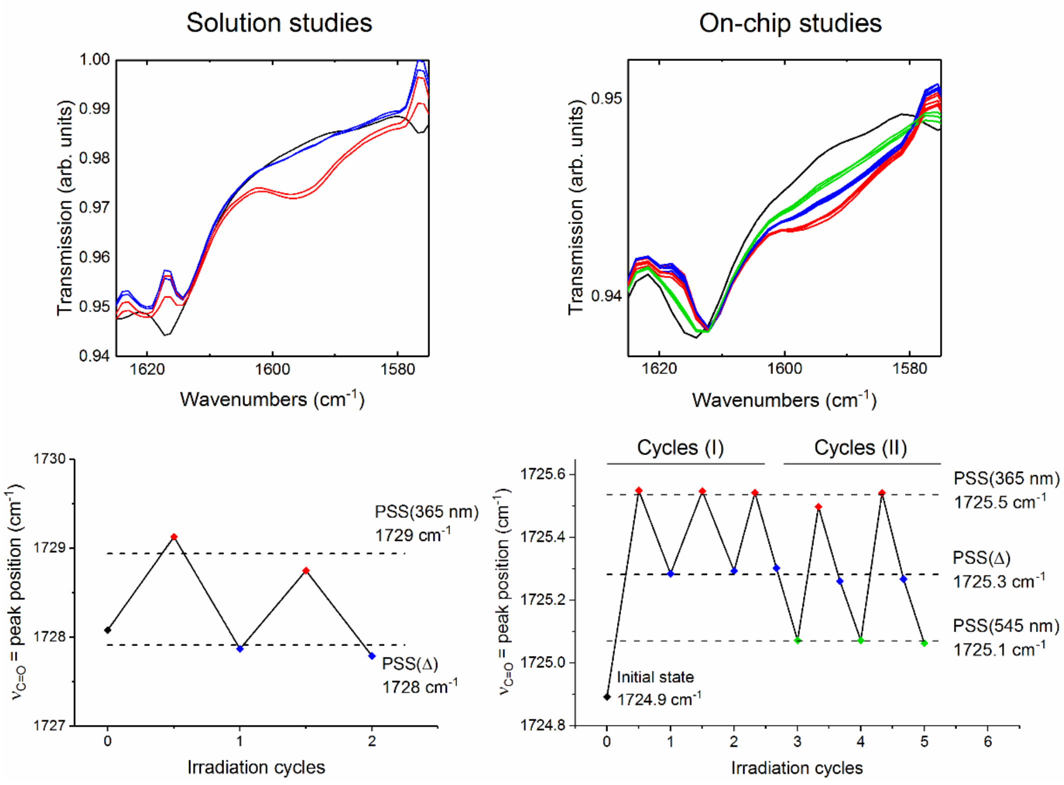

Figure 5.6. Differences between photochemical studies of naphthopyran-linker conjugate **71** in acetonitrile solution and naphthopyran-terminated SAMs on Si(111).

P-type and T-type photoswitchable SAMs on Si(111), exhibit different stability of their states during the photochemical studies. Fulgimide-terminated monolayers are strictly switched between two photostationary states, PSS(365 nm) and PSS(545 nm), upon irradiation with UV and visible light, respectively. Here, the influence of the underlying monolayer does not play significant role in the photochemical process. On the other side, the naphthopyran-terminated monolayer reaches three different states during one cycle, the PSS(365 nm), PSS(Δ) and PSS(545 nm). The highly polar carboxy-terminated monolayer underneath the naphthopyran moieties acts as a stabilization factor for the open forms (TC and TT), thus decreasing the rate of the thermal back reaction on the surface and facilitating accumulation of the open photoisomers. Upon visible light irradiation (λ_{irr} = 545 nm) the system reaches the third stable state for starting the complete cycle again.

6 Experimental Section

6.1 General Information

All starting materials and reagents were purchased in the highest available purity and were used without further purification, unless otherwise stated. Solvents used for extractions and purification (i.e. column chromatography, recrystallization) were of technical purity, and were dried and distilled prior to use: ethyl acetate over potassium carbonate; DCM, pentane, and cyclohexane over phosphorus pentoxide. Solvents used for reactions were of p.a. purity, and dried and distilled prior to use according to standard procedures:[203] toluene, dioxane, and THF over sodium/benzophenone, DCM over calcium hydride.

All reactions were monitored by analytical thin-layer chromatography (TLC, silica gel, Merck 60 F254 plates) and visualized by UV light (λ = 254 nm), and staining reagents: potassium permanganate, ninhydrine, or Seebach reagent (phosphomolybdic acid/$Ce(SO_4)_2$) stain. Preparative flash-chromatography was performed on MP Biomedicals GmbH silica gel 60 (32 – 63 µm, 60 Å). For purification of compound **47** Acros Organics neutral aluminium oxide (Brockmann I, 50-200 µm, 60 Å) was used. Solvents used as eluents are specified in the procedure for a particular substance.

^1H NMR spectra were recorded on a Bruker AvanceII 400 MHz spectrometer or a Bruker AvanceIII 500 MHz spectrometer. Chemical shifts are given as dimensionless δ-values in ppm, and coupling constants J are in Hz. Solvents are mentioned for the particular substances; their residual signals were used as internal standards: $CDCl_3$ δ = 7.26 ppm, MeOD-*d3* δ = 3.31 ppm, DMSO-*d6* δ = 2.50 ppm. The number of protons was determined by integration the corresponding signals. Multiplicities of the signals were abbreviated as follows: s = singlet, d = doublet, t = triplet, q = quartet, m = multiplet, b = broad. ^{13}C NMR spectra were recorded at 100 or 125 MHz on a Bruker AvanceII 400 MHz spectrometer or a Bruker AvanceIII 500 MHz spectrometer, respectively. Chemical shifts are given as dimensionless δ-values in ppm. Solvent residual signals were used as internal standards: $CDCl_3$ δ = 77.16 ppm, MeOD-*d3* δ = 49.00 ppm, DMSO-*d6* δ = 39.52 ppm. Correlation 2D NMR spectroscopy measurements (^1H-^1H COSY, ^1H-^{13}C HMQC,

^{1}H-^{13}C HMBC) were recorded on either a Bruker AvanceII or a Bruker AvanceIII spectrometer. All NMR spectra were measured at room temperature, unless otherwise stated.

Melting points were recorded on a Büchi M-560 melting point apparatus using open capillary tubes; the values remain uncorrected.

Infrared spectra were recorded as ATR (attenuated total reflectance) on Thermo Nicolet Magna-IR 750 FTIR spectrometer and are reported as wavenumbers in cm^{-1}. The intensity of the peaks were abbreviated as follows: s = strong, m = medium, w = weak, br = broad.

The samples for mass spectra and high-resolution MS were measured on a Finnigan MAT 95 S, and were ionized at an ionization potential of 70 eV. Ionization of the samples for the high-resolution MS measurement was carried out in positive ion mode by electron-spray ionization (ESI), unless otherwise specified.

Elemental analyses were performed on Thermo FlashEA 1112 Organic Elemental Analyzer.

6.2 Synthesis of Fulgimide-Linker Conjugate

1-(2-Methyl-1*H*-indol-3-yl)ethan-1-one (21)[81]

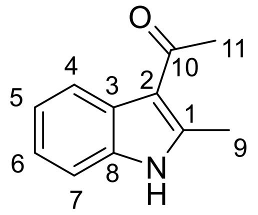

2-Methylindole (10.2 g, 77.8 mmol, 1.00 eq) was dissolved in *N*,*N*-dimethylacetamide (38.5 mL, 414.1 mmol, 5.32 eq) at 0 °C. Phosphoryl chloride (9 mL, 96.3 mmol, 1.24 eq) was added dropwise into the stirred reaction mixture over time of 20 min. The reaction mixture was refluxed at 80 °C for 2.5 h. After cooling to room temperature, the mixture was added to water (250 mL). The phases were separated, the water phase was extracted with DCM (5 × 100 mL). The water phase was set to pH = 10 with 20% aq NaOH, upon which the yellow solid precipitated. The solution was filtered, and the crude solid was recrystallized from ethanol. The compound **21** was obtained in 81 % yield (10.6 g, 62.8 mmol) as pale yellow solid.

Mp: 201 °C (Lit.: 197-200 °C)[204]. **R*f***: 0.52 (Pentane/EtOAc = 1:1). **^{1}H-NMR** (400 MHz, DMSO-*d6*): δ = 8.01 (m, 1H, H-4), 7.36 (m, 1H, H-7), 7.13 (m, 2H, H-5, H-6), 2.67 (s, 3H, H-9), 2.50 (s, 3H, H-11). **^{13}C-NMR** (100.6 MHz, DMSO-*d6*): δ = 193.0 (C-10), 144.2 (C-1), 134.7 (C-8), 126.9 (C-3), 121.7 (C-6), 121.3 (C-5), 120.6 (C-4), 113.5 (C-2), 111.2 (C-7), 30.9 (C-11), 15.0 (C-9). **IR** (ATR): ν = 3125 (m), 3093 (m), 3058 (m), 2969 (m), 2932 (m), 1610 (s), 1578 (s), 1443 (s), 1390 (s), 1193 (s), 1068 (m), 969 (m), 739 (s), 660 (m), 588 (s). **HR-MS** (ESI) for $C_{11}H_{12}NO$ $[M+H]^+$ calculated: m/z = 174.0913, found: m/z = 174.0908. **EA** for $C_{11}H_{11}NO$ calculated: C 76.28%, H 6.40%, N 8.09%, found: C 76.28%, H 6.35%, N 8.08%.

1-(2-Methyl-1-tosyl-1*H*-indol-3-yl)ethan-1-one (19)[81]

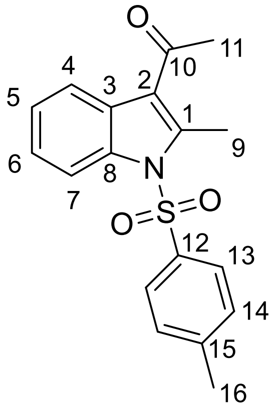

1-(2-Methyl-1*H*-indol-3-yl)ethanon (9.0 g, 52 mmol, 1.0 eq), *p*-toluenesulfonyl chloride (20.1 g, 105 mmol, 2.0 eq) and NaOH (4.2 g, 105 mmol, 2.0 eq) were dissolved DCM (technical grade, 350 mL) and stirred for 48 h at room temperature. The reaction mixture was washed with water (150 mL), the organic phase was separated, washed with brine (150 mL), dried over $MgSO_4$ and concentrated in vacuo. The crude product was recrystallized from cyclohexane, to give compound **19** as colourless solid in 84% yield (14.3 g, 43.7 mmol).

Mp: 108 °C (Lit.: 108 °C)[81]. **R*f***: 0.41 (Hexane/EtOAc = 3:1). **^{1}H-NMR** (400 MHz, $CDCl_3$): δ = 8.29 (m, 1H, H-4), 7.88 (m, 1H, H-7), 7.72 (m, 2H, H-13), 7.34 (m, 2H, H-5, H-6), 7.24 (m, 2H, H-14), 2.90 (s, 3H, H-9), 2.63 (s, 3H, H-11), 2.36 (s, 3H, H-16). **^{13}C-NMR** (100.6 MHz, $CDCl_3$): δ = 196.3 (C-10), 145.7 (C-15), 143.1 (C-1), 136.1 (C-8), 136.0 (C-12), 130.3 (C-14), 127.1 (C-3), 126.7 (C-13), 124.8 (C-6), 124.5 (C-5), 120.9 (C-2), 120.8 (C-7), 114.7 (C-4), 32.3 (C-11), 21.8 (C-16), 14.4 (C-9).[a] **IR** (ATR): ν = 2925 (w), 1669 (s), 1596 (m), 1540 (m), 1452 (m),1379 (s), 1359 (s), 1225 (m), 1172 (s), 1088 (m), 957 (m), 813 (m), 720 (m), 564 (s), 540 (s). **HR-MS** (ESI) for $C_{18}H_{18}NO_3S$ $[M+H]^+$ calculated m/z = 328.1002, found m/z = 328.0998. **EA** for $C_{18}H_{17}NO_3S$ calculated: C 66.04%, H 5.23%, N 4.28%, S 9.79%, found: C 66.20%, H 5.20%, N 4.12%, S 9.90%.

---

[a] In small concentrations in NMR, cyclohexane is visible: ^{1}H NMR ($CDCl_3$): δ = 1.43 (s). ^{13}C NMR ($CDCl_3$): δ = 26.9.[205].

3-(Ethoxycarbonyl)-4-(2-methyl-1-tosyl-1*H*-indol-3-yl)-2-(propan-2-ylidene)pent-3-enoic acid (22)[81]

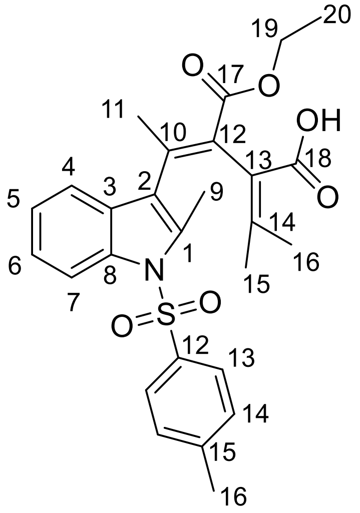

1-(2-Methyl-1-tosyl-1*H*-indol-3-yl)ethan-1-one (**19**) (3.0 g, 9.1 mmol, 1.00 eq) and isopropylidenesuccinic acid diethylester (**18**) (3.0 g, 14.0 mmol, 1.54 eq) were dissolved in dry THF (in 26 mL and 10 mL, respectively). The solutions were left stirring under inert atmosphere over molecular sieves (4 Å) over night. Diisopropylamine (2 mL, 14.3 mmol, 1.57 eq) and *n*-butyllithium (8.5 mL, 1.6 M in hexane, 13.6 mmol, 1.49 eq) were dissolved in dry THF (15 mL) under inert atmosphere at -78 °C. To this solution, previously dried isopropylidenesuccinic acid diethylester was added dropwise via cannula and stirred at -78 °C. After 90 min 1-(2-Methyl-1-tosyl-1*H*-indol-3-yl)ethan-1-one was added dropwise via cannula, and the reaction mixture was stirred for additional 1 h at -78 °C. The solution was left to warm up to the room temperature, and stirred for additional 2 days. The reaction mixture was acidified with ice cold 2 N aq. HCl solution (200 mL), the phases were separated and the aqueous phase was extracted with ethyl acetate (3 × 100 mL). The combined organic layers were washed with brine (100 mL), dried over $MgSO_4$, and the solvent was removed in vacuo. The crude product was purified by column chromatography on silica gel (first, cyclohexane/EtOAc = 1:2 + 0.1% NEt_3, and then cyclohexane/EtOAc = 1:2 + 0.2% AcOH). The product **22** was obtained as pale orange solid in 62 % yield (2.8 g, 5.6 mmol); ratio of isomers *E*:*Z* = 74:26, according to the ^{1}H-NMR.

Mp: 83-84°C (Lit.: *E-isomer*: 80-82 °C, *Z-isomer*: 84 °C)[81]. **R$_f$**: *E-isomer*: 0.37, *Z-isomer*: 0.14 (Pentane/EtOAc = 3:1). **^{1}H-NMR** (400 MHz, $CDCl_3$): *E-isomer*: δ = 8.11 (d, ^3J = 8.3 Hz, 1H, H-4), 7.60 (d, ^3J = 8.4 Hz, 2H, H-22), 7.22 (m, 3H, H-5, H-7, H-23), 7.12 (m, 1H, H-6), 4.27 (m, 2H, H-19), 2.38 (s, 3H, H-11), 2.33 (m, 6H, H-9, H-25), 1.71 (s, 3H, H-16), 1.60 (s, 3H, H-15), 1.30 (t, ^3J = 7.1 Hz, 3H, H-20). *Z-isomer*: δ = 8.16 (d, ^3J = 8.0 Hz, 1H, H-4), 7.68 (d, ^3J = 8.4 Hz, 2H, H-22), 7.22 (m, 4H, H-5, H-6, H-7, H-23), 3.64 (m, 2H, H-19), 2.49 (s, 3H, H-9), 2.33 (m, 3H, H-25), 2.26 (s, 3H, H-16), 1.97 (s, 3H, H-15), 1.94 (s, 3H, H-11), 0.52 (t, ^3J = 7.0 Hz, H-20). **^{13}C-NMR** (100.6 MHz, $CDCl_3$): *E-isomer*: δ = 171.6 (C-18), 167.6 (C-17), 153.8 (C-14), 144.8 (C-24), 144.1 (C-12), 136.4 (C-8), 136.3 (C-21), 132.8 (C-1), 131.4 (C-10), 130.0 (C-23), 128.0 (C-

3), 126.4 (C-22), 124.8 (C-13), 124.2 (C-5), 123.4 (C-6), 122.9 (C-2), 119.6 (C-7), 114.6 (C-4), 60.9 (C-19), 25.2 (C-15), 22.3 (C-16), 21.9 (C-11), 21.6 (C-25), 14.4 (C-20), 13.8 (C-9). *Z-isomer*: δ = 171.2 (C-18), 167.4 (C-17), 153.8 (C-14), 144.8 (C-24), 141.6 (C-10), 136.5 (C-21), 136.2 (C-8), 131.7 (2C, C-1, C-12), 130.0 (C-23), 129.5 (C-3), 126.5 (C-22), 124.2 (C-13), 124.1 (C-5), 123.7 (C-6), 123.3 (C-2), 119.1 (C-7), 114.6 (C-4), 60.5 (C-19), 24.6 (C-15), 22.7 (C-16), 22.3 (C-11), 21.6 (C-25), 13.6 (C-9), 13.3 (C-20).[a] **IR** (ATR): ν = 2979 (w), 1683 (m), 1598 (w), 1453 (m), 1373 (m), 1171 (s), 1091 (m), 1050 (m), 812 (w), 746 (m), 661 (s), 572 (s), 541 (s). **HR-MS** (ESI) for $C_{27}H_{30}NO_6S$ $[M+H]^+$ calculated: m/z = 496.1788, found m/z = 496.1788. **EA** for $C_{27}H_{29}NO_6S$ calculated: C 65.44%, H 5.90%, N 2.83%, S 6.47%, found: C 65.40%, H 5.98%, N 2.57%, S 5.90%.

3-(1-(2-methyl-1*H*-indol-3-yl)ethylidene)-4-(propan-2-ylidene)dihydrofuran-2,5-dione (16)[81]

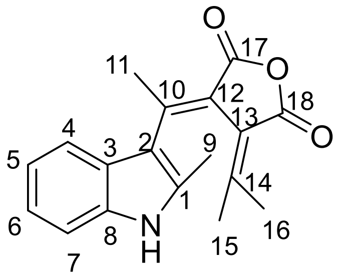

3-(ethoxycarbonyl)-4-(2-methyl-1-tosyl-1H-indol-3-yl)-2-(propan-2-ylidene)pent-3-enoic acid (**22**) (2.50 g, 5.0 mmol, 1.00 eq) was dissolved in abs. ethanol (50 mL). Upon adding a freshly prepared 20 % KOH aq solution (50 mL), the solution color changed to brown. The reaction mixture was refluxed at 80 °C, while stirring, for 24 hours. After cooling down to the room temperature, the reaction mixture was poured into an ice-cold 2 M aq. HCl solution (100 mL), upon which a yellow precipitate formed. The aqueous phase was saturated with NaCl, and extracted with EtOAc (3 × 100 mL). The combined organic phase was washed with brine (100 mL), dried over $MgSO_4$, and the solvent was removed under reduced pressure. The crude product was obtained as dark oil (1.61 g). The crude product was suspended in freshly distilled DCM (90 mL). To the solution, DCC (2.08 g, 10.1 mmol, 2.02 eq) was added, and the reaction mixture was stirred in the dark, at room temperature. The suspension was stirred for 2 hours (TLC monitoring). The solvent was partially removed under reduced pressure, and the white precipitate was filtered off. The solution was concentrated under reduced pressure, and purified by column chromatography (DCM). The product was obtained as a yellow solid in 49 % yield (0.73 g, 2.5 mmol), over 2 steps, ratio of the isomers E:Z = 85:15 (^{1}H NMR).

---

[a] In small concentrations in NMR, ethyl acetate is visible: ^{1}H NMR ($CDCl_3$): δ = 4.08 (m), 2.05 (s), 1.26 (t).[205].

Mp: 94 °C (decomposition) (Lit.: 92 °C (decomposition))[78]. **R*f***: 0.44 (Pentane/EtoAc = 3:1). **^{1}H-NMR** (500 MHz, DMSO-*d6*): *E-isomer*: δ = 11.51 (s, 1H, N*H*), 7.35 (d, ^3J = 8.0 Hz, 1H, H-4), 7.35 (d, ^3J = 8.5 Hz, 1H, H-7), 7.10 (m, 1H, H-6), 7.02 (m, 1H, H-7), 2.74 (s, 3H, H-11), 2.20 (s, 3H, H-9), 2.12 (s, 3H, H-16), 0.88 (s, 3H, H-15). *Z-isomer*: δ = 11.61 (s, 1H, N*H*), 7.57 (d, ^3J = 8.0 Hz, 1H, H-4), 2.38 (s, 3H, H-16), 2.35 (s, 3H, H-9), 2.31 (s, 3H, H-11), 1.99 (s, 3H, H-15). **^{13}C-NMR** (125.7 MHz, DMSO-*d6*): *E-isomer*: δ = 163.8 (C.17), 163.5 (C-18), 152.3 (C-14), 149.3 (C-10), 135.9 (C-1), 135.5 (C-8), 125.4 (C-3), 121.5 (C-6), 121.2 (C-13), 119.9 (C-5), 119.2 (C-4), 117.3 (C-12), 115.7 (C-2), 111.2 (C-7), 25.5 (C-15), 23.1 (C-11), 22.1 (C-16), 13.4 (C-9). *Z-isomer*: 26.8 (C-15), 24.4 (C-11), 21.8 (C-16), 13.0 (C-9).[a] **IR** (ATR): ν = 3335 (m), 2922 (w), 1798 (s), 1740 (s), 1588 (m), 1424 (m), 1230 (s), 1174 (m), 1135 (m), 973 (m), 926 (s), 745 (s), 722 (s), 620 (m). **HR-MS** (ESI) for $C_{18}H_{18}NO_3$ $[M+H]^+$ calculated: m/z = 296.1281, found m/z = 296.1275. **EA** for $C_{18}H_{17}NO_3$ calculated: C 73.20%, H 5.80%, N 4.74%, found: C 71.43%, H 5.84%, N 4.36%.

***tert*-Butyl (2-aminoethyl)carbamate (32)**[81]

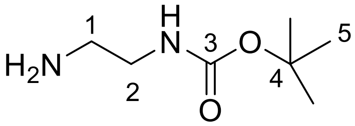

Ethylenediamine (5.75 mL, 85.5 mmol, 5.98 eq) was dissolved in 70 mL DCM, and stirred at room temperature. Di-*tert*-butyl dicarbonate (3.13 g, 14.3 mmol, 1.00 eq) was dissolved in DCM (150 mL), and added dropwise to the stirring reaction mixture over 6 h. The reaction mixture was stirred for additional 40 h, at room temperature, during which white precipitate formed. The reaction mixture was filtered, and the organic phase was washed with saturated aq. solution Na_2CO_3 (200 mL), and dried over $MgSO_4$. Solvent was removed under reduced pressure. The product was obtained without further purification as pale yellow oil (1.82 g, 11.4 mmol, 80 %).

---

[a] In small concentrations in NMR, DCM is visible: ^{1}H NMR (DMSO-*d6*): δ = 5.76 (s). ^{13}C NMR (DMSO-*d6*): δ = 54.8; and H grease: ^{1}H NMR (DMSO-*d6*): δ = 1.24 (s), 0.84 (s).[205].

R$_f$: 0.31 (MeOH). **^{1}H-NMR** (400 MHz, $CDCl_3$): δ = 5.05 (s, 1H, N*H*), 3.14 (q, ^{3}J = 5.8 Hz, 2H, H-2), 2.77 (t, ^{3}J = 5.8, 2H, H-1), 1.57 (m, 2H, N*H*), 1.41 (s, 9H, H-5). **^{13}C-NMR** (100.6 MHz, $CDCl_3$): δ = 156.3 (C-3), 79.2 (C-4), 43.3 (C-2), 41.9 (C-1), 28.5 (C-5). **IR** (ATR): ν = 3349 (m), 2976 (m), 2932 (m), 2869 (w), 1683 (s), 1521 (s), 1364 (m), 1275 (m), 1247 (m), 1164 (s), 872 (w), 636 (w). **HR-MS** (ESI) for $C_7H_{17}N_2O_2$ $[M+H]^+$ calculated: m/z = 161.1285, found m/z = 161.1282. **EA** for $C_7H_{16}N_2O_2$ calculated: C 52.48%, H 10.07%, N 17.49%, found: C 51.26%, H 9.90%, N 16.81%.

***tert*-Butyl-(2-(3-(1-(2-methyl-1H-indol-3-yl)ethylidene)-2,5-dioxo-4-(propan-2-ylidene)pyrrolidin-1-yl)ethyl)carbamate (34)**[81]

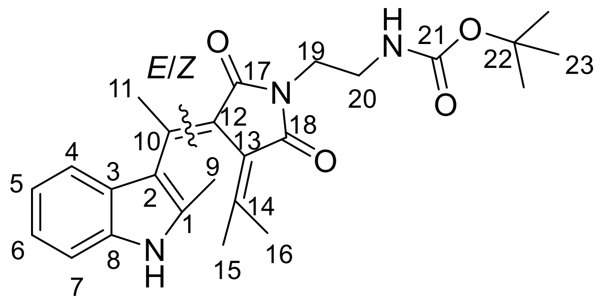

3-(1-(2-methyl-1*H*-indol-3-yl)ethylidene)-4-(propan-2-ylidene)dihydrofuran-2,5-dione (**16**, 0.86 g, 2.91 mmol, 1.00 eq) was dissolved in freshly distilled DCM. *tert*-Butyl (2-aminoethyl)carbamate (**32**, 0.52 g, 3.25 mmol, 1.12 eq) was added, and the reaction mixture was refluxed at 50 °C, in the dark, for 24 h. After cooling down to the room temperature, 1,1′-carbonyldiimidazole (0.96 g, 5.92 mmol, 2.03 eq), was added to the reaction mixture. It was stirred in the dark, at room temperature. Additional 0.12 g (0.74 mmol, 0.25 eq) CDI was added after 72 h, and the reaction mixture was stirred for additional 24 h. The reaction mixture was washed with water (100 mL), and the aqueous phase was extracted with DCM (4 × 40 mL). Combined organic phases were washed with brine (120 mL), and dried over $MgSO_4$. Solvent was removed under reduced pressure. The product was purified by column chromatography (DCM/MeCN = 10:1). The pure product **34** (*E*/*Z* = 85:15) was obtained as yellow solid (0.76 g, 1.74 mmol, 60 % over two steps).

Mp: 85 °C (Lit.: 85 °C)[81]. **R$_f$**: 0.32 (DCM/MeCN = 10:1). **^{1}H-NMR** (400 MHz, $CDCl_3$): *E-isomer*: δ = 8.48 (s, 1H, N*H*), 7.41 (d, ^{3}J = 7.7 Hz, 1H, H-4), 7.28 (d, ^{3}J = 7.8 Hz, 1H, H-7), 7.14 (m, 1H, H-7), 7.10 (m, 1H, H-5), 5.05 (m, 1H, N*H*), 3.78 (m, 2H, H-19), 3.41 (m, 2H, H-20), 2.78 (s, 3H, H-11), 2.17 (s, 6H, H-9, H-16), 1.40 (s, 9H, H-23), 0.95 (s, 3H, H-15). *Z-isomer*: δ = 8.71 (s, 1H, N*H*), 7.50 (d, ^{3}J = 7.7 Hz, 1H, H-4), 7.05 (m, 1H, H-5), 4.91 (m, 1H, N*H*), 3.60 (m, 2H, H-19), 3.24 (m, 2H, H-20), 2.45 (s, 3H, H-16), 2.37 (s, 3H, H-9), 2.31 (s, 3H, H-11), 1.98 (s, 3H, H-15), 1.43 (s, 9H, H-23). **^{13}C-NMR** (100.6 MHz, $CDCl_3$): *E-isomer*: δ = 169.4 (C-17), 168.9 (C-18), 156.1 (C-21), 148.1 (C-14), 143.8 (C-10), 135.7 (C-8), 132.9 (C-1), 126.4 (C-3), 123.8 (C-13), 122.8 (C-12), 122.0 (C-6), 120.5 (C-5), 119.7 (C-4), 117.5 (C-3), 110.7 (C-7), 79.3 (C-22), 39.9 (C-20), 37.5 (C-19), 28.5 (C-23), 26.2 (C-15), 22.5 (C-11), 22.1 (C-16), 13.6 (C-9). *Z-isomer*: δ = 169.0 (C-18), 166.3 (C-17), 156.1 (C-21), 147.1 (C-14), 142.4 (C-10)[a], 137.6 (C-1)*, 135.4 (C-8), 127.1 (C-3), 124.5 (C-13), 123.8 (C-12), 121.5 (C-6), 120.2 (C-5), 119.3 (C-4), 113.0 (C-2), 111.1 (C-7), 79.6 (C-22), 40.9 (C-20), 37.6 (C-19), 28.5 (C-23), 27.1 (C-15), 24.8 (C-11), 21.8 (C-16), 13.3 (C-9).[b,c] **IR** (ATR): ν = 2977 (m), 2931 (m), 2851 (w), 1686 (s), 1517 (m), 1427 (m), 1390 (s), 1366 (s), 1249 (m), 1169 (s), 1047 (m), 836 (m). **HR-MS** (ESI) for $C_{25}H_{32}N_3O_4$ $[M+H]^+$ calculated: m/z = 438.2387, found m/z = 438.2386. **EA** for $C_{25}H_{31}N_3O_4$ calculated: C 68.63%, H 7.14%, N 9.60%, found: C 66.79%, H 7.21%, N 8.69%.

1-(2-aminoethyl)-3-(1-(2-methyl-1H-indol-3-yl)ethylidene)-4-(propan-2-ylidene)pyrrolidine-2,5-dione (7)[81]

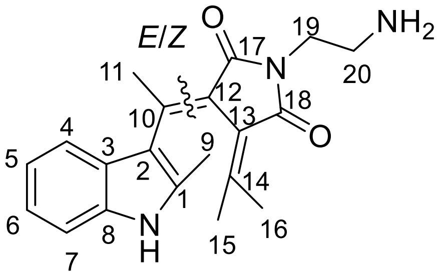

HCl in dioxane (4 M, 10 mL) was added dropwise to fulgimide **34** (0.19 g, 0.43 mmol), over 20 min, while stirring at 0 °C. The green reaction mixture was stirred for 1 h at 0 °C, and slowly warmed up to the room temperature while stirred for additional 1 h. The solvent was removed under reduced pressure. The crude product was dissolved in DCM (50 mL), and the solution was washed with aqueous NaOH solution (0.1 M, 50 mL). Organic phase was separated, and the aqueous phase was extracted with DCM (3 × 30 mL). Combined organic phase was washed with brine (50 mL), dried over $MgSO_4$, and the solvent was removed under reduced pressure. The product was purified by column chromatography (DCM/MeOH = 5:1). It was obtained 122 mg of the pure product **7** (0.36 mmol, 83 %), in the form of yellow solid (*E*/*Z* = 85:15).

---

[a] The signal not observable in ^{13}C NMR, found through the HMBC 2D NMR measurement.

[b] Traces of closed isomer (C) is also observed in the 1H NMR spectrum; due to the low intensity of the signals, those are not assigned.

[c] In small concentrations in NMR, DCM is visible: ^{1}H NMR ($CDCl_3$): δ = 5.30 (s). ^{13}C NMR ($CDCl_3$): δ = 53.5.[205].

Mp: 93 °C (Lit.: 90-92 °C)[81]. **R*f***: 0.17 (DCM/MeOH = 5:1). **^{1}H-NMR** (500 MHz, MeOD-*d3*): δ = 7.32 (d, ^3J = 7.8 Hz, 1H, H-4), 7.28 (d, ^3J = 8.0 Hz, 1H, H-7), 7.08 (m, 1H, H-6), 7.01 (m, 1H, H-5), 3.74 (m, 2H, H-19), 2.92 (m, 2H, H-20), 2.77 (s, 3H, H-11), 2.20 (s, 3H, H-9), 2.14 (s, 3H, H-16), 0.94 (s, 3H, H-15). **^{13}C-NMR** (125.7 MHz, MeOD-*d3*): δ = 170.6 (C-17), 170.1 (C-18), 150.0 (C-14), 146.7 (C-10), 137.4 (C-8), 135.4 (C-1), 127.3 (C-3), 125.1 (C-13), 122.9 (C-12), 122.5 (C-6), 120.9 (C-5), 120.3 (C-4), 117.9 (C-2), 111.9 (C-7), 40.0 (C-20), 36.3 (C-19), 26.2 (C-15), 23.1 (C-11), 22.1 (C-16), 13.4 (C-9).[a] **IR** (ATR): ν = .3355 (m), 3173 (w), 2993 (m), 2852 (w), 1736 (m), 1683 (s), 1592 (m), 1458 (m), 1427 (s), 1390 (s), 1217 (w), 1178 (w), 1146 (w), 1036 (w), 838 (m), 729 (m). **HR-MS** (ESI) for $C_{20}H_{24}N_3O_2$ $[M+H]^+$ calculated: m/z = 338.1863, found m/z = 338.1859. **EA** for $C_{20}H_{23}N_3O_2$ calculated: C 71.19%, H 6.87%, N 12.45%, found: C 68.37%, H 6.21%, N 10.14%.

---

[a] In small concentrations in NMR, DCM is visible: ^{1}H NMR (MeOD-*d3*): δ = 5.49 (s); and H grease: ^{1}H NMR (MeOD-*d3*): δ = 1.29 (s), 0.89 (m).[205].

6.3 Synthesis of Naphthopyran-Linker Conjugate

Methyl 1,4-dihydroxy-2-naphthoate (46)[108]

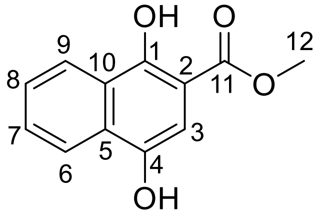

1,4-Dihydroxy-2-naphthoic acid (4.00 g, 19.6 mmol, 1.00 eq) and anhyd. $NaHCO_3$ (1.70 g, 20.2 mmol, 1.03 eq) were dissolved in dry DMF (40 mL) at room temperature, under inert conditions. MeI (1.32 mL, 21.2 mmol, 1.08 eq) was added dropwise within 20 min. The reaction mixture was stirred at room temperature for 2 days, until TLC monitoring indicated complete consumption of the starting material. The mixture was added to 1 M HCl solution (60 mL). The brown suspension was extracted with EtOAc (6 × 60 mL). Collected organic phase was washed with water (2 × 100 mL), dried over Na_2SO_4, filtered, and the organic solvent was removed under reduced pressure. The crude product was dissolved in heated EtOAc, filtered, and solvent was removed under reduced pressure. Finally, the pure product was obtained as a dark green solid (3.85 g, 17.6 mmol, 90 %) by flash column chromatography (pentane/EtOAc = 1:1).

Mp: 193°C (Lit.: 193 °C)[108]. **R$_f$** = 0.53 (Pentane/EtOAc = 5:1). **^{1}H-NMR** (400.1 MHz, MeOD-*d3*): δ = 8.30 (m, 1H, H-9), 8.14 (m, 1H, H-6), 7.60 (m, 1H, H-7), 7.52 (m, 1H, H-8), 7.08 (s, 1H, H-3), 3.96 (s, 3H, H-12). **^{13}C-NMR** (100.6 MHz, MeOD-*d3*): δ = 172.6 (C-11), 155.3 (C-1), 146.4 (C-4), 130.9 (C-5), 129.5 (C-7), 127.1 (C-8), 126.7 (C-10), 124.5 (C-9), 123.3 (C-6), 105.8 (C-2), 105.1 (C-3), 52.8 (C-12).[a] **IR** (ATR): ν = 3376 (m), 3193 (w), 2953 (w), 1634 (s), 1437 (s), 1354 (s), 1291 (s), 1254 (s), 1148 (s), 1073 (m), 990 (m), 792 (m), 762 (s), 662 (m), 472 (m). **HR-MS** (ESI) for $C_9H_{19}N_2O_2$ $[M+H]^+$: calculated: m/z = 219.0652, found: 219.0651. **EA** for $C_{12}H_{10}O_4$ calculated: C 66.05%, H 4.62%, found: C 64.93%, H 4.44%.

---

[a] In small concentrations in NMR, diethyl ether is visible: ^{1}H NMR (MeOD-*d3*): δ = 3.49 (q), 1.18 (t).[205].

1,1-diphenylprop-2-yn-1-ol (47)[93]

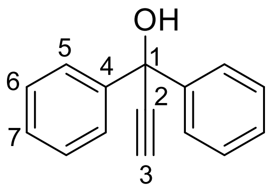

Benzophenone (18.2 g, 0.10 mol, 1.00 equiv) was dissolved in abs. THF (200 mL), at room temperature. Ethynylmagnesium chloride solution (0.6 M solution in THF/toluene, 330 mL, 0.20 mmol, 2.00 equiv) was added dropwise within 24 h. After complete addition, the reaction mixture was magnetically stirred for further 70 h at room temperature. The solution was diluted with 750 mL of diethyl ether and carefully hydrolyzed with 200 mL of a saturated NH_4Cl solution while stirring. The separated aqueous layer was extracted with Et_2O (3 × 300 mL). The combined organic layers where washed with brine (2 × 200 mL), dried over $MgSO_4$ and concentrated under reduced pressure. The crude alcohol **47** was purified by column chromatography on neutral Alox (pentane/EtOAc = 5:1) affording a colorless oil (16.1 g, 77.31 mmol, 77%).

R_f = 0.80 (Pentane/EtOAc = 5:1). **^{1}H-NMR** (400.1 MHz, $CDCl_3$): δ = 7.62 (m, 4H, H-5), 7.34 (m, 4H, H-6), 7.28 (m, 2H, H-7), 2.89 (s, 1H, H-3), 2.80 (b s, 1H, O*H*).[a] **^{13}C-NMR** (100.6 MHz, $CDCl_3$): δ = 144.6 (C-4), 128.5 (C-6), 128.0 (C-7), 126.1 (C-5), 86.5 (C-1), 75.7 (C-3), 74.5 (C-2). **IR** (ATR): ν = 3551 (s), 3273 (s), 3084 (w), 3061 (w), 3026 (w), 2116 (w), 1596 (w), 1489 (s), 1448 (s), 1324 (m), 1155 (s), 1001 (s), 888 (s), 752 (s), 642 (s), 540 (m). **HR-MS** (ESI) for $C_{15}H_{13}O$ $[M-H]^+$: calculated: m/z = 209.0961, found: m/z = 209.0962. **EA** for $C_{15}H_{12}O$ calculated: C 86.51%, H 5.81%, found: C 85.16%, H 5.70%.

Methyl 6-hydroxy-2,2-diphenyl-2H-benzo[h]chromene-5-carboxylate (45)[87]

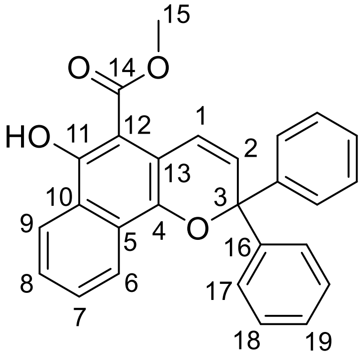

Under inert atmosphere, methyl 1,4-dihydroxy-2-naphthoate (**46**) (3.00 g, 13.75 mmol, 1.00 eq) and 1,1-diphenylprop-2-yn-1-ol (**47**) (2.86 g, 13.75 mmol, 1.00 eq) were dissolved in abs. toluene (180 mL). To the solution, acidic aluminium oxide (activated, Brockmann I; 11.00 g, 104.90 mmol, 7.6 eq) was added, and the reaction mixture was refluxed for 24 h. The reaction mixture was filtered warm, washed with hot toluene (4 × 50 mL) and acetone (3 × 30 mL). The solvent was removed under reduced pressure. The product was purified by column chromatography (pentane/DCM = 1:1), to afford the pure product (1.12 g, 2.74 mmol, 20 %) as yellow-orange solid.

---

[a] In small concentrations in NMR, DCM is visible: ^{1}H NMR ($CDCl_3$): δ = 5.30 (s).[205].

Mp: 137 °C. **R$_f$** = 0.28 (Pentane/DCM = 5:1). **^{1}H-NMR** (400.1 MHz, CDCl$_3$): δ = 12.21 (s, 1H, O*H*), 8.37 (d, ^3J = 8.0 Hz, 1H, H-6), 8.35 (d, ^3J = 7.8 Hz, 1H, H-9), 7.66 (m, 1H, H-7), 7.52 (m, 5H, H-8, H-17), 7.44 (d, ^3J = 10.0 Hz, 1H, H-1), 7.30 (m, 4H, H-18), 7.23 (m, 2H, H-19), 6.20 (d, ^3J = 10.0 Hz, 1H, H-2), 4.02 (s, 3H, H-15).[a] **^{13}C-NMR** (100.6 MHz, CDCl$_3$): δ = 172.5 (C-14), 157.2 (C-11), 144.9 (C-16), 141.3 (C-4), 129.8 (C-7), 128.9 (C-5), 128.2 (C-18), 127.6 (C-19), 127.3 (C-2), 126.9 (C-17), 126.7 (C-8), 125.5 (C-10), 124.3 (C-9), 124.0 (C-1), 122.1 (C-6), 113.3 (C-13), 102.2 (C-12), 81.5 (C-3), 52.5 (C-15). **IR** (ATR): ν = 3060 (w), 2949 (w), 1648 (s), 1579 (m), 1489 (m), 1446 (s), 1329 (s), 1234 (s), 1169 (s), 1101 (m), 1015 (m), 810 (w), 764 (s), 698 (s), 636 (w). **HR-MS** (ESI) for $C_{27}H_{21}O_4$ [M+H]$^+$: calculated: m/z = 409.1434, found: m/z = 409.1436. **EA** for $C_{27}H_{20}O_4$ calculated: C 79.40%, H 4.94%, found: C 77.18%, H 4.88%.

Methyl 2-(4-iodophenyl)acetate (61)[113]

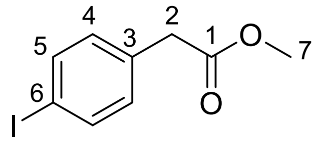

To a solution of 2-(4-iodophenyl)acetic acid (4.03 g, 15.38 mmol, 1.00 eq.) in methanol (30 mL) concentrated sulfuric acid was added (98.00%, 2.20 mL, 2.65 eq.) and the reaction mixture was heated under reflux for 4 h. After cooling down to room temperature, methanol was removed under reduced pressure, and water (80 mL) was added to the residue. The mixture was then extracted with DCM (3 × 50 mL), the combined organic layers were washed with saturated aqueous solution NaHCO$_3$ (50 mL), water (100 mL) and brine (100 mL). The organic phase was dried with Na$_2$SO$_4$ and the solvent was removed under reduced pressure. The product (3.00 g, 14.11 mmol, 97 %) was obtained as yellow oil.

R$_f$ = 0.89 (Pentane:EtOAc = 1:1). **^{1}H-NMR** (400.1 MHz, CDCl$_3$): δ = 7.65 (m, 2H, H-5), 7.03 (m, 2H, H-4), 3.69 (s, 3H, H-7), 3.57 (s, 2H, H-2). **^{13}C-NMR** (100.6 MHz, CDCl$_3$): δ = 171.6 (C-1), 137.8 (C-5), 133.7 (C-6), 131.4 (C-4), 92.8 (C-3), 52.3 (C-7), 40.8 (C-2). **IR** (ATR): ν = 2950 (m),

---

[a] In small concentrations in NMR, DCM is visible: ^{1}H NMR (CDCl$_3$): δ = 5.30 (s); and pentane 1.27 (m), 0.88 (m).[205].

1733 (s), 1591 (w), 1484 (s), 1434 (s), 1252 (s), 1158 (s), 1060 (m), 1007 (s), 797 (s), 565 (w). **HR-MS** (ESI) for $C_9H_9IO_2$ $[M]^+$ calculated: m/z = 275.9642, found: m/z = 275.9641. **EA** for $C_9H_9IO_2$ calculated C 39.16%, H 3.29%, found: C 40.32%, H 3.65%.

tert-Butyl piperazine-1-carboxylate (62)[115]

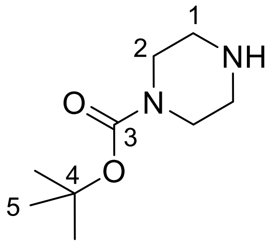

Piperazine (6.30 g, 73.14 mmol, 3.12 eq) was dissolved in DCM (200 mL) and cooled to 0 °C. Boc_2O (5.11 g, 23.37 mmol, 1.00 eq) was dissolved in DCM (200 mL), and added dropwise to the stirred piperazine solution within 4 h, while stirring at 0°C. The reaction mixture was stirred overnight and let to warm up to room temperature. The mixture was filtered, the precipitate was washed with ice cold DCM (2 × 30 mL). The organic solvent was removed under reduced pressure. The oil residue was dissolved in water. The precipitate was filtered off, washed with water, and the aqueous phase was saturated with K_2CO_3, and the product was extracted with Et_2O (3 × 70 mL). The organic phase was dried over Na_2SO_4, filtered, and the solvent was removed under reduced pressure. The product (3.84 g, 20.62 mmol, 89%) was obtained as colourless oil.

R$_f$ = 0.24 (MeOH). **^{1}H-NMR** (400.1 MHz, $CDCl_3$): δ = 3.45 (m, 4H, H-2), 2.87 (m, 4H, H-1), 1.45 (s, 9H, H-5). **^{13}C-NMR** (100.6 MHz, $CDCl_3$): δ = 154.9 (C-3), 79.9 (C-4), 51.4 (C-2), 45.8 (C-1), 28.5 (C-5). **IR** (ATR): ν = 3218 (m), 2936 (s), 2823 (s), 2804 (s), 2745 (m), 1689 (s), 1415 (s), 1243 (s), 1168 (s), 1132 (s), 1002 (m), 833 (s), 769 (m), 617 (m). **HR-MS** (ESI) for $C_9H_{19}N_2O_2$ $[M-H]^+$: calculated: m/z = 187.1441, found: m/z = 187.1441.

tert-Butyl 4-(4-(2-methoxy-2-oxoethyl)phenyl)piperazine-1-carboxylate (63)

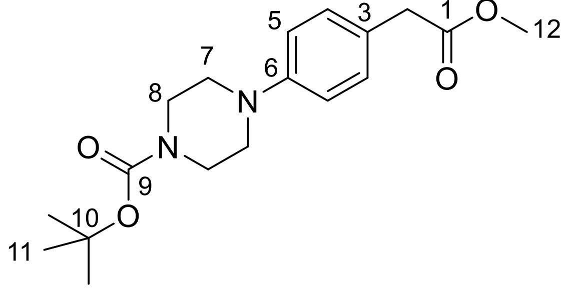

Under a nitrogen atmosphere methyl 2-(4-iodophenyl) acetate (**61**) (3.24 g, 11.74 mmol, 1.00 eq.) was added to a solution of *tert*-butyl piperazine-1-carboxylate (**62**) (2.77 g, 14.87 mmol, 1.27 eq.) in abs. toluene (15 mL) and stirred for one hour over molecular sieves. The dried solution was then added to a solution of $Pd_2(dba)_3$ (0.14 g, 0.15 mmol, 0.03 eq.), tri-*tert*-butylphosphane (0.60 g, 2.95 mmol, 0.25 eq.) and Cs_2CO_3 (5.86 g, 17.82 mmol, 1.52 eq.) in abs. toluene (10 mL). The reaction mixture was stirred for 20 h at 100 °C. Additional $Pd_2(dba)_3$ (0.05 g, 0.06 mmol, 0.0008 eq.) was added to the reaction mixture, which was stirred for additional 22 h at 100 °C. The mixture was filtered and the solvent removed under reduced pressure. The product was purified by column chromatography (pentane/EtOAc = 5:1) to afford the product as orange oil (1.57 g, 4.70 mmol, 40%, abs. yield, 45% rel. yield (88% conv.)).

R_f = 0.32 (Pentane/EtOAc = 5:1). **^{1}H-NMR** (400.1 MHz, $CDCl_3$): δ = 7.20 (d, ^3J = 8.2 Hz, 2H, H-5), 6.97 (m, 2H, H-4), 3.68 (s, 3H, H-12), 3.62 (m, 4H, H-8), 3.56 (s, 2H, H-2), 3.14 (m, 4H, H-7), 1.48 (s, 9H, H-11). **^{13}C-NMR** (100.6 MHz, $CDCl_3$): δ = 172.4 (C-1), 154.8 (C-9), 130.3 (C-4), 129.1 (C-3)[a], 117.3 (C-5), 80.2 (C-10), 52.1 (C-12), 50.1 (C-8), 43.3 (C-7), 40.4 (C-2), 28.5 (C-11). **IR** (ATR): ν = 2977 (m), 1735 (m), 1689 (s), 1615 (m), 1516 (s), 1419 (s), 1364 (m), 1249 (s), 1228 (s), 1160 (s), 1121 (s), 1001 (m), 915 (m), 810 (m), 770 (w), 528 (w). **HR-MS** (ESI) for $C_{18}H_{27}N_2O_4$ $[M+H]^+$ calculated: m/z = 335.1965, found: m/z = 335.1971. **EA** for $C_{18}H_{26}N_2O_4$ calculated C 64.65%, H 7.84%, N 8.38%, found: C 64.60%, H 7.97%, N 8.29%.

2-(4-(4-(tert-Butoxycarbonyl)piperazin-1-yl)phenyl)acetic acid (70)

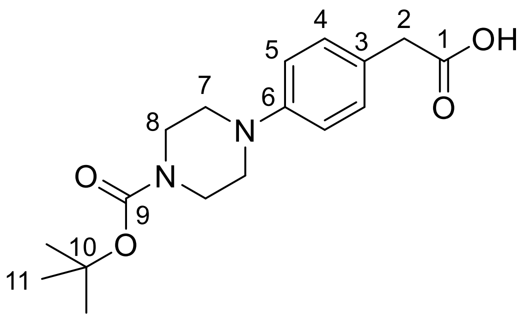

To a solution of *tert*-butyl 4-(4-(2-methoxy-2-oxoethyl)phenyl)piperazine-1-carboxylate (**63**) (1.59 g, 4.75 mmol, 1 eq.) in THF (15 mL), 2 M NaOH (10 mL) was added dropwise and the reaction mixture was stirred at room temperature for 21 h. The solvent was removed under reduced pressure, and the aqueous phase extracted with EtOAc (3 × 30 mL). The aqueous phase was carefully acidified to pH = 4 with 1 M HCl and then extracted with EtOAc (3 × 50 mL). The combined organic layers were washed with brine (50 mL), dried over Na_2SO_4, filetered and the solvent was removed in vacuo to yield 2-(4-(4-(tert-butoxycarbonyl)piperazin-1-yl)phenyl)acetic acid (**69**) as orange solid (1.44 g, 4.49 mmol, 94 %).

---

[a] The signal not observable in ^{13}C NMR, found through the HMBC 2D NMR measurement.

Mp.: 119 °C. **R$_f$** = 0.40 (pentane/EtOAc = 1:2). **^{1}H-NMR** (400.1 MHz, CDCl$_3$): δ = 7.19 (d, ^3J = 8.5 Hz, 2H, H-5), 6.92 (m, 2H, H-4), 3.57 (m, 6H, H-2, H-8), 3.12 (m, 4H, H-7), 1.48 (s, 9H, H-11). **^{13}C-NMR** (100.6 MHz, CDCl$_3$): δ = 177.3 (C-1), 154.9 (C-9), 130.3 (C-4), 117.1 (C-5), 80.2 (C-10), 49.8 (C-8), 43.7 (C-7), 40.2 (C-2), 28.6 (C-11). **IR** (ATR): ν = 3188 (m), 2968 (w), 2928 (w), 2813 (w), 1731 (s), 1659 (s), 1619 (s), 1520 (m), 1464 (m), 1437 (s), 1371 (s), 1319 (w), 1255 (m), 1203 (w), 1169 (s), 1134 (s), 1084 (w), 1045 (m), 1003 (m), 912 (s), 828 (m), 805 (s), 761 (s), 743 (w), 707 (w), 649 (w), 605 (w), 529 (w), 453 (w). **HR-MS** (ESI) for $C_{17}H_{23}N_2O_4$ [M-H]$^-$ calculated: m/z = 319.1663, found: m/z = 319.1653. **EA** for $C_{17}H_{24}N_2O_4$ calculated: C 63.73%, H 7.55%, N 8.74%, found: C 63.03%, H 7.48%, N 8.18%.

tert-Butyl 4-(4-(2-((5-(methoxycarbonyl)-2,2-diphenyl-2Hbenzo[h]chromen-6-yl)oxy)-2-oxoethyl)phenyl)piperazine-1-carboxylate (71)

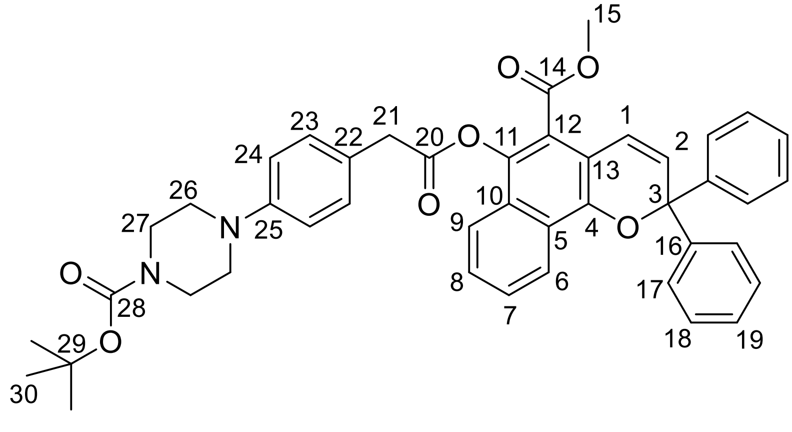

A mixture of 2-(4-(4-(tert-butoxycarbonyl)piperazin-1-yl)phenyl)acetic acid (**70**) (0.100 g, 0.312 mmol, 1.1 eq.) and DCC (0.064 g, 0.312 mmol, 1.1 eq.) in DCM was cooled to 0 °C and stirred for 15 min. Methyl 6-hydroxy-2,2-diphenyl-2H-benzo[h]chromene-5-carboxylate (**45**) (0.116 g, 0.284 mmol, 1 eq.) and DMAP (0.0173 g, 0.142 mmol, 0.5 eq.) were added and the suspension was stirred in the dark for 48 h at room temperature. After completion of the reaction, the mixture was filtered and water was added to the residue before it was extracted with DCM (3 x 50 mL). The combined organic layers were washed with NaHCO$_3$ and brine and were then dried over Na$_2$SO$_4$. The solvent was removed under reduced pressure to get the crude material. The crude product was dissolved in ice cold Et$_2$O and filtered. The solvent from the filtrate was removed under reduced pressure. Finally, the product was purified by column chromatography (pentane/EtOAc = 5:1 + 0.1 % Et_3N) to yield the pure product as an orange solid (0.141g, 0.199 mmol, 70 %).

Mp: 135 °C. **R_f** = 0.85 (Pentane/EtOAc = 1:1). **^{1}H-NMR** (500.1 MHz, DMSO-*d6*): δ = 8.43 (d, ^3J = 8.8 Hz, 1H, H-6), 7.73 (m, 2H, H-7, H-9), 7.61 (m, 1H, H-8), 7.52 (m, 4H, H-17), 7.36 (m, 4H, H-18), 7.27 (m, 4H, H-19, H-23), 6.97 (d, ^3J = 8.8 Hz, 2H, H-24), 6.87 (d, ^3J = 10.1 Hz, 1H, H-1), 6.66 (d, ^3J = 10.1 Hz, 1H, H-2), 3.99 (s, 2H, H-21), 3.77 (s, 3H, H-15), 3.46 (m, 4H, H-27), 3.09 (m, 4H, H-26), 1.42 (s, 9H, H-30).[a] **^{13}C-NMR** (125.7 MHz, DMSO-*d6*): *δ* = 170.3 (C-20), 165.0 (C-14), 153.9 (C-28), 150.1 (C-25), 145.2 (C-4), 144.3 (C-16), 138.6 (C-11), 130.2 (C-23), 129.2 (C-2), 128.5 (C-7), 128.4 (C-18), 128.2 (C-8), 127.7 (C-19), 126.6 (C-10), 126.0 (C-17), 125.3 (C-5), 124.2 (C-22), 122.5 (C-9), 121.9 (C-6), 120.5 (C-1), 119.6 (C-12), 116.0 (C-24), 112.8 (C-13), 82.3 (C-3), 79.0 (C-29), 52.7 (C-15), 48.4 (C-26), 43.2 (C-27)[b], 39.0 (C-21)[c], 28.1 (C-30). **IR** (ATR): ν = 2928 (m), 1764 (s), 1722 (w), 1689 (s), 1616 (m), 1517 (s), 1449 (w), 1422 (w), 1388 (w), 1364 (s), 1286 (s), 1225 (s), 1167 (s), 1101 (s), 1013 (m), 1000 (s), 969 (w), 913 (m), 866 (w), 809 (w), 753 (s), 699 (s), 529 (w), 468 (m). **HR-MS** (ESI) for $C_{44}H_{43}N_2O_7$ $[M+H]^+$ calculated: m/z = 711.3065, found: m/z = 711.3057. **EA** for $C_{44}H_{42}N_2O_7$ calculated: C 74.35%, H 5.96%, N 3.94%, found: C 73.19%, H 6.02%, N 3.85%.

---

[a] In small concentrations in NMR, pentane is visible: ^{1}H NMR (DMSO-*d6*): δ = 1.27 (m), 0.86 (m).[205].

[b] The signal not observable in ^{13}C NMR, found through the HMBC 2D NMR measurement.

[c] The signal is detected by HMBC 2D NMR spectra, however not observed in ^{13}C NMR because of the overlap with the solvent peak.

4-(4-(2-((5-(Methoxycarbonyl)-2,2–diphenyl-2H-benzo[h]chromen-6-yl)oxy)-2-oxoethyl)phenyl)piperazin-1-ium chloride (8)

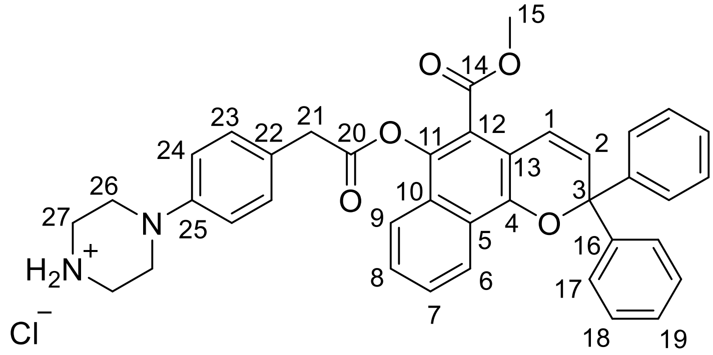

Under cooling at 0 °C, a solution of 4 M HCl in dioxane (5 mL) was added dropwise to *tert*-butyl 4-(4-(2-((5-(methoxycarbonyl)-2,2-diphenyl-2H-benzo[h]chromen-6-yl)oxy)-2-oxoethyl)phenyl)piperazine-1-carboxylate (**71**) (0.052 g, 0.073 mmol, 1.00 eq) and stirred for 1.5 h. After the reaction was complete, the solvent was removed under reduced pressure, and the pure product was obtained without further purification as orange solid (0.047 g, 0.073 mmol, quant.).

Mp.: 97 °C. **^{1}H-NMR** (500.1 MHz, DMSO-*d6*): δ = 8.98 (s b, 2H, NH_2), 8.44 (d, ^3J = 8.3 Hz, 1H, H-6), 7.74 (m, 2H, H-7, H-9), 7.62 (m, 1H, H-8), 7.52 (m, 4H, H-17), 7.36 (m, 4H, H-18), 7.28 (m, 4H, H-19, H-23), 7.01 (d, ^3J = 8.8 Hz, 2H, H-24), 6.86 (d, ^3J = 10.1 Hz, 1H, H-1), 6.66 (d, ^3J = 10.1 Hz, 1H, H-2), 4.01 (s, 2H, H-21), 3.77 (s, 3H, H-15), 3.35 (m, 4H, H-26), 3.22 (s, 4H, H-27). **^{13}C-NMR** (125.7 MHz, DMSO-*d6*): δ = 170.3 (C-20), 165.1 (C-14), 149.2 (C-25), 145.2 (C-4), 144.3 (C-16), 138.8 (C-11), 130.5 (C-23), 129.3 (C-2), 128.6 (C-7), 128.5 (C-18), 128.3 (C-8), 127.8 (C-19), 126.6 (C-10), 126.0 (C-17), 125.4 (C-5), 125.0 (C-22), 122.5 (C-9), 122.0 (C-6), 120.6 (C-1), 119.7 (C-12), 116.2 (C-24), 112.9 (C-13), 82.3 (C-4), 52.8 (C-15), 45.6 (C-26), 42.7 (C-27), 39.4 (C-5)[a].[b] **IR** (ATR): ν = 2950 (m), 1759 (m), 1715 (m), 1615 (m), 1517 (m), 1491 (m), 1449 (s), 1367 (s), 1288 (s), 1225 (s), 1169 (m), 1110 (s), 1013 (s), 1000 (s), 960 (m), 915 (w), 883 (w), 810 (w), 749 (s), 698 (s), 536 (m), 485 (s), 449 (m). **HR-MS** (ESI) for $C_{39}H_{35}N_2O_5$ $[M+H]^+$ calculated: m/z = 611.2540, found: m/z = 611.2539. **EA** for $C_{39}H_{35}N_2O_5Cl$ calculated: C 72.38%, H 5.45%, N 4.33%, found: C 69.54%, H 6.23%, N 2.96%.

---

[a] The signal is detected by HMBC 2D NMR spectra, however not observed in ^{13}C NMR because of the overlap with the solvent peak.

[b] In small concentrations in NMR, dioxane is visible: ^{1}H NMR (DMSO-*d6*): δ = 3.57 (s). ^{13}C NMR (DMSO-*d6*): δ = 66.4.[205].

6.4 Preparation of the Self-Assembled Monolayers on Si(111) and Si(100) Surfaces

6.4.1 General Information

Reagents were purchased in the highest available purity, and solvents were obtained in p.a. or spectroscopic grade purity; all were used without purification, unless otherwise stated. Hexane and dichloromethane (stabilized with amylene) was purchased from Acros Organics. Acetonitrile and acetone were purchased from Roth. Ethanol, methanol and toluene were purchased from Fisher Scientific. Toluene for silanization reactions was distilled over Na/benzophenone, stored over molecular sieves in the glove box, and filtered through a syringe filter (Phenomenex, PTFE membrane, 0.45 μm) immediately before use. The water concentration in toluene was determined by Karl-Fisher titration.[206] The toluene sample saturated with water was obtained by adding a drop of water to 5 mL toluene, and shaking the solution in order to saturate it with water; the concentration of water in this sample was not determined. Hydrogen peroxide (H_2O_2, 31%), sulfuric acid (H_2SO_4, 96%), and ammonium fluoride (NH_4F, 40%) were of VLSI grade (very large scale integration grade), purchased from BASF. Hydrofluoric acid (HF, 49.5-50.5%) was purchased from Sigma Aldrich and used diluted as 2.5% solution. Trichloroethylene (p.a., >99.5%) and (3-glycidyloxypropyl)trimethoxysilane (GPTMS) were purchased from Sigma-Aldrich. Trimethoxy(propyl)silane was ordered from Alfa Aesar. Methyl undec-10-enoate (97%) was purchased from Sigma-Aldrich, distilled twice under reduced pressure (124 °C, 14 mbar), and stored in a glovebox. 1-Decene (94%) was distilled three times under reduced pressure (98 °C, 111 mbar), and stored in a glovebox; before the last distillation, 1-decen was refluxed over sodium under inert atmosphere for 1 h. Ultrapure Milli-Q water (18 MΩ cm) was obtained from a MilliPore four-bowl system.

Samples for attenuated total reflection Fourier-transform infrared spectroscopy (ATR-FTIR) were cut in rectangle shape, dimensions 1.1 × 2.5 cm, from silicon wafers (*Sil'tronix*, double side polished Si(111) ± 0.02°, FZ, n-type (P-doped), R = 10-30 Ωcm, d = 500-550 μm; *Sil'tronix*, double side polished Si(100) ± 0.5°, FZ, non-doped, R = 1000-1600 Ωcm, d = 500-550 μm). The short side was grinded at 45° angle with a commercially available wet sandpapers in an ascending grit order (P180 – P1200, grain sizes 82 – 15 μm; usually used eight different grit sizes of grit paper, or as many different sizes in the range P180 - P1200 as commercially available). The samples were further polished with a polycrystalline diamond-tipped polishing paste (DP paste) of a grain size of 6 µm, 3 µm and 1 µm, using a polishing solution for cooling (DP-Lubricant Green) and special polishing cloths as pads (MD-Pan, Ø = 250 mm), obtained from *Struer*. The prepared ATR crystals were, prior to use, carefully scratched along the longer side of the sample.

ATR-FTIR spectra were recorded on a Bruker Vertex70v ATR-FTIR spectrometer containing a liquid nitrogen-cooled mercury−cadmium−telluride (MCT) detector, while the sample compartment was kept under nitrogen. The spectral range between 370 and 4000 cm^{-1} was investigated, with 4 cm^{-1} resolution. The irradiation was carried out with a set-up equipped with LED diodes that directly attaches to the sample holder, and irradiates both sides of the silicon ATR wafer. IR data were analyzed using the software OPUS 6.5 (Bruker).

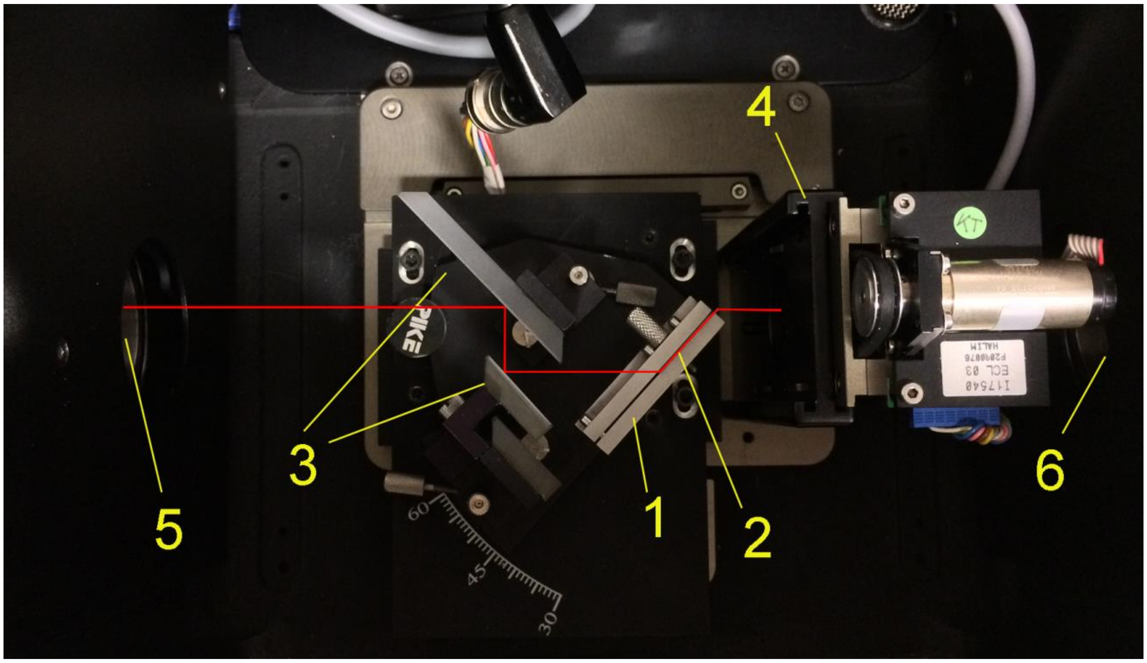

Figure 6.1. Sample compartment of the Bruker ATR-FTIR spectrometer: (1) sample holder, (2) silicon ATR wafer, (3) mirrors, (4) polarizator, (5) detector, (6) light source. The red line is drawn to guide the eye by following the IR light beam during the measurement.

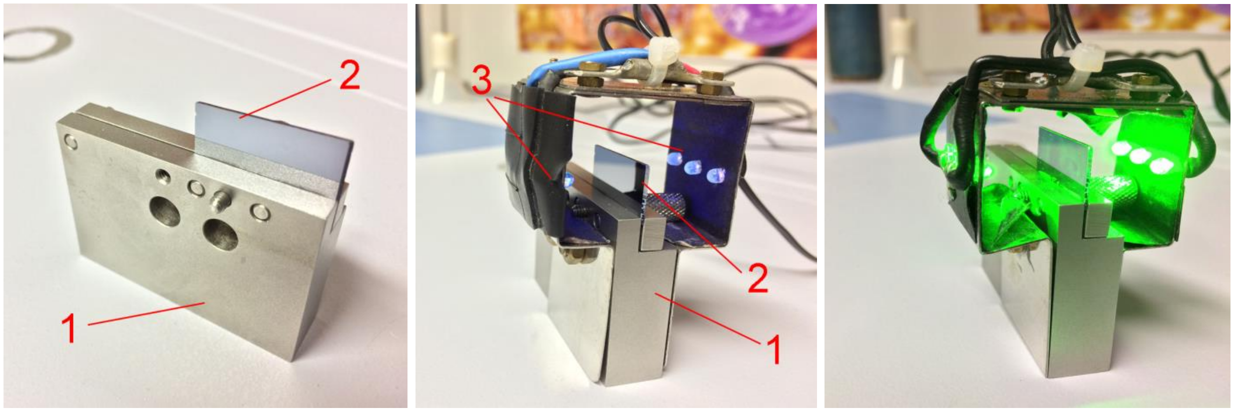

Figure 6.2. Sample holder unit (1) of the Bruker ATR-FTIR spectrometer with a self-prepared ATR silicon wafer (2), and irradiation elements equipped with LED diodes for both UV (365 nm) and visible light (545 nm) irradiation (3).

Samples for X-ray photoelectron spectroscopy (XPS) were cut in rectangle shape, dimensions 1 cm × 1 cm, from silicon wafers (*Silchem*, single side polished Si(111), n-type, 7.5 Ω cm, thickness 525 µm; *Sil'tronix*, double side polished Si(100) ± 0.5°, FZ, non-doped, R = 1000-1600 Ωcm, d = 500-550 µm).

XPS measurements on Si(111) wafers were performed by the research group of Prof. Dr. Arne Thomas (Institute of Chemistry, Technische Universität Berlin). The measurements were carried out using a Thermo Scientific K-Alpha$^+$ X-ray Photoelectron Spectrometer. All samples were analyzed using a microfocused, monochromated Al K α X-ray source (1486.68 eV; 400 µm spot size). The K-Alpha$^+$ charge compensation system was employed during analysis to prevent any localized charge buildup. The samples were mounted on conductive carbon tape and resulting spectra analyzed using the Avantage software from Thermo Scientific. Before the last synthesis step, the sample was broken into two 1 cm × 1 cm pieces in order to evaluate the last coupling reaction.

XPS measurements on Si(100) wafers were performed by the research group of Prof. Dr. Wolfgang Unger (BAM Federal Institute for Materials Research and Testing, Berlin). The measurements were carried out by an AXIS Ultra DLD electron spectrometer manufactured by Kratos Analytical, UK. XPS spectra were recorded using monochromated Al Kα excitation at pass energy of 80 eV for survey spectra and 20 eV for highly-resolved core level spectra. The electron emission angle was 0 degree and the source-to-analyzer angle was 60 degree. The binding energy scale of the instrument was calibrated following a Kratos Analytical procedure which uses ISO 15472 binding

energy data.[207] Spectra were taken by setting the instrument to the hybrid lens mode and the slot mode providing approximately a 300 x 700 µm^2 analysis area. Charge neutralization was used. The binding energy scale was corrected for charging[208] using an electron binding energy of 285.0 eV[209] for the C1s photoemission of aliphatic hydrocarbons. Before the last synthesis step, the sample was broken into two 1 cm × 1 cm pieces in order to evaluate the last coupling reaction.
Samples for ellipsometry measurements were prepared for the previously produced ATR crystals. The measurements were performed by Dr. Jürgen Bruns (research group of Prof. Dr. Klaus Petermann, Institute of Hochfrequenztechnik-Photonik, Technische Universität Berlin). The layer thickness measurements were carried out with a Sentech SE 850 ellipsometer. The angle of incidence of light was 70°, the measurements were performed in the wavelength range 300-800 nm. For the analysis of the measurements the software SpectraRay3 was used. Initially, the thickness of the SiO_2 layer was determined from reference samples. The thickness of the epoxy-terminated monolayer was calculated using a two layer SiO_2/epoxysilane monolayer model. The refractive indices of the epoxysilane monolayer and the silicon oxide are assumed to be constant and equal to the bulk values of 1.429 and 1.461, respectively.

Static water contact angle measurements were performed on an Easydrop instrument (Krüss, Germany) using the sessile drop method. All measurements were carried out at ambient temperature and humidity. Each sample was prepared in triplicate at least. Usually five or more drops of MilliQ water with a volume of ~1 µL were placed on each sample and imidiatelly measured. Each sample was prepared in triplicate. The data was analysed using Drop Shape Analysis, DSA1 1.90 software. The typical average error was ±3° at maximum, obtained as the fitting error of each measurement. Measurements of the irradiated silicon samples were conducted in the dark.

6.4.2 Procedures on Si(111)

6.4.2.1 Procedure for cleaning of the Si(111) wafers

The wafer was cleaned two times in trichloroethylene at 60°C, for 40 minutes, in order to remove the residual wax from the preparation of the ATR crystals. Further, the wafer was cleaned by sonication in different solvents: acetone, dichloromethane, methanol and acetonitrile, each 15 minutes in a Teflon vial, and dried under reduced pressure ($\sim 2\cdot 10^{-2}$ mbar). The wafer was then oxidized in *Piranha* solution (H_2SO_4/H_2O_2, 3:1, V/V), at 100 °C for 30 minutes, thoroughly rinsed with MilliQ water, and dried under reduced pressure ($\sim 2\cdot 10^{-2}$ mbar) for 5 minutes. (Caution: *Piranha* solution reacts violently with organic materials and must be handled with extreme care!) The oxidized sample was etched in 40% aq. NH_4F solution, containing 50 mM $(NH_4)_2SO_3$, in a Teflon vial, in order to prepare H-terminated Si(111) wafer. Upon 15 minute at room temperature, the wafer was quickly rinsed with MilliQ water, and dried under reduced pressure ($\sim 2\cdot 10^{-2}$ mbar), and stored under argon.

6.4.2.2 Procedures for the hydrosilylation reaction on Si(111)

Preparation of ester-terminated monolayers on Si(111)

The freshly prepared H-terminated Si(111) wafer was transferred to a glove box, and immersed into methyl undec-10-enoate (5 mL). The closed glass vial was heated to 160 °C for 2 h. After cooling down to the room temperature, the sample was removed from the glove box, cleaned twice with the following solvents: hexane (3 × 5 mL), and DCM (3 × 5 mL). The wafer was dried under reduced pressure, and stored under argon.

Preparation of diluted ester-terminated monolayers on Si(111)

The freshly prepared H-terminated Si(111) wafer was transferred to a glove box, and immersed into 5 mL solution of methyl undec-10-enoate / 1-decene (V/V, 1:1). The closed glass vial was heated to 160 °C for 2 h. After cooling down to the room temperature, the sample was removed from the glove box, cleaned twice with the following solvents: hexane (3 × 5 mL), and DCM (3 × 5 mL). The wafer was dried under reduced pressure, and stored under argon.

6.4.2.3 Procedure for the preparation of the carboxy-terminated monolayers on Si(111)

For the hydrolysis of the ester-terminated monolayer, an aqueous solution of HCl (5.5 M, 10 mL)[a] was prepared, and degassed under sonication with an argon stream for at least 1 h, prior to the reaction. The wafer with the ester-terminated monolayer was immersed with a help of tweezers, under argon stream, into previously heated HCl solution (40 °C). After 3 h, the wafer was thoroughly washed with MilliQ water, acetone (3 × 5 mL), and DCM (3 × 5 mL), then dried under reduced pressure, and stored under argon.

6.4.2.4 Procedures for the photoswitch attachment to the carboxy-terminated monolayers on Si(111)

Preparation of the fulgimide-terminated monolayer on Si(111)

In glove box, in a glass vial, (*E/Z*)-fulgimide-linker conjugate **7** (*E/Z* = 85:15) (8.2 mg, 0.024 mmol, 5 mM) was dissolved in acetonitrile/DIPEA solution (5 mL)[b]. To the solution, HCTU (21 mg, 0.050 mmol, 10 mM) were added. The wafer with the carboxy-terminated monolayer was immersed into the solution with a help of tweezers, at room temperature under dark conditions. After 2 h, under dark conditions, the wafer was washed with acetonitrile (5 mL) in the glove box, further washed with acetonitrile outside the glove box (4 × 5 mL) and DCM (2 × 5 mL), dried under reduced pressure, and stored under argon.

---

[a] The dilution of the conc. HCl was prepared with the MilliQ water.

[b] The stock solution was previously prepared in acetonitrile: 86 µL DIPEA (0.50 mmol, 10 mM) in 50 mL acetonitrile. The solution was used in period no longer than 6 months after the preparation.

Test coupling of the piperazine **62** to the carboxy-terminated monolayer on Si(111)

Coupling with HCTU: In a glass vial (glove box), Boc-piperazine **62** (5 mg, 0.027 mmol, 5 mM) was dissolved in acetonitrile/DIPEA solution (5 mL)[a]. To the solution, HCTU (20.6 mg, 0.050 mmol, 10 mM) was added. The wafer with the carboxy-terminated monolayer was immersed into the solution, and the solution was heated to 50 °C for 5 h. The wafer was washed with acetonitrile (5 mL) in the glove box, further washed with acetonitrile outside the glove box (4 × 5 mL) and DCM (2 × 5 mL), dried under reduced pressure, and stored under argon.

Coupling with HATU In a glass vial (glove box), Boc-piperazine **62** (5 mg, 0.027 mmol, 5 mM) was dissolved in acetonitrile/DIPEA solution (5 mL)[*]. To the solution, HATU (19 mg, 0.050 mmol, 10 mM) was added. The wafer with the carboxy-terminated monolayer was immersed into the solution, and the solution was heated to 50 °C for 5 h. The wafer was washed with acetonitrile (5 mL) in the glove box, further washed with acetonitrile outside the glove box (4 × 5 mL) and DCM (2 × 5 mL), dried under reduced pressure, and stored under argon.

Preparation of the naphthopyran-terminated monolayer on Si(111)

In a glass vial (glove box), naphthopyran-linker conjugate **8** (16 mg, 0.025 mmol, 5 mM) was dissolved in acetonitrile/DIPEA solution (5 mL)[*]. To the solution, HCTU (21 mg, 0.050 mmol, 10 mM) and additional DIPEA (8 µL, 0.10 mmol) were added. The wafer with the carboxy-terminated monolayer was immersed into the solution, and the solution was heated to 50 °C for 18 h, under dark conditions. The wafer was washed with acetonitrile (5 mL) in the glove box, further washed with acetonitrile outside the glove box (4 × 5 mL) and DCM (2 × 5 mL), dried under reduced pressure, and stored under argon.

---

[a] The stock solution was previously prepared in acetonitrile: 86 µL DIPEA (0.50 mmol, 10 mM) in 50 mL acetonitrile. The solution was used in period no longer than 6 months after the preparation.

6.4.3 Procedures on Oxidized Si(100)

6.4.3.1 Procedure for cleaning of the Si(100) wafers

The wafer was cleaned two times in trichloroethylene at 60°C, for 40 minutes, in order to remove the residual wax from the preparation of the ATR crystals. Further, the wafer was cleaned by sonication in different solvents: acetone, dichloromethane, methanol and acetonitrile, each 15 minutes in a Teflon vial, and dried under reduced pressure ($\sim 2 \cdot 10^{-2}$ mbar). The wafer was then oxidized in *Piranha* solution (H_2SO_4/H_2O_2, 3:1, v/v), at 100 °C for 1 h, thoroughly rinsed with MilliQ water, and dried under reduced pressure ($\sim 2 \cdot 10^{-2}$ mbar) for 5 minutes. The oxidized sample was etched in 2.5% aq. HF solution, in a Teflon vial, for 1 minute at room temperature, then quickly rinsed with MilliQ water, and dried under reduced pressure. Finally, the wafer was reoxidized in *Piranha* solution, at 100 °C for 1 h, thoroughly rinsed with MilliQ water, dried under reduced pressure ($\sim 2 \cdot 10^{-2}$ mbar) for 5 minutes, and stored under argon.

6.4.3.2 Procedures for the silanization reaction on Si(100) wafers

Preparation of the epoxy-terminated monolayers on Si(100)

Formation of the monolayer was done by immersion of the oxidized wafer into 5 mL of the freshly prepared solution of (3-glycidyloxypropyl)trimethoxysilane in toluene (1%, volume concentration), in a nitrogen flushed glove box. The wafer was left to react at room temperature for 24 h. After removing the wafer from the glovebox, three different work-up procedures were examined: Procedure A) Washing of the wafer with toluene (3 × 5 mL) and ethanol (3 × 5 mL), and subsequent sonication in ethanol for 20 minutes, Procedure B) Washing of the wafer with toluene (3 × 5 mL) and ethanol (3 × 5 mL), and subsequent sonication in toluene for 20 minutes, Procedure C) Washing of the wafer with toluene (5 × 5 mL) and subsequent sonication in toluene for 10 minutes. Then, the wafer was baked in the oven at 150 °C for 10 minutes, and stored under argon at room temperature.

Preparation of the alkyl-terminated monolayers on Si(100)

Formation of the monolayer was done by immersion of the oxidized wafer into 5 mL of the freshly prepared solution of trimethoxy(propyl)silane in toluene (1%, volume concentration), in a nitrogen flushed glove box. After 24 h at room temperature, the wafer was removed from the glove box, washed with toluene (5 × 5 mL), sonicated in toluene for 10 minutes (Procedure C), and dried under reduced pressure ($\sim 2 \cdot 10^{-2}$ mbar). The wafer was baked in the oven at 150 °C for 10 minutes, and stored under argon at room temperature.

6.4.3.3 Procedures for modification of epoxy-terminated monolayers on Si(100)

Preparation of the acetylene-terminated monolayers on Si(100)

The wafer with the epoxy-terminated monolayer was immersed into a solution of propargylamine (50 µL, 781 µmol, 156 mM) in 5 mL toluene, under inert conditions (in a glove box), and heated to 80 °C. After 24 h, the wafer was removed from the glove box, washed three times with 5 mL of toluene and once with 5 mL of abs. ethanol, dried under reduced pressure ($\sim 2 \cdot 10^{-2}$ mbar), and stored under argon.

Preparation of the fulgimide-terminated monolayers on Si(100)

The wafer with the epoxy-terminated monolayer was immersed into a (*E/Z*)-fulgimide-linker conjugate **7** (*E/Z* = 85:15) (10 mg, 27 µmol, 5.4 mM) solution in 5.5 mL toluene/1,4-dioxane (10:1) mixture, under inert conditions (in a glove box). The solution was heated to 90 °C, while mildly stirring, not to damage the wafer. After 24 h, the wafer was removed from the glove box, washed three times with 5 mL toluene and once with 5 mL abs. ethanol, dried under reduced pressure ($\sim 2 \cdot 10^{-2}$ mbar), and stored under argon.

6.5 Photochromic Investigations

6.5.1 UV/Vis Measurements

The UV/Vis spectra were recoded using the AvaSpec Dual-channel Fiber Optic Spectrometer, equipped with the AvaLight-DH-S-BAL light source. The measurements were carried out inside a 10 mm Quartz SUPRASIL cuvette (Hellma Analytics).

The LED lights for the irradiation were obtained from Thorlabs, their intensity determined to be: 1) 365 nm (bandwidth (FWHM): 9 nm), 85 mW/cm^2; 2) 505 nm (bandwidth (FWHM): 30 nm), 110 mW/cm^2, 3) 565 nm (bandwidth (FWHM): 104 nm), 130 mW/cm^2. For the LED output intensity spectra, see Chapter 7.1. The irradiation and recording of the absorption spectra were carried out simultaneously on the set-up shown in Figure 6.3. The spectra were analyzed using the software AvaSoft 8.5 (Avantes).

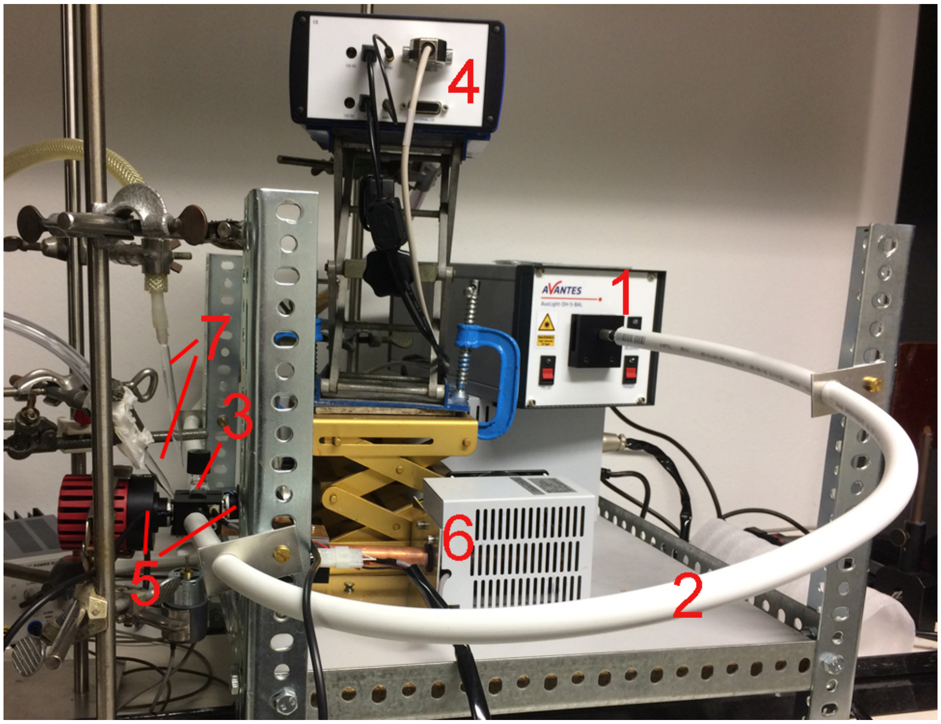

Figure 6.3. UV/Vis set-up: (1) light source, (2) optical cable, (3) sample holder with a cuvette, (4) detector, (5) LED lights, (6) temperature regulator, (7) air stream cooling.

The samples for photochemical studies were prepared in concentrations of $1.5 \cdot 10^{-5}$ M in solvents of spectroscopic purity. The prepared solutions were degassed with stream of argon for 15 min prior to the measurement, to avoid irradiation induced radical side reaction with oxygen present in the solvent. The samples were termoregulated and stirred at all time during the measurement (Figure 6.4). Because of the thermoregulation being slow in cooling down the sample compartment, additional cooling by the air stream was incorporated (Figure 6.4, 7).

The constructed set-up also allows for installing two LED lights at the same time (Figure 6.4), thus subsequent irradiations were carried out without required time in between for changing the light source.

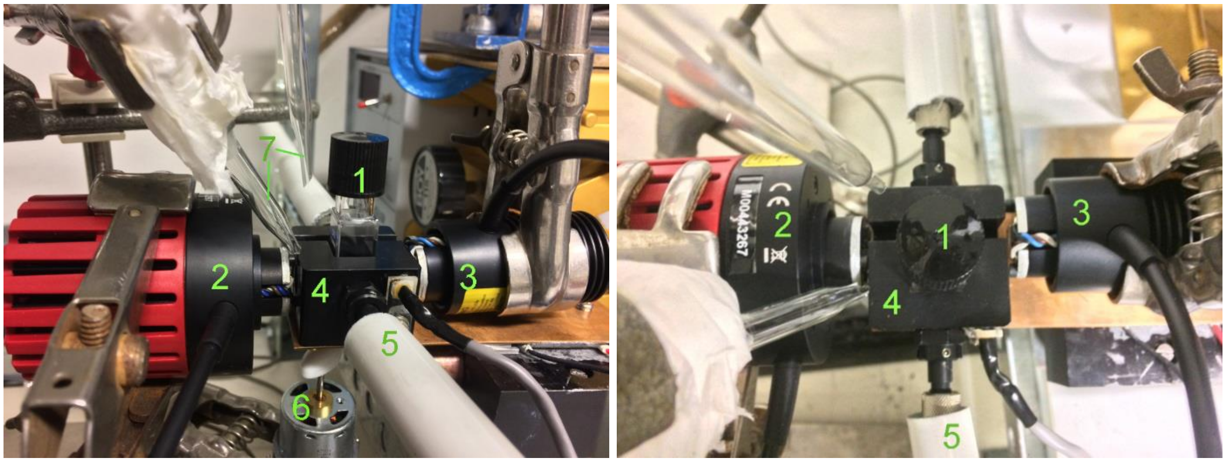

Figure 6.4. Sample compartment of the UV/Vis set-up: (1) cuvette, (2) 1st LED light, (3) 2nd LED light, (4) sample holder with thermoregulation, (5) optical cable, (6) stirring mechanism, (7) air stream cooling.

6.5.2 NMR Measurements

The photochemical studies in the NMR spectrometer were carried out in acetonitrile-*d3* at 0°C. The samples (concentration 10^{-2} M) were irradiated directly in the NMR tube, via self-constructed insert connected to the optical fiber (Figure 6.5), and coupled with the LED light source (Figure 6.6). The intensity of the light reaching the NMR tube was determined to be: 1) 365 nm (bandwidth (FWHM): 9 nm), 0.45 mW/cm^2; 2) 505 nm (bandwidth (FWHM): 30 nm), 1.5 mW/cm^2. ^{1}H NMR spectra were recorded at 500 MHz on an Avance III (Bruker) in regular time periods, and data were processed and analyzed using TopSpin software from Bruker. Solvent residual signals were used as internal standards, MeCN-*d3* $\delta = 1.94$ ppm.

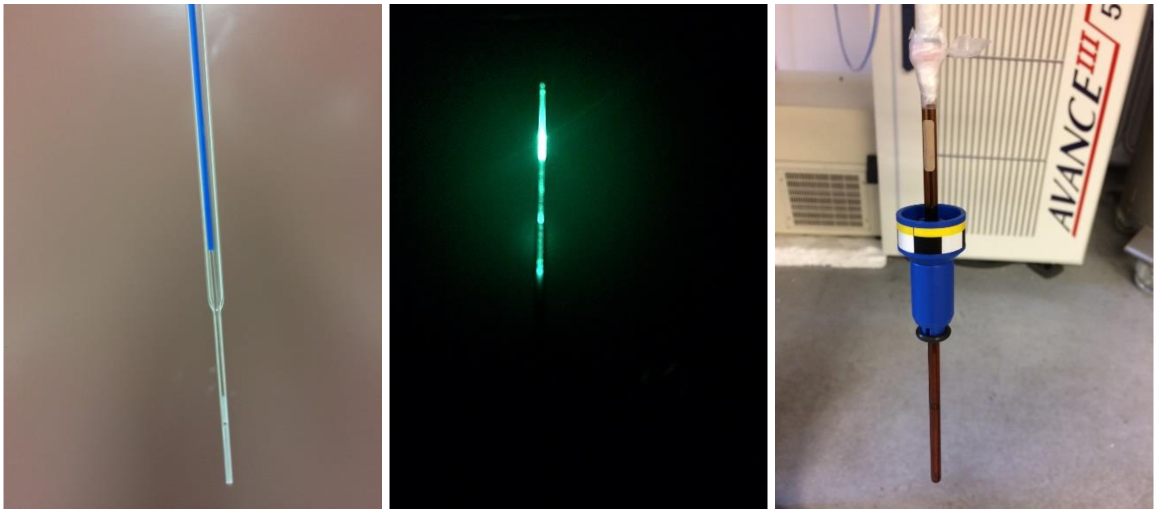

Figure 6.5. The etched insert at the end of the optical cable; with the LED turned on, the light is distributed over the whole length of the etched insert. NMR tube mounted to the optical cable, with a spinner for inserting the tube into the NMR machine.

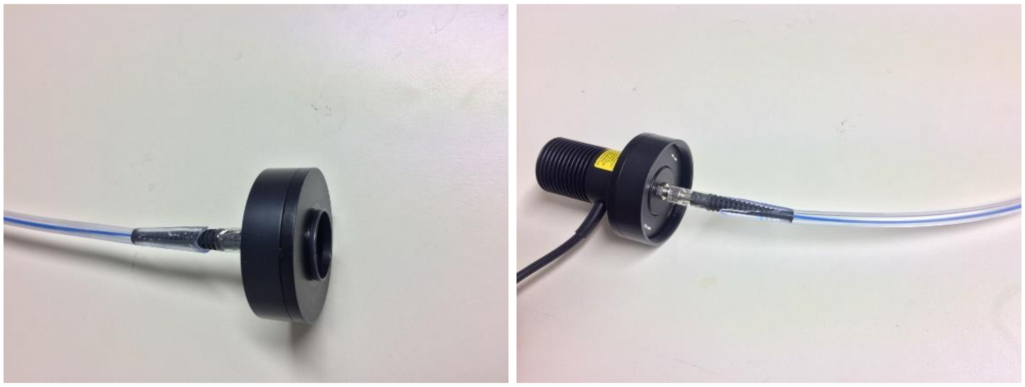

Figure 6.6. Adapter for an LED attachment to the optical cable, with and without the LED attached.

Table 6.1. Irradiation conditions of the NMR photochemical studies of the naphthopyrans **45** and **71**.

Compound	**Irradiation time,** λ_{irr} **= 365 nm** (min)	**Thermal relaxation time** (min)	**Irradiation time,** λ_{irr} **= 505 nm** (min)
Naphthopyran **45**	30	150	-
Naphthopyran **71**	30	45	10

6.5.3 Infrared Measurements

The infrared measurements in solution were recorded on a Bruker Vertex70v ATR-FTIR spectrometer, using deuterated Lanthanum α-alanine doped triglycine sulphate (DLaTGS) detector. The sample compartment was kept under nitrogen. The measurements were carried out in a standard cuvette (two sodium chloride slides, 21 mm × 14 mm) (Figure 6.7). For all the samples, the used concentration was $3\cdot10^{-2}$ M. The irradiation was carried out with a set-up equipped with LED diodes (λ_{irr} = 365 nm), that directly attaches to the cuvette (Figure 6.7). The spectral range between 370 and 4000 cm^{-1} was investigated, with 4 cm^{-1} resolution. IR data were analyzed using the software OPUS 6.5 (Bruker).

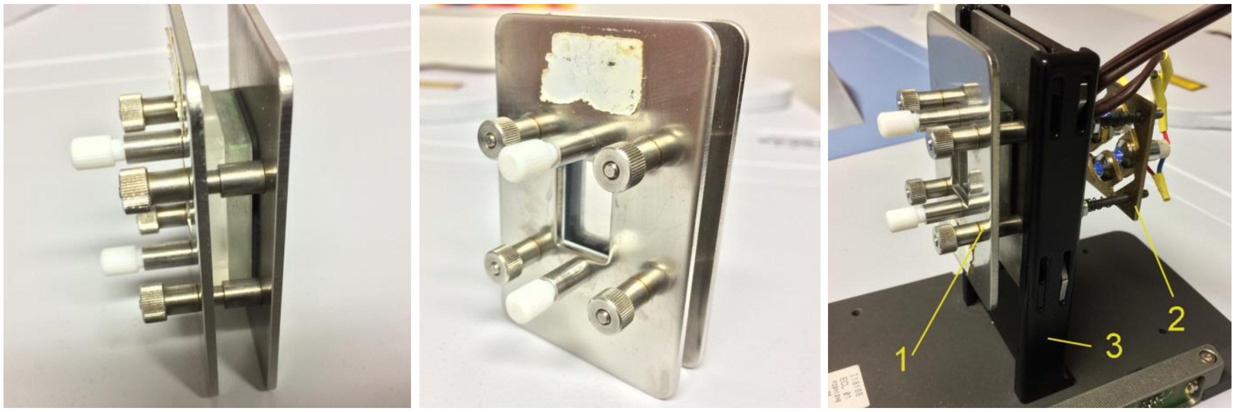

Figure 6.7. Cuvette for the IR measurements (1); equipped with the LED diodes set-up for irradiation (2), mounted on the cuvette holder (3).

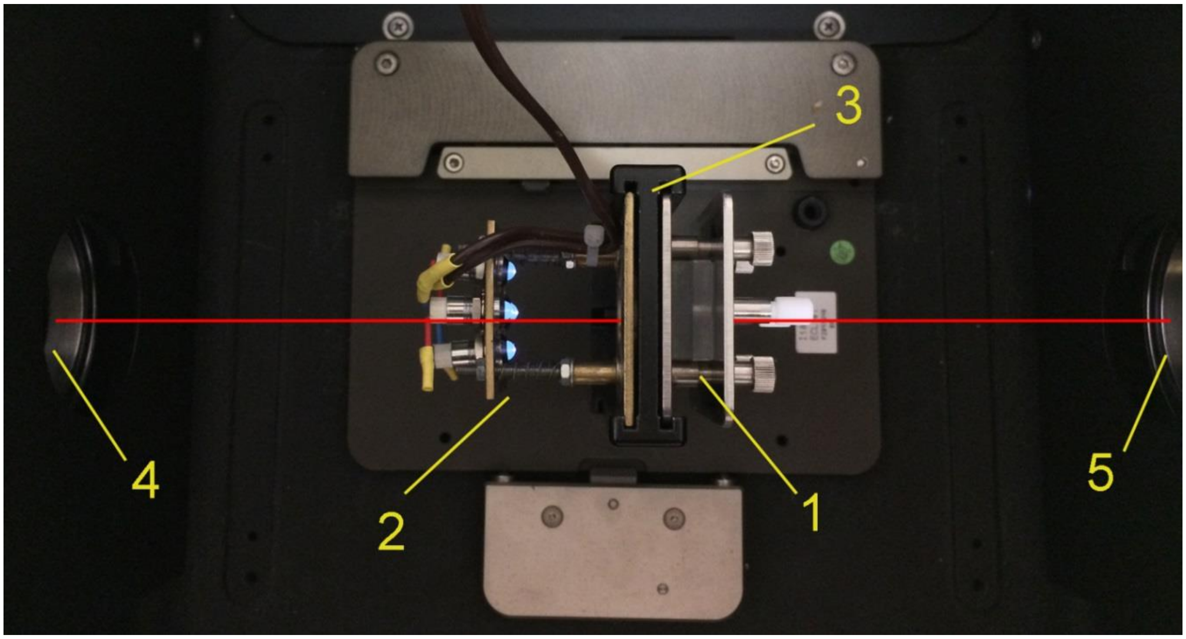

Figure 6.8. Sample compartment of the Bruker FTIR spectrometer: (1) cuvette, (2) set-up with LED diodes for irradiation of the sample, (3) cuvette holder, (4) detector, (5) light source. The red line is drawn to guide the eye by following the IR light beam during the measurement.

Table 6.2. Conditions of the in-solution FTIR photochemical studies of the naphthopyrans **45** and **71**.

Compound	**Solvent**	**Irradiation time, λ = 365 nm** (min)	**Thermal relaxation time** (min)
Naphthopyran **45**	TCE	10	30
	MeCN	10	20
	DCE	15	30
Naphthopyran **71**	TCE	10	20
	MeCN	10	20
	DCE	10	20

7 Appendix

7.1 Photochemical Data

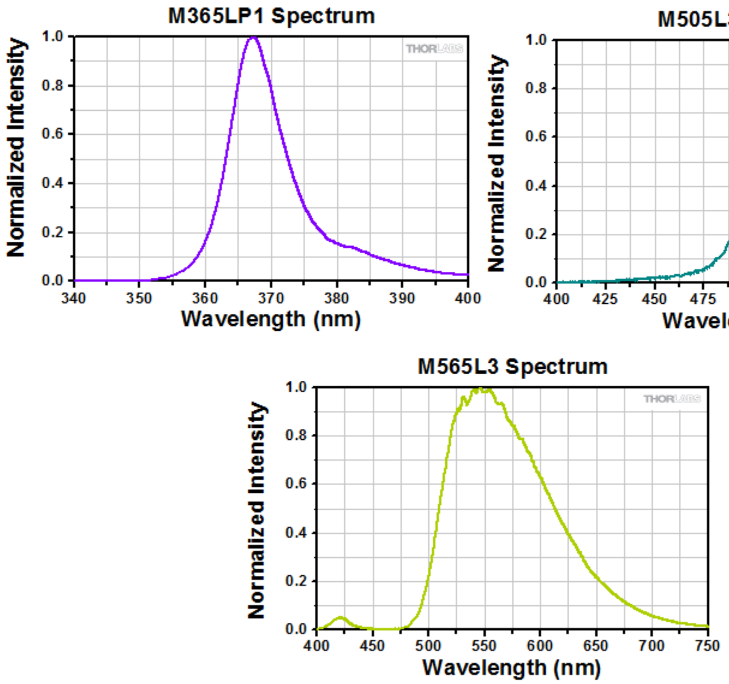

Figure 7.1. Output spectra of the LEDs used in this work.

7.1.1 UV/Vis Data

3-(1-(2-methyl-1*H*-indol-3-yl)ethylidene)-4-(propan-2-ylidene)dihydrofuran-2,5-dione (16)

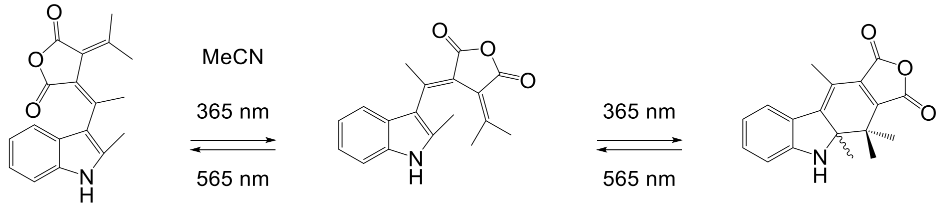

16-*Z* **16**-*E* **16**-*C*

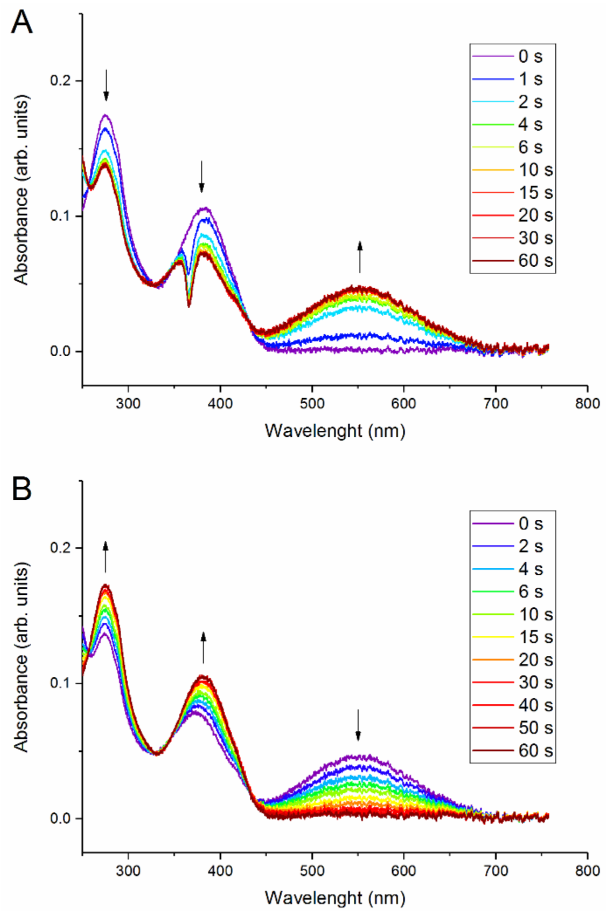

Figure 7.2. Absorption spectra of fulgide **16** in MeCN (9.6 · 10^{-6} M), taken periodically upon (A) UV light irradiation (λ_{irr} = 365 nm, 85 mW/cm^2), (B) visible light irradiation (λ_{irr} = 565 nm, 130 mW/cm^2). The artefacts at ~365 nm is because of the increase in irradiation power in that region, due to simultaneous irradiation and recording of the spectra.

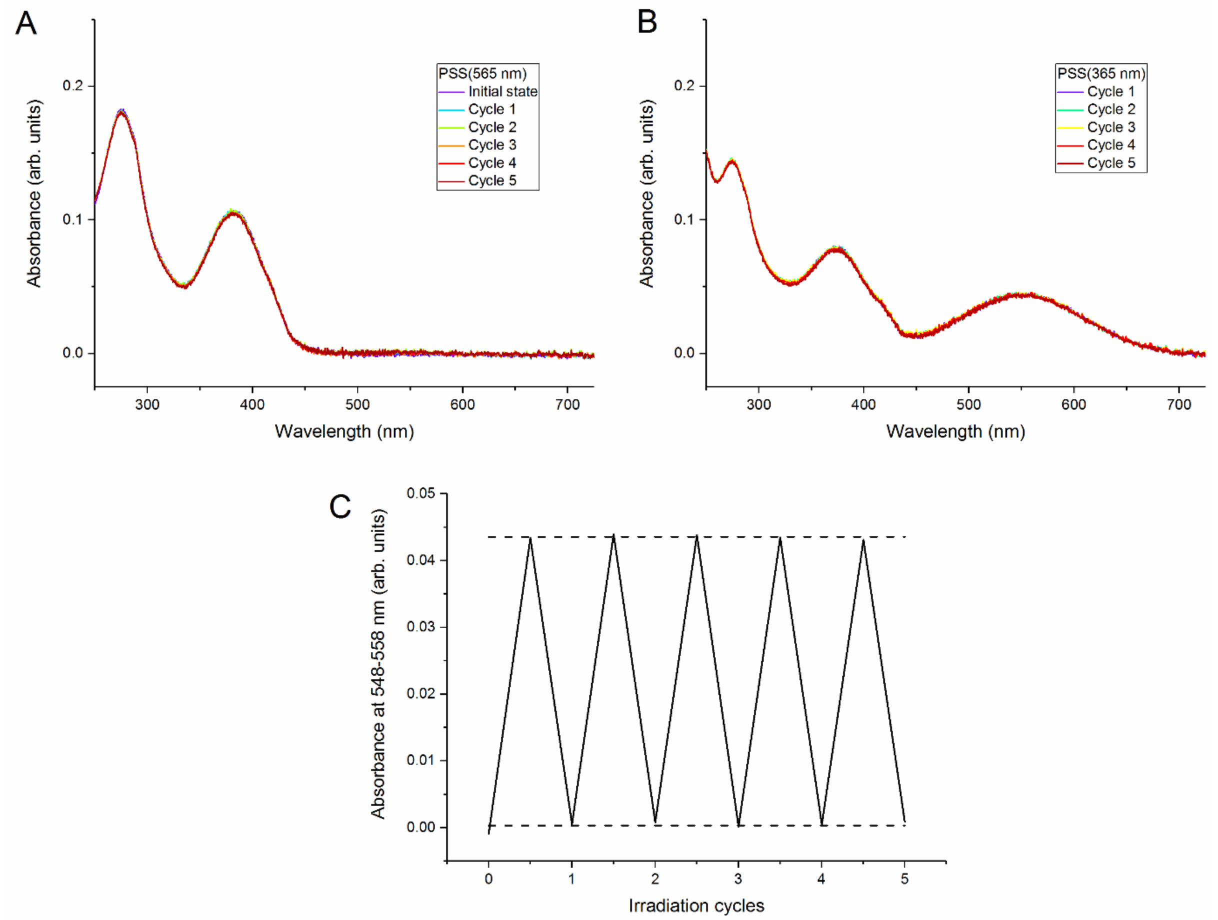

Figure 7.3. Photochemical studies of fulgide **16** in MeCN ($9.6 \cdot 10^{-6}$ M), over 5 irradiation cycles. Irradiation conditions for the cycles: 50 s irradiation with UV light (λ_{irr} = 365 nm, 5 mW/cm^2), 120 s irradiation with visible light (λ_{irr} = 565 nm, 130 mW/cm^2). (A) The spectrum of the initial state (violet) and comparison with spectra of the PSS(565 nm), over 5 cycles. (B) The spectra upon reaching the PSS(365 nm), over 5 cycles.

3-(1-(2-methyl-1*H*-indol-3-yl)ethylidene)-4-(propan-2-ylidene)dihydrofuran-2,5-dione (16)

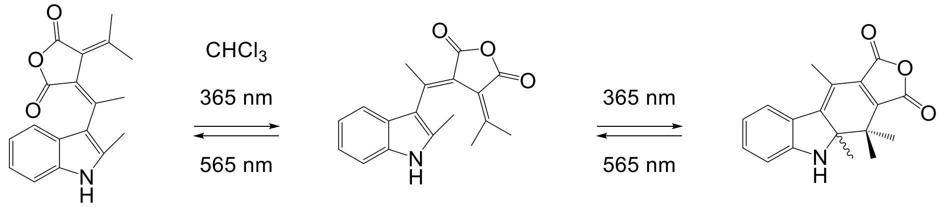

16-*Z* **16**-*E* **16**-*C*

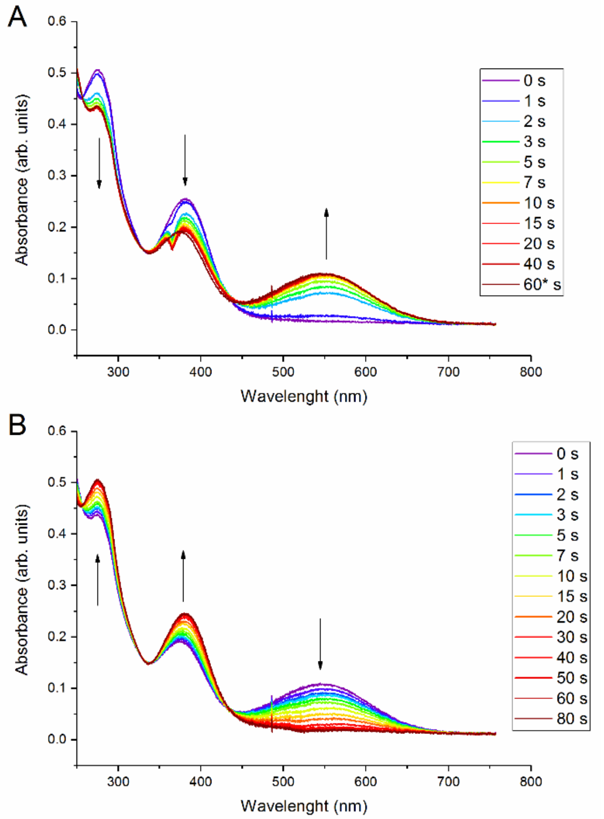

Figure 7.4. Absorption spectra of fulgide **16** in CHCl$_3$ ($2.07 \cdot 10^{-5}$ M), taken periodically upon (A) UV light irradiation (λ_{irr} = 365 nm, 85 mW/cm^2), (B) visible light irradiation (λ_{irr} = 565 nm, 130 mW/cm^2). The artefact at ~365 nm is because of the increase in irradiation power in that region, due to simultaneous irradiation and recording of the spectra.

tert-butyl-(2-(3-(1-(2-methyl-1H-indol-3-yl)ethylidene)-2,5-dioxo-4-(propan-2-ylidene)pyrrolidin-1-yl)ethyl)carbamate (34)

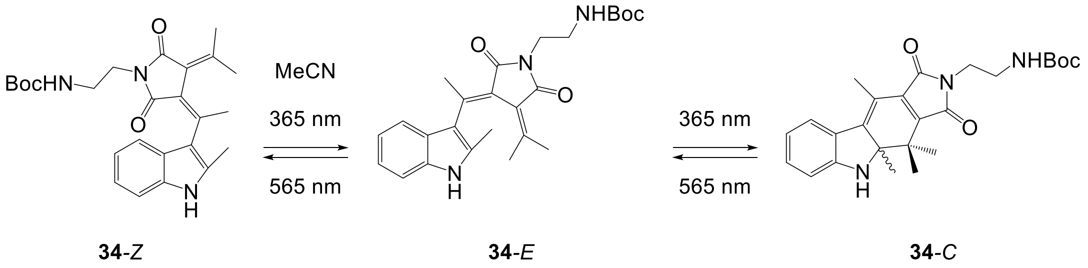
BocHN
MeCN
365 nm
565 nm
NHBoc
365 nm
565 nm
NHBoc
34-*Z*
34-*E*
34-*C*

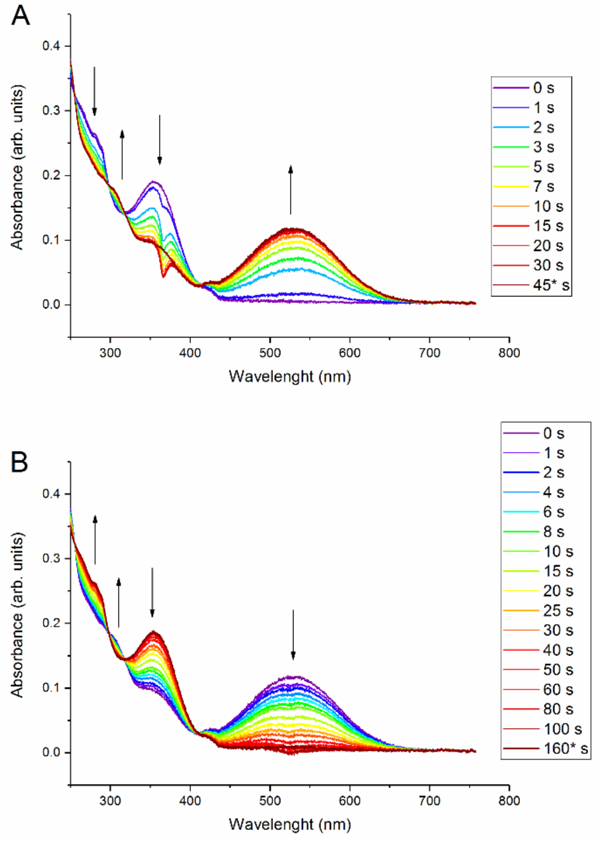

Figure 7.5. Absorption spectra of fulgimide **34** in MeCN ($2.21 \cdot 10^{-5}$ M), taken periodically upon (A) UV light irradiation (λ_{irr} = 365 nm, 85 mW/cm^2), (B) visible light irradiation (λ_{irr} = 565 nm, 130 mW/cm^2). The artefact at ~365 nm is because of the increase in irradiation power in that region, due to simultaneous irradiation and recording of the spectra.

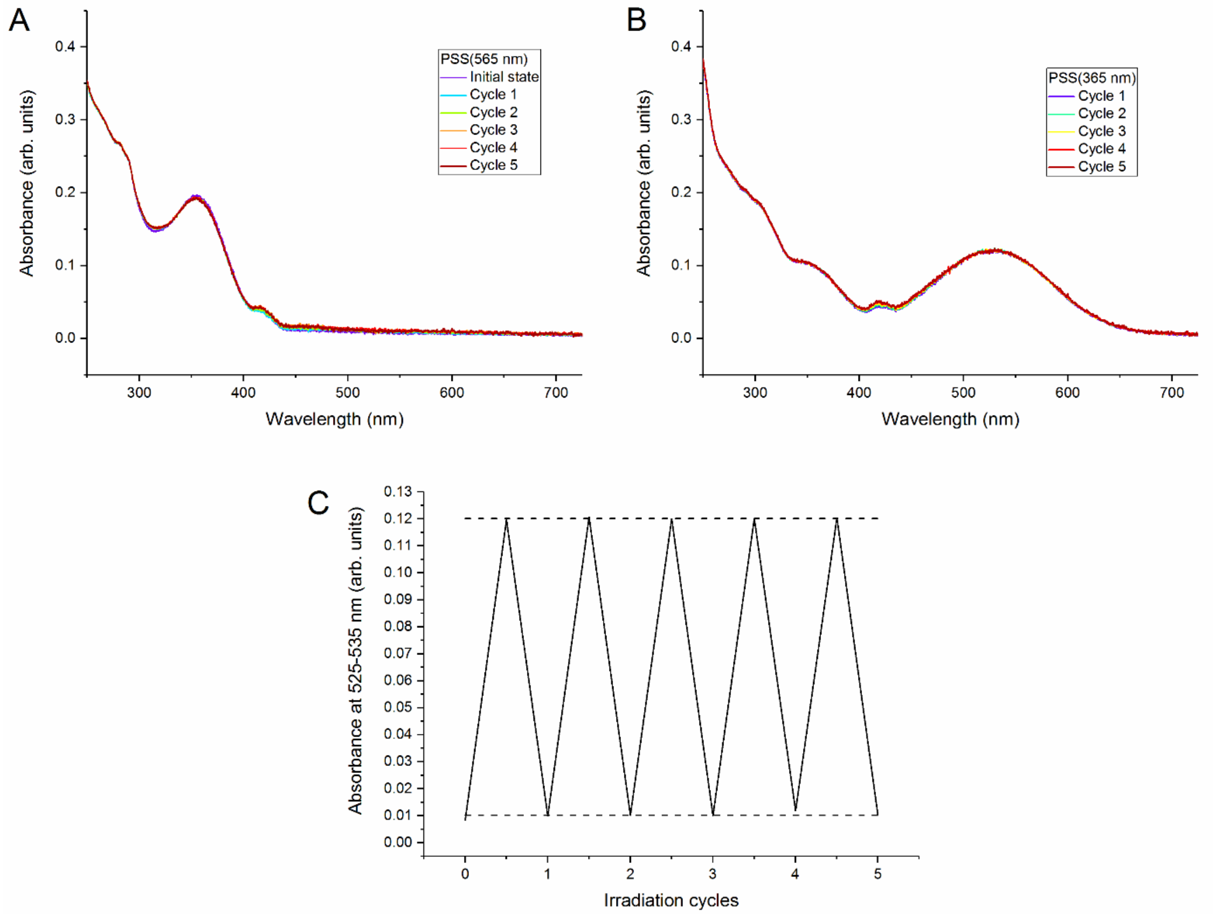

Figure 7.6. Photochemical studies of fulgimide **34** in MeCN ($2.21 \cdot 10^{-5}$ M), over 5 irradiation cycles. Irradiation conditions for the cycles: 30 s irradiation with UV light (λ_{irr} = 365 nm, 85 mW/cm^2), 120 s irradiation with visible light (λ_{irr} = 565 nm, 130 mW/cm^2). (A) The spectrum of the initial state (violet) and comparison with spectra of the PSS(565 nm), over 5 cycles. (B) The spectra upon reaching the PSS(365 nm), over 5 cycles.

tert-butyl-(2-(3-(1-(2-methyl-1H-indol-3-yl)ethylidene)-2,5-dioxo-4-(propan-2-ylidene)pyrrolidin-1-yl)ethyl)carbamate (34)

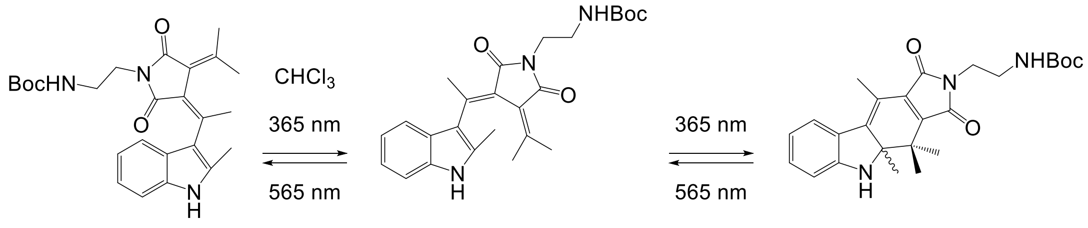

34-*Z* **34**-*E* **34**-*C*

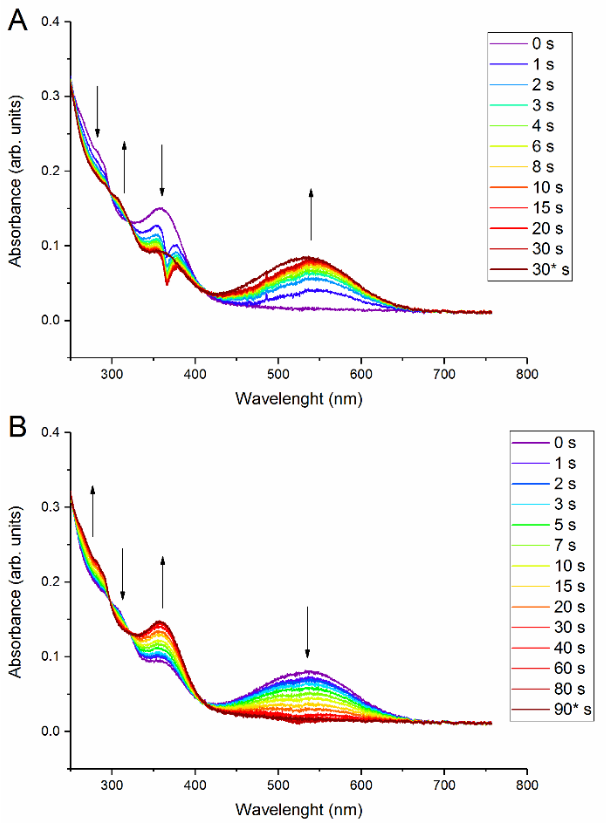

Figure 7.7. Absorption spectra of fulgimide **34** in $CHCl_3$ ($2.53 \cdot 10^{-5}$ M), taken periodically upon (A) UV light irradiation (λ_{irr} = 365 nm, 85 mW/cm^2), (B) visible light irradiation (λ_{irr} = 565 nm, 130 mW/cm^2). The artefacts at ~365 nm is because of the increase in irradiation power in that region, due to simultaneous irradiation and recording of the spectra.

Methyl 6-hydroxy-2,2-diphenyl-2H-benzo[h]chromene-5-carboxylate (45)

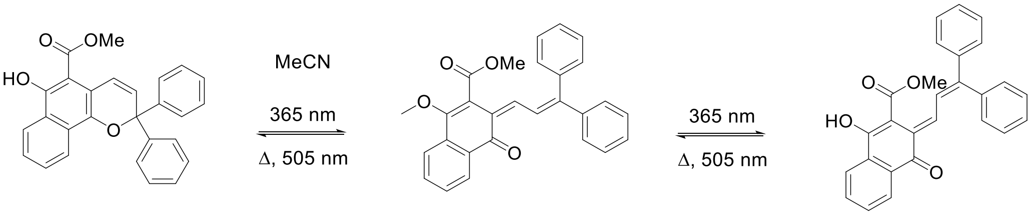

45-*CF* **45**-*TC* **45**-*TT*

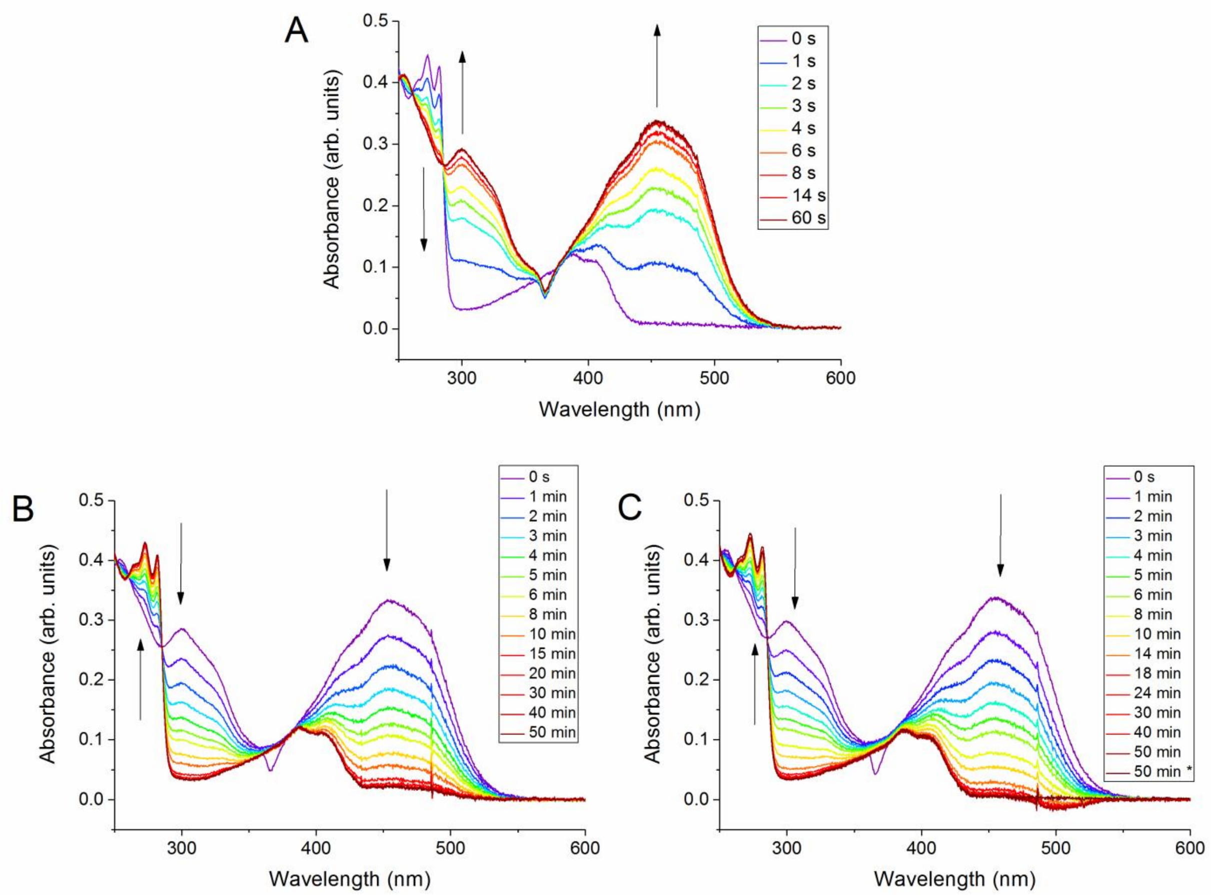

Figure 7.8. Absorption spectra of naphthopyran **45** in MeCN ($9.4 \cdot 10^{-6}$ M), taken periodically upon (A) UV light irradiation (λ_{irr} = 365 nm, 85 mW/cm^2), (B) thermal relaxation. and (C) visible light irradiation (λ_{irr} = 505 nm, 110 mW/cm^2). The artefacts at ~365 nm and ~505 nm are because of the increase in irradiation power in that region, due to simultaneous irradiation and recording of the spectra. (C) The temperature increased over time due to irradiation with the LED (505 nm) light, from 21.8 °C at the beginning of the measurement, to 27.3 °C after 50 min of irradiation. The *50 min** spectra was recorded upon cooling down to the initial temperature.

tert-Butyl 4-(4-(2-((5-(methoxycarbonyl)-2,2-diphenyl-2Hbenzo[h]chromen-6-yl)oxy)-2-oxoethyl)phenyl)piperazine-1-carboxylate (71)

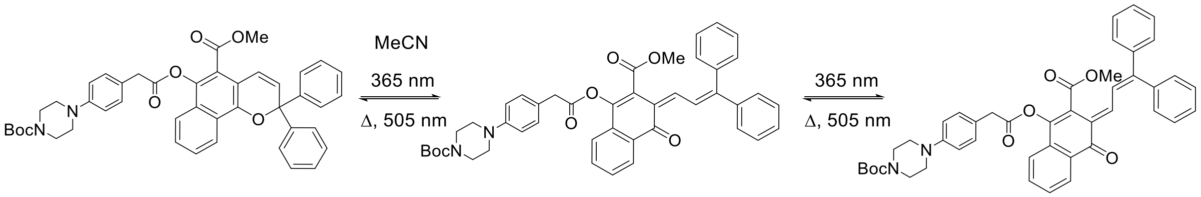
O
OMe
O
O
BocN
N
O
MeCN
365 nm
Δ, 505 nm
O
OMe
O
O
BocN
N
O
365 nm
Δ, 505 nm
O
OMe
O
O
BocN
N
O

71-*CF* **71**-*TC* **71**-*TT*

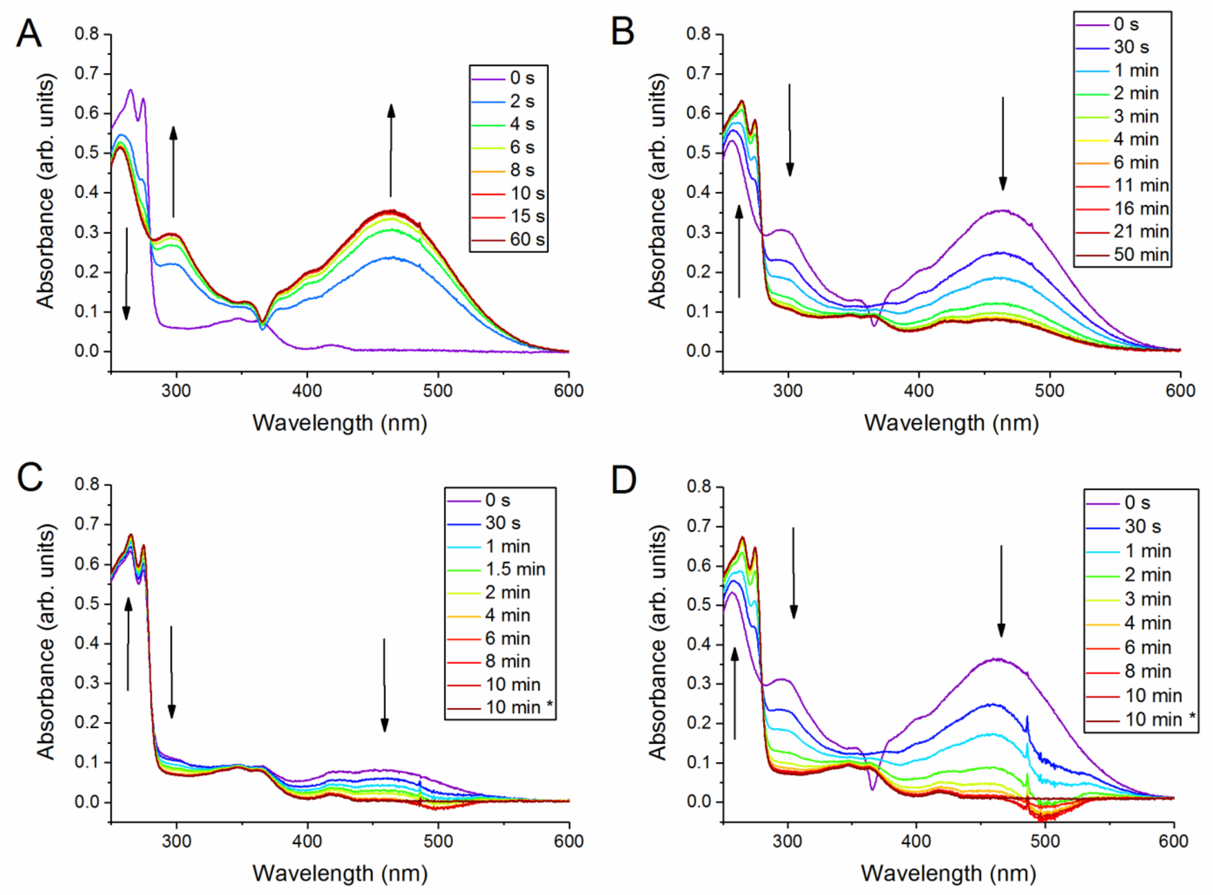

Figure 7.9. Absorption spectra of naphthopyran **71** in MeCN ($9.8 \cdot 10^{-6}$ M), taken periodically upon (A) UV light irradiation (λ_{irr} = 365 nm, 85 mW/cm^2), (B) thermal relaxation. and (C, D) visible light irradiation (λ_{irr} = 505 nm, 110 mW/cm^2). The artefacts at ~365 nm and ~505 nm are because of the increase in irradiation power in that region, due to simultaneous irradiation and recording of the spectra.

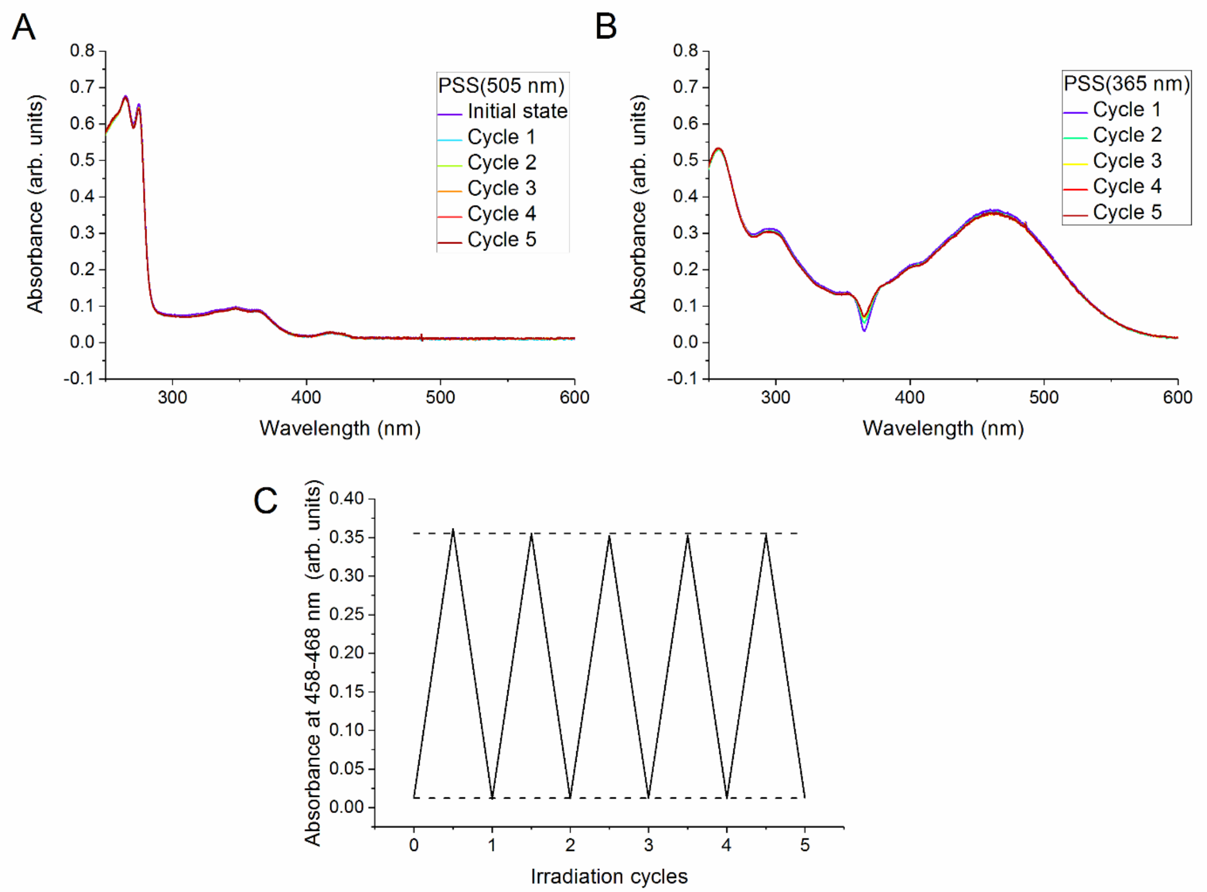

Figure 7.10. Photochemical studies of the naphthopyran **71** in MeCN ($9.8 \cdot 10^{-6}$ M), over 5 irradiation cycles. Irradiation conditions for the cycles: 60 s irradiation with UV light (λ_{irr} = 365 nm85 mW/cm^2), 10 min irradiation with visible light (λ_{irr} = 505 nm, 110 mW/cm^2). (A) The spectrum of the initial state (violet) and comparison with spectra of the PSS(505 nm), over 5 cycles. The temperature increased upon irradiation with 505 nm LED light (from 21.8 °C to ~25.5 °C), so the spectra of the PSS(505 nm) were taken upon cooling down to the initial temperature. (B) The spectra upon reaching the PSS(365 nm), over 5 cycles. The artefact at ~365 nm is because of the increase in irradiation power in that region, due to simultaneous irradiation and recording of the spectra.

tert-Butyl 4-(4-(2-((5-(methoxycarbonyl)-2,2-diphenyl-2Hbenzo[h]chromen-6-yl)oxy)-2-oxoethyl)phenyl)piperazine-1-carboxylate (71)

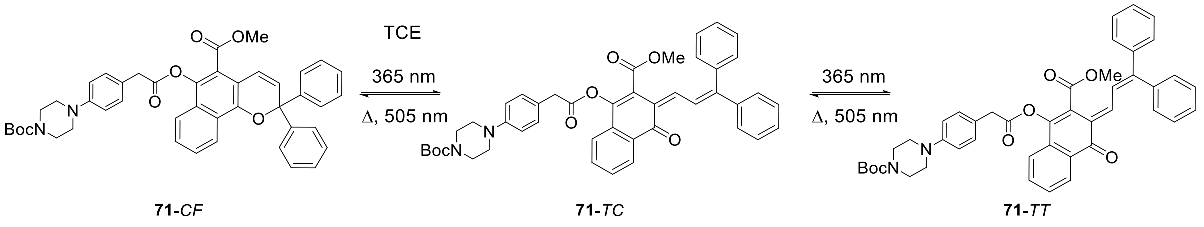
O
OMe
O
O
BocN
N
O
TCE
365 nm
Δ, 505 nm
O
OMe
O
O
BocN
N
O
365 nm
Δ, 505 nm
O
OMe
O
O
BocN
N
O
71-*CF*
71-*TC*
71-*TT*

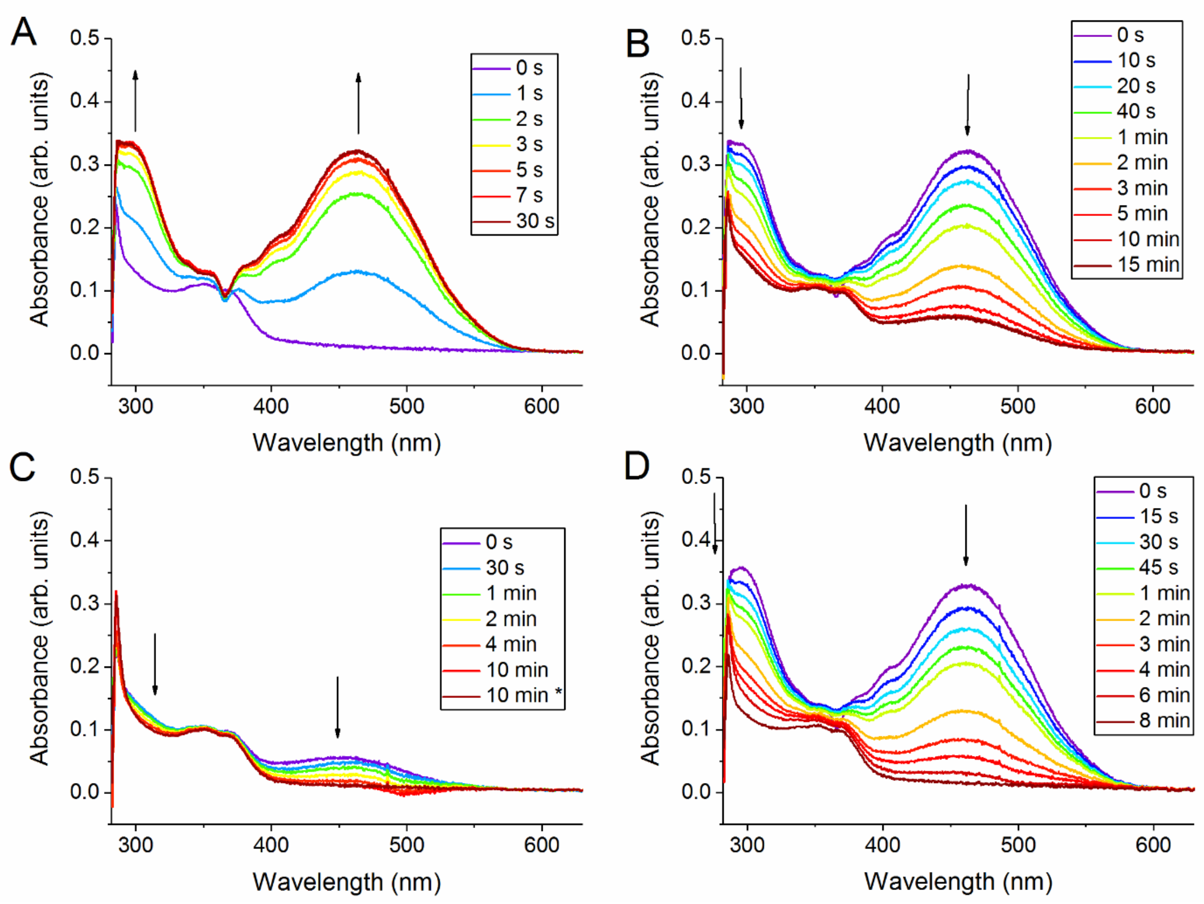

Figure 7.11. Absorption spectra of naphthopyran **71** in TCE ($9.4 \cdot 10^{-6}$ M), taken periodically upon (A) UV light irradiation (λ_{irr} = 365 nm, 85 mW/cm^2), (B) thermal relaxation, and (C, D) visible light irradiation (λ_{irr} = 505 nm, 110 mW/cm^2). The artefacts at ~365 nm and ~505 nm are because of the increase in irradiation power in that region, due to simultaneous irradiation and recording of the spectra.

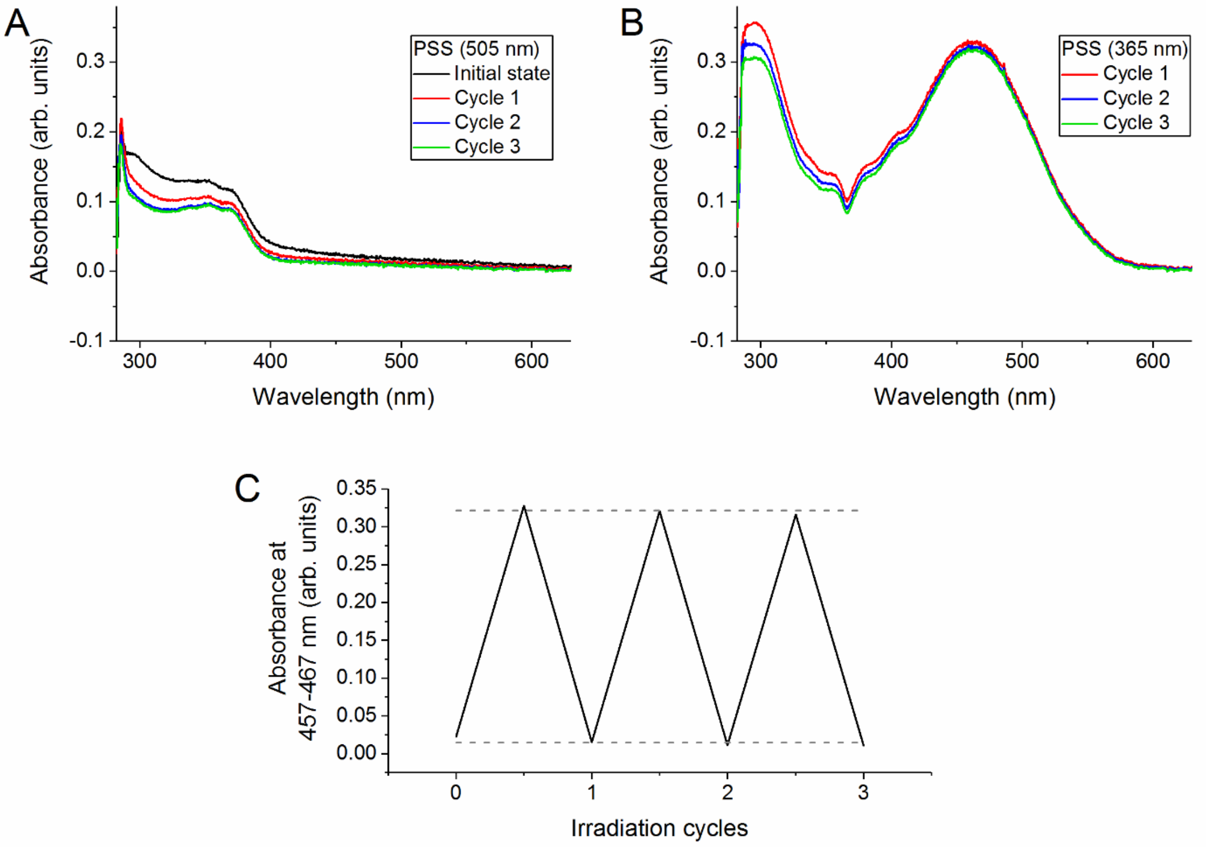

Figure 7.12. Photochemical studies of the naphthopyran **71** in TCE ($9.4 \cdot 10^{-6}$ M), over 3 irradiation cycles. Irradiation conditions for the cycles: 30 s irradiation with visible light ($\lambda_{irr} = 365$ nm, 85 mW/cm^2), 8 min irradiation with visible light ($\lambda_{irr} = 505$ nm, 110 mW/cm^2). (A) The spectrum of the initial state (black line) and comparison with spectra of the PSS(505 nm), over 3 cycles. The temperature increased upon irradiation with 505 nm LED light (from 21.8 °C to ~24 °C), so the spectra of the PSS were taken upon cooling down to the initial temperature. (B) The spectra upon reaching the PSS(365 nm), over 3 cycles. The artefact at ~365 nm is because of the increase in irradiation power in that region, due to simultaneous irradiation and recording of the spectra.

7.1.2 NMR Data

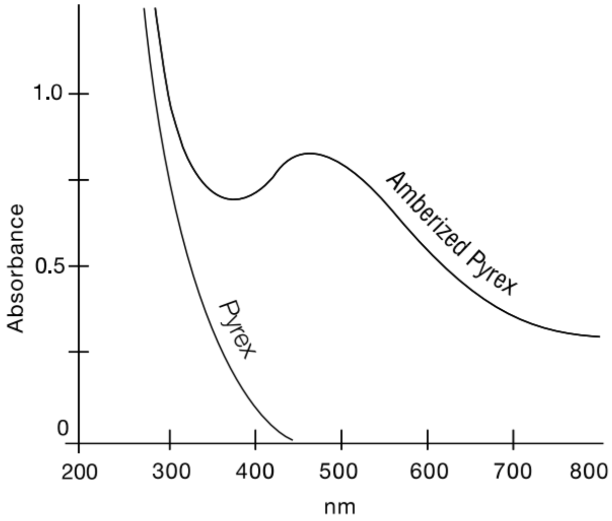

Figure 7.13. Transmission curve of the amberized Pyrex glass of the NMR tube used for photochemical investigations.

Methyl 6-hydroxy-2,2-diphenyl-2H-benzo[h]chromene-5-carboxylate (45)

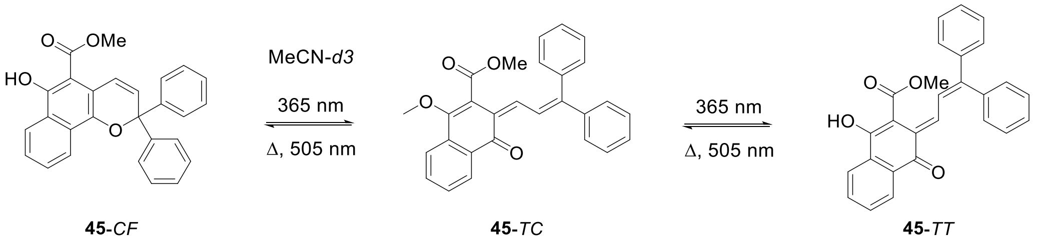
O
OMe
HO
O
MeCN-d3
365 nm
Δ, 505 nm
O
OMe
O
O
365 nm
Δ, 505 nm
O
OMe
HO
O
45-CF
45-TC
45-TT

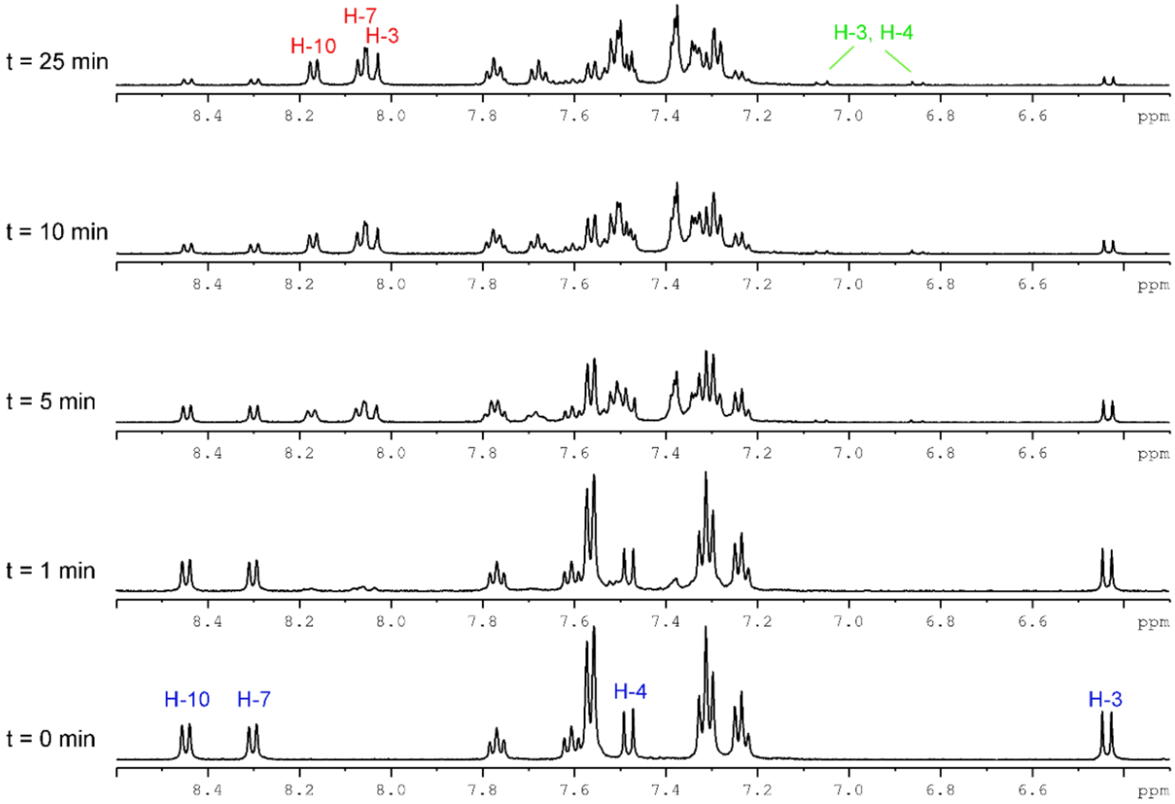

Figure 7.14. ^{1}H NMR spectra of naphthopyran **45** in MeCN-*d3* (10^{-2} M), taken periodically upon irradiation with 365 nm LED light (0.45 mW/cm^2) at 0 °C. Signal assignments are color-coded as following: CF – blue, TC – red, TT – green.

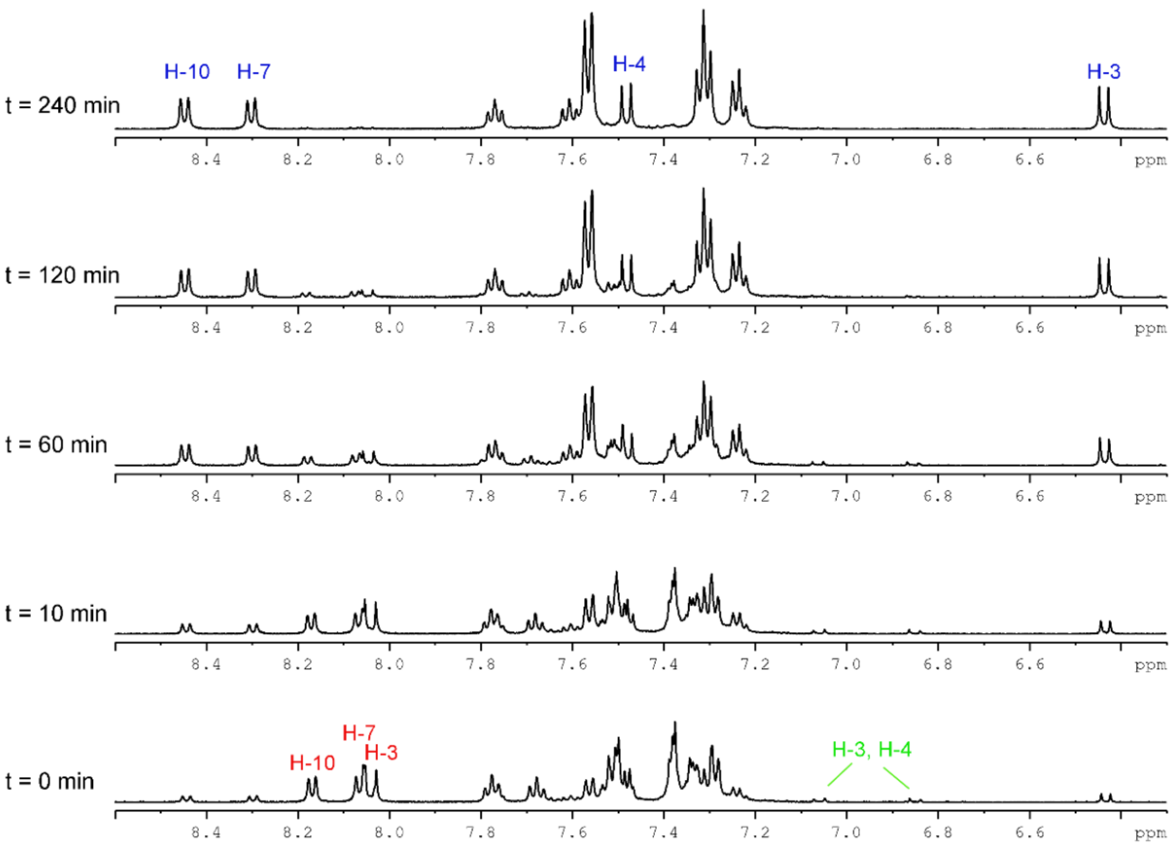

Figure 7.15. ^{1}H NMR spectra of naphthopyran **45** in MeCN-*d3* (10^{-2} M), taken periodically upon thermal relaxation reaction in the dark at 0 °C. Signal assignments are color-coded as following: CF – blue, TC – red, TT – green.

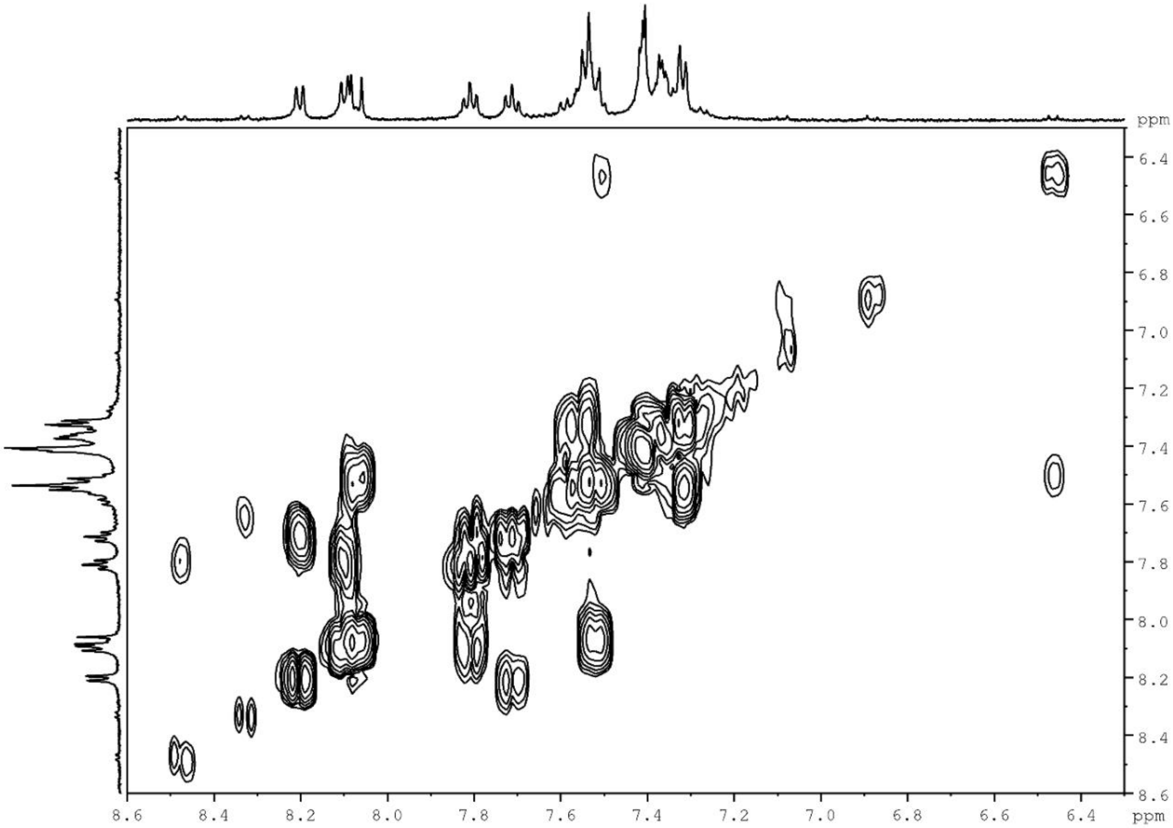

Figure 7.16. H,H-COSY of naphthopyran **45** in MeCN-*d3* (10^{-2} M), recorded upon reaching the PSS(365 nm) at 0 °C.

tert-Butyl 4-(4-(2-((5-(methoxycarbonyl)-2,2-diphenyl-2Hbenzo[h]chromen-6-yl)oxy)-2-oxoethyl)phenyl)piperazine-1-carboxylate (71)

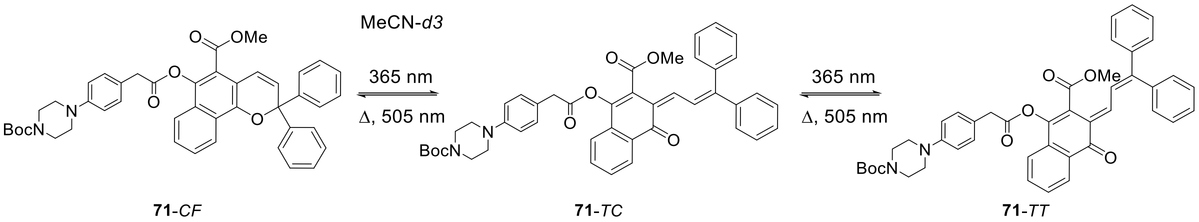
MeCN-*d3*
365 nm
Δ, 505 nm
365 nm
Δ, 505 nm
OMe
BocN
N
O
71-*CF*
71-*TC*
71-*TT*

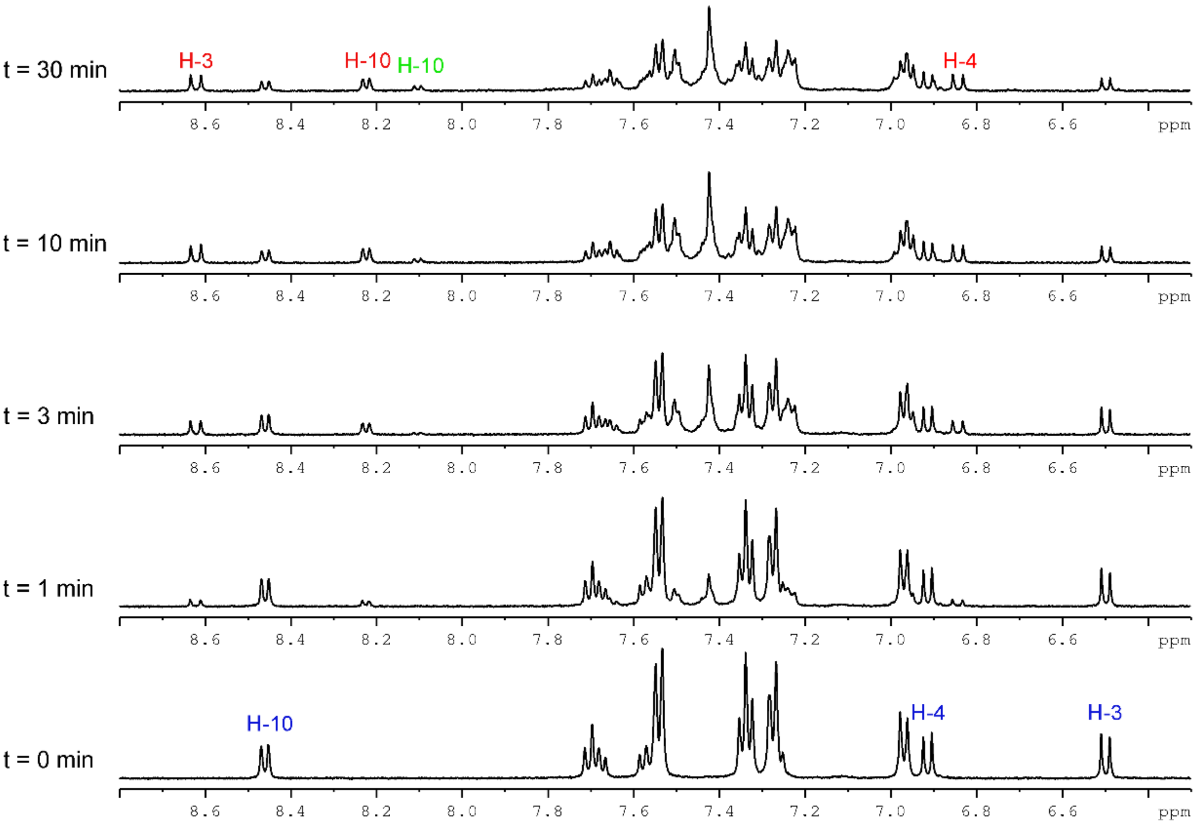

Figure 7.17. ^{1}H NMR spectra of naphthopyran **71** in MeCN-*d3* (10^{-2} M), taken periodically upon irradiation with 365 nm LED light (0.45 mW/cm^2) at 0 °C. Signal assignments are color-coded as following: CF – blue, TC – red, TT – green.

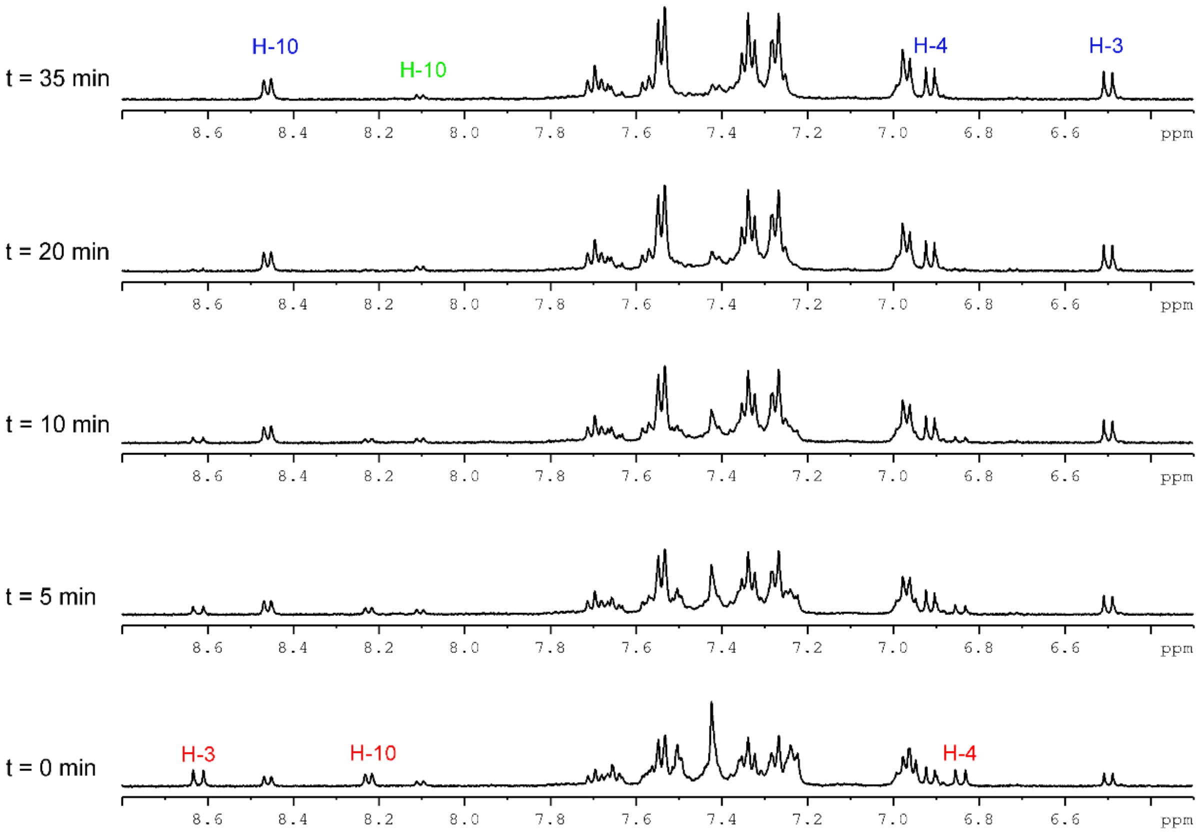

Figure 7.18. ^{1}H NMR spectra of naphthopyran **71** in MeCN-*d3* (10^{-2} M), taken periodically upon thermal relaxation reaction in the dark at 0 °C. Signal assignments are color-coded as following: CF – blue, TC – red, TT – green.

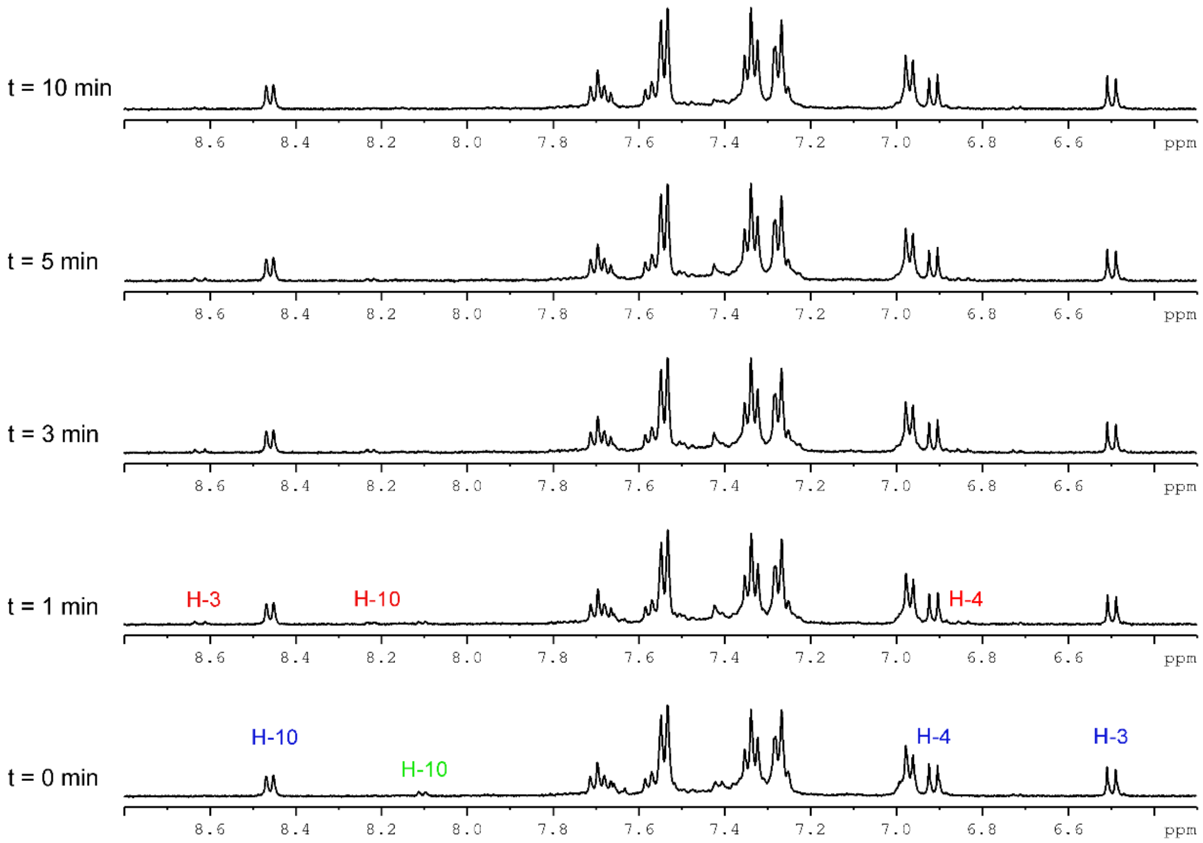

Figure 7.19. ^{1}H NMR spectra of naphthopyran **71** in MeCN-*d3* (10^{-2} M), taken periodically upon irradiation with 505 nm LED light (1.5 mW/cm^2) at 0 °C. Signal assignments are color-coded as following: CF – blue, TC – red, TT – green.

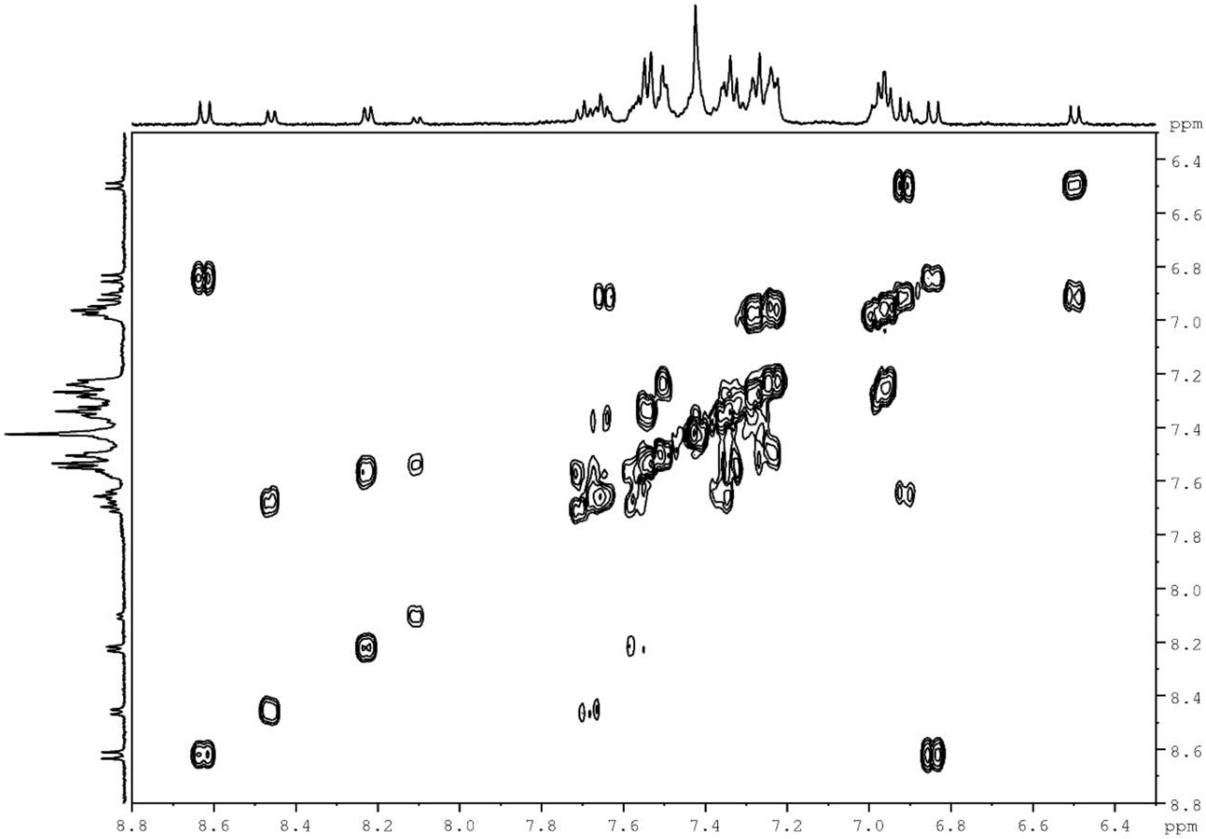

Figure 7.20. H,H-COSY of naphthopyran **71** in MeCN-*d3* (10^{-2} M), recorded upon reaching the PSS(365 nm) at 0 °C.

7.1.3 Infrared Data

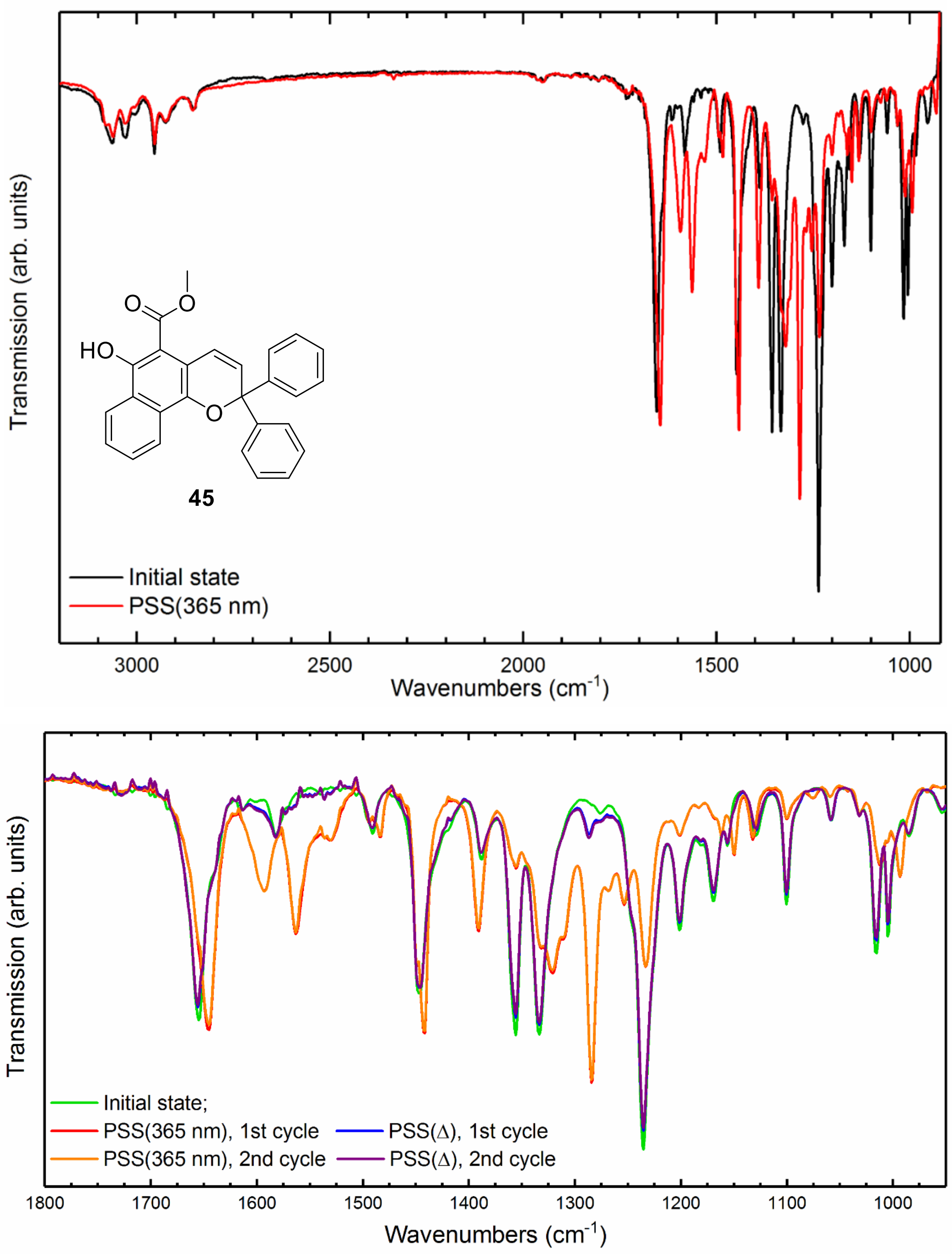

Figure 7.21 IR spectra of the photochemical studies of naphthopyran **45** in TCE.

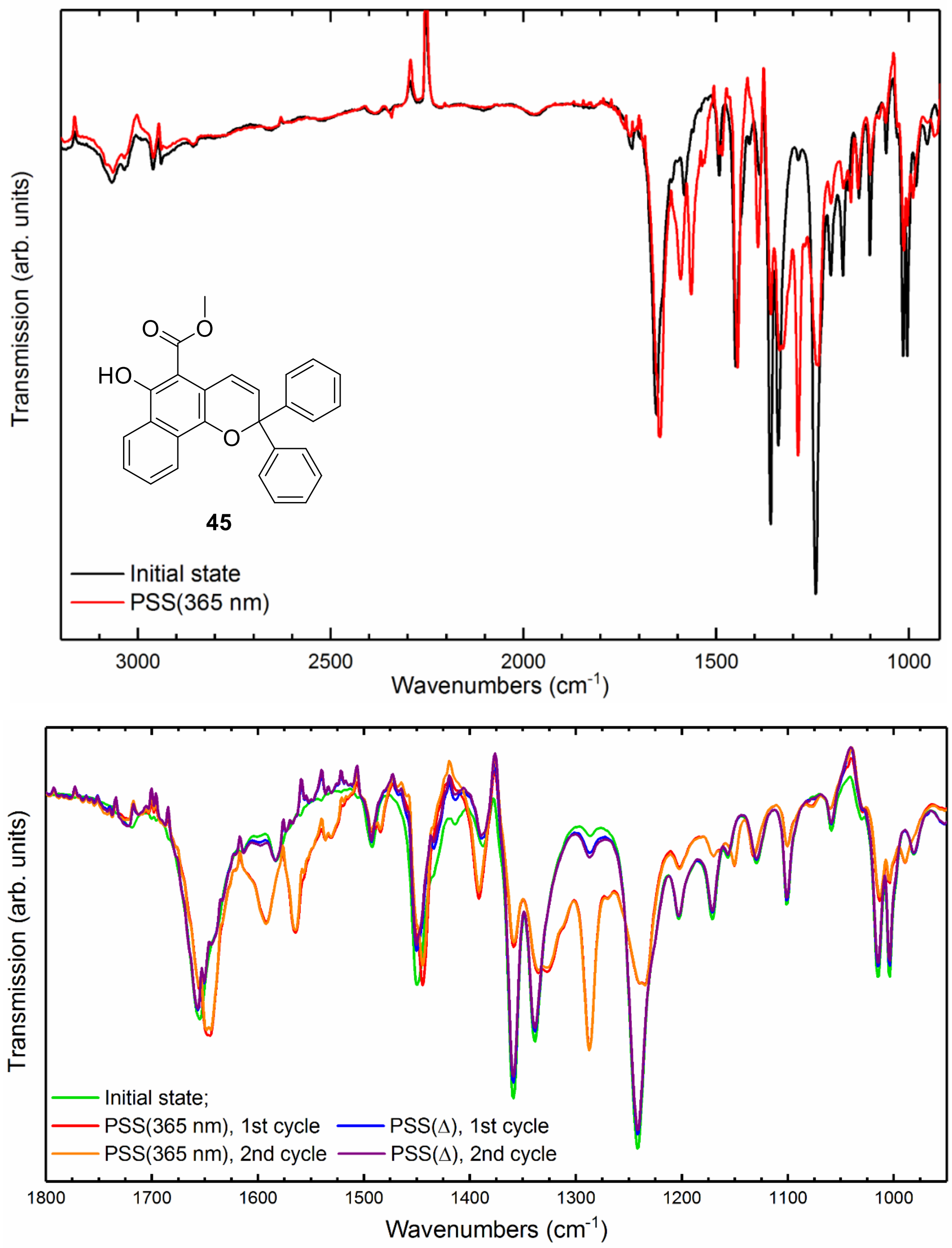

Figure 7.22. IR spectra of the photochemical studies of naphthopyran **45** in MeCN.

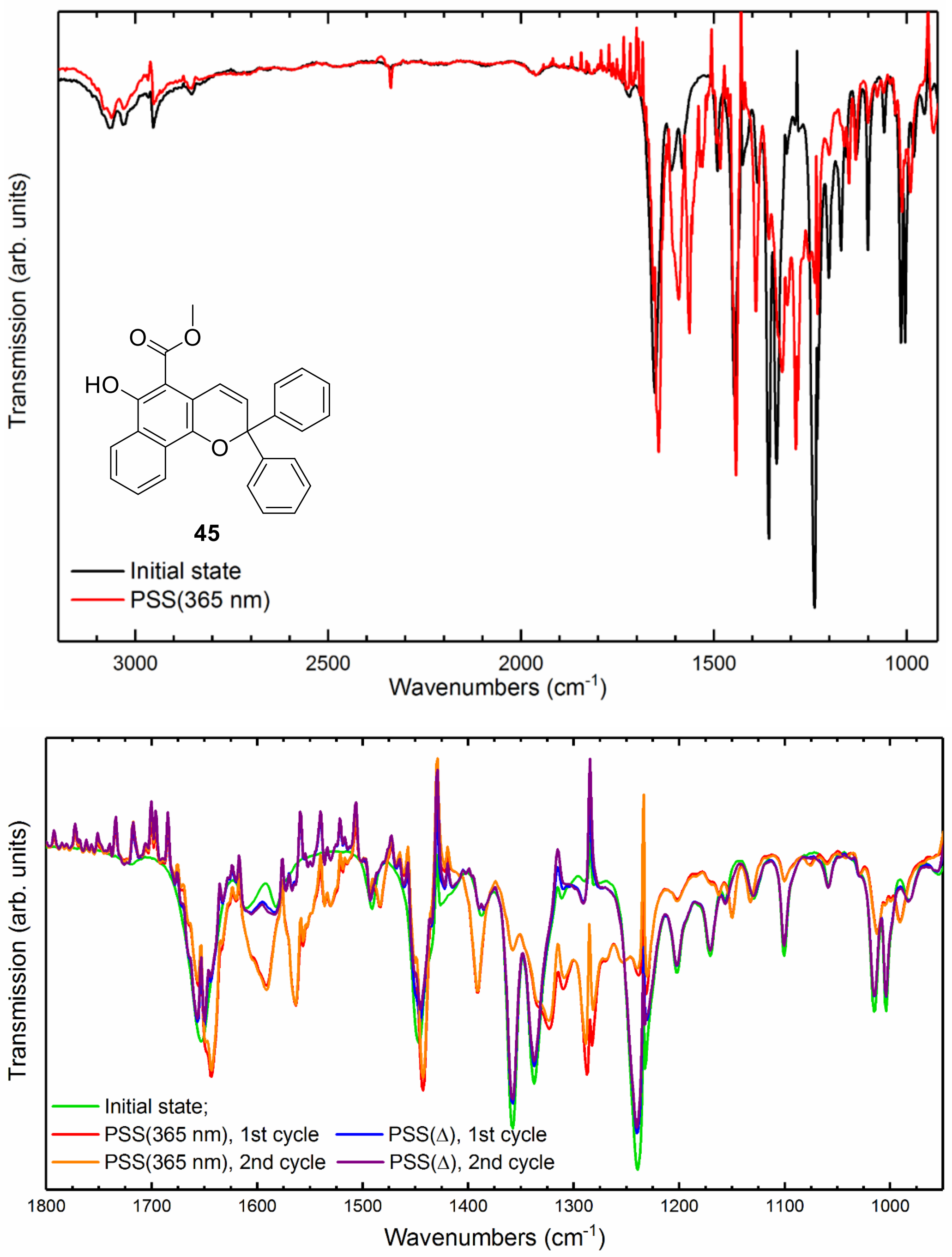

Figure 7.23. IR spectra of the photochemical studies of naphthopyran **45** in DCE.

Table 7.1. IR absorption and band assignments of the initial state of the naphthopyran **45**, measured in solution in TCE, MeCN and DCE. The literature references are taken from ref. 136. Assignments next to the literature range suggest the relative intensity of the band: s - strong; m - medium; w - weak; v - variable. The values in shaded rows of the table specify the bands that significantly increase in the intensity upon the ring-opening reaction.

IR absorption bands (cm^{-1})			**Assignment**[a]	**Literature** (cm^{-1})[136]
TCE	MeCN	DCE		
3064	3067	3068	ν_{as}(C-H) arom.	3105-3000 (m)
3028	3036	3032		
2955	2961	2954	ν_{as}(CH_3)	2975-2925 (m)
2853	2856	2854	ν_{sym}(CH_3)	2880-2820 (m)
	1719		ν(C=O) ester, non H-bonded	1740-1705 (s)
1655	1655	1653	ν(C=O) ester, H-bonded[b]	~ 1650 (s)
1593	1592	1591	C=C conjugated with C=C or C=O	1660-1580 (s-m)
1563	1565	1563	-C=C- aromatic ring str	(1600-1500) (v)
1530	1531	1530	extended conjugation	
1583	1583	1583	-C=C- aromatic ring str	1590-1575 (v)
1491	1492	1491		1525-1470 (v)
1448	1450	1447	asym CH_3 def vib	1475-1445 (m-s)
1388	1388	1388	-C=C- aromatic (naph.) str	1400-1370 (m)
1356	1359	1358	COH bending (phenol)	1410-1310 (s)
1344	1339	1338	in-plane O-H def vib (phenol)	1410-1310 (s)
1284	1287	1287	ν(C-CO-C) aryl ketone	~ 1300 (m)
1235	1242	1239	ν_{asym}(C-O-C) ester	1275-1185 (s)
1202	1202	1203	ν(C-O) ester	1260-1180 (s)
1170	1171	1171	ν(O-C) methyl ester	1175-1155 (s)
1100	1101	1100	sym C-O-C ester	1150-1100 (s)
1015	1015	1015	ν(C-O-C) ether	1120-1020 (s)
1005	1004	1004	C-H rocking (CH_3)	1060-900 (m-w)
771	775	773	out of plane C-H arom. (naph.)	780-760 (s)
699	704	705	C-H out of plane bending	730-650 (s)

---

[a] Abbreviations: str – stretching, def – deformation, vib – vibration.

[b] The -CH=CH-, in conjugation with aryl moiety, shows a vibration of a medium intensity in the range 1640-1610 cm^{-1}. However, this band is only observable as a shoulder of a more intense C=O stretching vibration. Additionally, the shoulder also present in the sample measured in MeCN, is assigned to the bending vibration of the water impurities (~1640 cm^{-1}) from the solvent.

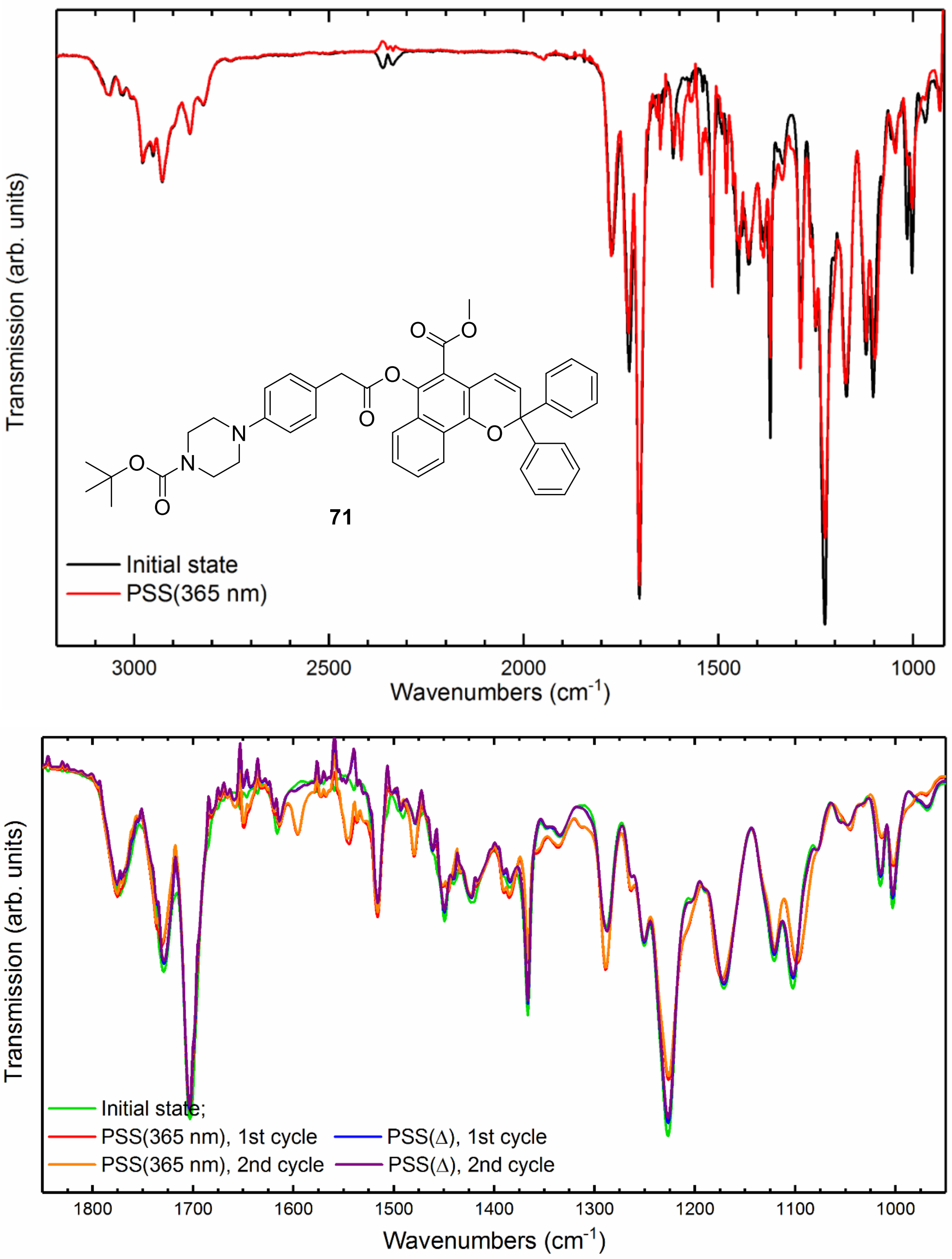

Figure 7.24. IR spectra of the photochemical studies of naphthopyran **71** in TCE.

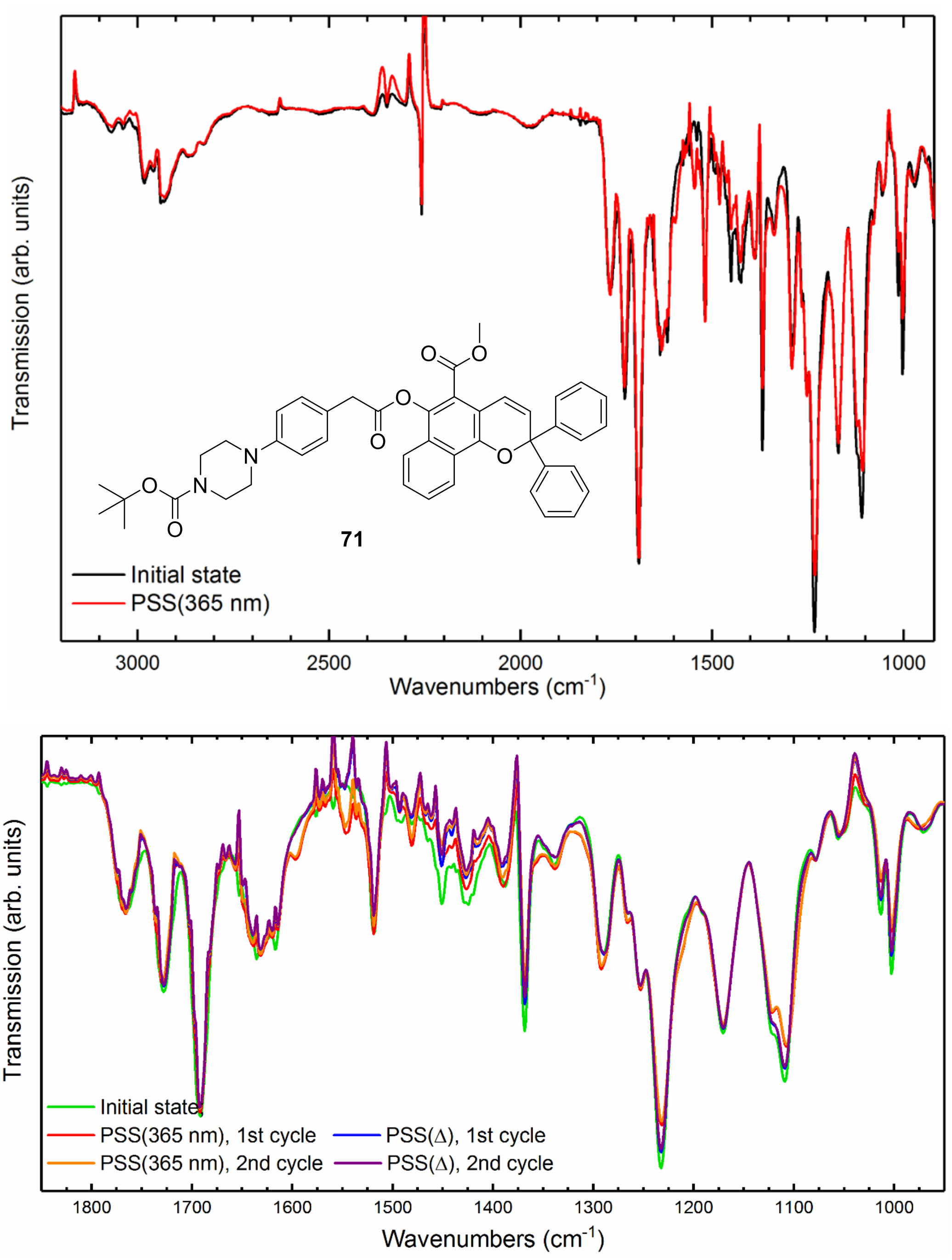

Figure 7.25. IR spectra of the photochemical studies of naphthopyran **71** in MeCN.

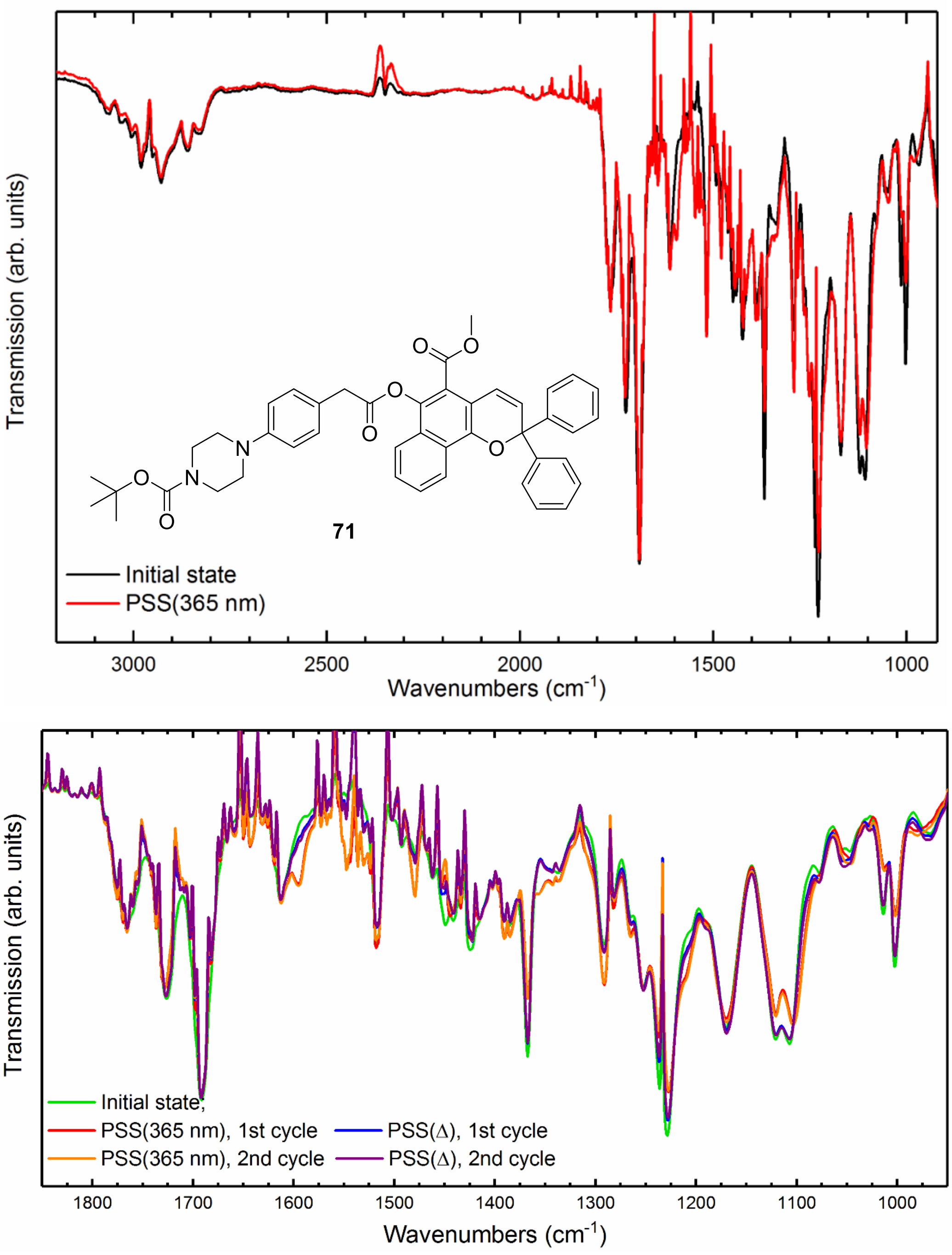

Figure 7.26. IR spectra of the photochemical studies of naphthopyran **71** in DCE.

Table 7.2. IR absorption and band assignments of the initial state of the naphthopyran **71**, measured in solution in TCE, MeCN and DCE. The literature references are taken from ref. 136. Assignments next to the literature range suggest the relative intensity of the band: s - strong; m - medium; w – weak; and v- variable. The values in shaded rows of the table specify the bands that significantly increase in the intensity upon the ring-opening reaction.

IR absorption bands ($\mathrm{cm^{-1}}$)			**Assignment**[a]	**Literature** ($\mathrm{cm^{-1}}$)[136]
TCE	MeCN	DCE		
3066	3069	3063	ν_{as}(C-H) arom.	3105-3000 (m)
3030	3039	3034		
2979	2983	2981	$\nu_{as}(\mathrm{CH_3})$	3030-2950 (m-w)
2952	2959	2951	$\nu_{as}(\mathrm{CH_3})$	2975-2925 (m)
2929	2939	2929	$\nu_{as}(\mathrm{CH_2})$	2940-2915 (m)
2857	2868	2861	$\nu_{sym}(\mathrm{CH_2})$	2890-2850 (m)
2824	2828	2827	$\nu_{sym}(\mathrm{CH_3})$	2880-2820 (m)
1773	1768	1766	ν(C=O) phenyl ester	1800-1750 (s)
1729	1728	1726	ν(C=O) methyl ester	1740-1705 (s)
1703	1692	1692	ν(C=O) carbamate	1740 – 1680 (s)
1650	- [b]	1650	ν(C=O) ketone conjugated	1680-1650 (s)
1595	1597	1595	-C=C- aromatic ring str extended conjugation	(1600-1500) (v)
1545	1548	1548		
1616	- [b]	1613	-C=C- aromatic ring str	1620-1580 (v)
1516	1519	1517		1525-1470 (v)
1449	1451	1449	asym $\mathrm{CH_3}$ def vib	1475-1445 (m-s)
1385	1388	1386	-C=C- aromatic (naph.) str	1400-1370 (m)
1367	1368	1367	$\mathrm{-C(CH_3)_3}$, asym $\mathrm{CH_3}$ def vib	1395-1350 (m-s)
1288	1290	1291	ν(O-C(aromatic))	1310-1230 (s)
1227	1232	1229	ν_{as}(C-O-C) ester	1275-1185 (s)
1172	1171	1170	O-C str, methyl ester	1175-1155 (s)
1121	1122	1121	ν_{sym}(C-O-C) ester	1150-1100 (s)
1102	1109	1107	ν_{sym}(C-O-C) ester	1150-1100 (s)
1015	1014	1015	ν(C-O-C) (ether)	1120-1020 (s)
1003	1003	1003	C-H rocking ($\mathrm{CH_3}$)	1060-900 (m-w)
772	773	773	out of plane C-H arom. (naph)	780-760 (s)
699	704	709	CH out of plane bending	730-650 (s)

---

[a] Abbreviations: str – stretching, def – deformation, vib – vibration.

[b] The absorption bands in the region 1660-1600 $\mathrm{cm^{-1}}$ are hidden due to overlapping with the O-H bending vibration of the water impurities in MeCN. Thus, the bands expected to be observed in this region are not possible to identify and assign.

7.2 Surface Analysis

Table 7.3. IR absorptions and band assignments of the ester- and carboxy-terminated neat SAMs on Si(111).

IR absorption bands (cm^{-1})	Assignments
Ester-terminated monolayer	
2956	$\nu_{as}(CH_3)$
2922	$\nu_{as}(CH_2)$
2852	$\nu_{sym}(CH_2)$
1746	$\nu(C{=}O)$
1466	$\delta(CH_2)$ scissoring mode
1440	$\delta_{as}(CH_3)$
1365	$\delta_{sym}(CH_3)$
1172	$\nu(C\text{-}O)$
Carboxy-terminated monolayer	
2923	$\nu_{as}(CH_2)$
2853	$\nu_{sym}(CH_2)$
1714	$\nu(C{=}O)$
1466	$\delta(CH_2)$ scissoring mode
1415	$\delta(OH)$
1161	$\nu(C\text{-}O)$

Table 7.4. IR absorptions and band assignments of the ester- and carboxy-terminated diluted SAMs on Si(111).

IR absorption bands (cm^{-1})	Assignments
Ester-terminated monolayer	
2958	$\nu_{as}(CH_3)$
2922	$\nu_{as}(CH_2)$
2852	$\nu_{sym}(CH_2)$
1746	$\nu(C=O)$
1466	$\delta(CH_2)$ scissoring mode
1440	$\delta_{as}(CH_3)$
1161	$\nu(C-O)$
Carboxy-terminated monolayer	
2958	$\nu_{as}(CH_3)$
2923	$\nu_{as}(CH_2)$
2852	$\nu_{sym}(CH_2)$
1714	$\nu(C=O)$
1463	$\delta(CH_2)$ scissoring mode
1440	$\delta_{as}(CH_3)$
1410	$\delta(OH)$
1161	$\nu(C-O)$

Table 7.5. IR absorptions and band assignments of the fulgimide-terminated neat and diluted SAMs on Si(111) in PSS(545 nm) and PSS(365 nm).

IR absorption bands (cm^{-1})		**Assignments**
Fulgimide-terminated neat monolayer		
PSS(545 nm)	**PSS(365 nm)**	
2922	2923	$\nu_{as}(CH_2)$
2852	2852	$\nu_{sym}(CH_2)$
1741 (1739)[a]	1758	$\nu_{sym}(C=O)$ imide
1691 (1689)[a]	1695	$\nu_{as}(C=O)$ imide
1649	1649	$\nu(C=O)$ amide I
1601	1604	$\nu(C=C)$ conjugated
1547	1548	$\nu(CNH)$ amide II
Fulgimide-terminated diluted monolayer		
PSS(545 nm)	**PSS(365 nm)**	
2922	2922	$\nu_{as}(CH_2)$
2852	2852	$\nu_{sym}(CH_2)$
1741 (1739)[a]	1757	$\nu_{sym}(C=O)$ imide
1691 (1689)[a]	1693	$\nu_{as}(C=O)$ imide
1658	1658	$\nu(C=O)$ amide I
1595	1598	$\nu(C=C)$ conjugated
1548	1548	$\nu(CNH)$ amide II

---

[a] Value of the absorption band upon the immobilization of (*E*/*Z*)-fulgimide.

Table 7.6. IR absorptions and band assignments of the naphthopyran-terminated neat SAMs on Si(111) in PSS(545 nm) and PSS(365 nm).

IR absorption bands (cm^{-1})		Assignments
Naphthopyran-terminated monolayer		
PSS(545 nm)	**PSS(365 nm)**	
2925	2925	$\nu_{as}(CH_2)$
2853	2853	$\nu_{sym}(CH_2)$
1765	1765	ν(C=O) phenylacetic acid ester
1725	1726	ν(C=O) methyl ester
1641	1641	ν(C=O) amide
1612 (1614)[a]	1612	Aromatic ring stretch
-	1595	ν(C=C) conjugated
1517	1516	Aromatic ring stretch
1465	1465	$\delta(CH_2)$ scissoring mode
1446	1446	$\delta_{as}(CH_3)$ methyl ester
1368	1368	$\delta_{sym}(CH_3)$ methyl ester
1230	1230	ν_{as}(C-O-C) arom. acid ester

---

[a] Value of the absorption band upon the immobilization of naphthopyran conjugate **8**.

Table 7.7. IR absorption and band assignments of epoxy-, alkyl-, acetylene- and fulgimide-terminated monolayers on oxidized Si(100).

IR absorption bands (cm^{-1})			**Assignments**
Epoxy-terminated monolayer			
10 ppm	**66 ppm**	**Sat.**	
2963	2965	-[†]	$\nu_{as}(CH_3)$
2931	2934	2934	$\nu_{as}(CH_2)$
2869	2871	2876	$\nu_{sym}(CH_2)$
1434	1434	1434	$\delta(CH_2)_3$ scissoring mode
1280-1000[a]			ν(C-O), ν(Si-O)
[†] the CH_3 stretching vibration not observed due to all Si-OCH_3 groups being hydrolyzed in procedure with toluene with the highest water content.			
Alkyl-terminated monolayer			
10 ppm	**66 ppm**		
2960	2964		$\nu_{as}(CH_3)$
2927	2931		$\nu_{as}(CH_2)$
2860	2871		$\nu_{sym}(CH_2)$
1412	1412		$\delta(CH_2)_3$ scissoring mode
1280-1000*			ν(C-O), ν(Si-O)
Acetylene-terminated monolayer			
2960			$\nu_{as}(CH_3)$
2929			$\nu_{as}(CH_2)$
2863			$\nu_{sym}(CH_2)$
2121			ν(C≡C)
1612			δ(N-H) bending δ(O-H) bending
1438			$\delta(CH_2)_3$ scissoring mode
1373			δ(C-H) deformation in alcohol (in H-C-OH) sec. alcohol O-H in plane deformation
1280-1000*			ν(C-O), ν(Si-O)

---

[a] A proper assignment of the absorption bands in the region from 1280-1000 cm^{-1} is difficult, due to the number of bands overlapping in this area: ν(C-O), ν(Si-O-C), Si-O-Si TO, Si-O-Si LO.

Table 7.8. IR absorptions and band assignments of the fulgimide-terminated SAMs on oxidized Si(100) in PSS(545 nm) and PSS(365 nm).

IR absorption bands (cm^{-1})		**Assignments**
Fulgimide-terminated monolayer		
2963	2963	$\nu_{as}(CH_3)$
2923	2923	$\nu_{as}(CH_2)$
2868	2868	$\nu_{sym}(CH_2)$
1699	1700	$\nu_{as}(C=O)$
1608	1608	δ(N-H) bending δ(O-H) bending
1280-1000[a]		ν(C-O), ν(Si-O)

---

[a] A proper assignment of the absorption bands in the region from 1280-1000 cm^{-1} is difficult, due to the number of bands overlapping in this area: ν(C-O), ν(Si-O-C), Si-O-Si TO, Si-O-Si LO.

Table 7.9. Contact angle data of prepared epoxy-, alkyl-, and fulgimide-terminated monolayers on oxidized Si(100). The contact angle values are obtained as an average over 5 measurements on a sample, each sample was prepared in triplicate at least. Calculated errors are the maximum fitting error obtained for each measurement.

Sample	**Contact angle** (°)	**Calculated error** (±)
Epoxy-terminated monolayer (~10 ppm)	54.1	2.7
Epoxy-terminated monolayer (66 ppm)	62.0	2.5
Alkyl-terminated monolayer (~10 ppm)	51.2	2.3
Alkyl-terminated monolayer (66 ppm)	64.2	2.9
Fulgimide-terminated monolayer (average, PSS 365 nm)	62.2	3.0
Fulgimide-terminated monolayer (average, PSS 545 nm)	58.2	3.0

Table 7.10. Ellipsometry measurements of the freshly prepared silicon oxide layer, and silicon oxide and the epoxy-terminated monolayer of the freshly prepared SAMs on oxidized Si(100).

Sample	**Thickness of the layer** (nm)
Silicon oxide	1.49
Silicon oxide under the monolayer	130-1.42
Epoxy-terminated monolayer	0.90

7.3 NMR Spectra

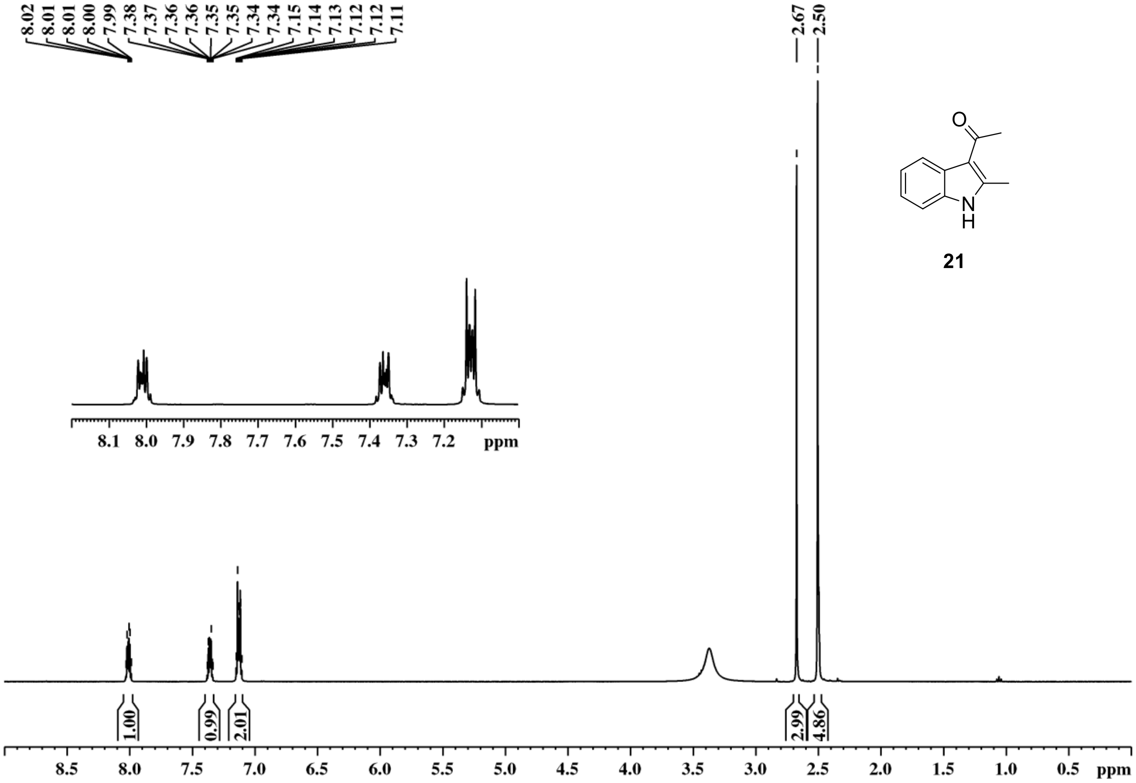

21

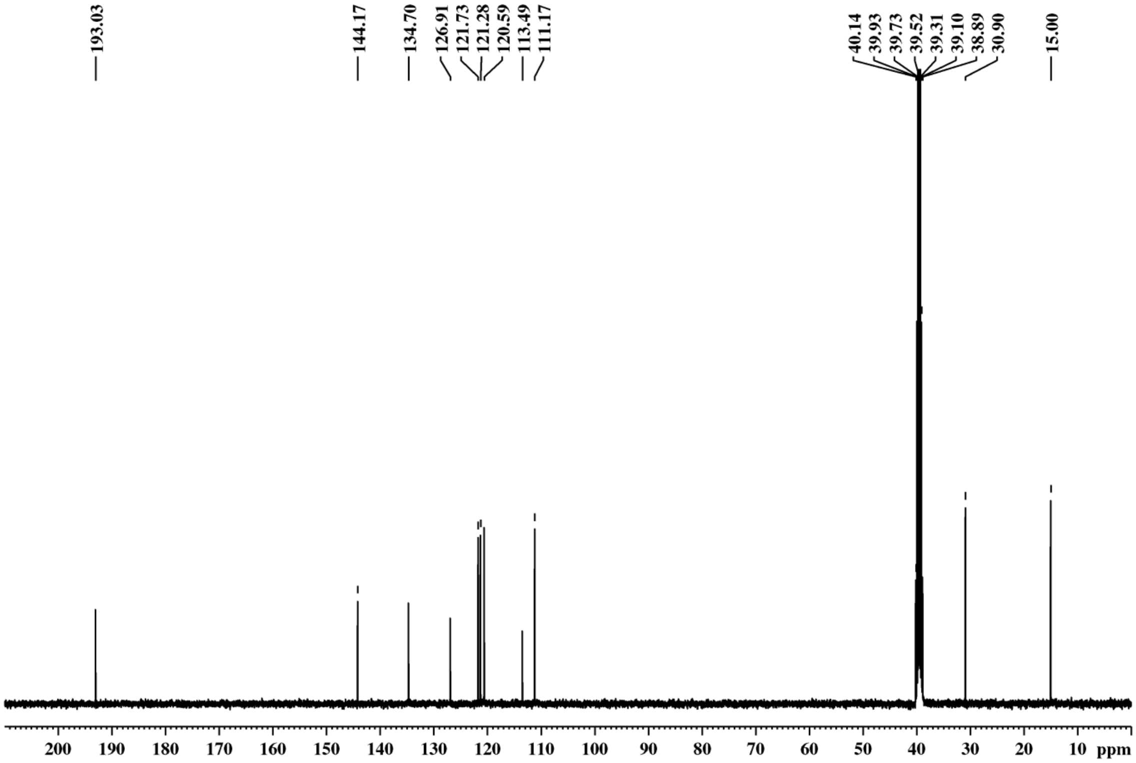

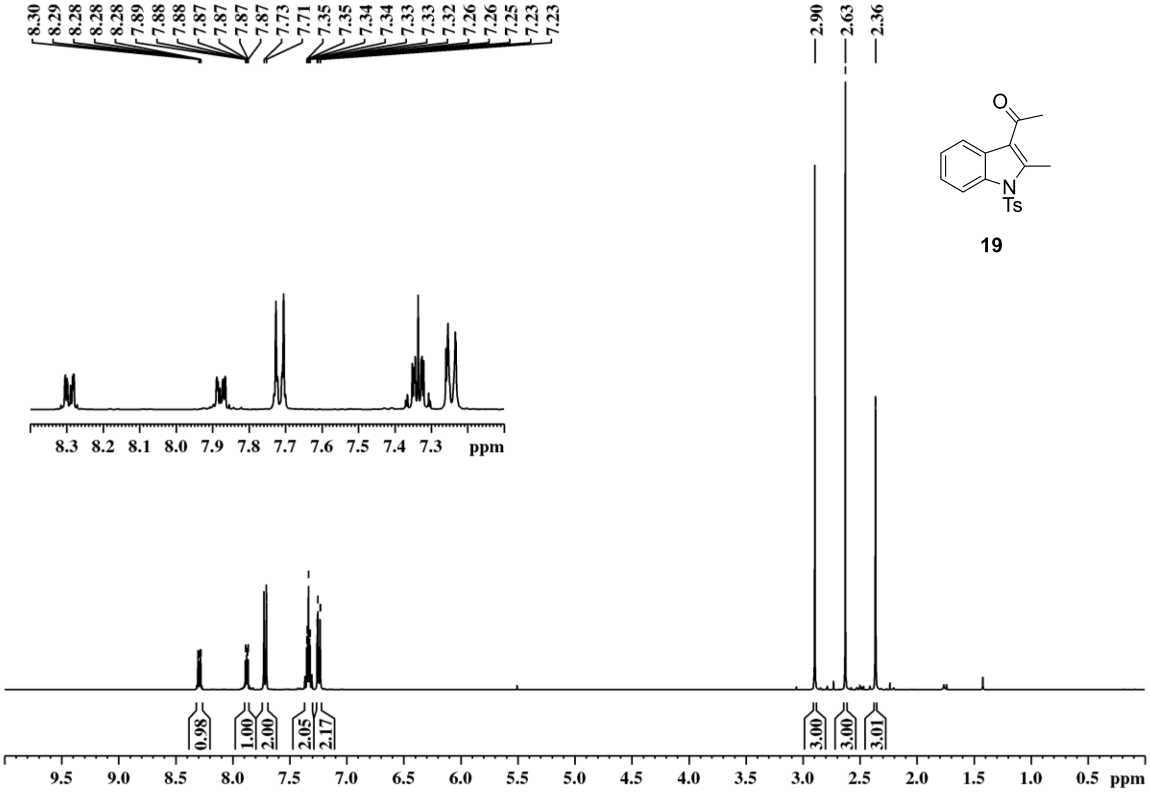
8.30
8.29
8.28
8.28
8.28
7.89
7.88
7.88
7.87
7.87
7.87
7.87
7.73
7.71
7.35
7.35
7.34
7.34
7.33
7.33
7.32
7.26
7.26
7.25
7.23
7.23
2.90
2.63
2.36
O
N
Ts
8.3 8.2 8.1 8.0 7.9 7.8 7.7 7.6 7.5 7.4 7.3 ppm
0.98
1.00
2.00
2.05
2.17
3.00
3.00
3.01
9.5 9.0 8.5 8.0 7.5 7.0 6.5 6.0 5.5 5.0 4.5 4.0 3.5 3.0 2.5 2.0 1.5 1.0 0.5 ppm

19

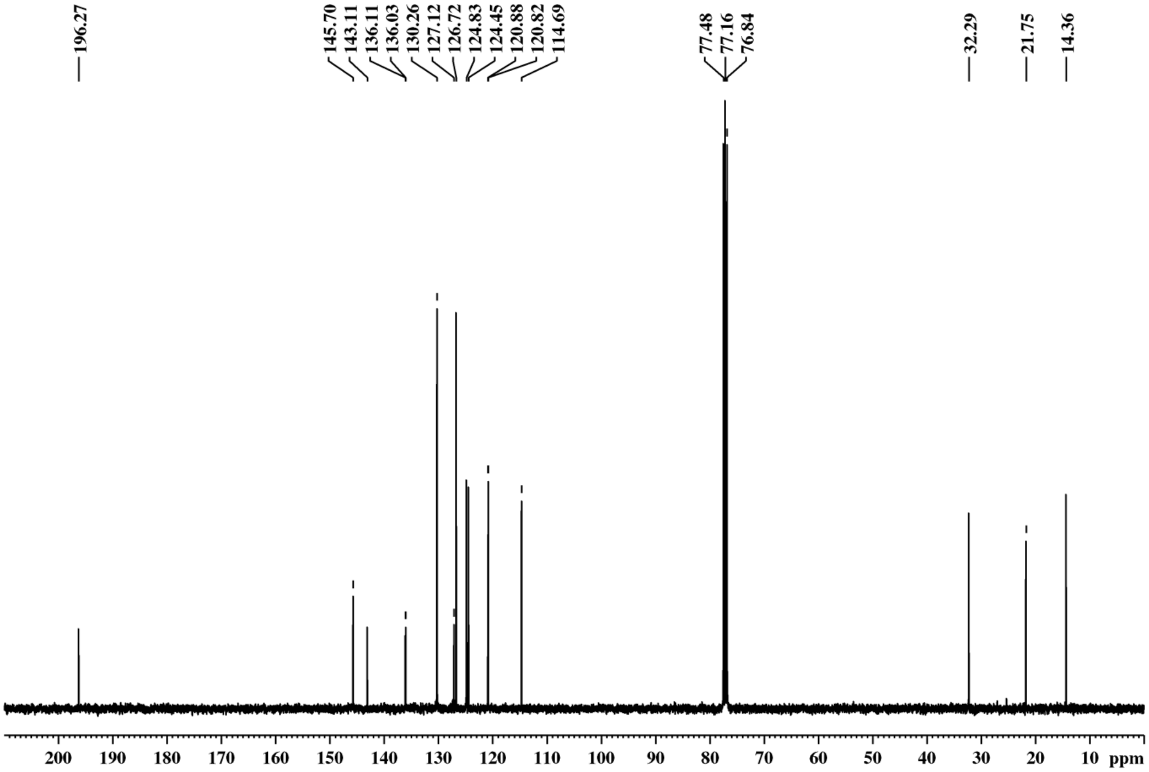
196.27
145.70
143.11
136.11
136.03
130.26
127.12
126.72
124.83
124.45
120.88
120.82
114.69
77.48
77.16
76.84
32.29
21.75
14.36
200 190 180 170 160 150 140 130 120 110 100 90 80 70 60 50 40 30 20 10 ppm

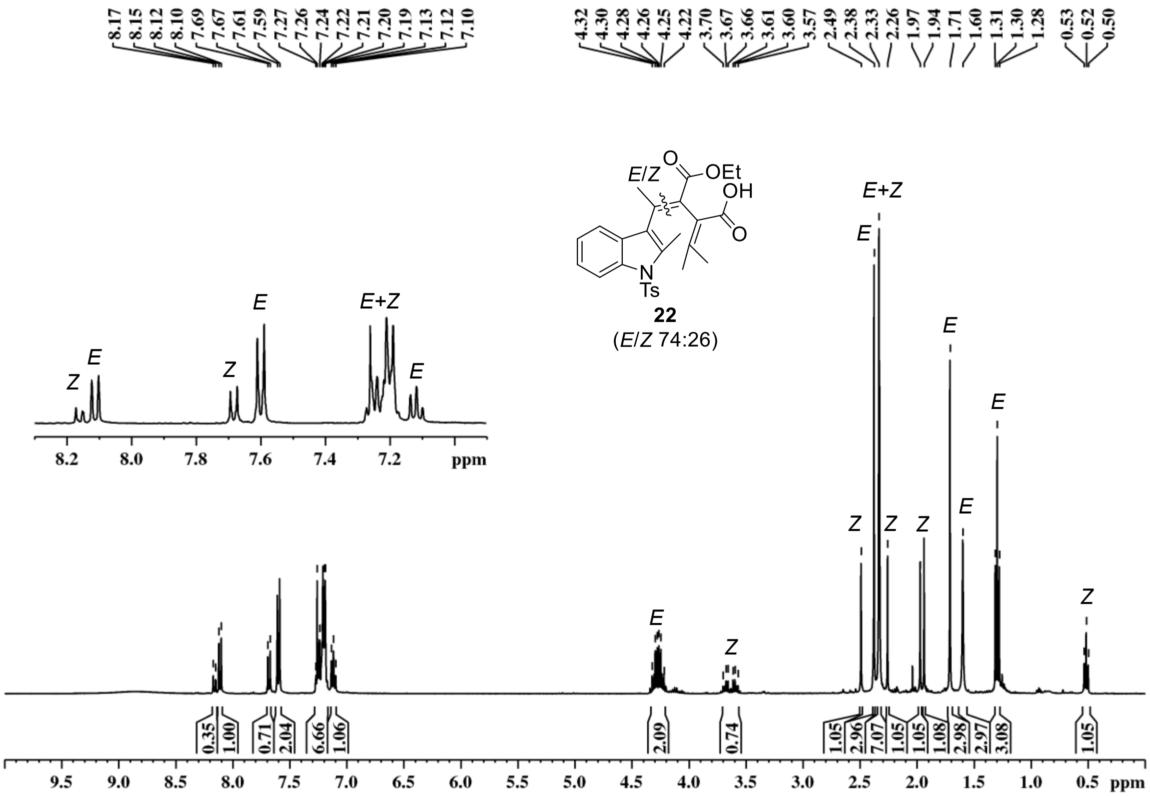
22
(*E*/*Z* 74:26)
8.17
8.15
8.12
8.10
7.69
7.67
7.61
7.59
7.27
7.26
7.24
7.22
7.21
7.20
7.19
7.13
7.12
7.10
4.32
4.30
4.28
4.26
4.25
4.22
3.70
3.67
3.66
3.61
3.60
3.57
2.49
2.38
2.33
2.26
1.97
1.94
1.71
1.60
1.31
1.30
1.28
0.53
0.52
0.50
E/Z
O
OEt
OH
O
N
Ts
E+Z
E
Z
E
Z
E
E+Z
E
8.2
8.0
7.8
7.6
7.4
7.2
ppm
E
Z
Z
Z
Z
E
E
E
Z
0.35
1.00
0.71
2.04
6.66
1.06
2.09
0.74
1.05
2.96
7.07
1.05
1.08
2.98
2.97
3.08
1.05
9.5
9.0
8.5
8.0
7.5
7.0
6.5
6.0
5.5
5.0
4.5
4.0
3.5
3.0
2.5
2.0
1.5
1.0
0.5
ppm

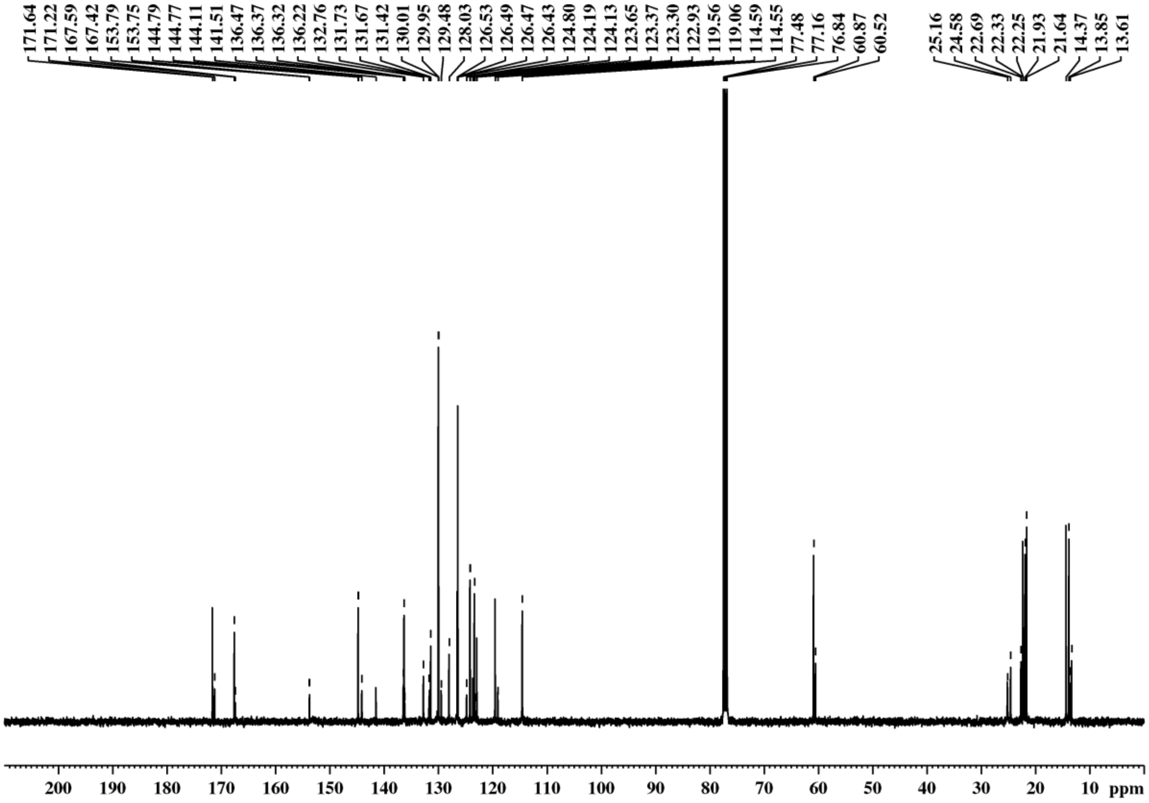
171.64
171.22
167.59
167.42
153.79
153.75
144.79
144.77
144.11
141.51
136.47
136.37
136.32
136.22
132.76
131.73
131.67
131.42
130.01
129.95
129.48
128.03
126.53
126.49
126.47
126.43
124.80
124.19
124.13
123.65
123.37
123.30
122.93
119.56
119.06
114.59
114.55
77.48
77.16
76.84
60.87
60.52
25.16
24.58
22.69
22.33
22.25
21.93
21.64
14.37
13.85
13.61
200
190
180
170
160
150
140
130
120
110
100
90
80
70
60
50
40
30
20
10
ppm

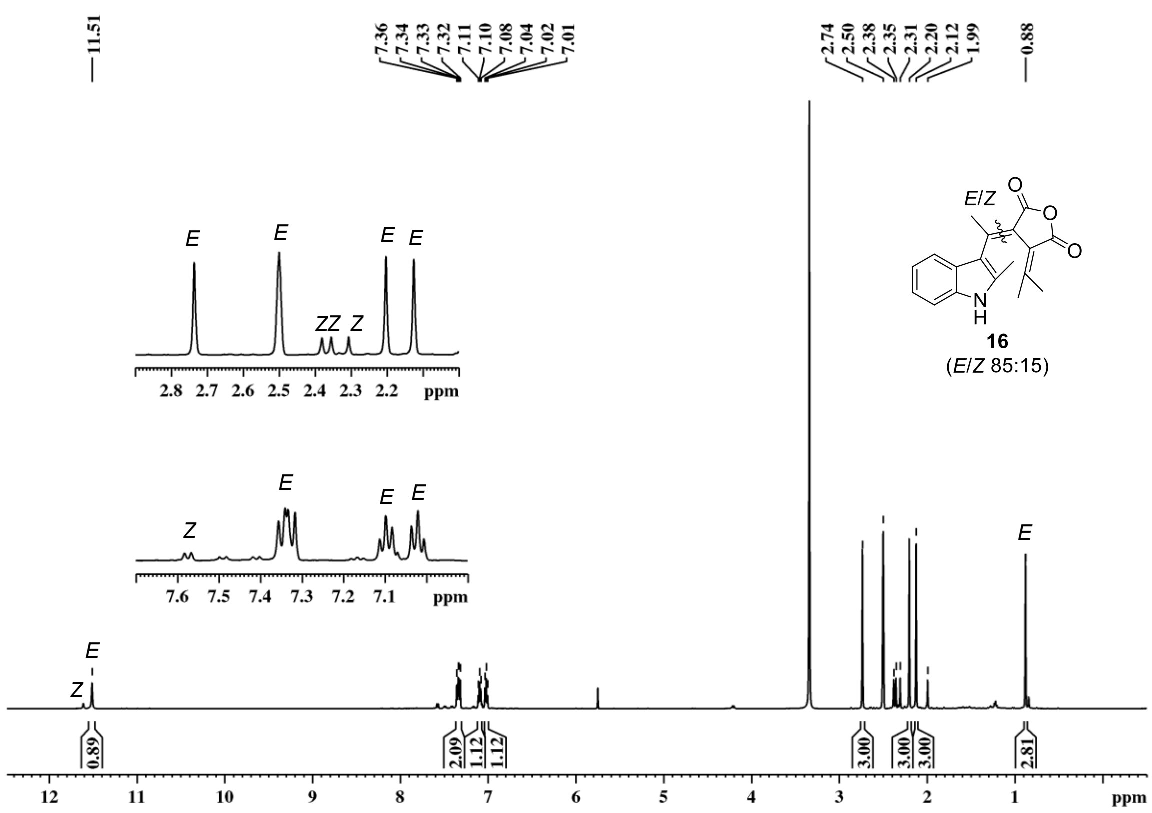
11.51
7.36
7.34
7.33
7.32
7.11
7.10
7.08
7.04
7.02
7.01
2.74
2.50
2.38
2.35
2.31
2.20
2.12
1.99
0.88
E/Z
O
O
O
N
H
E
E
ZZ Z
E E
2.8 2.7 2.6 2.5 2.4 2.3 2.2 ppm
Z
E
E E
7.6 7.5 7.4 7.3 7.2 7.1 ppm
E
Z
E
0.89
2.09
1.12
1.12
3.00
3.00
3.00
2.81
12 11 10 9 8 7 6 5 4 3 2 1 ppm

16
(E/Z 85:15)

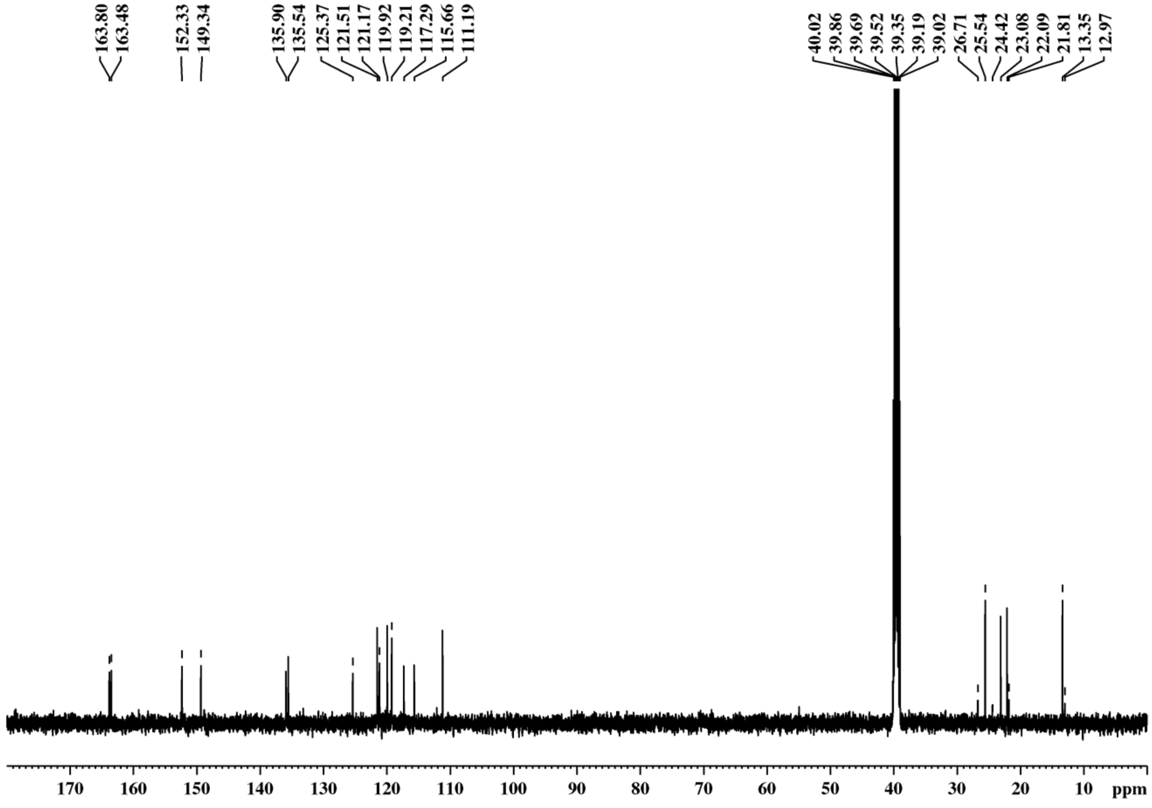
163.80
163.48
152.33
149.34
135.90
135.54
125.37
121.51
121.17
119.92
119.21
117.29
115.66
111.19
40.02
39.86
39.69
39.52
39.35
39.19
39.02
26.71
25.54
24.42
23.08
22.09
21.81
13.35
12.97
170 160 150 140 130 120 110 100 90 80 70 60 50 40 30 20 10 ppm

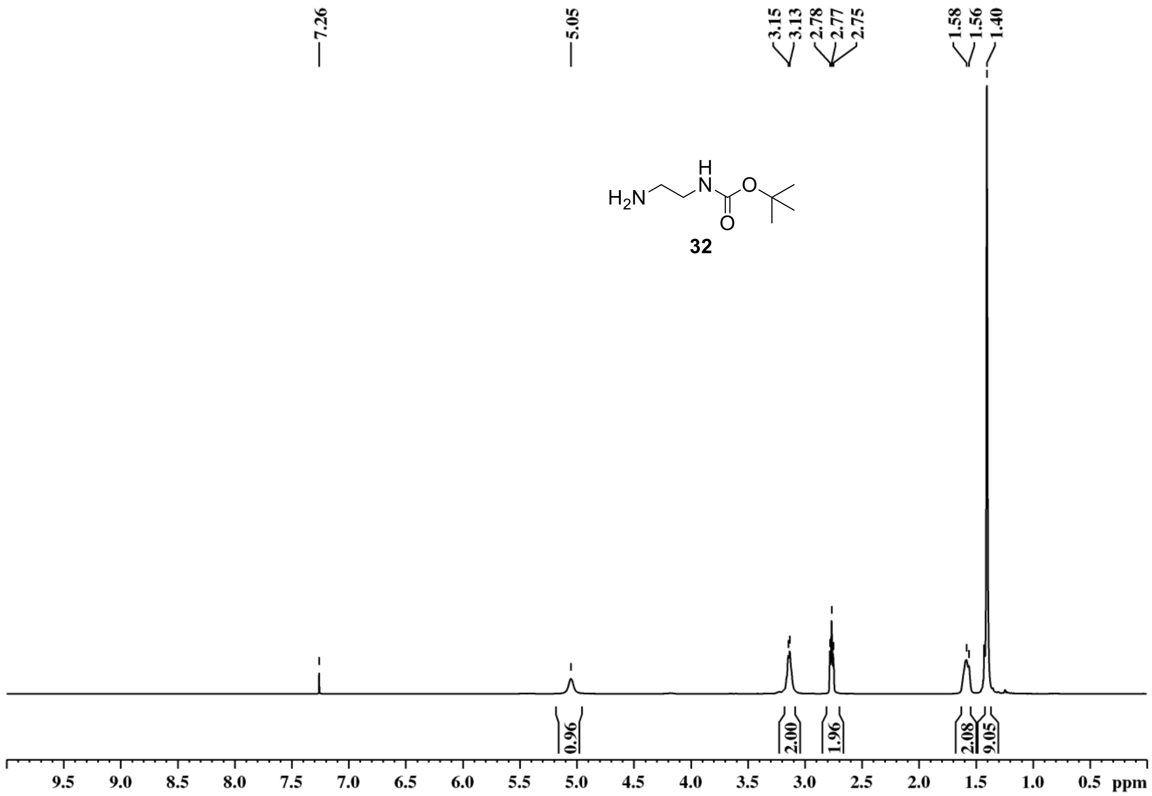
7.26
5.05
3.15
3.13
2.78
2.77
2.75
1.58
1.56
1.40
H
H₂N
N
O
O
0.96
2.00
1.96
2.08
9.05
9.5 9.0 8.5 8.0 7.5 7.0 6.5 6.0 5.5 5.0 4.5 4.0 3.5 3.0 2.5 2.0 1.5 1.0 0.5 ppm

32

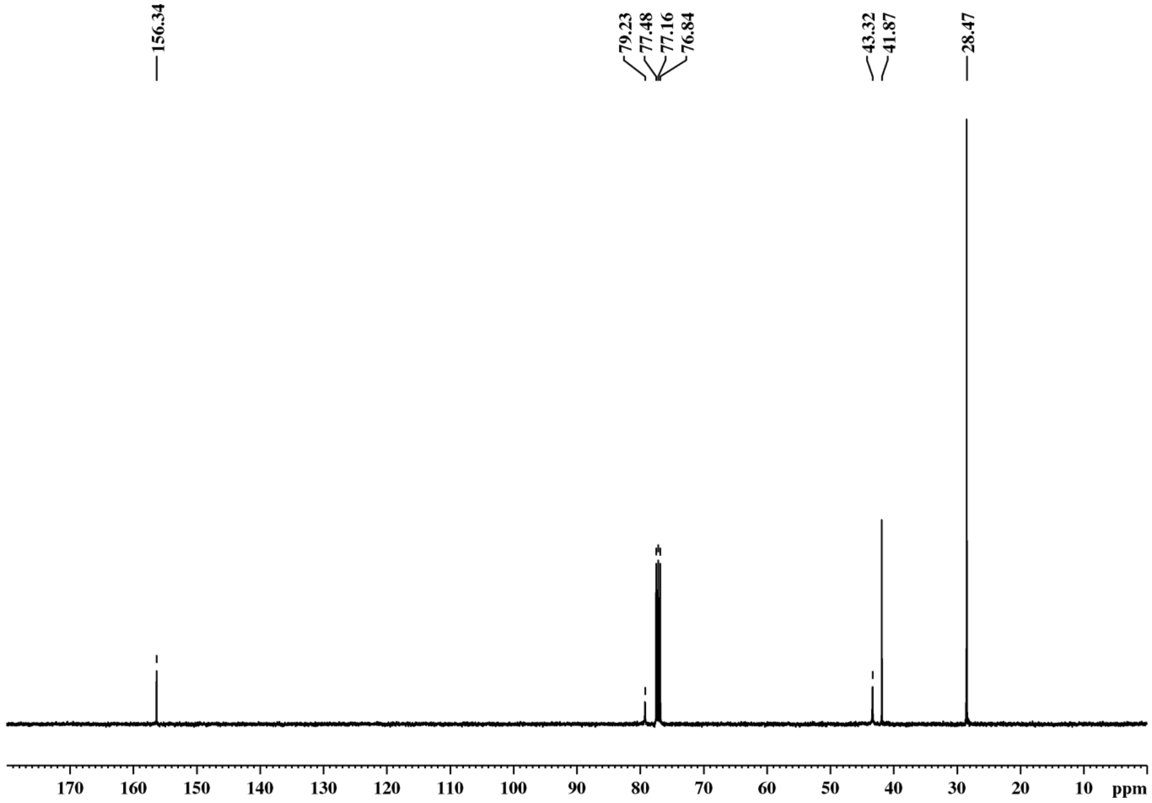
156.34
79.23
77.48
77.16
76.84
43.32
41.87
28.47
170 160 150 140 130 120 110 100 90 80 70 60 50 40 30 20 10 ppm

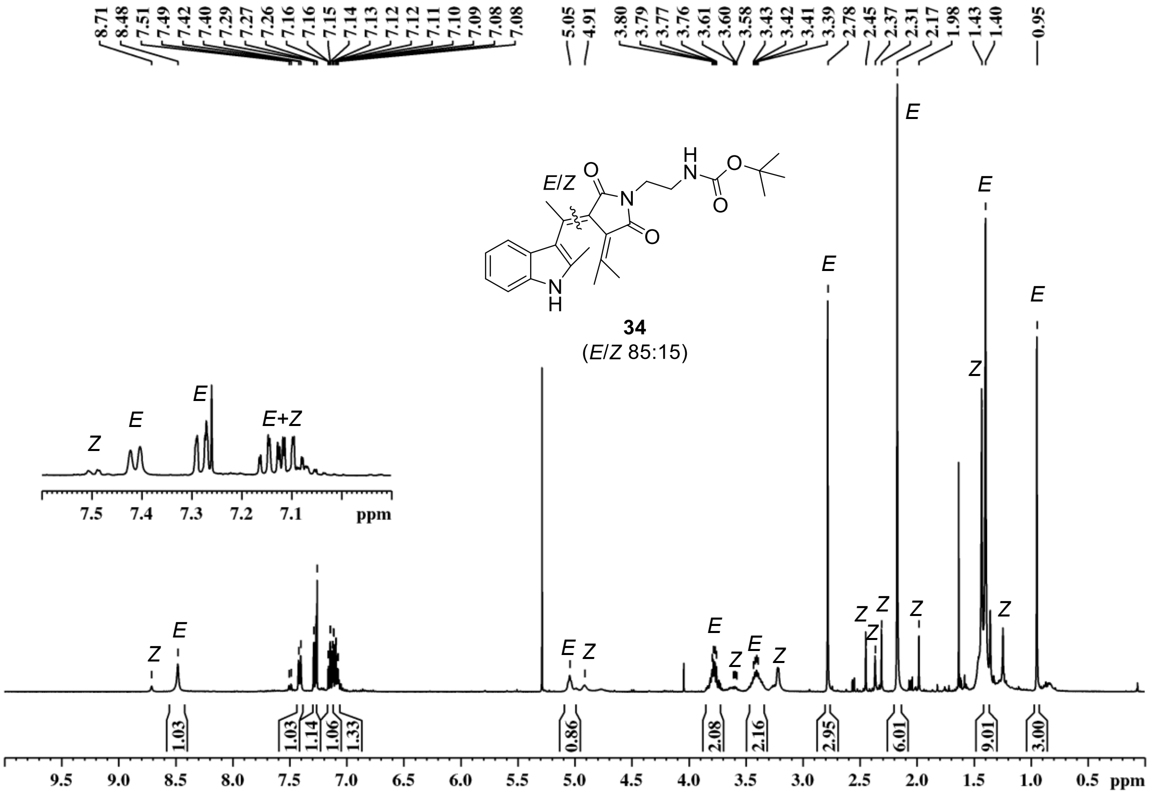
8.71
8.48
7.51
7.49
7.42
7.40
7.29
7.27
7.26
7.16
7.16
7.15
7.14
7.13
7.12
7.12
7.11
7.10
7.09
7.08
7.08
5.05
4.91
3.80
3.79
3.77
3.76
3.61
3.60
3.58
3.43
3.42
3.41
3.39
2.78
2.45
2.37
2.31
2.17
1.98
1.43
1.40
0.95
E/Z
O
N
H
N
O
O
O
N
H
E
E
E
E
Z
E
E+Z
Z
7.5
7.4
7.3
7.2
7.1
ppm
Z
E
E
Z
E
Z
E
Z
Z
Z
Z
Z
Z
1.03
1.03
1.14
1.06
1.33
0.86
2.08
2.16
2.95
6.01
9.01
3.00
9.5
9.0
8.5
8.0
7.5
7.0
6.5
6.0
5.5
5.0
4.5
4.0
3.5
3.0
2.5
2.0
1.5
1.0
0.5
ppm

34
(*E*/*Z* 85:15)

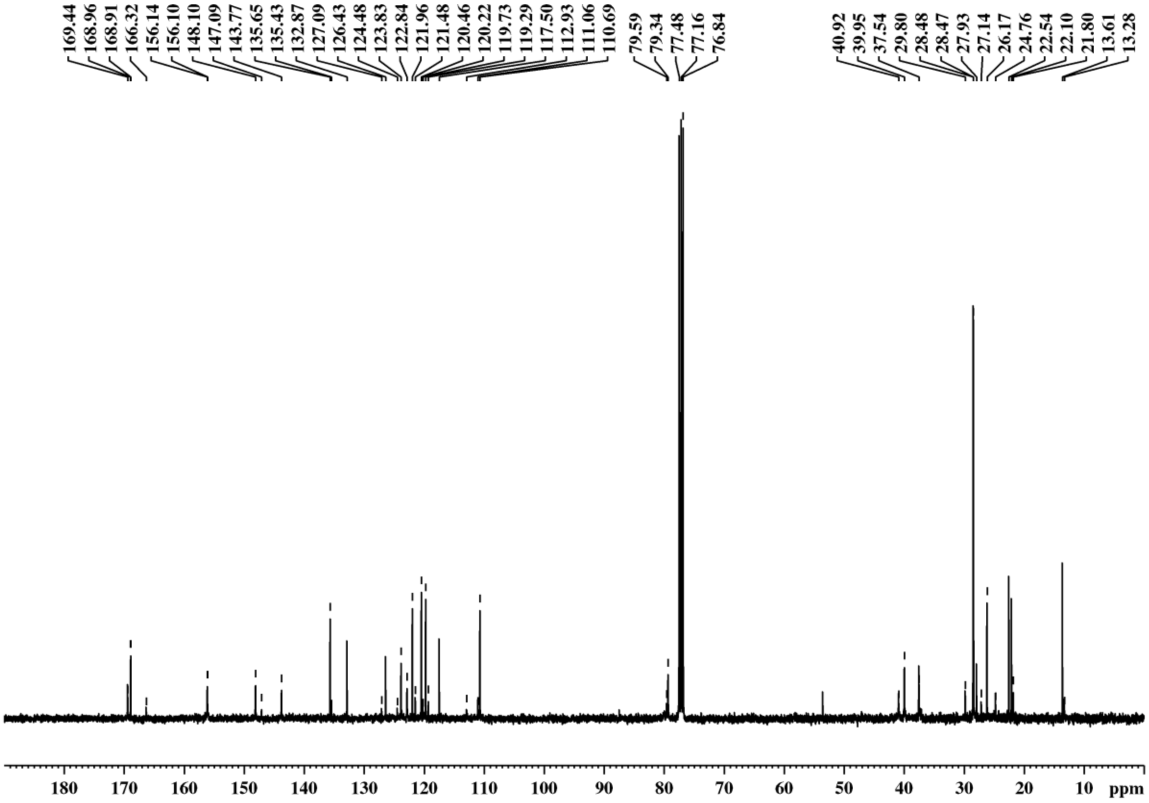
169.44
168.96
168.91
166.32
156.14
156.10
148.10
147.09
143.77
135.65
135.43
132.87
127.09
126.43
124.48
123.83
122.84
121.96
121.48
120.46
120.22
119.73
119.29
117.50
112.93
111.06
110.69
79.59
79.34
77.48
77.16
76.84
40.92
39.95
37.54
29.80
28.48
28.47
27.93
27.14
26.17
24.76
22.54
22.10
21.80
13.61
13.28
180
170
160
150
140
130
120
110
100
90
80
70
60
50
40
30
20
10
ppm

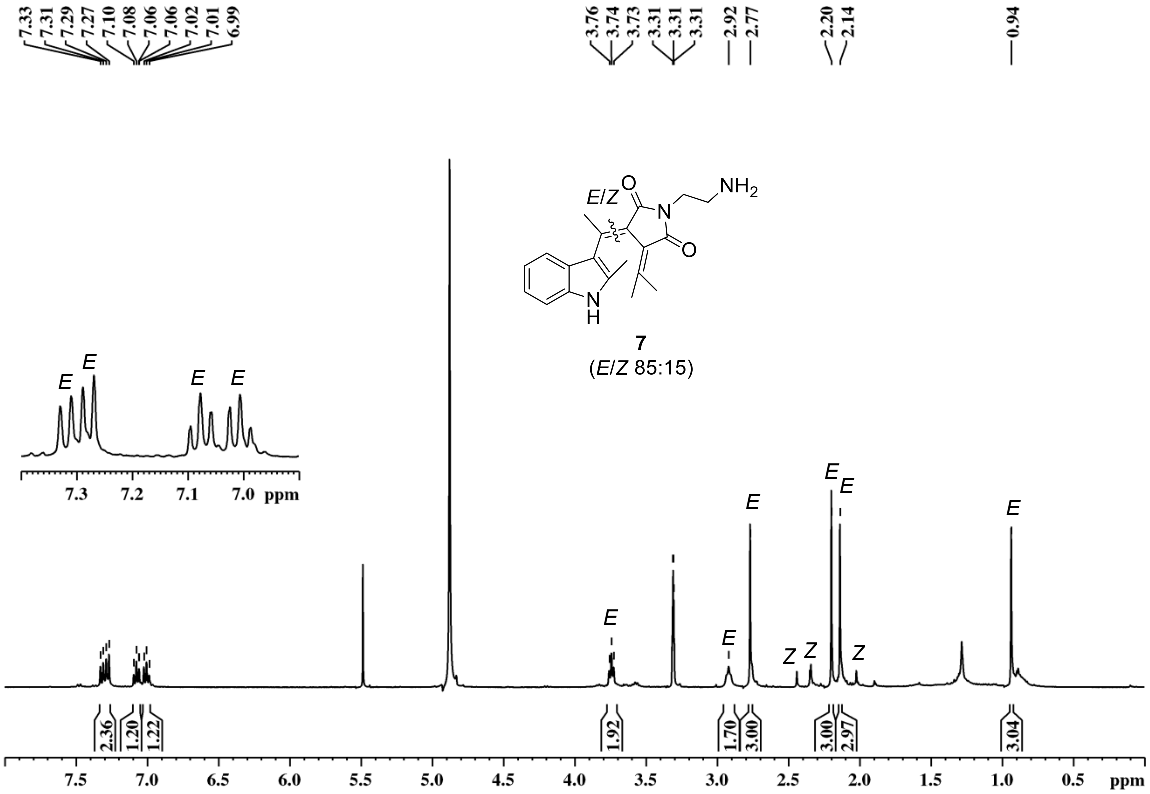
7.33
7.31
7.29
7.27
7.10
7.08
7.06
7.06
7.02
7.01
6.99
3.76
3.74
3.73
3.31
3.31
3.31
2.92
2.77
2.20
2.14
0.94
E/Z
O
N
NH2
O
N
H
E
E
E
E
7.3
7.2
7.1
7.0 ppm
E
E
E
E
E
Z
Z
Z
E
2.36
1.20
1.22
1.92
1.70
3.00
3.00
2.97
3.04
7.5
7.0
6.5
6.0
5.5
5.0
4.5
4.0
3.5
3.0
2.5
2.0
1.5
1.0
0.5
ppm

7
(*E*/*Z* 85:15)

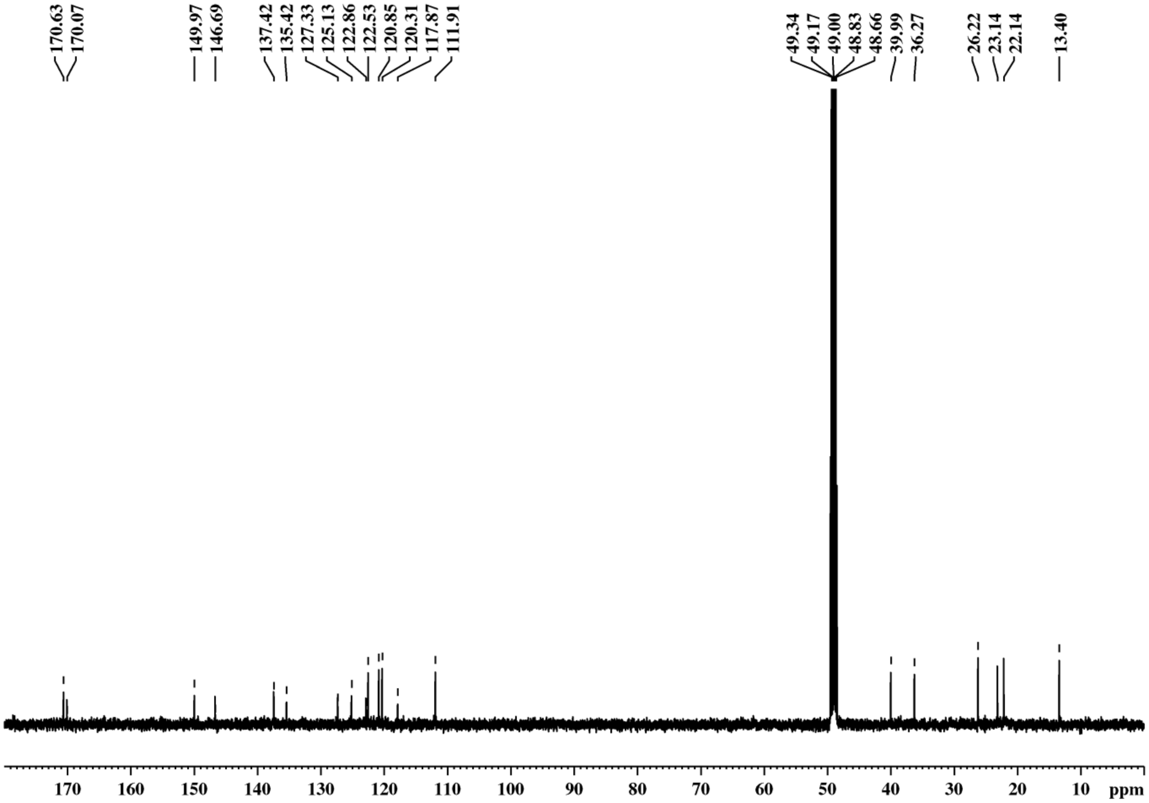
170.63
170.07
149.97
146.69
137.42
135.42
127.33
125.13
122.86
122.53
120.85
120.31
117.87
111.91
49.34
49.17
49.00
48.83
48.66
39.99
36.27
26.22
23.14
22.14
13.40
170
160
150
140
130
120
110
100
90
80
70
60
50
40
30
20
10
ppm

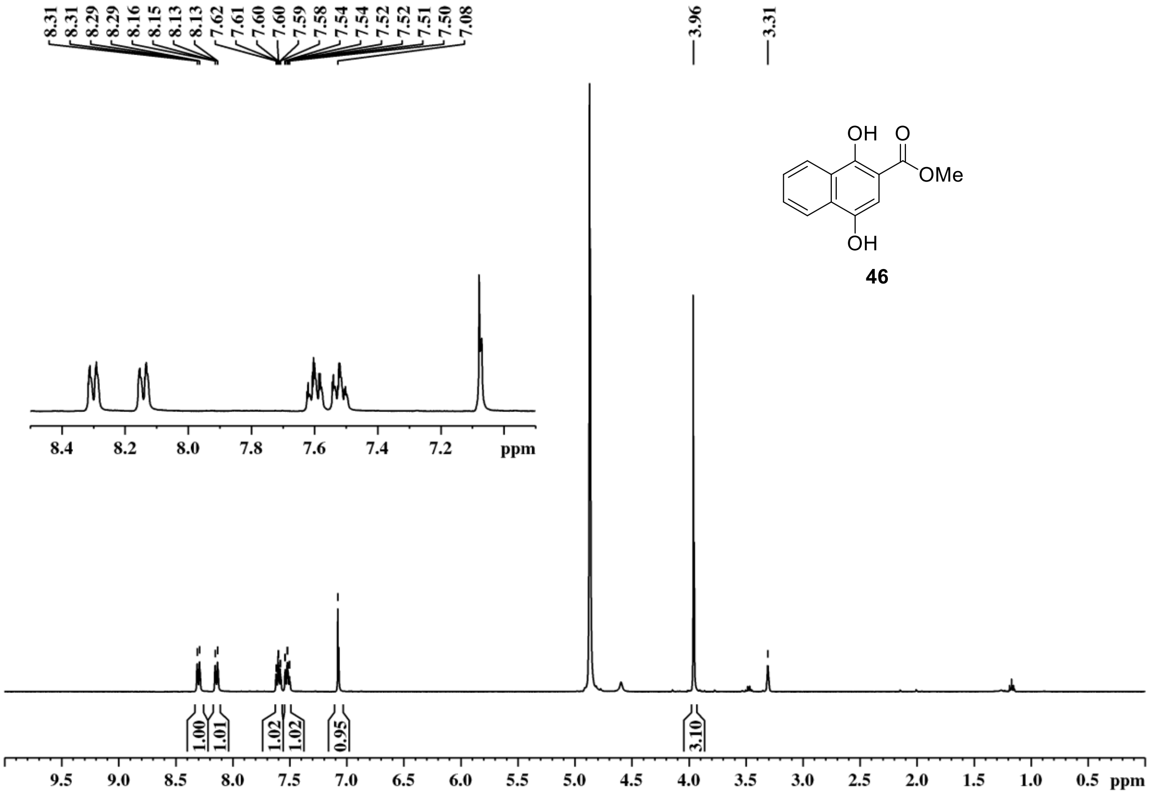
8.31
8.31
8.29
8.29
8.16
8.15
8.13
8.13
7.62
7.61
7.60
7.60
7.59
7.58
7.54
7.54
7.52
7.52
7.51
7.50
7.08
3.96
3.31
OH
O
OMe
OH
8.4
8.2
8.0
7.8
7.6
7.4
7.2
ppm
1.00
1.01
1.02
1.02
0.95
3.10
9.5
9.0
8.5
8.0
7.5
7.0
6.5
6.0
5.5
5.0
4.5
4.0
3.5
3.0
2.5
2.0
1.5
1.0
0.5
ppm

46

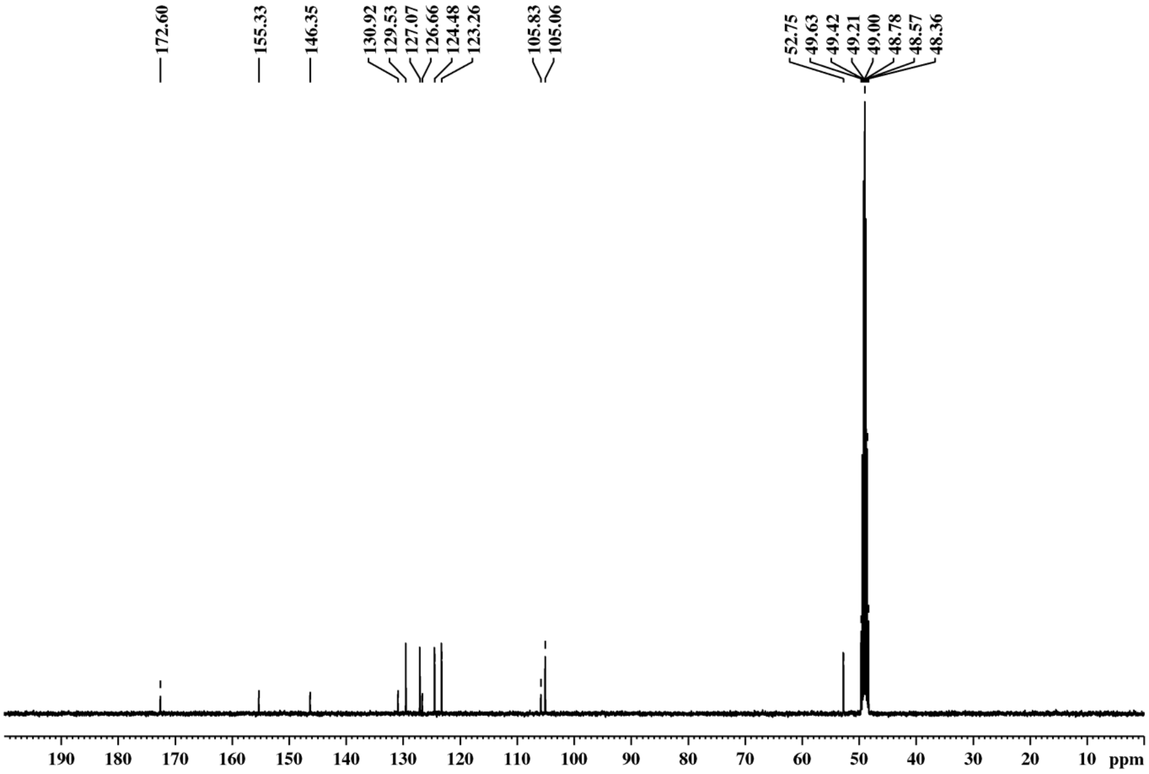
172.60
155.33
146.35
130.92
129.53
127.07
126.66
124.48
123.26
105.83
105.06
52.75
49.63
49.42
49.21
49.00
48.78
48.57
48.36
190
180
170
160
150
140
130
120
110
100
90
80
70
60
50
40
30
20
10
ppm

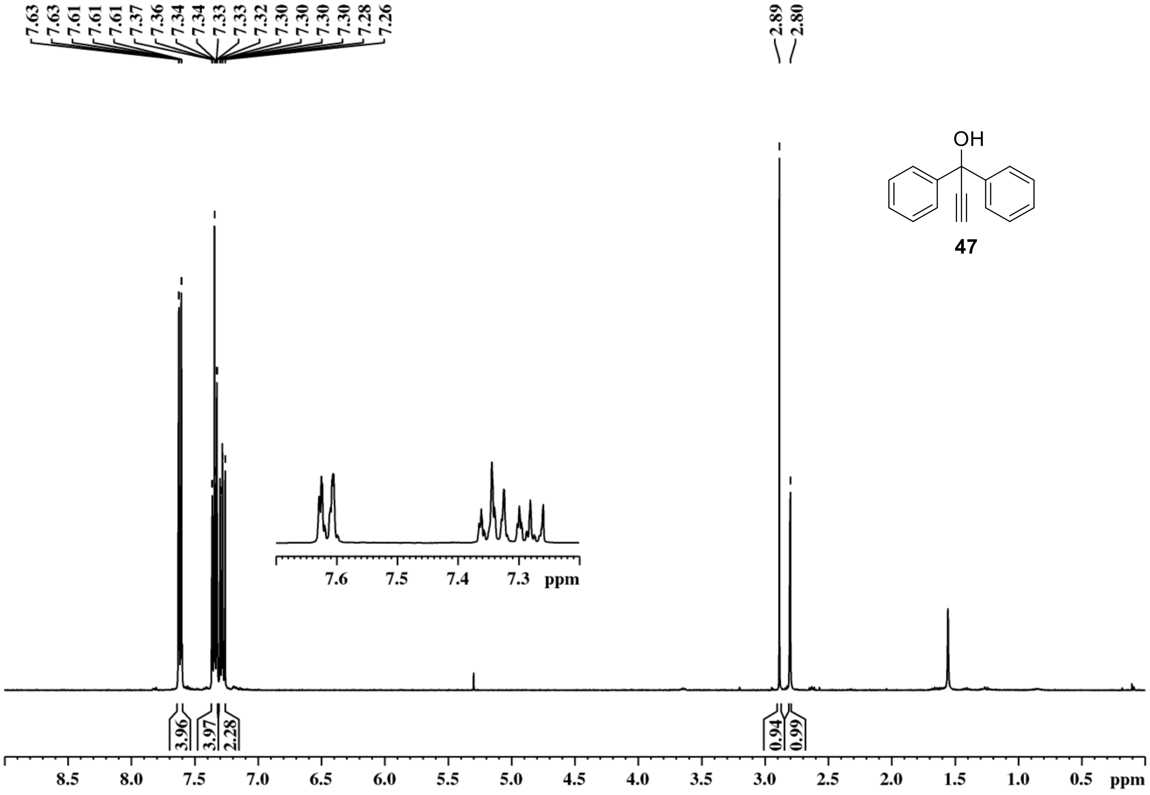
7.63
7.63
7.61
7.61
7.61
7.37
7.36
7.34
7.34
7.33
7.33
7.32
7.30
7.30
7.30
7.30
7.28
7.26
2.89
2.80
OH
7.6
7.5
7.4
7.3
ppm
3.96
3.97
2.28
0.94
0.99
8.5
8.0
7.5
7.0
6.5
6.0
5.5
5.0
4.5
4.0
3.5
3.0
2.5
2.0
1.5
1.0
0.5
ppm

47

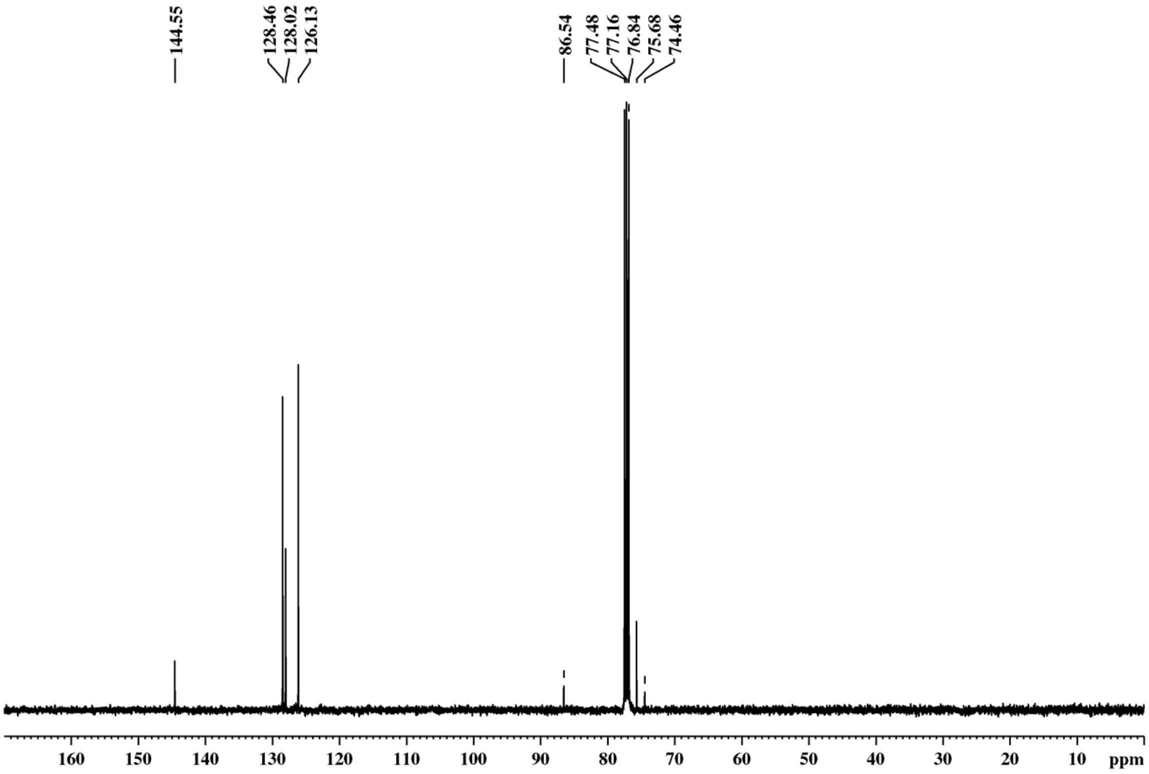
144.55
128.46
128.02
126.13
86.54
77.48
77.16
76.84
75.68
74.46
160
150
140
130
120
110
100
90
80
70
60
50
40
30
20
10
ppm

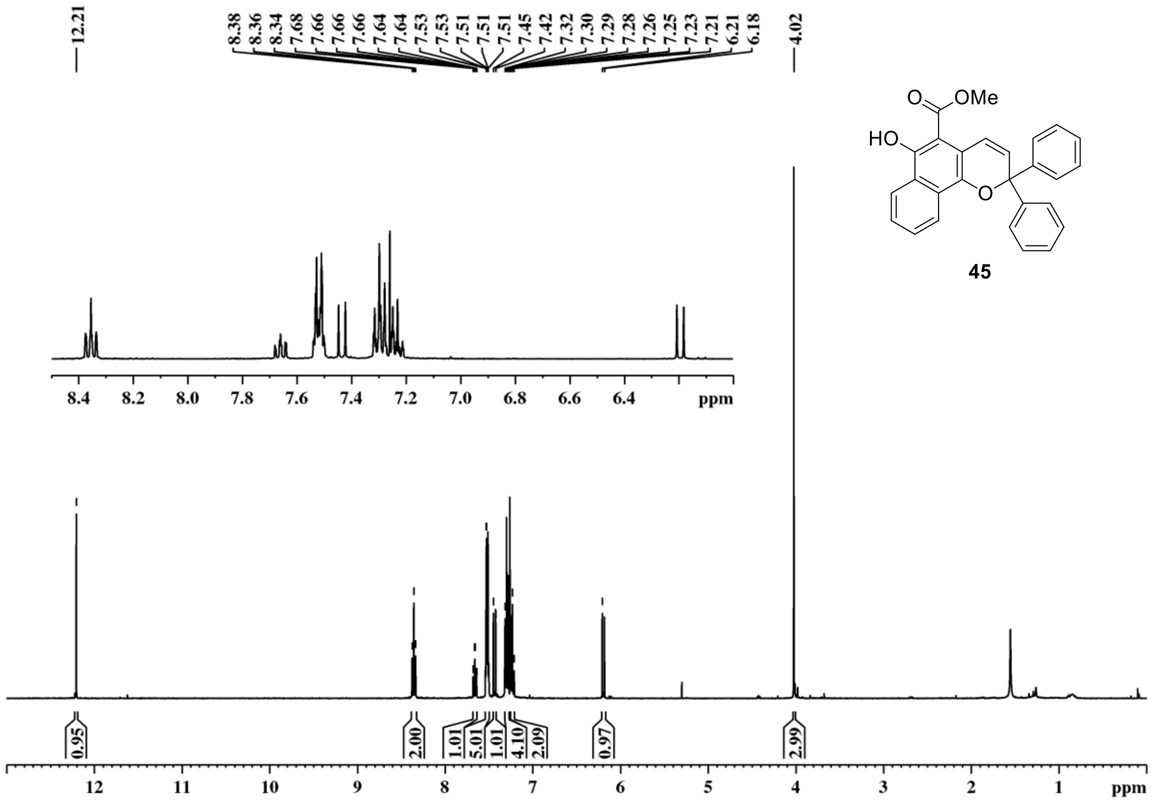
12.21
8.38
8.36
8.34
7.68
7.66
7.66
7.66
7.64
7.64
7.53
7.53
7.51
7.51
7.51
7.45
7.42
7.32
7.30
7.29
7.28
7.26
7.25
7.23
7.21
6.21
6.18
4.02
O
OMe
HO
O
45
8.4
8.2
8.0
7.8
7.6
7.4
7.2
7.0
6.8
6.6
6.4
ppm
0.95
2.00
1.01
5.01
1.01
4.10
2.09
0.97
2.99
12
11
10
9
8
7
6
5
4
3
2
1
ppm

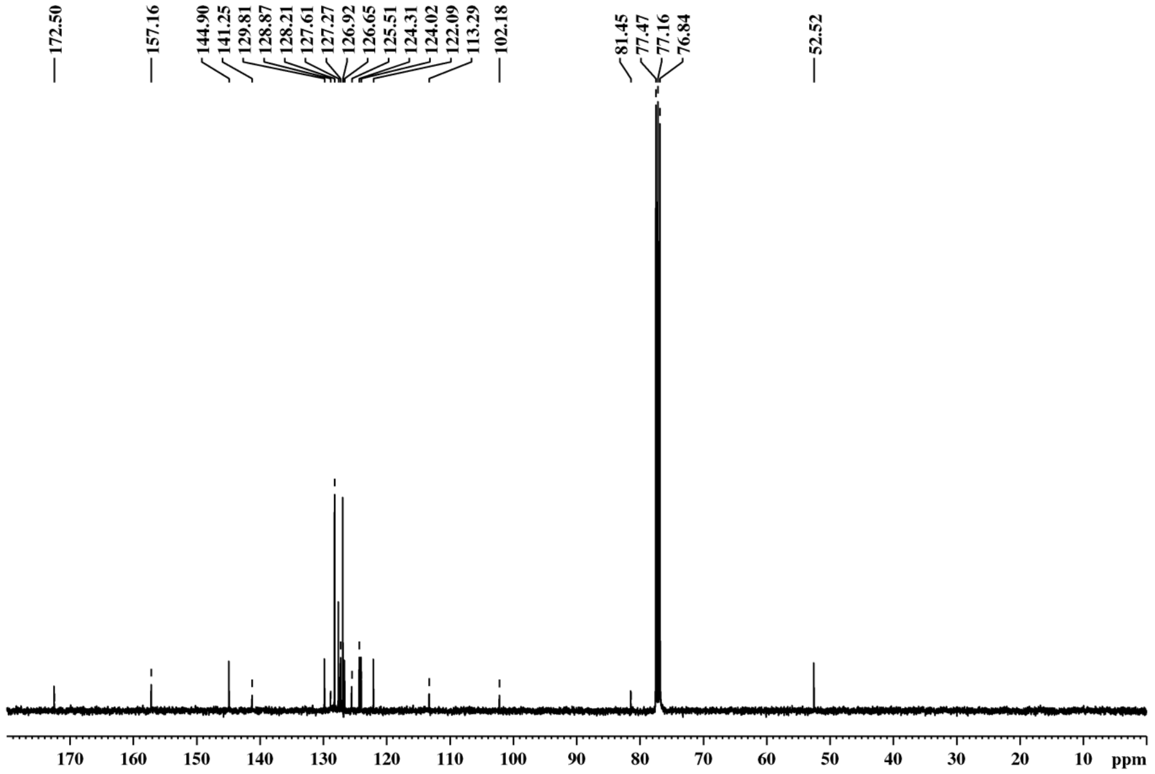
172.50
157.16
144.90
141.25
129.81
128.87
128.21
127.61
127.27
126.92
126.65
125.51
124.31
124.02
122.09
113.29
102.18
81.45
77.47
77.16
76.84
52.52
170
160
150
140
130
120
110
100
90
80
70
60
50
40
30
20
10
ppm

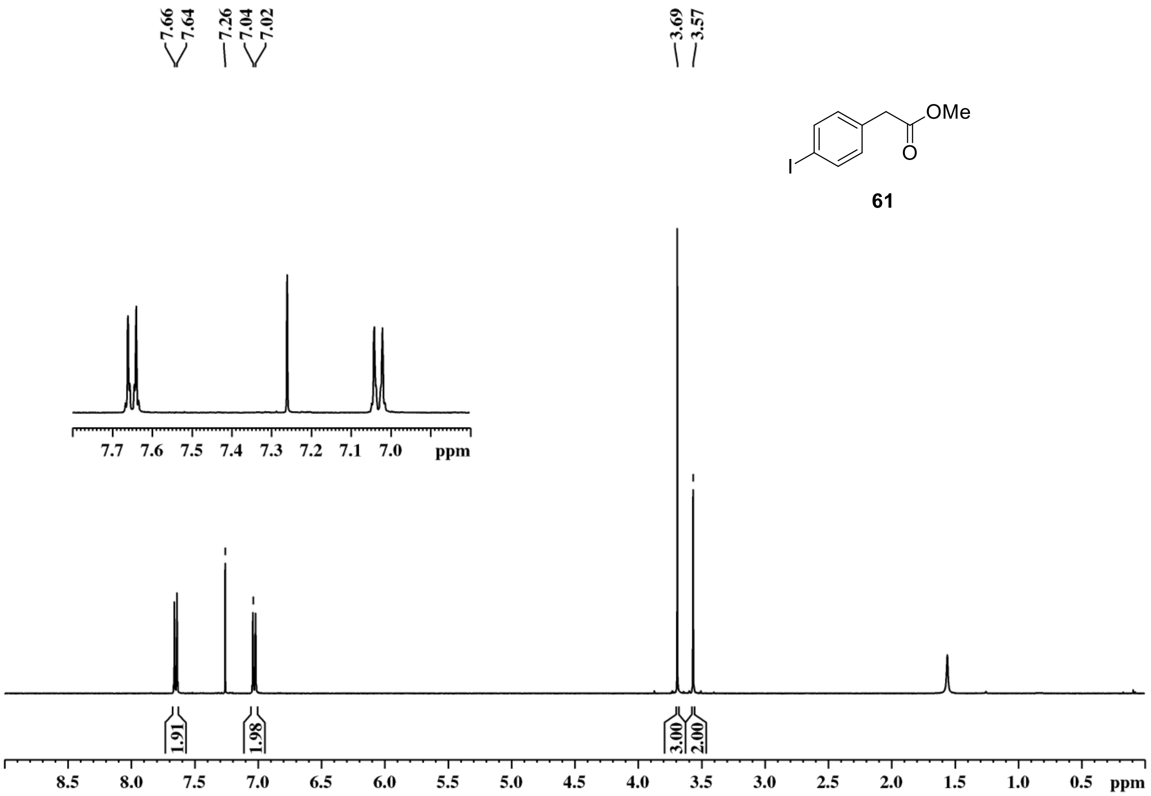
7.66
7.64
7.26
7.04
7.02
3.69
3.57
OMe
O
I
61
7.7 7.6 7.5 7.4 7.3 7.2 7.1 7.0 ppm
1.91
1.98
3.00
2.00
8.5 8.0 7.5 7.0 6.5 6.0 5.5 5.0 4.5 4.0 3.5 3.0 2.5 2.0 1.5 1.0 0.5 ppm

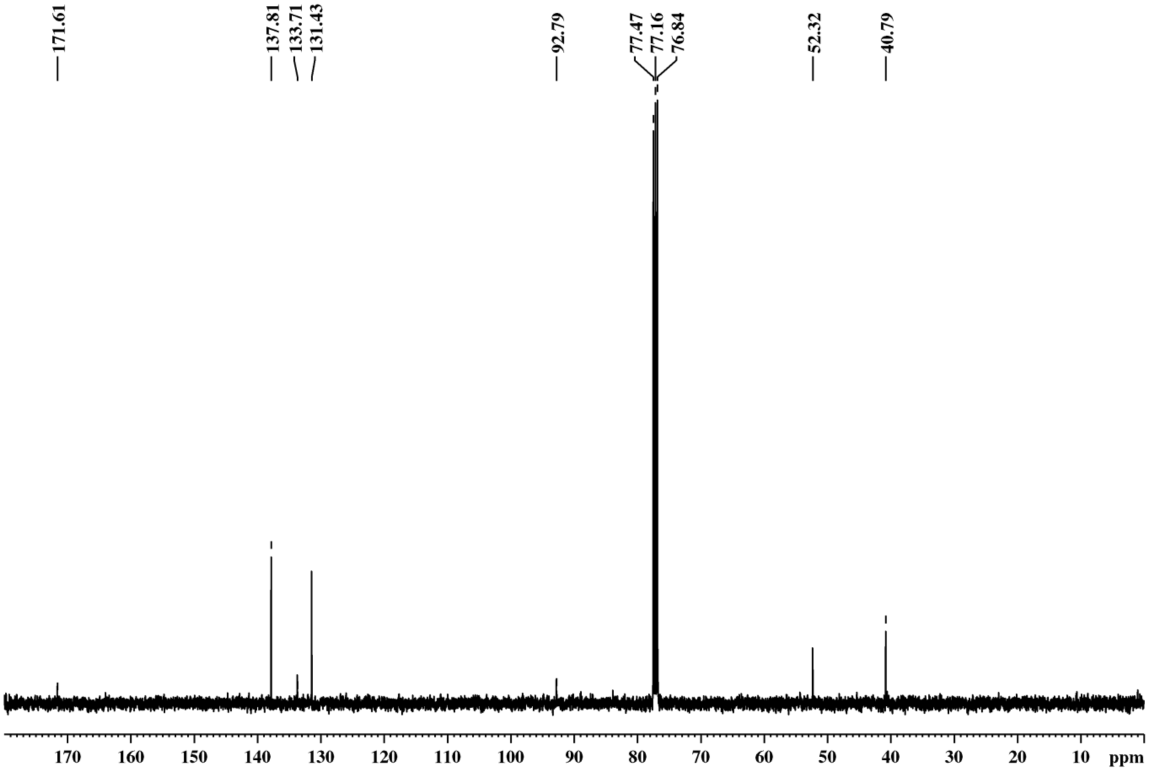
171.61
137.81
133.71
131.43
92.79
77.47
77.16
76.84
52.32
40.79
170 160 150 140 130 120 110 100 90 80 70 60 50 40 30 20 10 ppm

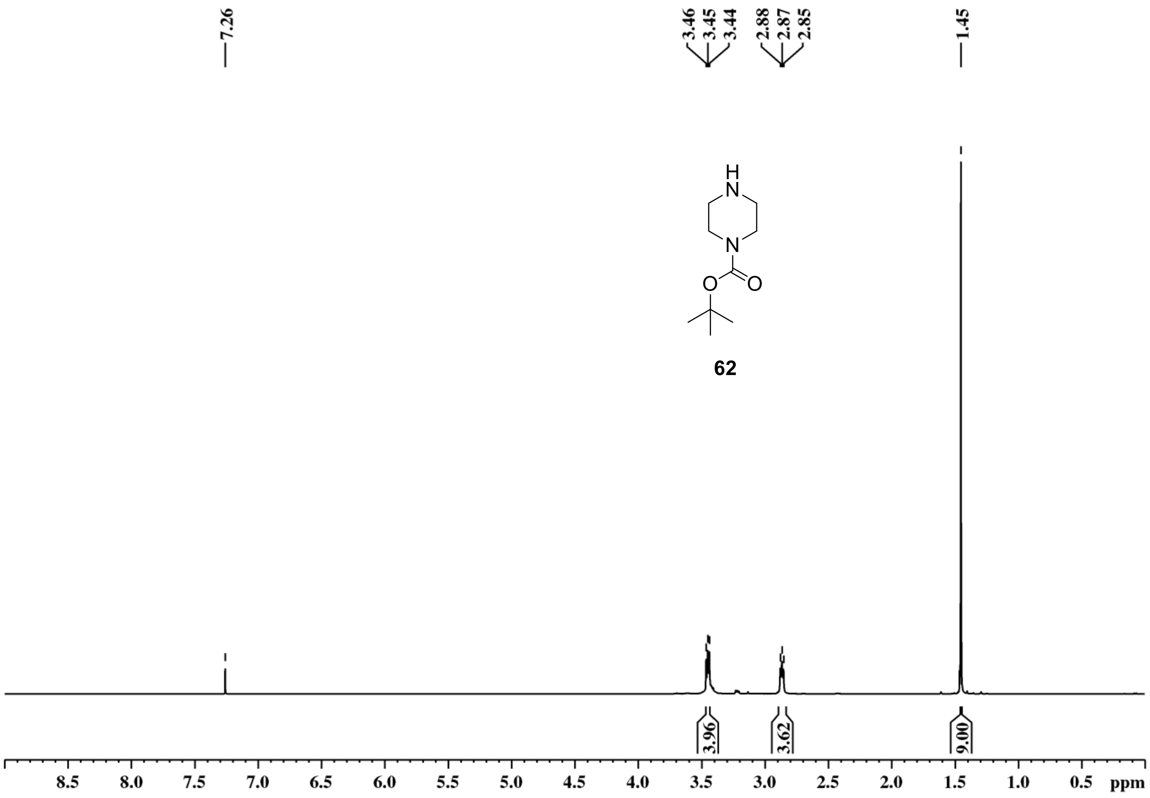

62

7.26
3.46
3.45
3.44
2.88
2.87
2.85
1.45
3.96
3.62
9.00
8.5
8.0
7.5
7.0
6.5
6.0
5.5
5.0
4.5
4.0
3.5
3.0
2.5
2.0
1.5
1.0
0.5
ppm

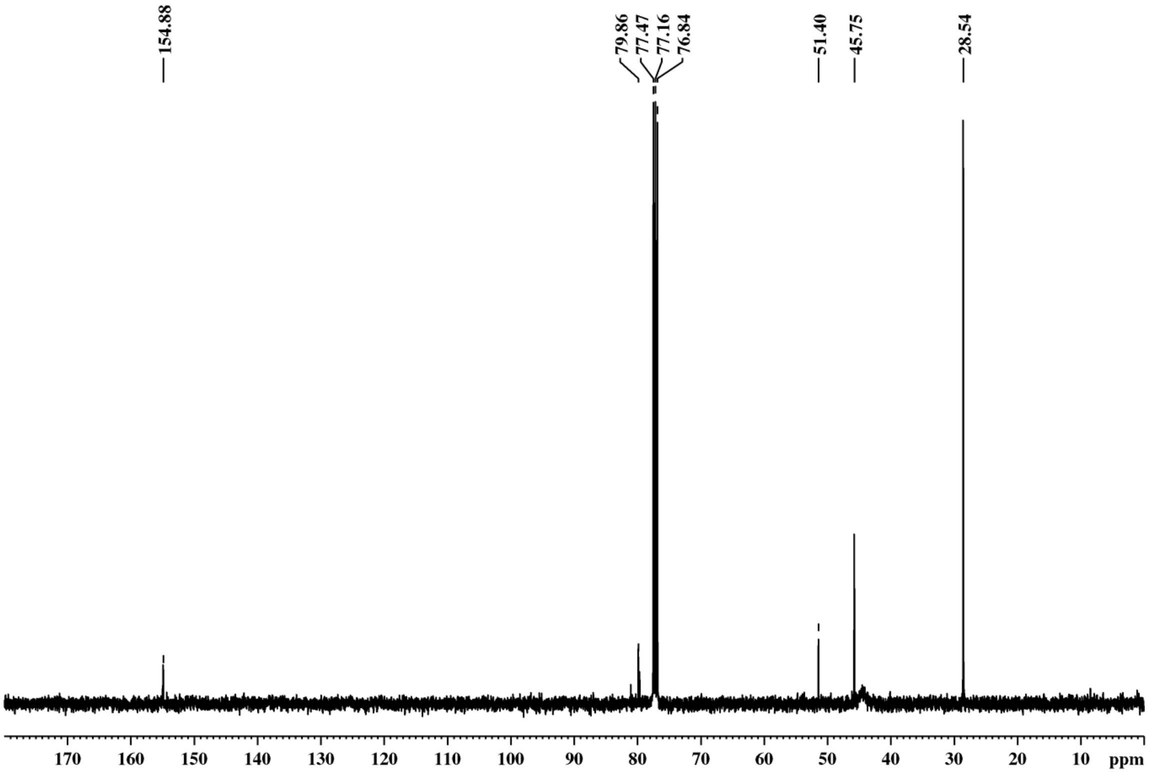

154.88
79.86
77.47
77.16
76.84
51.40
45.75
28.54
170
160
150
140
130
120
110
100
90
80
70
60
50
40
30
20
10
ppm

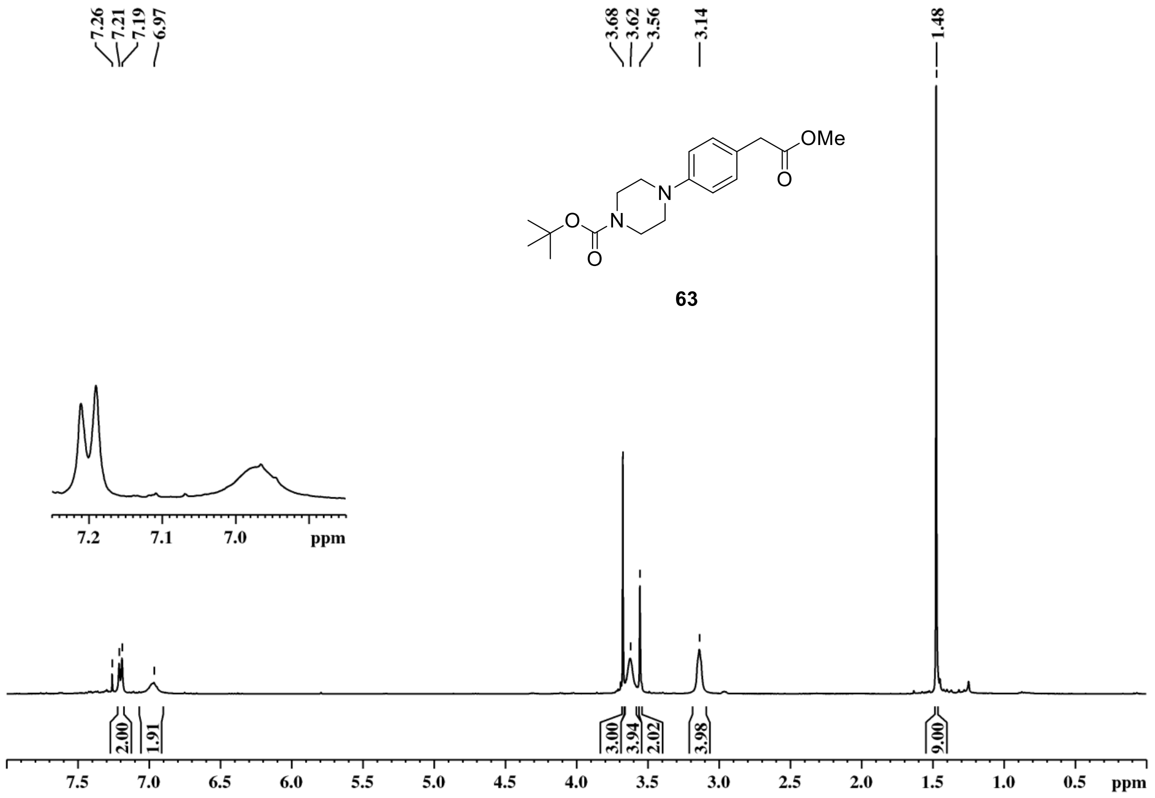
7.26
7.21
7.19
6.97
3.68
3.62
3.56
3.14
1.48
OMe
N
N
O
O
O
63
7.2
7.1
7.0
ppm
2.00
1.91
3.00
3.94
2.02
3.98
9.00
7.5
7.0
6.5
6.0
5.5
5.0
4.5
4.0
3.5
3.0
2.5
2.0
1.5
1.0
0.5
ppm

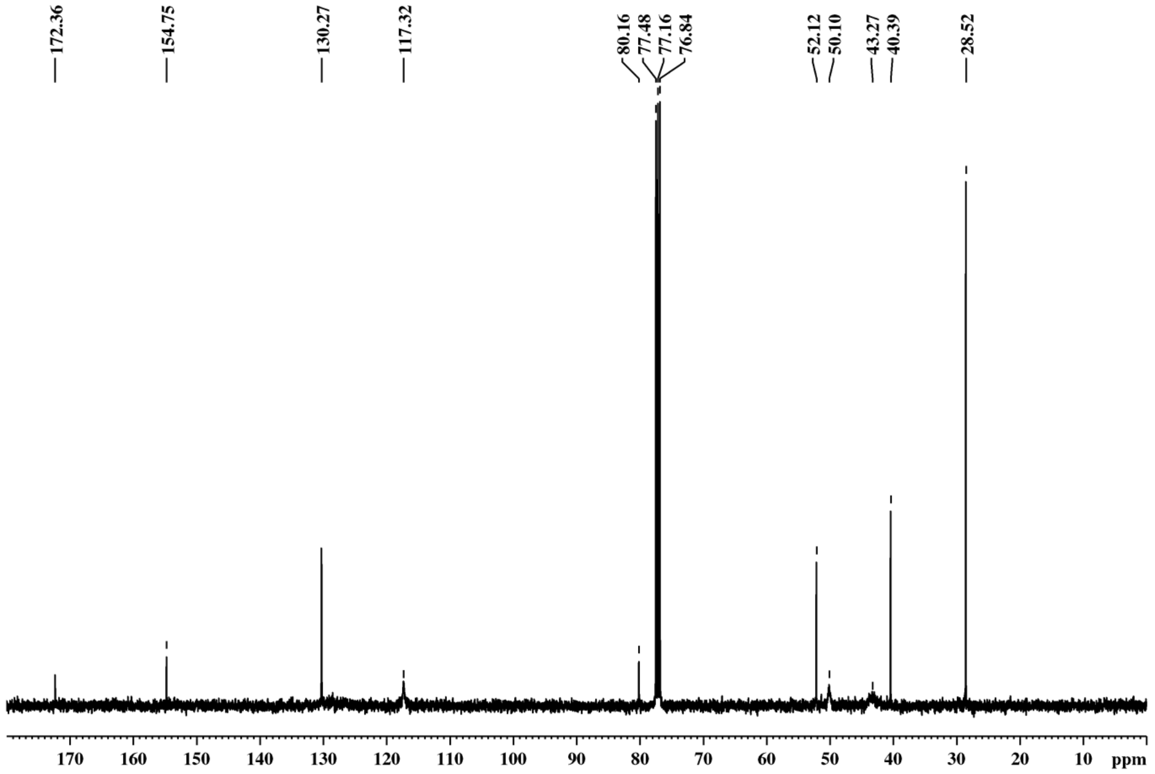
172.36
154.75
130.27
117.32
80.16
77.48
77.16
76.84
52.12
50.10
43.27
40.39
28.52
170
160
150
140
130
120
110
100
90
80
70
60
50
40
30
20
10
ppm

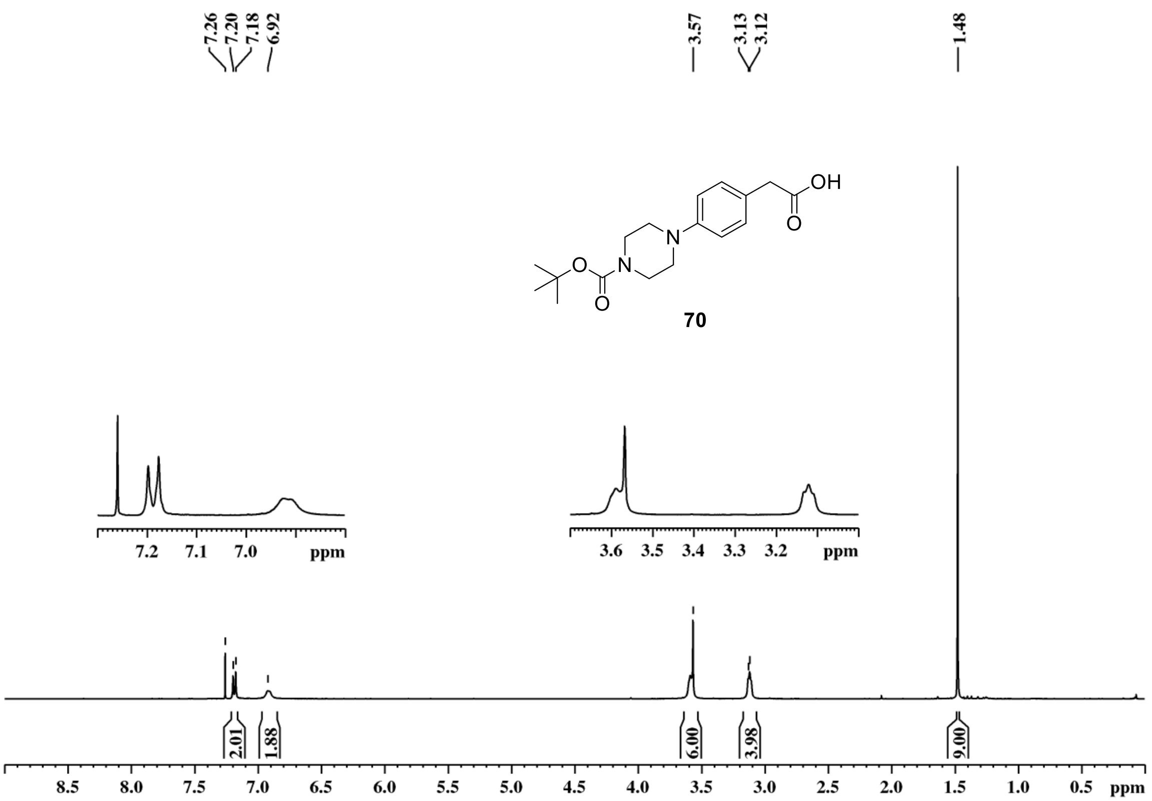
7.26
7.20
7.18
6.92
3.57
3.13
3.12
1.48
OH
O
N
N
O
O
70
7.2 7.1 7.0 ppm
3.6 3.5 3.4 3.3 3.2 ppm
2.01
1.88
6.00
3.98
9.00
8.5 8.0 7.5 7.0 6.5 6.0 5.5 5.0 4.5 4.0 3.5 3.0 2.5 2.0 1.5 1.0 0.5 ppm

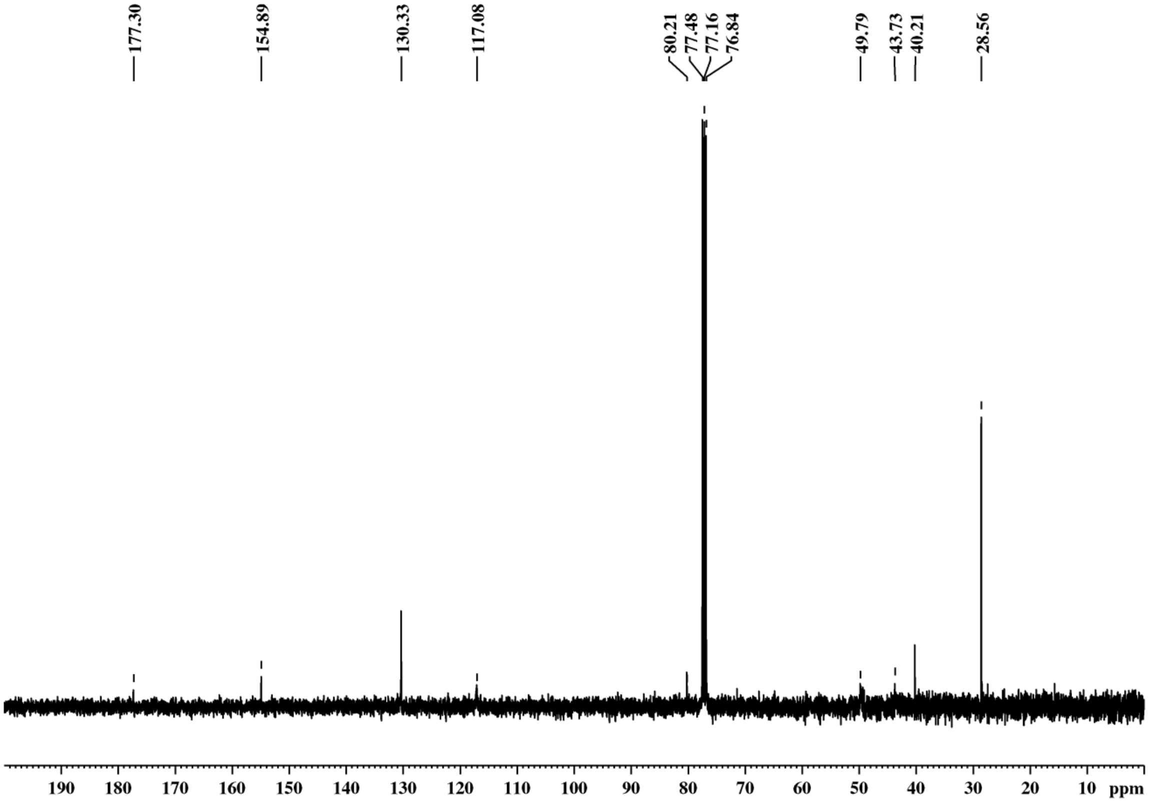
177.30
154.89
130.33
117.08
80.21
77.48
77.16
76.84
49.79
43.73
40.21
28.56
190 180 170 160 150 140 130 120 110 100 90 80 70 60 50 40 30 20 10 ppm

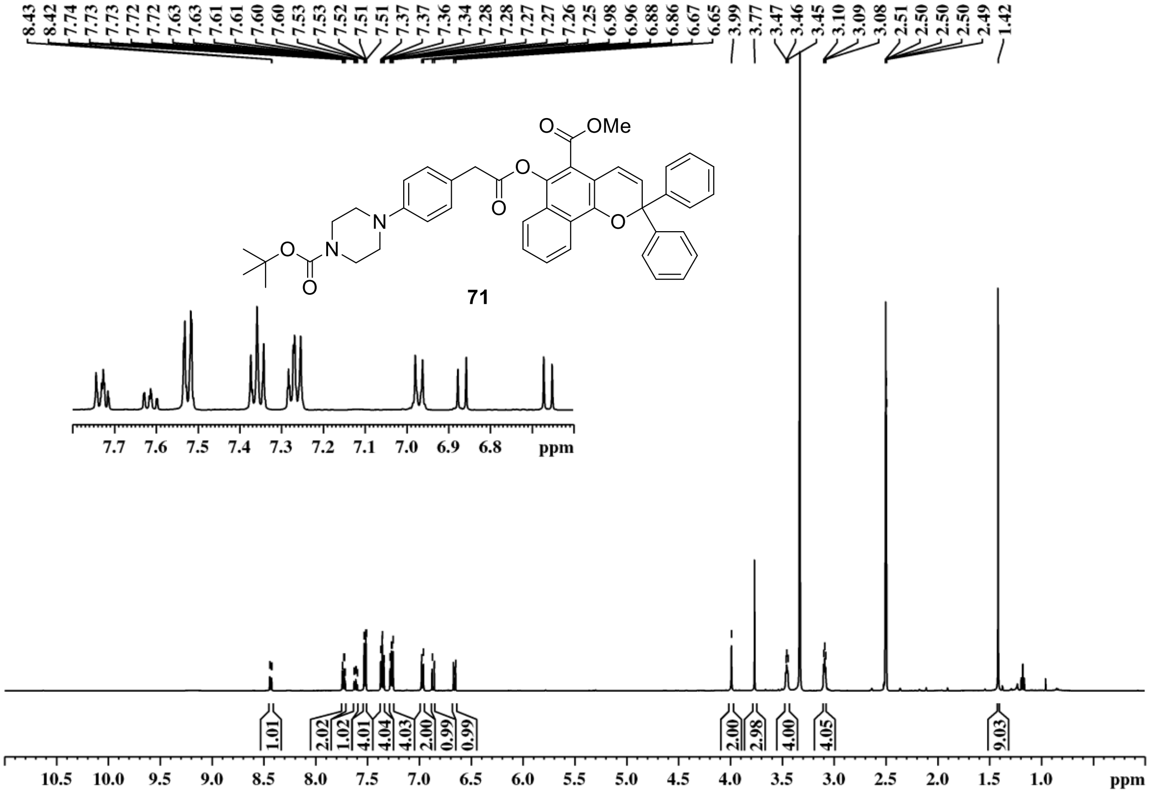
8.43
8.42
7.74
7.73
7.73
7.72
7.72
7.72
7.63
7.63
7.61
7.61
7.60
7.60
7.53
7.53
7.52
7.51
7.51
7.37
7.37
7.36
7.34
7.28
7.28
7.27
7.27
7.26
7.25
6.98
6.96
6.88
6.86
6.67
6.65
3.99
3.77
3.47
3.46
3.45
3.10
3.09
3.08
2.51
2.50
2.50
2.50
2.49
1.42
OMe
O
N
1.01
2.02
1.02
4.01
4.04
4.03
2.00
0.99
0.99
2.00
2.98
4.00
4.05
9.03
7.7 7.6 7.5 7.4 7.3 7.2 7.1 7.0 6.9 6.8 ppm
10.5 10.0 9.5 9.0 8.5 8.0 7.5 7.0 6.5 6.0 5.5 5.0 4.5 4.0 3.5 3.0 2.5 2.0 1.5 1.0 ppm

71

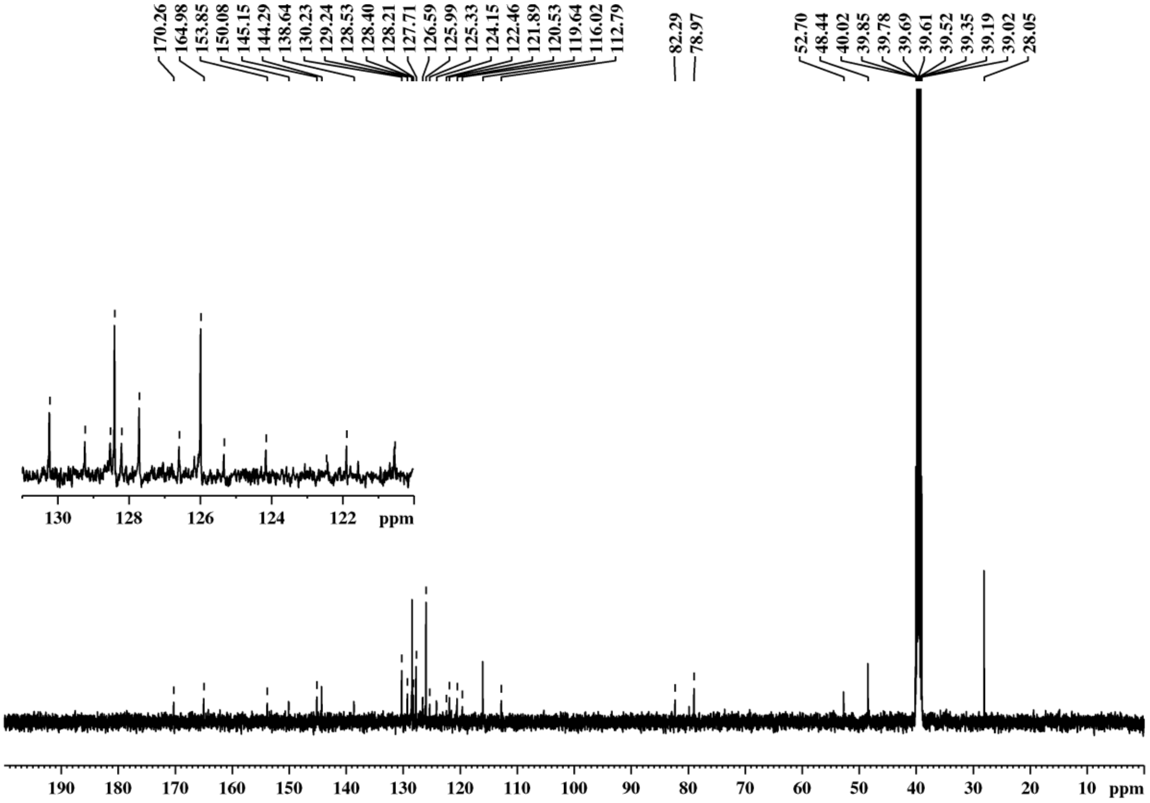
170.26
164.98
153.85
150.08
145.15
144.29
138.64
130.23
129.24
128.53
128.40
128.21
127.71
126.59
125.99
125.33
124.15
122.46
121.89
120.53
119.64
116.02
112.79
82.29
78.97
52.70
48.44
40.02
39.85
39.78
39.69
39.61
39.52
39.35
39.19
39.02
28.05
130 128 126 124 122 ppm
190 180 170 160 150 140 130 120 110 100 90 80 70 60 50 40 30 20 10 ppm

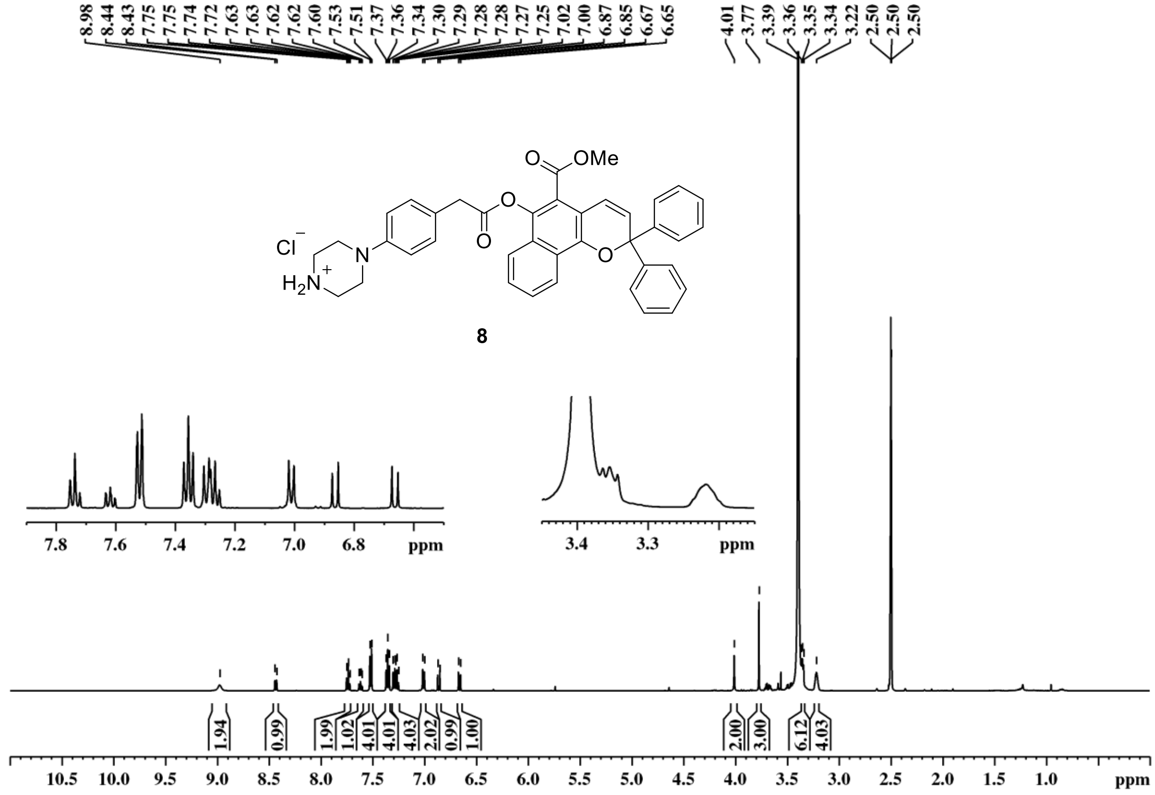
8.98
8.44
8.43
7.75
7.75
7.74
7.72
7.63
7.63
7.62
7.62
7.60
7.53
7.51
7.37
7.36
7.34
7.30
7.29
7.28
7.28
7.27
7.25
7.02
7.00
6.87
6.85
6.67
6.65
4.01
3.77
3.39
3.36
3.35
3.34
3.22
2.50
2.50
2.50
OMe
O
O
O
O
N
Cl^-
H_2N^+
8
7.8
7.6
7.4
7.2
7.0
6.8
ppm
3.4
3.3
ppm
1.94
0.99
1.99
1.02
4.01
4.01
4.03
2.02
0.99
1.00
2.00
3.00
6.12
4.03
10.5
10.0
9.5
9.0
8.5
8.0
7.5
7.0
6.5
6.0
5.5
5.0
4.5
4.0
3.5
3.0
2.5
2.0
1.5
1.0
ppm

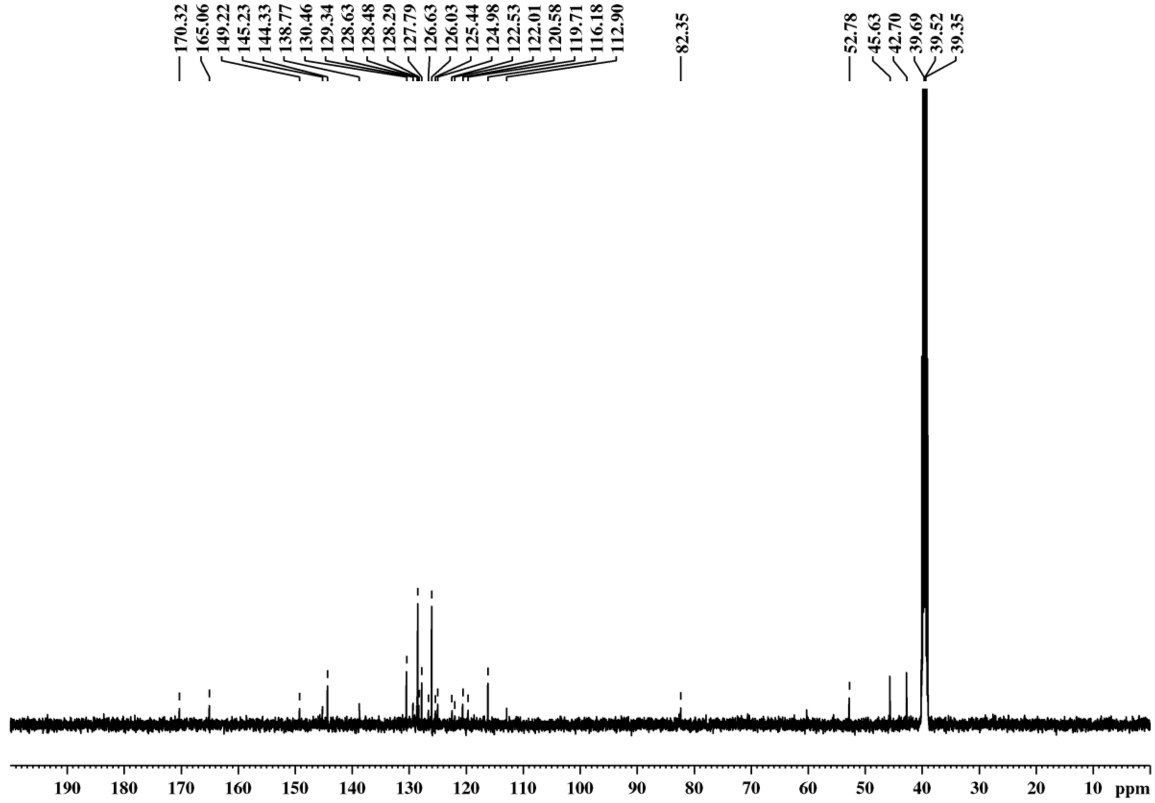
170.32
165.06
149.22
145.23
144.33
138.77
130.46
129.34
128.63
128.48
128.29
127.79
126.63
126.03
125.44
124.98
122.53
122.01
120.58
119.71
116.18
112.90
82.35
52.78
45.63
42.70
39.69
39.52
39.35
190
180
170
160
150
140
130
120
110
100
90
80
70
60
50
40
30
20
10
ppm

8 References

(1) Bouas-Laurent, H.; Dürr, H. Organic photochromism (IUPAC Technical Report). *Pure and Applied Chemistry* **2001**, *73*, 639.

(2) Yokoyama, Y. Fulgides for Memories and Switches. *Chem. Rev.* **2000**, *100*, 1717–1740.

(3) Hepworth, J. D.; Heron, B. M. Photochromic Naphthopyrans, 85–135.

(4) Helmy, S.; Leibfarth, F. A.; Oh, S.; Poelma, J. E.; Hawker, C. J.; Read de Alaniz, J. Photoswitching using visible light: A new class of organic photochromic molecules. *J. Am. Chem. Soc.* **2014**, *136*, 8169–8172.

(5) Hemmer, J. R.; Poelma, S. O.; Treat, N.; Page, Z. A.; Dolinski, N.; Diaz, Y. J.; Tomlinson, W.; Clark, K. D.; Hooper, J. P.; Hawker, C. J. *et al.* Tunable Visible and Near Infrared Photoswitches. *J. Am. Chem. Soc.* **2016**.

(6) Szymański, W.; Beierle, J. M.; Kistemaker, H. A. V.; Velema, W. A.; Feringa, B. L. Reversible photocontrol of biological systems by the incorporation of molecular photoswitches. *Chem. Rev.* **2013**, *113*, 6114–6178.

(7) Beharry, A. A.; Woolley, G. A. Azobenzene photoswitches for biomolecules. *Chem. Soc. Rev.* **2011**, *40*, 4422–4437.

(8) Hoppmann, C.; Schmieder, P.; Domaing, P.; Vogelreiter, G.; Eichhorst, J.; Wiesner, B.; Morano, I.; Rück-Braun, K.; Beyermann, M. Photocontrol of contracting muscle fibers. *Angew. Chem. Int. Ed.* **2011**, *50*, 7699–7702.

(9) Zeyat, G.; Rück-Braun, K. Building photoswitchable 3,4'-AMPB peptides: Probing chemical ligation methods with reducible azobenzene thioesters. *Beilstein J. Org. Chem.* **2012**, *8*, 890–896.

(10) Kitzig, S.; Thilemann, M.; Cordes, T.; Rück-Braun, K. Light-Switchable Peptides with a Hemithioindigo Unit: Peptide Design, Photochromism, and Optical Spectroscopy. *ChemPhysChem* **2016**, *17*, 1252–1263.

(11) Kitzig, S.; Rück-Braun, K. Synthesis of hemithioindigo-based chromopeptides by using the Tmb auxiliary in native chemical ligation studies. *J. Pept. Sci.* **2017**, *23*, 567–573.

(12) Irie, M.; Fukaminato, T.; Matsuda, K.; Kobatake, S. Photochromism of diarylethene molecules and crystals: Memories, switches, and actuators. *Chem. Rev.* **2014**, *114*, 12174–12277.

(13) Villeneuve, C. H. de; Michalik, F.; Chazalviel, J. N.; Rück-Braun, K.; Allongue, P. Photochromes: Quantitative IR Readout of Fulgimide Monolayer Switching on Si(111) Surfaces. *Adv. Mater.* **2013**, *25*, 415.

(14) Rück-Braun, K.; Petersen, M. Å.; Michalik, F.; Hebert, A.; Przyrembel, D.; Weber, C.; Ahmed, S. A.; Kowarik, S.; Weinelt, M. Formation of Carboxy- and Amide-Terminated Alkyl Monolayers on Silicon(111) Investigated by ATR-FTIR, XPS, and X-ray Scattering: Construction of Photoswitchable Surfaces. *Langmuir* **2013**, *29*, 11758–11769.

(15) Schulze, M.; Utecht, M.; Hebert, A.; Rück-Braun, K.; Saalfrank, P.; Tegeder, P. Reversible Photoswitching of the Interfacial Nonlinear Optical Response. *J. Phys. Chem. Lett.* **2015**, *6*, 505–509.

(16) Walz, J.; Ulrich, K.; Port, H.; Wolf, H. C.; Wonner, J.; Effenberger, F. Fulgides as switches for intramolecular energy transfer. *Chem. Phys. Lett.* **1993**, *213*, 321–324.

(17) Nemnes, G. A.; Visan, C. Electron transport properties of fulgide-based photochromic switches. *RSC Adv.* **2015**, *5*, 26438–26442.

(18) Matsui, F.; Taniguchi, H.; Yokoyama, Y.; Sugiyama, K.; Kurita, Y. Application of Photochromic 5-Dimethylaminoindolylfulgide to Photon-Mode Erasable Optical Memory Media with Non-Destructive Readout Ability Based on Wavelength Dependence of Bleaching Quantum Yield. *Chem. Lett.* **1994**, *23*, 1869–1872.

(19) Janicki, S. Z.; Schuster, G. B. A Liquid Crystal Opto-optical Switch: Nondestructive Information Retrieval Based on a Photochromic Fulgide as Trigger. *J. Am. Chem. Soc.* **1995**, *117*, 8524–8527.

(20) Yu, C.-M.; Hu, B.-C.; Gong, Z.-H.; Liu, C.; Li, J.-T. A novel photochromic fulgide based on porphyrin for nondestructive information processing. *Chin. Chem. Lett.* **2016**, *27*, 1767–1770.

(21) Delaire, J. A.; Nakatani, K. Linear and Nonlinear Optical Properties of Photochromic Molecules and Materials. *Chem. Rev.* **2000**, *100*, 1817–1846.

(22) Yokoyama, Y.; Nakatani, K. *Photon-Working Switches*; Springer Japan: Tokyo, 2017.

(23) van Gemert, B. *Organic Photochromic and Thermochromic Compounds, Vol. 1: Benzo and Naphthopyrans (Chromenes)*; Plenum Press: New York, 1999.

(24) Crano, J. C.; Flood, T.; Knowles, D.; Kumar, A.; van Gemert, B. Photochromic compounds: Chemistry and application in ophthalmic lenses. *Pure Appl. Chem.* **1996**, *68*.

(25) Pinto, T. V.; Costa, P.; Sousa, C. M.; Sousa, C. A. D.; Monteiro, A.; Pereira, C.; Soares, Olívia Salomé G P; Silva, C. S. M.; Pereira, M. F. R.; Coelho, P. J. *et al.* Naphthopyran-Based Silica Nanoparticles as New High-Performance Photoresponsive Materials. *ACS Appl. Mater. Interfaces* **2016**, *8*, 7221–7231.

(26) Ho, M.-L.; Yu, Y.-P.; Chen, Y.-T.; Lin, M.-H. Solid state photochromism of pyrano[3,2-c]chromen-5-one moiety with the assistance of localized surface plasmons. *CrystEngComm* **2012**, *14*, 4049.

(27) Such, G.; Evans, R. A.; Yee, L. H.; Davis, T. P. Factors Influencing Photochromism of Spiro-Compounds Within Polymeric Matrices. *Journal of Macromolecular Science, Part C.* **2003**, *43*, 547–579.

(28) Zhang, M.-D.; Zhang, Y.-F.; Li, D.-H.; Wang, G.; Li, J.-X. The high stability of merocyanine and significant slow fading speed of naphthopyran in layer-by-layer assembled films via hydrogen bonding. *New J. Chem.* **2013**, *37*, 1385.

(29) Han, S.; Chen, Y. Modification of a photochromic 3-aryl-3-(α-naphthalene)-3H-naphtho[2,1-b]pyran system with a fast fading speed in solution and in a rigid polymer matrix. *J. Mater. Chem.* **2011**, *21*, 4961.

(30) Evans, R. A.; Hanley, T. L.; Skidmore, M. A.; Davis, T. P.; Such, G. K.; Yee, L. H.; Ball, G. E.; Lewis, D. A. The generic enhancement of photochromic dye switching speeds in a rigid polymer matrix. *Nat. Mater.* **2005**, *4*, 249–253.

(31) Aldib, M.; Christie, R. M. Textile applications of photochromic dyes. Part 5: Application of commercial photochromic dyes to polyester fabric by a solvent-based dyeing method. *Coloration Technol.* **2013**, *129*, 131–143.

(32) Pinto, T. V.; Costa, P.; Sousa, C. M.; Sousa, C. A. D.; Pereira, C.; Silva, C. J. S. M.; Pereira, M. F. R.; Coelho, P. J.; Freire, C. Screen-Printed Photochromic Textiles through New Inks Based on SiO2@naphthopyran Nanoparticles. *ACS applied materials & interfaces* **2016**, *8*, 28935–28945.

(33) Moorthy, J. N.; Mandal, S.; Mukhopadhyay, A.; Samanta, S. Helicity as a steric force: Stabilization and helicity-dependent reversion of colored o-quinonoid intermediates of helical chromenes. *J. Am. Chem. Soc.* **2013**, *135*, 6872–6884.

(34) Browne, W. R.; Feringa, B. L. Light switching of molecules on surfaces. *Annu. Rev. Phys. Chem.* **2009**, *60*, 407–428.

(35) Gooding, J. J.; Ciampi, S. The molecular level modification of surfaces: from self-assembled monolayers to complex molecular assemblies. *Chem. Soc. Rev.* **2011**, *40*, 2704.

(36) Vilan, A.; Yaffe, O.; Biller, A.; Salomon, A.; Kahn, A.; Cahen, D. Molecules on Si: Electronics with Chemistry. *Adv. Mater.* **2010**, *22*, 140–159.

(37) Haensch, C.; Ott, C.; Hoeppener, S.; Schubert, U. S. Combination of different chemical surface reactions for the fabrication of chemically versatile building blocks onto silicon surfaces. *Langmuir* **2008**, *24*, 10222–10227.

(38) Boukherroub, R.; Morin, S.; Bensebaa, F.; Wayner, D. D. M. New Synthetic Routes to Alkyl Monolayers on the Si(111) Surface 1. *Langmuir* **1999**, *15*, 3831–3835.

(39) Ciampi, S.; Harper, J. B.; Gooding, J. J. Wet chemical routes to the assembly of organic monolayers on silicon surfaces via the formation of Si-C bonds: Surface preparation, passivation and functionalization. *Chem. Soc. Rev.* **2010**, *39*, 2158–2183.

(40) Veerbeek, J.; Huskens, J. Applications of Monolayer-Functionalized H-Terminated Silicon Surfaces: A Review. *Small Methods* **2017**, *1*, 1700072.

(41) Haensch, C.; Hoeppener, S.; Schubert, U. S. Chemical modification of self-assembled silane based monolayers by surface reactions. *Chem. Soc. Rev.* **2010**, *39*, 2323–2334.

(42) Pujari, S. P.; Scheres, L.; Marcelis, A. T. M.; Zuilhof, H. Covalent Surface Modification of Oxide Surfaces. *Angew. Chem. Int. Ed.* **2014**, *53*, 6322–6356.

(43) Oh, S. J.; Hong, B. J.; Choi, K. Y.; Park, J. W. Surface modification for DNA and protein microarrays. *OMICS: A Journal of Integrative Biology* **2006**, *10*, 327–343.

(44) Pirrung, M. C. How to Make a DNA Chip. *Angew. Chem. Int. Ed.* **2002**, *41*, 1276–1289.

(45) Wilson, D. S.; Nock, S. Recent Developments in Protein Microarray Technology. *Angew. Chem. Int. Ed.* **2003**, *42*, 494–500.

(46) Bañuls, M.-J.; Puchades, R.; Maquieira, Á. Chemical surface modifications for the development of silicon-based label-free integrated optical (IO) biosensors: A review. *Analytica Chimica Acta* **2013**, *777*, 1–16.

(47) Lapin, N. A.; Chabal, Y. J. Infrared Characterization of Biotinylated Silicon Oxide Surfaces, Surface Stability, and Specific Attachment of Streptavidin. *J. Phys. Chem. B* **2009**, *113*, 8776–8783.

(48) Potyrailo, R. A.; Conrad, R. C.; Ellington, A. D.; Hieftje, G. M. Adapting Selected Nucleic Acid Ligands (Aptamers) to Biosensors. *Anal. Chem.* **1998**, *70*, 3419–3425.

(49) Shircliff, R. A.; Stradins, P.; Moutinho, H.; Fennell, J.; Ghirardi, M. L.; Cowley, S. W.; Branz, H. M.; Martin, I. T. Angle-resolved XPS analysis and characterization of monolayer and multilayer silane films for DNA coupling to silica. *Langmuir* **2013**, *29*, 4057–4067.

(50) Demirel, G. B.; Dilsiz, N.; Ergün, M. A.; Çakmak, M.; Çaykara, T. Photocontrollable DNA hybridization on reversibly photoresponsive surfaces. *J. Mater. Chem.* **2011**, *21*, 10415.

(51) Böcking, T.; Kilian, K. A.; Gaus, K.; Gooding, J. J. Single-step DNA immobilization on antifouling self-assembled monolayers covalently bound to silicon (111). *Langmuir* **2006**, *22*, 3494–3496.

(52) Qin, G.; Santos, C.; Zhang, W.; Li, Y.; Kumar, A.; Erasquin, U. J.; Liu, K.; Muradov, P.; Trautner, B. W.; Cai, C. Biofunctionalization on alkylated silicon substrate surfaces via "click" chemistry. *J. Am. Chem. Soc.* **2010**, *132*, 16432–16441.

(53) Rosso, M.; Giesbers, M.; Schroën, K.; Zuilhof, H. Controlled oxidation, biofunctionalization, and patterning of alkyl monolayers on silicon and silicon nitride surfaces using plasma treatment. *Langmuir* **2010**, *26*, 866–872.

(54) Awsiuk, K.; Budkowski, A.; Psarouli, A.; Petrou, P.; Bernasik, A.; Kakabakos, S.; Rysz, J.; Raptis, I. Protein adsorption and covalent bonding to silicon nitride surfaces modified with organo-silanes: Comparison using AFM, angle-resolved XPS and multivariate ToF-SIMS analysis. *Colloids and Surfaces B: Biointerfaces* **2013**, *110*, 217–224.

(55) Aissaoui, N.; Bergaoui, L.; Landoulsi, J.; Lambert, J.-F.; Boujday, S. Silane layers on silicon surfaces: Mechanism of interaction, stability, and influence on protein adsorption. *Langmuir* **2012**, *28*, 656–665.

(56) Escorihuela, J.; Bañuls, M.-J.; Puchades, R.; Maquieira, Á. Site-specific immobilization of DNA on silicon surfaces by using the thiol–yne reaction. *J. Mater. Chem. B* **2014**, *2*, 8510–8517.

(57) Defrancq, E.; Hoang, A.; Vinet, F.; Dumy, P. Oxime bond formation for the covalent attachment of oligonucleotides on glass support. *Bioorganic Med. Chem. Lett.* **2003**, *13*, 2683–2686.

(58) Cattaruzza, F.; Cricenti, A.; Flamini, A.; Girasole, M.; Longo, G.; Prosperi, T.; Andreano, G.; Cellai, L.; Chirivino, E. Controlled loading of oligodeoxyribonucleotide monolayers onto unoxidized crystalline silicon; fluorescence-based determination of the surface coverage and of the hybridization efficiency; parallel imaging of the process by Atomic Force Microscopy. *Nucl Acids Res* **2006**, *34*, e32.

(59) Voicu, R.; Boukherroub, R.; Bartzoka, V.; Ward, T.; Wojtyk, J. T. C.; Wayner, D. D. M. Formation, characterization, and chemistry of undecanoic acid-terminated silicon surfaces: Patterning and immobilization of DNA. *Langmuir* **2004**, *20*, 11713–11720.

(60) Coffinier, Y.; Olivier, C.; Perzyna, A.; Grandidier, B.; Wallart, X.; Durand, J.-O.; Melnyk, O.; Stiévenard, D. Semicarbazide-functionalized Si(111) surfaces for the site-specific immobilization of peptides. *Langmuir* **2005**, *21*, 1489–1496.

(61) Strother, T.; Cai, W.; Zhao, X.; Hamers, R. J.; Smith, L. M. Synthesis and Characterization of DNA-Modified Silicon (111) Surfaces. *J. Am. Chem. Soc.* **2000**, *122*, 1205–1209.

(62) Condorelli, G. G.; Motta, A.; Favazza, M.; Gurrieri, E.; Betti, P.; Dalcanale, E. Molecular recognition of halogen-tagged aromatic VOCs at the air-silicon interface. *Chem. Commun.* **2010**, *46*, 288–290.

(63) van der Veen, N. J.; Flink, S.; Deij, M. A.; Egberink, R. J. M.; van Veggel, F. C. J. M.; Reinhoudt, D. N. Monolayer of a Na + -Selective Fluoroionophore on Glass: Connecting the Fields of Monolayers and Optical Detection of Metal Ions. *J. Am. Chem. Soc.* **2000**, *122*, 6112–6113.

(64) Ayadim, M.; Habib Jiwan, J. L.; Silva, A. P. de; Soumillion, J.P. Photosensing by a fluorescing probe covalently attached to the silica. *Tetrahedron Lett.* **1996**, *37*, 7039–7042.

(65) Dietrich, P.; Michalik, F.; Schmidt, R.; Gahl, C.; Mao, G.; Breusing, M.; Raschke, M. B.; Priewisch, B.; Elsässer, T.; Mendelsohn, R. *et al.* An anchoring strategy for photoswitchable biosensor technology: Azobenzene-modified SAMs on Si(111). *Appl. Phys. A* **2008**, *93*, 285–292.

(66) Min, M.; Bang, G. S.; Lee, H.; Yu, B.-C. A photoswitchable methylene-spaced fluorinated aryl azobenzene monolayer grafted on silicon. *Chem. Commun.* **2010**, *46*, 5232–5234.

(67) Uchida, K.; Yamanoi, Y.; Yonezawa, T.; Nishihara, H. Reversible on/off conductance switching of single diarylethene immobilized on a silicon surface. *J. Am. Chem. Soc.* **2011**, *133*, 9239–9241.

(68) Kehrlösser, D.; Träger, J.; Kim, H.-C.; Hampp, N. Synthesis and photochemistry of coumarin-based self-assembled monolayers on silicon oxide surfaces. *Langmuir* **2010**, *26*, 3878–3882.

(69) Demirel, G. B.; Dilsiz, N.; Çakmak, M.; Çaykara, T. Molecular design of photoswitchable surfaces with controllable wettability. *J. Mater. Chem.* **2011**, *21*, 3189.

(70) Aburaya, Y.; Nomura, H.; Kageshima, M.; Naitoh, Y.; Li, Y. J.; Sugawara, Y. Switching surface polarization of atomic force microscopy probe utilizing photoisomerization of photochromic molecules. *J. Appl. Phys.* **2011**, *109*, 64308.

(71) Bunker, B. C.; Kim, B. I.; Houston, J. E.; Rosario, R.; Garcia, A. A.; Hayes, M.; Gust, D.; Picraux, S. T. Direct Observation of Photo Switching in Tethered Spiropyrans Using the Interfacial Force Microscope. *Nano Lett.* **2003**, *3*, 1723–1727.

(72) Claus, T. K.; Telitel, S.; Welle, A.; Bastmeyer, M.; Vogt, A. P.; Delaittre, G.; Barner-Kowollik, C. Light-driven reversible surface functionalization with anthracenes: Visible light writing and mild UV erasing. *Chem. Commun.* **2017**, *53*, 1599–1602.

(73) Fan, M.-G.; Yu, L.; Zhao, W. *Organic Photochromic and Thermochromic Compounds, Vol. 1: Fulgide Family Compounds: Synthesis, Photochromism, and Application*; Plenum Press: New York, 1999.

(74) Kaneko, A.; Tomoda, A.; Ishizuka, M.; Suzuki, H.; Matsushima, R. Photochemical Fatigue Resistances and Thermal Stabilities of Heterocyclic Fulgides in PMMA Film. *Bull. Chem. Soc. Jpn* **1988**, *61*, 3569–3573.

(75) Uchida, S.; Yamada, S.; Yokoyama, Y.; Kurita, Y. Steric Effects of Substituents on the Photochromism of Indolylfulgides. *Bull. Chem. Soc. Jpn* **1995**, *68*, 1677–1682.

(76) Yokoyama, Y.; Kurita, Y. Photochromism of Fulgides and Related Compounds. *Molecular Crystals and Liquid Crystals Science and Technology. Section A. Molecular Crystals and Liquid Crystals* **1994**, *246*, 87–94.

(77) Matsushima, R.; Sakaguchi, H. Comparison of the photochromic properties of fulgides and fulgimides. *J. Photochem. Photobiol. A* **1997**, *108*, 239–245.

(78) Mayer, K. Dissertation: Entwicklung wasserlöslicher schaltbarer Fluorophore, Technical University, Berlin, 2014.

(79) Zarwell, S.; Dietrich, S.; Schulz, C.; Dietrich, P.; Michalik, F.; Rück-Braun, K. Preparation of an Indolylfulgimide-Adamantane Linker Conjugate with Nitrile Anchoring Groups through Palladium-Catalyzed Transformations. *Eur. J. Org. Chem.* **2009**, *2009*, 2088–2095.

(80) Dietrich, S. Dissertation: Synthese und photochrome Eigenschaften funktionalisierter Indolylfulgimide, Technical University, Berlin, 2006.

(81) Michalik, F. Dissertation: Photoschaltbare Monolagen auf Silizium(111): Design und Synthese, Technical University, Berlin, 2011.

(82) Hebert, A. Dissertation: Herstellung schaltbarer Hybridsysteme und ihre IR-spektroskopische Charakterisierung, Technical University, Berlin, 2014.

(83) Stobbe, H. Eine neue Synthese der Teraconsäure. *Ber. Dtsch. Chem. Ges.* **1893**, *26*, 2312–2319.

(84) Johnson, W. S.; McCloskey, A. L.; Dunnigan, D. A. The Mechanism of the Stobbe Condensation. *J. Am. Chem. Soc.* **1950**, *72*, 514–517.

(85) Selinger, Z.; Lapidot, Y. Synthesis of fatty acid anhydrides by reaction with dicyclohexylcarbodiimide. *J. Lipid Res.* **1966**, *7*, 174–175.

(86) Schulz, C. Dissertation: Beiträge zur Chemie funktionalisierter Indolylfulgimide: Synthese und Anwendungen, Technical University, Berlin, 2009.

(87) Heron, B. M.; D. Gabbutt, C.; D. Hepworth, J.; A. Thomas, D.; Kilner, C.; M. Partington, S. Synthesis and Photochromic Properties of Methoxy Substituted 2,2-Diaryl-2H-naphtho[1,2-b]pyrans. *Heterocycles,* **2004**, *63*, 567.

(88) Hepworth, J. D.; Gabbutt, C. D.; Heron, B. M. *Colour Science '98, Vol. 1: Dyes and Pigment Chem.*; University of Leeds: UK, 1999.

(89) Ercole, F.; Malic, N.; Davis, T. P.; Evans, R. A. Optimizing the photochromic performance of naphthopyrans in a rigid host matrix using poly(dimethylsiloxane) conjugation. *J. Mater. Chem.* **2009**, *19*, 5612.

(90) Kumar, A.; van Gemert, B.; Knowles, D. B. Substituted naphthopyrans, Patent. US 5458814.

(91) Zayat, M.; Levy, D. Photochromic naphthopyrans in sol–gel ormosil coatings. *J. Mater. Chem.* **2003**, *13*, 727–730.

(92) Gabbutt, C. D.; Gelbrich, T.; Hepworth, J. D.; Heron, B.M.; Hursthouse, M. B.; Partington, S. M. Synthesis and photochromic properties of some fluorine-containing naphthopyrans. *Dyes and Pigments* **2002**, *54*, 79–93.

(93) Böttcher, C.; Zeyat, G.; Ahmed, S. A.; Irran, E.; Cordes, T.; Elsner, C.; Zinth, W.; Rueck-Braun, K. Synthesis of novel photochromic pyrans via palladium-mediated reactions. *Beilstein J. Org. Chem.* **2009**, *5*, 25.

(94) Sousa, C. M.; Berthet, J.; Delbaere, S.; Coelho, P. J. Photochromic fused-naphthopyrans without residual color. *J. Org. Chem.* **2012**, *77*, 3959–3968.

(95) Sousa, C. M.; Berthet, J.; Delbaere, S.; Polónia, A.; Coelho, P. J. Fast Color Change with Photochromic Fused Naphthopyrans. *J. Org. Chem.* **2015**, *80*, 12177–12181.

(96) Sousa, C. M.; Berthet, J.; Delbaere, S.; Polónia, A.; Coelho, P. J. Control of the Switching Speed of Photochromic Naphthopyrans through Restriction of Double Bond Isomerization. *J. Org. Chem.* **2017**, *82*, 12028–12037.

(97) Inagaki, Y.; Kobayashi, Y.; Mutoh, K.; Abe, J. A Simple and Versatile Strategy for Rapid Color Fading and Intense Coloration of Photochromic Naphthopyran Families. *J. Am. Chem. Soc.* **2017**, *139*, 13429–13441.

(98) Delbaere, S.; Micheau, J.-C.; Vermeersch, G. NMR kinetic investigations of the photochemical and thermal reactions of a photochromic chromene. *J. Org. Chem.* **2003**, *68*, 8968–8973.

(99) Delbaere, S.; Micheau, J.-C.; Vermeersch, G. Multinuclear NMR Structural Characterization of an Unprecedented Photochromic Allene Intermediate. *Org. Lett.* **2002**, *4*, 3143–3145.

(100) Delbaere, S.; Vermeersch, G. NMR characterization of allenyl-naphthol in the photochromic process of 3,3-diphenyl-[3H]-naphtho[2-1,b]pyran. *J. Photochem. Photobiol. A* **2003**, *159*, 227–232.

(101) Delbaere, S.; Vermeersch, G. NMR proofs of the involvement of an allenyl-naphthol as a key-intermediate in the photochromic process of [3H]-naphthopyrans. *Tetrahedron Lett.* **2003**, *44*, 259–262.

(102) Maurel, F.; Delbaere, S.; Truong, S. L.; Couesnon, T.; Dubest, R.; Vermeersch, G.; Aubard, J. Combined NMR, SERRS, and DFT study of photochemical and thermal reactions of acetylene- and thienylacetylene-substituted chromenes. *J. Phys. Org. Chem.* **2007**, *20*, 944–952.

(103) Sallenave, X.; Delbaere, S.; Vermeersch, G.; Saleh, A.; Pozzo, J.-L. Photoswitch based on remarkably simple naphthopyrans. *Tetrahedron Lett.* **2005**, *46*, 3257–3259.

(104) Aiken, S.; Booth, K.; Gabbutt, C. D.; Mark Heron, B.; Rice, C. R.; Charaf-Eddin, A.; Jacquemin, D. The first structural and spectroscopic characterisation of a ring-opened form of a 2H-naphtho1,2-bpyran: A novel photomerocyanine. *Chem. Commun.* **2014**, *50*, 7900–7903.

(105) Coelho, P. J.; Carvalho, L. M.; Vermeersch, G.; Delbaere, S. Thermally reversible photochromic behaviour of new naphthopyrans involving an intramolecular [2+2] cyclization reaction. *Tetrahedron* **2009**, *65*, 5369–5376.

(106) Delbaere, S.; Micheau, J.-C.; Frigoli, M.; Vermeersch, G. Unexpected halogen substituent effects on the complex thermal relaxation of naphthopyrans after UV irradiation. *J. Org. Chem.* **2005**, *70*, 5302–5304.

(107) Sousa, C. M.; Coelho, P. J.; Vermeersch, G.; Berthet, J.; Delbaere, S. Synthesis and photochemical reactivity of new 4-substituted naphtho[1,2-b]pyran derivatives. *J. Photochem. Photobiol. A* **2010**, *216*, 73–78.

(108) Liebmann, D. Dissertation: Synthesen von photoschaltbaren Hybridsystemen, Technical University, Berlin, 2014.

(109) Bulman Page, P. C.; Chan, Y.; Noor Armylisas, A. H.; Alahmdi, M. Asymmetric epoxidation of chromenes mediated by iminium salts: Synthesis of mollugin and (3S,4R)-trans-3,4-dihydroxy-3,4-dihydromollugin. *Tetrahedron* **2016**, *72*, 8406–8416.

(110) Gabbutt, C. D.; Heron, B. M.; Instone, A. C.; Thomas, D. A.; Partington, S. M.; Hursthouse, M. B.; Gelbrich, T. Observations on the Synthesis of Photochromic Naphthopyrans. *Eur. J. Org. Chem.* **2003**, *2003*, 1220–1230.

(111) Gabbutt, C. D.; Heron, B. M.; Kilner, C.; Kolla, S. B. The influence of a 1,1-diarylvinyl moiety on the photochromism of naphthopyrans. *Org. Biomol. Chem.* **2010**, *8*, 4874–4883.

(112) Gabbutt, C. D.; Heron, B. M.; Instone, A. C.; Horton, P. N.; Hursthouse, M. B. Synthesis and photochromic properties of substituted 3H-naphtho[2,1-b]pyrans. *Tetrahedron* **2005**, *61*, 463–471.

(113) Yu, G.; Chowdhury, M. A.; Abdellatif, K. R. A.; Dong, Y.; Praveen Rao, P. N.; Das, D.; Velázquez, C. A.; Suresh, M. R.; Knaus, E. E. Phenylacetic acid regioisomers possessing a N-difluoromethyl-1,2-dihydropyrid-2-one pharmacophore: Evaluation as dual inhibitors of cyclooxygenases and 5-lipoxygenase with anti-inflammatory activity. *Bioorganic Med. Chem. Lett.* **2010**, *20*, 896–902.

(114) Greene, T. W.; Wuts, P. G. M. *Protective Groups in Organic Synthesis*, 3rd ed.; Wiley: New York, Chichester, 2002.

(115) Gobbo, P.; Gunawardene, P.; Luo, W.; Workentin, M. Synthesis of a Toolbox of Clickable Rhodamine B Derivatives. *Synlett* **2015**, *26*, 1169–1174.

(116) Guram, A. S.; Rennels, R. A.; Buchwald, S. L. A Simple Catalytic Method for the Conversion of Aryl Bromides to Arylamines. *Angew. Chem. Int. Ed. Engl.* **1995**, *34*, 1348–1350.

(117) Louie, J.; Hartwig, J. F. Palladium-catalyzed synthesis of arylamines from aryl halides. Mechanistic studies lead to coupling in the absence of tin reagents. *Tetrahedron Lett.* **1995**, *36*, 3609–3612.

(118) Sandanayaka, V.; Singh, J.; Zhou, L.-M.; Gurney, M. E. Biaryl nitrogen-heterocycle inhibitors of lta4h for treating inflammation, Patent. US20070149544 A1.

(119) Hooper, M. W.; Utsunomiya, M.; Hartwig, J. F. Scope and mechanism of palladium-catalyzed amination of five-membered heterocyclic halides. *J. Org. Chem.* **2003**, *68*, 2861–2873.

(120) Hartwig, J. F.; Richards, S.; Barañano, D.; Paul, F. Influences on the Relative Rates for C−N Bond-Forming Reductive Elimination and β-Hydrogen Elimination of Amides. A Case Study on

the Origins of Competing Reduction in the Palladium-Catalyzed Amination of Aryl Halides. *J. Am. Chem. Soc.* **1996**, *118*, 3626–3633.

(121) Ozawa, F.; Fujimori, M.; Yamamoto, T.; Yamamoto, A. Mechanism of the reaction of trans-bis(diethylphenylphosphine)di-m-tolylpalladium(II) with methyl iodide affording m-xylene. Evidence for a reductive elimination process involving the intermolecular exchange of organic groups. *Organometallics* **1986**, *5*, 2144–2149.

(122) Ullmann, F. Ueber eine neue Bildungsweise von Diphenylaminderivaten. *Ber. Dtsch. Chem. Ges.* **1903**, *36*, 2382–2384.

(123) Sambiagio, C.; Marsden, S. P.; Blacker, A. J.; McGowan, P. C. Copper catalysed Ullmann type chemistry: From mechanistic aspects to modern development. *Chem. Soc. Rev.* **2014**, *43*, 3525–3550.

(124) Saruta, K.; Hayashi, N.; Sakurai, O.; Sawamoto, H.; Oboki, E. Aromatic heterocyclic compound, Patent. EP2862856.

(125) Li, H.; Johansson Seechurn, C. C. C.; Colacot, T. J. Development of Preformed Pd Catalysts for Cross-Coupling Reactions, Beyond the 2010 Nobel Prize. *ACS Catal.* **2012**, *2*, 1147–1164.

(126) Christmann, U.; Vilar, R. Monoligated palladium species as catalysts in cross-coupling reactions. *Angew. Chem. Int. Ed.* **2005**, *44*, 366–374.

(127) Surry, D. S.; Buchwald, S. L. Dialkylbiaryl Phosphines in Pd-Catalyzed Amination: A User's Guide. *Chem. Sci.* **2011**, *2*, 27–50.

(128) Fleckenstein, C. A.; Plenio, H. Sterically demanding trialkylphosphines for palladium-catalyzed cross coupling reactions-alternatives to PtBu3. *Chem. Soc. Rev.* **2010**, *39*, 694–711.

(129) Neises, B.; Steglich, W. Simple Method for the Esterification of Carboxylic Acids. *Angew. Chem. Int. Ed. Engl.* **1978**, *17*, 522–524.

(130) Kitamura, M.; Takahashi, S.; Okauchi, T. Rh-Catalyzed Cyclization of 3-Aryloxycarbonyldiazonaphthoquinones for the Synthesis of β-Phenylnaphthalene Lactones and Formal Synthesis of Pradimicinone. *J. Org. Chem.* **2015**, *80*, 8406–8416.

(131) Delbaere, S.; Vermeersch, G. NMR spectroscopy applied to photochromism investigations. *J. Photochem. Photobiol. C: Photochem. Rev.* **2008**, *9*, 61–80.

(132) Kinder, M. A.; Meyer, L.; Margaretha, P. Photocycloaddition of Isocoumarins and Isothiocoumarins to Alkenes. *Helv. Chim. Acta.* **2001**, *84*, 2373–2378.

(133) Delbaere, S.; Luccioni-Houze, B.; Bochu, C.; Teral, Y.; Campredon, M.; Vermeersch, G. Kinetic and structural studies of the photochromic process of 3H-naphthopyrans by UV and NMR spectroscopy. *J. Chem. Soc., Perkin Trans. 2* **1998**, 1153–1158.

(134) Malic, N.; Campbell, J. A.; Ali, A. S.; York, M.; D'Souza, A.; Evans, R. A. Controlling Molecular Mobility in Polymer Matrices: Synchronizing Switching Speeds of Multiple Photochromic Dyes. *Macromolecules* **2010**, *43*, 8488–8501.

(135) Suzuki, T.; Lin, F.-T.; Priyadashy, S.; Weber, S. G. Stabilization of the merocyanine form of photochromic compounds in fluoro alcohols is due to a hydrogen bond. *Chem. Commun.* **1998**, 2685–2686.

(136) *Infrared and raman characteristic group frequencies: Tables and charts;* Socrates, G., Ed., 3rd ed.; John Wiley & Sons: West Sussex, 2007.

(137) Kamlet, M. J.; Abboud, J. L. M.; Abraham, M. H.; Taft, R. W. Linear solvation energy relationships. 23. A comprehensive collection of the solvatochromic parameters, .pi.*, .alpha., and .beta., and some methods for simplifying the generalized solvatochromic equation. *J. Org. Chem.* **1983**, *48*, 2877–2887.

(138) Rijksen, B.; van Lagen, B.; Zuilhof, H. Mimicking the silicon surface: Reactivity of silyl radical cations toward nucleophiles. *J. Am. Chem. Soc.* **2011**, *133*, 4998–5008.

(139) Cicero, R. L.; Linford, M. R.; Chidsey, C. E. D. Photoreactivity of Unsaturated Compounds with Hydrogen-Terminated Silicon(111). *Langmuir* **2000**, *16*, 5688–5695.

(140) Cicero, R. L.; Chidsey, C. E. D.; Lopinski, G. P.; Wayner, D. D. M.; Wolkow, R. A. Olefin Additions on H−Si(111): Evidence for a Surface Chain Reaction Initiated at Isolated Dangling Bonds. *Langmuir* **2002**, *18*, 305–307.

(141) Takeuchi, N.; Kanai, Y.; Selloni, A. Surface reaction of alkynes and alkenes with H-Si(111): A density functional theory study. *J. Am. Chem. Soc.* **2004**, *126*, 15890–15896.

(142) Boukherroub, R.; Morin, S.; Sharpe, P.; Wayner, D. D. M.; Allongue, P. Insights into the Formation Mechanisms of Si−OR Monolayers from the Thermal Reactions of Alcohols and Aldehydes with Si(111)−H 1. *Langmuir* **2000**, *16*, 7429–7434.

(143) Hacker, C. A.; Anderson, K. A.; Richter, L. J.; Richter, C. A. Comparison of Si-O-C interfacial bonding of alcohols and aldehydes on Si(111) formed from dilute solution with ultraviolet irradiation. *Langmuir* **2005**, *21*, 882–889.

(144) Effenberger, F.; Götz, G.; Bidlingmaier, B.; Wezstein, M. Photoactivated Preparation and Patterning of Self-Assembled Monolayers with 1-Alkenes and Aldehydes on Silicon Hydride Surfaces. *Angew. Chem. Int. Ed.* **1998**, *37*, 2462–2464.

(145) Asanuma, H.; Lopinski, G. P.; Yu, H.-Z. Kinetic control of the photochemical reactivity of hydrogen-terminated silicon with bifunctional molecules. *Langmuir* **2005**, *21*, 5013–5018.

(146) Boukherroub, R.; Wojtyk, J. T. C.; Wayner, D. D. M.; Lockwood, D. J. Thermal Hydrosilylation of Undecylenic Acid with Porous Silicon. *J. Electrochem. Soc.* **2002**, *149*, H59.

(147) Voicu, R.; Boukherroub, R.; Bartzoka, V.; Ward, T.; Wojtyk, J. T. C.; Wayner, D. D. M. Formation, characterization, and chemistry of undecanoic acid-terminated silicon surfaces: Patterning and immobilization of DNA. *Langmuir* **2004**, *20*, 11713–11720.

(148) Faucheux, A.; Gouget-Laemmel, A. C.; Henry de Villeneuve, C.; Boukherroub, R.; Ozanam, F.; Allongue, P.; Chazalviel, J.-N. Well-defined carboxyl-terminated alkyl monolayers grafted onto H-Si(111): Packing density from a combined AFM and quantitative IR study. *Langmuir* **2006**, *22*, 153–162.

(149) Eves, B. J.; Lopinski, G. P. Formation of organic monolayers on silicon via gas-phase photochemical reactions. *Langmuir* **2006**, *22*, 3180–3185.

(150) Sieval, A. B.; Demirel, A. L.; Nissink, J. W. M.; Linford, M. R.; van der Maas, J. H.; Jeu, W. H. de; Zuilhof, H.; Sudhölter, E. J. R. Highly Stable Si−C Linked Functionalized Monolayers on the Silicon (100) Surface. *Langmuir* **1998**, *14*, 1759–1768.

(151) Sun, Q.-Y.; Smet, L. C. P. M. de; van Lagen, B.; Giesbers, M.; Thüne, P. C.; van Engelenburg, J.; Wolf, F. A. de; Zuilhof, H.; Sudhölter, E. J. R. Covalently attached monolayers on crystalline hydrogen-terminated silicon: Extremely mild attachment by visible light. *J. Am. Chem. Soc.* **2005**, *127*, 2514–2523.

(152) Aureau, D.; Ozanam, F.; Allongue, P.; Chazalviel, J.-N. The titration of carboxyl-terminated monolayers revisited: In situ calibrated fourier transform infrared study of well-defined monolayers on silicon. *Langmuir* **2008**, *24*, 9440–9448.

(153) Dutta, S.; Perring, M.; Barrett, S.; Mitchell, M.; Kenis, P. J. A.; Bowden, N. B. Cross metathesis on olefin-terminated monolayers on Si(111) using the Grubbs' catalyst. *Langmuir* **2006**, *22*, 2146–2155.

(154) Allongue, P.; Kieling, V.; Gerischer, H. Etching mechanism and atomic structure of H• Si(111) surfaces prepared in NH4F. *Electrochim. Acta* **1995**, *40*, 1353–1360.

(155) Allongue, P.; Henry de Villeneuve, C.; Morin, S.; Boukherroub, R.; Wayner, D. D.M. The preparation of flat H–Si(111) surfaces in 40% NH4F revisited. *Electrochim. Acta* **2000**, *45*, 4591–4598.

(156) Fukidome, H.; Matsumura, M. Electrochemical study of atomically flattening process of silicon surface in 40% NH4F solution. *Appl. Surf. Sci.* **1998**, *130-132*, 146–150.

(157) Higashi, G. S.; Chabal, Y. J.; Trucks, G. W.; Raghavachari, K. Ideal hydrogen termination of the Si (111) surface. *Appl. Phys. Lett.* **1990**, *56*, 656–658.

(158) Queeney, K. T.; Weldon, M. K.; Chang, J. P.; Chabal, Y. J.; Gurevich, A. B.; Sapjeta, J.; Opila, R. L. Infrared spectroscopic analysis of the Si/SiO[sub 2] interface structure of thermally oxidized silicon. *J. Appl. Phys.* **2000**, *87*, 1322.

(159) Porter, M. D.; Bright, T. B.; Allara, D. L.; Chidsey, C. E. D. Spontaneously organized molecular assemblies. 4. Structural characterization of n-alkyl thiol monolayers on gold by optical ellipsometry, infrared spectroscopy, and electrochemistry. *J. Am. Chem. Soc.* **1987**, *109*, 3559–3568.

(160) McKittrick, P. T.; Katon, J. E. Infrared and Raman Group Frequencies of Cyclic Imides. *Appl. Spectrosc.* **2016**, *44*, 812–817.

(161) Valley, D. T.; Onstott, M.; Malyk, S.; Benderskii, A. V. Steric hindrance of photoswitching in self-assembled monolayers of azobenzene and alkane thiols. *Langmuir* **2013**, *29*, 11623–11631.

(162) Liu, L.; Zhang, Y.; Wang, G.; Zhang, M.; Guan, H. High stability of photoinduced merocyanine in naphthopyran-doped polyvinylpyrrolidone electrospun nanofibers. *Polym. Int.* **2014**, *63*, 1991–1996.

(163) McGovern, M. E.; Kallury, K. M. R.; Thompson, M. Role of Solvent on the Silanization of Glass with Octadecyltrichlorosilane. *Langmuir* **1994**, *10*, 3607–3614.

(164) Ko, S.; Han, G.; Lee, J. K. Surface organic chemistry for application to organic electronics. *Tetrahedron Lett.* **2015**, *56*, 3721–3731.

(165) Rye, R. R.; Nelson, G. C.; Dugger, M. T. Mechanistic Aspects of Alkylchlorosilane Coupling Reactions. *Langmuir* **1997**, *13*, 2965–2972.

(166) Luzinov, I.; Julthongpiput, D.; Liebmann-Vinson, A.; Creggerm T.; Foster, M. D.; Tsukruk, V. V. Epoxy-Terminated Self-Assembled Monolayers: Molecular Glues for Polymer Layers. *Langmuir* **2000**, *16*, 504–516.
(167) Desbief, S.; Patrone, L.; Goguenheim, D.; Guérin, D.; Vuillaume, D. Impact of chain length, temperature, and humidity on the growth of long alkyltrichlorosilane self-assembled monolayers. *Phys. Chem. Chem. Phys.* **2011**, *13*, 2870–2879.
(168) Pasternack, R. M.; Rivillon Amy, S.; Chabal, Y. J. Attachment of 3-(Aminopropyl)triethoxysilane on Silicon Oxide Surfaces: Dependence on Solution Temperature. *Langmuir* **2008**, *24*, 12963–12971.
(169) Tsukruk, V. V.; Luzinov, I.; Julthongpiput, D. Sticky Molecular Surfaces: Epoxysilane Self-Assembled Monolayers. *Langmuir* **1999**, *15*, 3029–3032.
(170) Zhang, F.; Sautter, K.; Larsen, A. M.; Findley, D. A.; Davis, R. C.; Samha, H.; Linford, M. R. Chemical Vapor Deposition of Three Aminosilanes on Silicon Dioxide: Surface Characterization, Stability, Effects of Silane Concentration, and Cyanine Dye Adsorption. *Langmuir* **2010**, *26*, 14648–14654.
(171) Sagiv, J. Organized monolayers by adsorption. 1. Formation and structure of oleophobic mixed monolayers on solid surfaces. *J. Am. Chem. Soc.* **1980**, *102*, 92–98.
(172) Wang, Y.; Lieberman, M. Growth of Ultrasmooth Octadecyltrichlorosilane Self-Assembled Monolayers on SiO 2. *Langmuir* **2003**, *19*, 1159–1167.
(173) Dinh, D. H.; Vellutini, L.; Bennetau, B.; Dejous, C.; Rebière, D.; Pascal, É.; Moynet, D.; Belin, C.; Desbat, B.; Labrugère, C. *et al.* Route to Smooth Silica-Based Surfaces Decorated with Novel Self-Assembled Monolayers (SAMs) Containing Glycidyl-Terminated Very Long Hydrocarbon Chains. *Langmuir* **2009**, *25*, 5526–5535.
(174) Hang, T. C.; Guiseppi-Elie, A. Frequency dependent and surface characterization of DNA immobilization and hybridization. *Biosens. Bioelectron.* **2004**, *19*, 1537–1548.
(175) Knorr, D. B.; Jaye, C.; Fischer, D. A.; Shoch, A. B.; Lenhart, J. L. Manipulation of Interfacial Amine Density in Epoxy-Amine Systems as Studied by Near-Edge X-ray Absorption Fine Structure (NEXAFS). *Langmuir* **2012**, *28*, 15294–15304.
(176) Lemieux, M.; Minko, S.; Usov, D.; Stamm, M.; Tsukruk, V. V. Direct Measurement of Thermoelastic Properties of Glassy and Rubbery Polymer Brush Nanolayers Grown by “Grafting-from” Approach. *Langmuir* **2003**, *19*, 6126–6134.
(177) Leipert, D.; Nopper, D.; Bauser, M.; Gauglitz, G.; Jung, G. Investigation of the Molecular Recognition of Amino Acids by Cyclopeptides with Reflectometric Interference Spectroscopy. *Angew. Chem. Int. Ed.* **1998**, *37*, 3308–3311.
(178) Maskos, U.; Southern, E. M. Oligonucleotide hybridisations on glass supports: a novel linker for oligonucleotide synthesis and hybridisation properties of oligonucleotides synthesised in situ. *Nucl Acids Res* **1992**, *20*, 1679–1684.
(179) Minko, S.; Patil, S.; Datsyuk, V.; Simon, F.; Eichhorn, K.-J.; Motornov, M.; Usov, D.; Tokarev, I.; Stamm, M. Synthesis of Adaptive Polymer Brushes via “Grafting To” Approach from Melt. *Langmuir* **2002**, *18*, 289–296.

(180) Karabudak, E.; Kas, R.; Ogieglo, W.; Rafieian, D.; Schlautmann, S.; Lammertink, R. G. H.; Gardeniers, Han J. G. E.; Mul, G. Disposable Attenuated Total Reflection-Infrared Crystals from Silicon Wafer: A Versatile Approach to Surface Infrared Spectroscopy. *Anal. Chem.* **2013**, *85*, 33–38.

(181) Aswal, D. K.; Lenfant, S.; Guerin, D.; Yakhmi, J. V.; Vuillaume, D. Self assembled monolayers on silicon for molecular electronics. *Anal. Chim. Acta* **2006**, *568*, 84–108.

(182) Tian, R.; Seitz, O.; Li, M.; Hu, W. W.; Chabal, Y. J.; Gao, J. Infrared characterization of interfacial Si-O bond formation on silanized flat SiO2/Si surfaces. *Langmuir* **2010**, *26*, 4563–4566.

(183) da Fonseca, C.; Ozanam, F.; Chazalviel, J.-N. In situ infrared characterisation of the interfacial oxide during the anodic dissolution of a silicon electrode in fluoride electrolytes. *Surf. Sci.* **1996**, *365*, 1–14.

(184) Clark, I. T.; Aldinger, B. S.; Gupta, A.; Hines, M. A. Aqueous Etching Produces Si(100) Surfaces of Near-Atomic Flatness: Strain Minimization Does Not Predict Surface Morphology. *J. Phys. Chem. C* **2010**, *114*, 423–428.

(185) Parikh, A. N.; Allara, D. L.; Azouz, I. B.; Rondelez, F. An Intrinsic Relationship between Molecular Structure in Self-Assembled n-Alkylsiloxane Monolayers and Deposition Temperature. *J. Phys. Chem.* **1994**, *98*, 7577–7590.

(186) Blaudez, D.; Bonnier, M.; Desbat, B.; Rondelez, F. Two-Dimensional Polymerization in Langmuir Films: A PM-IRRAS Study of Octadecyltrimethoxysilane Monolayers. *Langmuir* **2002**, *18*, 9158–9163.

(187) Šapić, I. M.; Bistričić, L.; Volovšek, V.; Dananić, V.; Furić, K. DFT study of molecular structure and vibrations of 3-glycidoxypropyltrimethoxysilane. *Spectrochim. Acta A* **2009**, *72*, 833–840.

(188) Innocenzi, P.; Figus, C.; Takahashi, M.; Piccinini, M.; Malfatti, L. Structural Evolution during Evaporation of a 3-Glycidoxypropyltrimethoxysilane Film Studied in Situ by Time Resolved Infrared Spectroscopy. *J. Phys. Chem. A* **2011**, *115*, 10438–10444.

(189) Kurth, D. G.; Bein, T. Surface reactions on thin layers of silane coupling agents. *Langmuir* **1993**, *9*, 2965–2973.

(190) Aureau, D.; Varin, Y.; Roodenko, K.; Seitz, O.; Pluchery, O.; Chabal, Y. J. Controlled Deposition of Gold Nanoparticles on Well-Defined Organic Monolayer Grafted on Silicon Surfaces. *J. Phys. Chem. C* **2010**, *114*, 14180–14186.

(191) Boukherroub, R.; Morin, S.; Wayner, D. D. M.; Bensebaa, F.; Sproule, G. I.; Baribeau, J.-M.; Lockwood, D. J. Ideal Passivation of Luminescent Porous Silicon by Thermal, Noncatalytic Reaction with Alkenes and Aldehydes. *Chem. Mater.* **2001**, *13*, 2002–2011.

(192) Kim, J.; Seidler, P.; Wan, L. S.; Fill, C. Formation, structure, and reactivity of amino-terminated organic films on silicon substrates. *J. Colloid. Interface Sci.* **2009**, *329*, 114–119.

(193) Michalak, D. J.; Amy, S. R.; Estève, A.; Chabal, Y. J. Investigation of the Chemical Purity of Silicon Surfaces Reacted with Liquid Methanol. *J. Phys. Chem. C* **2008**, *112*, 11907–11919.

(194) Funk, C.; Dietrich, P. M.; Gross, T.; Min, H.; Unger, W. E. S.; Weigel, W. Epoxy-functionalized surfaces for microarray applications: Surface chemical analysis and fluorescence labeling of surface species. *Surf. Interface Anal.* **2012**, *44*, 890–894.

(195) Zhu, M.; Lerum, M. Z.; Chen, W. How To Prepare Reproducible, Homogeneous, and Hydrolytically Stable Aminosilane-Derived Layers on Silica. *Langmuir* **2012**, *28*, 416–423.

(196) Wanunu, M.; Livne, S.; Vaskevich, A.; Rubinstein, I. Assembly of Coordination Nanostructures via Ligand Derivatization of Oxide Surfaces. *Langmuir* **2006**, *22*, 2130–2135.

(197) Weber, T.; Gies, Y.; Terfort, A. Bacteria-repulsive polyglycerol surfaces by grafting polymerization onto aminopropylated surfaces. *Langmuir* **2012**, *28*, 15916–15921.

(198) Alderman, N.; Danos, L.; Fang, L.; Grossel, M. C.; Markvart, T. Light harvesting in silicon(111) surfaces using covalently attached protoporphyrin IX dyes. *Chem. Commun.* **2017**, *53*, 12120–12123.

(199) Barron, A. R.; Flood, D. J. *XPS of Carbon Nanomaterials.: In OpenStax CNX*, 2013.

(200) Kamra, T.; Chaudhary, S.; Xu, C.; Johansson, N.; Montelius, L.; Schnadt, J.; Ye, L. Covalent immobilization of molecularly imprinted polymer nanoparticles using an epoxy silane. *J. Colloid. Interface Sci.* **2015**, *445*, 277–284.

(201) Ulrich, S.; Jung, U.; Strunskus, T.; Schütt, C.; Bloedorn, A.; Lemke, S.; Ludwig, E.; Kipp, L.; Faupel, F.; Magnussen, O. *et al.* X-ray spectroscopy characterization of azobenzene-functionalized triazatriangulenium adlayers on Au(111) surfaces. *Phys. Chem. Chem. Phys.* **2015**, *17*, 17053–17062.

(202) *Spektroskopische Methoden in der organischen Chemie;* Hesse, M.; Meier, H.; Zeeh, B., Eds., 7., überarb. Aufl.; Thieme: Stuttgart, New York, 2005.

(203) Perrin, D. D.; Armarego, W. L. F. *Purification of Laboratorial Chemicals*; Wiley-VCH: Weinheim.

(204) Dave, V.; Warnhoff, E. W. New reactions of 2-substituted indoles. *Can. J. Chem.* **1976**, *54*, 1020–1028.

(205) Fulmer, G. R.; Miller, A. J. M.; Sherden, N. H.; Gottlieb, H. E.; Nudelman, A.; Stoltz, B. M.; Bercaw, J. E.; Goldberg, K. I. NMR Chemical Shifts of Trace Impurities: Common Laboratory Solvents, Organics, and Gases in Deuterated Solvents Relevant to the Organometallic Chemist. *Organometallics* **2010**, *29*, 2176–2179.

(206) Fischer, K. Neues Verfahren zur maßanalytischen Bestimmung des Wassergehaltes von Flüssigkeiten und festen Körpern. *Angew. Chem.* **1935**, *48*, 394–396.

(207) ISO 15472:2010, Surface chemical analysis - X-ray photoelectron spectrometers - Calibration of energy scales.

(208) ISO 19318:2004, Surface chemical analysis - X-ray photoelectron spectroscopy - Reporting of methods used for charge control and charge correction.

(209) Beamson, G.; Briggs, D. *High Resolution XPS of Organic Polymers – The Scienta ESCA300 Database*; Wiley, 1992.

Acknowledgements

First and foremost, I would like to thank Prof. Dr. Karola Rück-Braun, for giving me an opportunity to work in her research group on the topics I find great interest in. Moreover, I would like to thank her for guidance and supervision during my work, for valuable help and advice over the past few years.

I thank Prof. Dr. Petra Tegeder for accepting the role of the external examiner.

I thank Prof. Dr. Marga Lensen for accepting the role of the chairperson of the examination committee.

I would like to thank staff working at the Institute. In particular, I would like to thank Dr. Kemper and Ms. Voges for the help with the NMR spectrometer. Dr. Schlangen and Mr. Griffel I thank for the measurements on mass spectrometer. Additionally, I would like to thank Ms. Fischer and Ms. Krone for caring out the IR and elemental analysis measurements.

I would also like to thank all the people from the research group for the pleasant working atmosphere and constructive discussions over the years. Here I thank Sebastian, Miro, Nandor, Anne, Junjie, Christoph and Longying. Thank you for mutual support and understanding, for always being open for discussion and exchange of ideas, and for providing the necessary motivation when needed. Furthermore, I thank Andreas, Diana, Kim, Kerstin and Denis. I thank my bachelor student Valeria for her contribution and work.

I would like to thank people I collaborated with over the years, who helped with measurements and useful insights. I would like to thank Dr. Johannes Schmidt for taking XPS measurements, Dr. Jürgen Bruns for taking ellipsometry measurements. Furthermore, I would like to thank Prof. Dr. Wolfgang Unger from BAM for carrying out the XPS measurements. Additionally, I thank Stefan Schutte for doing the Karl-Fisher measurements.

I would like to thank my friends, in particular, Anita, Boris, Milan, Jovan, Milan, Sarah for your support and encouraging words when I needed them.

I would like to thank my family. Hvala mama i tata za podršku i veru, hvala na strpljenju, ljubavi i brizi, i svim rečima podrške koje su mi uvek značile. Katarina, hvala na bodrenju i brizi, nadam se da ću umeti uzvratiti bar istom merom sada kad je na tebe red da prođeš ovaj put. Njako, hvala na razumevanju, i što si imala prave reči kad su mi trebale. Hvala vam! Gorane, hvala ti za pozitivnu enegriju, ljubav i podršku.

Parts of the work presented in this thesis have been previously reported:

1. Parts of Chapter 3.2 and Chapter 4.1 have been previously published as:
   Vlajić, M.; Schmidt, J.; Thomas, A.; Rück-Braun, K. 2H-Naphthopyran-Based Three-State Systems: From Solution Studies to Photoresponsive Organic/Inorganic Hybrid Materials. *ChemPhotoChem*, ahead of print. DOI: 10.1002/cptc.201800118. Copyright Wiley-VCH Verlag GmbH & Co. KGaA. Reproduced with permission.

2. Parts of Chapter 4.1 and Chapter 4.2 have been previously published as:
   Vlajić, M.; Unger, W.; Bruns, J.; Rück-Braun, K. Photoswitching of fulgimides in different environments on silicon surfaces. *Appl. Surf. Sci.*, ahead of print. DOI: 10.1016/j.apsusc.2018.09.159.